Univerzita Karlova

Lékařská fakulta v Plzni

Šiklův ústav patologie Fakultní nemocnice Plzeň

Disertační práce

Studijní program: Patologie

Korelace molekulárně-biologických a imunohistochemických
metod v diagnostice nádorů hlavy a krku

Correlation of molecular-biological and imunohistochemical
methods in the diagnostics of head and neck tumors

Školitel: prof. MUDr. Alena Skálová, CSc.

Plzeň 2024   Natálie Klubíčková

Prohlášení

Poděkování

Abstrakt

Rozvoj použití metod molekulární genetiky přinesl v posledních desetiletích možnost přesněji klasifikovat nádory hlavy a krku, řada nových jednotek byla recentně definována mimo jiné mezi nádory salivárními a mesenchymálními či nádory sinonasální oblasti. Zatímco v některých případech napomáhá přesná klasifikace predikci průběhu onemocnění a volbě adekvátní intenzity léčby, v jiných případech s mutacemi targetovatelnými cílenou terapií mají výsledky molekulárně-biologických metod přímou implikaci v terapii. Zároveň se stávají dostupnými nové imunohistochemické markery, které mohou v některých případech část genetické analýzy spolehlivě nahradit, což s sebou přináší ekonomické výhody a kratší dobu potřebnou k provedení bioptického vyšetření.

V disertační práci je shrnuta a komentována publikační činnost autorky týkající se salivárních a sinonasálních a mesenchymálních nádorů, důraz je kladen na jejich molekulárně-genetický podklad a imunohistochemické nálezy.

V oblasti salivárních nádorů je pojednáno o možnostech detekce rearanže genů *NR4A3* a *NR4A2* v acinickém karcinomu, následně je diskutováno genetické pozadí sklerózujícího polycystického adenomu a jeho implikace v morfologii a imunoprofilu jednotlivých případů. Dále jsou uvedeny čtyři publikace prezentující případy sinonasálních tumorů, od vzácných typů sinonasálních adenokarcinomů s fúzí *ETV6::NTRK3* či deficiencí SMARCB1, přes raritní případ bifenotypického sinonasálního sarkomu transformujícího do high-grade rhabdomyosarkomu, po soubor případů nově definovaného agresivního sarkomu s fúzí *EWSR1::POU2AF3*. Nakonec jsou diskutovány další mesenchymální nádory vyskytující se v oblasti hlavy a krku: v publikaci o mesenchymálních tumorech s aberacemi kinázových genů jsou prezentována nová morfologická, imunohistochemická a především molekulárně-genetická data včetně významných poznatků z metylačního profilování těchto nádorů, dále je v souboru sedmi případů popsán unikátní myxoidní fibroblastický tumor hlasivky s rekurentní fúzí *TIMP3::ALK*, jako poslední je uveden vzácný epiteloidní mesenchymální tumor měkkého patra s fúzí *PTCH1::GLI1*.

Abstract

The increasing use of molecular-genetic methods in recent decades has facilitated precise classification of head and neck tumors. This has led to the identification of new entities among salivary, mesenchymal, and sinonasal tumors. Accurate classification not only aids in predicting disease course and determining appropriate treatment intensity but also holds significance in cases where mutations can be targeted with specific therapy. Additionally, newly available immunohistochemical markers can in some cases reliably replace part of the genetic analysis, which brings with it economic advantages and a shorter time needed to examine the biopsy material.

The dissertation summarizes and comments on the publication activity of the author regarding salivary, sinonasal and mesenchymal tumors, with a particular focus on their molecular-genetic background and immunohistochemical findings.

In the field of salivary tumors, the discussion revolves around the detection of *NR4A3* and *NR4A2* gene rearrangements in acinic cell carcinoma, as well as the genetic background of sclerosing polycystic adenoma and its implications on morphology and immunoprofile of individual cases. Furthermore, the dissertation lists four publications presenting various cases of sinonasal tumors, ranging from rare types of sinonasal adenocarcinomas with *ETV6::NTRK3* fusion or SMARCB1 deficiency, through a rare case of biphenotypic sinonasal sarcoma transforming into high-grade rhabdomyosarcoma, to a series of cases featuring a newly defined aggressive sarcoma with *EWSR1::POU2AF3* fusion. Lastly, other mesenchymal tumors occurring in the head and neck region are discussed: in the publication on mesenchymal tumors with kinase gene aberrations, new morphological, immunohistochemical and, above all, molecular-genetic data are presented, including significant findings from the methylation profiling of these tumors; a unique myxoid fibroblastic tumor of the vocal cord with a recurrent *TIMP3::ALK* fusion is described in a collection of seven cases, and finally a rare epithelioid mesenchymal tumor of the soft palate with a *PTCH1::GLI1* fusion is reported.

Předmluva

Konvergence různých oborů medicíny vede často k hlubokému poznání a inovativnímu náhledu na problematiku. V patologii tumorů hlavy a krku dochází v poslední době díky aplikaci molekulárně-genetických metod a dostupnosti nových protilátek pro imunohistochemii k dynamickému vývoji diagnostických i terapeutických možností, zároveň však tato nově získaná data vyžadují nejen dobrou orientaci v aspektech medicínských, ale také pochopení studovaných molekulárně-biologických procesů i metod užívaných k jejich analýze. Mé duální vzdělání v medicíně a molekulární biologii umožňuje tuto plodnou symbiózu, o čemž svědčí i tato disertační práce.

Mé doktorské studium probíhalo na Šiklově ústavu patologie Lékařské fakulty v Plzni, jež úzce spolupracuje také se výjimečnou plzeňskou Bioptickou laboratoří. Prof. Michal vybudoval v obou institucích nesmírně podporující prostředí zaměstnávající vynikající patology a akademické pracovníky, což mi umožnilo od počátku mé vědecké kariéry vést kvalitní projekty s klinickým přesahem. Během doktorského studia jsem měla příležitost spolupracovat s prof. Skálovou, světovou špičkou v oboru patologie slinných žláz, která mi byla jako vedoucí doktorského studia inspirací a průvodcem a umožnila mi se podílet na vědecké práci s mnohými dalšími vynikajícími zahraničními odborníky zabývajícími se salivární a sinonasální patologií.

S doc. Michalem jsem se zároveň ponořila do patologie měkkotkáňových nádorů, které nevzácně postihují oblast hlavy a krku, některé jsou dokonce pro tuto lokalizaci specifické. Vrcholem naší spolupráce je rozsáhlá publikace „Comprehensive clinicopathological, molecular, and methylation analysis of mesenchymal tumors with *NTRK* and other kinase gene aberrations", v které aplikujeme nejmodernější metody molekulární genetiky včetně metylačního profilování a prokazujeme jednotný genetický podklad všech studovaných lézí.

Významným cílem jsou též implikace našich poznatků v léčbě pacientů postižených popisovanými tumory, které jsou v několika zde uvedených příkladech značně agresivní a v současné době jen omezeně terapeuticky ovlivnitelné. Prvním krokem k optimální léčbě je zcela přesná diagnostika až na úroveň jednotlivých genetických aberací hrajících roli v patogenezi studovaných nádorů. Tímto způsobem jsou v poslední době definovány nové, geneticky uniformní jednotky, často se vyčleňující ze skupin doposud dále nespecifikovatelných maligních tumorů. V některých případech je navíc již nyní dostupná cílená léčba, kterou je možno v případě detekce příslušných alterací indikovat, často s velmi dobrým terapeutickým efektem.

Obsah

Seznam zkratek

AciCC	Acinický karcinom
CK	Cytokeratin
CNV	Copy-number variant
DNA	Deoxyribonukleová kyselina
DNA-seq	DNA sekvenace
FISH	Fluorescenční in-situ hybridizace
HGT	High-grade transformace
IMT	Inflamatorní myofibroblastický tumor
ITAC	Adenokarcinom intestinálního typu
MR	Magnetická rezonance
Non-ITAC	Adenokarcinom non-intestinálního typu
PAS	Periodic acid-Schiff
RNA	Kyselina ribonukleová
RNA-seq	RNA sekvenace
SMA	Hladkosvalový aktin
SPA	Sklerózující polycystický adenom
WHO	Světová zdravotnická organizace

1 Úvod

1.1 Salivární nádory

Nádory slinných žláz jsou vzácné zhoubné i benigní léze vyskytující se v zemích západního světa s incidencí přibližně 2,5 – 3/100 000, přičemž ve většině případů se jedná o tumory benigní – především Warthinův tumor a pleomorfní adenom (1,2). Incidence maligních salivárních nádorů celosvětově nepřesahuje 1/100 000 (standardizováno na věk). Incidence maligních salivárních nádorů v České republice je 0,67/100 000, mortalita dosahuje 0,25/100 000. V Evropě je Česká republika v incidenci na 8. místě, nejvyšší incidence je v Itálii, kde dosahuje 0,9/100 000 (3).

V současnosti se pro klasifikaci salivárních nádorů používá 5. vydání WHO klasifikace tumorů hlavy a krku vydané v roce 2022 (4). V kapitole salivárních nádorů je klasifikováno 15 benigních epiteliálních nádorů, 21 karcinomů, 1 benigní mesenchymální tumor specificky se vyskytující v slinných žlázách – sialolipom, a 2 nenádorové epiteliální léze.

1.1.1 Acinický karcinom

Acinický karcinom (AciCC) je častým maligním salivárním tumorem, představuje asi 10 % salivárních karcinomů. Po mukoepidermoidním karcinomu je druhým nejčastějším pediatrickým maligním nádorem slinných žláz (4), většinou však postihuje dospělé pacienty středního věku. Nejčastěji roste v příušní žláze, v malých slinných žlázách je zcela raritní.

V typických dobře diferencovaných případech mají nádorové buňky serózní acinickou morfologii a obsahují cytoplazmatická PAS-pozitivní granula, onkocytická nebo světlobuněčná přeměna však není výjimkou. Především v těchto případech nabývají na významu pomocné imunohistochemické a molekulárně-genetické metody, protože prostá morfologická diagnostika může být značně obtížná. Nejčastější růstový vzor je solidně-mikrocystický s bohatým lymfoidním stromatem i s dobře formovanými lymfoidními folikly se zárodečnými centry, lze se ale také setkat s případy s kribriformní, makrocystickou, tubulární či papilární architekturou, možné jsou také kombinace několika růstových vzorů.

Zatímco prognóza pacientů s klasickým dobře diferencovaným AciCC je vynikající, s 5letým a 10letým přežitím 97 % a 94 % (4-5), některé případy vykazují takzvanou high-grade transformaci (HGT) v agresivně se chovající novotvar s vysokou mortalitou (6), charakterizovaný přítomností ložisek nízce diferencovaného karcinomu či adenokarcinomu rostoucího většinou v solidních hnízdech s centrální nekrózou, vykazujícího výrazné jaderné atypie a vysokou mitotickou aktivitu, a zároveň přítomností struktur klasického low-grade AciCC. V některých případech low-grade komponenta již není zastižena, tyto případy jsou označovány jako high-grade AciCC.

Nádorové buňky exprimují marker DOG1, s typickou apikální/kanalikulární imunohistochemickou pozitivitou. Zatímco marker SOX10 je imunohistochemicky

pozitivní, S100 protein je negativní, stejně jako markery p40 a p63. Nově je pro imunohistochemii dostupná protilátka NR4A3.

Geneticky vzniká naprostá většina AciCC na podkladě translokace t(4;9)(q13;q31), která vede k tzv. enhancer hijackingu (únosu enhanceru). Silný enhancer z oblasti clusteru genů *SCPP* na dlouhém raménku 4. chromosomu se translokací dostává do blízkosti genu *NR4A3* (*Nor1*) na dlouhém raménku 9. chromosomu (7). To způsobuje nadměrnou expresi genu *NR4A3*, přičemž produkt tohoto genu lze detekovat imunohistochemicky. Pro potvrzení přítomnosti translokace je metodou volby FISH s break-apartovou sondou detekující zlom genu *NR4A3* (7). Jelikož není výsledkem translokace rekurentní patogenní fúzní gen, není RNA sekvenace (RNA-seq) vhodným nástrojem pro potvrzení diagnózy.

1.1.2 Sklerózující polycystický adenom

Tato jednotka byla původně pod názvem sklerózující polycystická adenóza považována za nenádorovou reaktivní lézi. Již v roce 2006 však byla pomocí assaye HUMARA, jež testuje vzorec inaktivace chromosomu X, prokázána klonalita, respektive nádorová povaha této jednotky (8). Recentně byly pomocí sekvenačních metod navíc ve sklerózujícím polycystickém adenomu (SPA) detekovány rekurentní aberace signální kaskády PI3K (9-10).

Jedná se o benigní salivární tumor postihující především dospělé pacienty středního věku, mírně častěji se vyskytující u žen a většinou rostoucí v příušní žláze. Histologicky je typické multilobulární uspořádání nádorové proliferace tvořené dukty vystlanými luminálními buňkami značně variabilní morfologie a aciny tvořenými velkými buňkami s objemnými eosinofilními granuly, přičemž ve všech epiteliálních strukturách zůstává zachována abluminální vrstva myoepitelií. Ve stromatu jsou ložiska výrazné hyalinizace a sklerotizace. Imunohistochemický marker SOX10 je pozitivní ve všech epitelálních strukturách, myoepitelie jsou dále pozitivní v imunohistochemickém průkazu p40, p63 či SMA (4). Luminální buňky mohou vykazovat ztrátu imunohistochemické exprese PTEN. V některých případech lze zastihnout exuberantní intraluminální mikropapilární, kribriformní nebo i solidní epiteliální proliferaci a vzácně byl reportován vznik karcinomu ze SPA (10).

1.2 Sinonasální nádory

Mezi sinonasální nádory řadí WHO klasifikace rozmanité epiteliální, mesenchymální i neuroektodermální tumory, které spojuje jejich růst v nosní dutině a paranasálních sinusech. Jsou to léze extrémně vzácné, spolehlivé údaje o jejich incidenci proto nejsou dobře dostupné. Maligní sinonasální nádory mají incidenci přibližně 0,56/100 000 (11), mortalita je poměrně vysoká, v některých evropských populacích dosahuje až 0,33/100 000 (12), protože se často jedná o značně agresivní nádorové jednotky.

Současná WHO klasifikace sinonasálních nádorů je poměrně komplexní – jednotky jsou rozděleny do 4 skupin, a to hamartomy, léze vznikající z epitelu respiračního traktu, mesenchymální tumory specificky se vyskytující v sinonasální oblasti a ostatní sinonasální tumory. Celkem klasifikace popisuje 24 jednotek.

1.2.1 Sinonasální adenokarcinom

Sinonasální adenokarcinomy *sensu stricto* vznikají z epitelu respiračního traktu. V této lokalizaci se mohou raritně vyskytovat rovněž nádory salivární, tyto nádory zde však diskutovány nebudou.

Primární sinonasální adenokarcinomy jsou velmi vzácné nádory, které se dělí do dvou základních skupin: adenokarcinom intestinálního typu (ITAC) a adenokarcinom non-intestinálního typu (non-ITAC). V nedávné době byl dále popsán SMARCB1-deficientní adenokarcinom, který se ve WHO klasifikaci řadí mezi sinonasální karcinomy s deficiencí SWI/SNF komplexu (4). Sinonasální adenokarcinomy většinou postihují starší dospělé pacienty, ale věkové rozmezí je značně široké. Častěji vznikají u mužů (4).

ITAC je morfologicky blízký primárním gastrointestinálním adenokarcinomům, je tvořen hlenotvornými kolumnárními a pohárkovými buňkami uspořádanými v papilárních a glandulárních strukturách. Zatímco lépe diferencované případy mají papilární a tubulární architekturu, hůře diferencované adenokarcinomy mívají kribriformní a solidní úpravu, s častými centrálními nekrózami. V některých případech může adenokarcinom vykazovat extenzivní extracelulární hlenotvorbu. Imunohistochemicky jsou nádorové buňky pozitivní v průkazu CK20, CDX2 a SATB2, variabilně je exprimován CK7 (13-14). Biologickým chováním se jedná o poměrně agresivní, často rekurující nádory; pět let přežívá přibližně jedna polovina pacientů (15). Pokročilost tumoru je pro prognózu významnější než grade (15).

Morfologické spektrum non-ITAC je velmi široké. Na dobře diferencovaném konci spektra stojí nádory s papilární či tubulární úpravou tvořené jen mírně atypickými cylindrickými či kuboidálními buňkami. Špatně diferencované tumory rostou spíše v solidních hnízdech jen s ojedinělými žlázovými strukturami, běžný je výskyt centrálních nekróz. Další variantou je disociovaný infiltrativní růst mucin-produkujících nádorových buněk, některé případy vykazují světlobuněčnou přeměnu. Imunohistochemický profil je nespecifický, není však přítomna difúzní exprese gastrointestinálních markerů CDX2 a SATB2. Zatímco většina pacientů s dobře diferencovanými non-ITAC dlouhodobě přežívá, prognóza pacientů se špatně diferencovanými tumory je značně nepříznivá a většina pacientů zemře na komplikace lokálně pokročilého tumoru do pěti let (16).

SMARCB1-deficientní sinonasální adenokarcinom je extrémně vzácný nádor definovaný ztrátou exprese genu *SMARCB1*, a tedy deficitem funkce proteinového komplexu SWI/SNF, a zároveň přítomností jednoznačných glandulárních struktur. Nádorové buňky mají většinou plasmacytoidní, onkocytoidní či rhabdoidní vzhled a bryskní proliferační aktivitu. Nevzácně jsou přítomna ložiska připomínající tumor ze žloutkového váčku i s odpovídajícím imunoprofilem. Dále je ve většině případů

imunohistochemicky pozitivní průkaz CK7 a negativní je barvení s protilátkou proti SMARCB1 (17). Pomocí FISH či DNA sekvenace (DNA-seq) lze detekovat delece či mutace menšího rozsahu postihující gen *SMARCB1*.

1.2.2 Bifenotypický sinonasální sarkom

Bifenotypický sinonasální sarkom (BSNS) je indolentní mesenchymální nádor vykazující podvojnou neurální a myogenní diferenciaci. Vzniká u dospělých pacientů, častěji postihuje ženy. Roste infiltrativně do přilehlých měkkých tkání i do lebečních kostí a je možná i intracerebrální extenze, vzdálené metastázy však nevznikají.

Morfologicky je BSNB tvořen denzní uniformní, nepříliš mitoticky aktivní vřetenobuněčnou proliferací uspořádanou do fasciklů, někdy s architekturou rybí kosti. Časté jsou invaginace reaktivně změněného povrchového epitelu. Typická je koexprese imunohistochemických markerů SMA a S100 při negativitě SOX10. Až 90 % případů vykazuje též fokální expresi markeru kosterní svaloviny MyoD1, vzácně mohou být nalezeny rhabdomyoblasty (18-19). Exprese dalšího markeru kosterní svaloviny myogeninu je vzácnější (18, 20).

Většina případů vzniká na podkladě patogenní fúze genu *PAX3*, jeho nejčastějším fúzním partnerem je gen *MAML3*, možná je však i přítomnost jiných fúzních partnerů (20). Pro detekci aberace a konfirmaci diagnózy lze využít FISH s break-apartovými sondami detekujícími zlomy genů *PAX3* a *MAML3*, případně lze fúzní produkty detekovat targetovanou RNA-seq.

1.2.3 *EWSR1::POU2AF3* sarkom

Vzhledem k tomu, že byl *EWSR1::POU2AF3* sarkom poprvé identifikován v roce 2022 na základě molekulárně-genetické analýzy obtížně klasifikovatelných mesenchymálních nádorů v rámci běžné klinické praxe (21), není dosud součástí platné WHO klasifikace. Jedná se o nádor postihující široké věkové rozmezí převážně dospělých pacientů, jeden pacient byl v době první resekce adolescentního věku. Nádor vykazuje predilekci pro sinonasální oblast, kde roste destruktivně v měkkých tkáních i kostech, dále byly reportovány případy vyrůstající v kostech pánve, v hrudní stěně, orbitě a mozku (21-22).

V první práci byla popsána nepříznačná morfologie atypických krátce vřetenitých až oválných a kulatých epiteloidních buněk s jemně zrnitým jaderným chromatinem, uspořádaných v plochách, vágních fasciklech a hnízdech s četnými nekrotickými ložisky. Nebyly přítomny přesvědčivé známky specifického směru jakékoli diferenciace (21). V další práci pak byl prezentován nález bifázické morfologie, s oblastmi tvořenými epiteloidními kulatými nádorovými buňkami a oblastmi s bohatším kolagenním stromatem a vřetenitými nádorovými buňkami. Ani v této práci nebyla prokázána specifická linie diferenciace (22). Imunoprofil je nepříliš specifický, v některých případech byla detekována slabá pozitivita markeru CD99, některé tumory byly fokálně pozitivní v průkazu cytokeratinů, EMA, p16 či CD56 (21-22).

Větší význam pro diagnostiku tohoto sarkomu má molekulárně-genetická analýza. Fúzi *EWSR1::POU2AF3* lze detekovat pomocí targetované RNA-seq, analýzu lze rovněž doplnit metodou FISH za použití komerčně dostupných break-apartových sond detekujících zlom genu *EWSR1*. Ve dvou případech byla namísto fúze *EWSR1::POU2AF3* detekována alternativní fúze *FUS::POU2AF3*. Proteinové produkty genů *EWSR1* a *FUS* patří do rodiny FET, mají homologní strukturu a obdobou funkci: jedná se v obou případech o RNA-vazebné proteiny, které ovlivňují transkripci a zpracovávání RNA (23).

Prognóza pacientů s *EWSR1::POU2AF3* je nepříznivá, a to i přes užití multimodální intenzivní terapie. Přibližně u dvou třetin pacientů vznikají vzdálené metastázy a/nebo tumor opakovaně recidivuje, v některých případech již bez možnosti onemocnění lokálně kontrolovat (21-22).

1.3 Další měkkotkáňové nádory hlavy a krku

Benigní měkkotkáňové nádory jsou výrazně častější než nádory maligní. Statistická epidemiologická data nejsou příliš přesná, jejich incidence je přibližně 300/100 000 (24). Maligní měkkotkáňové nádory jsou velmi vzácné, představují méně než 1 % všech malignit (25-26), pětileté přežití je přibližně 50 %. Méně než 10 % všech měkkotkáňových tumorů vyrůstá v oblasti hlavy a krku, incidence je vyšší u dětí (27).

WHO klasifikace tumorů hlavy a krku uvádí 32 benigních a maligních jednotek řazených do 10 kapitol dle histogeneze (4). Tyto jednotky jsou zcela specifické pro oblast hlavy a krku, nebo se v ní vyskytují velmi frekventně. V praxi je však možné se v konkrétních případech setkat i s řadou jiných měkkotkáňových nádorů, které nejsou pro oblast hlavy a krku typické – tyto jednotky kategorizuje WHO klasifikace kostních a měkkotkáňových nádorů (25).

1.3.1 Mesenchymální nádory s aberacemi kinázových genů

Měkkotkáňové novotvary s aberacemi kinázových genů jsou v současné klasifikaci WHO kostních a měkkotkáňových tumorů (25) zařazeny v kategorii fibroblastických a myofibroblastických nádorů pod dvěma jednotkami: infantilní fibrosarkom a adultní fibrosarkom. V kategorii nádorů nejisté histogeneze je navíc řazena další příbuzná entita, a to *NTRK*-rearanžované vřetenobuněčné tumory.

Pravděpodobně se jedná o blízce příbuzné jednotky pohybující se na morfologickém spektru od low-grade vřetenobuněčných proliferací s nízkou celularitou, minimální mitotickou aktivitou až po agresivně vyhlížející, vysoce mitoticky aktivní nádory tvořené atypickými vřetenitými buňkami (28-29). Fúze *ETV6::NTRK3* je charakteristická pro infantilní fibrosarkom, všechny nádory z této širší skupiny však sdílí obdobné patogenní mutace, a to fúze genů pro tyrosin- nebo serin-threonin kinázy (*NTRK1-3*, *MET*, *RET*, *RAF1* nebo *BRAF*), povětšinou s geny pro různé transkripční faktory nebo DNA- či RNA-vazebné proteiny. Častá je také imunohistochemická koexprese markerů S100 a CD34. V případě fúzí genů *NTRK1-3* jsou nádorové buňky

rovněž pozitivní v imunohistochemickém průkazu panTrk. Pro průkaz kanonické fúze *ETV6::NTRK3* v infantilním fibrosarkomu je zcela dostačující molekulárně-genetická analýza pomocí FISH, vzhledem k počtu možných fúzních partnerů v ostatních nádorech této skupiny je však výhodnější využití RNA-seq.

Nádory se vyskytují v jakémkoli věku, mohou být i kongenitální. Lokalizovány jsou většinou v hlubokých měkkých tkáních končetin, trupu a hlavy a krku (25). Pacienti ženského a mužského pohlaví jsou postiženi přibližně stejně často. Většina případů je pouze lokálně agresivní, při nepříznivé lokalizaci však mohou být obtížně operovatelné, přibližně v 20 % případů rekurují. Metastazují především nádory s high-grade morfologií, vzdálené metastázy postihují celkově méně než 10 % pacientů (29). Mimo možnosti chirurgického řešení a chemoterapeutické režimy jsou dostupné inhibiční molekuly cílící na aberantně aktivované proteiny NTRK a RET (entrektinib, larotrektinib, kabozantinib), které jsou používané v léčbě lokálně pokročilých inoperabilních nebo metastatických případů.

1.3.2 Inflamatorní myofibroblastický tumor

Inflamatorní myofibroblastický tumor (IMT) je vzácný tumor postihující především mladší dospělé pacienty a pediatrickou populaci. Nejčastěji vzniká v plicích, mesenteriu, omentu a močových cestách, asi 15 % případů je lokalizováno v oblasti hlavy a krku včetně horních cest dýchacích (30). Přibližně u čtvrtiny pacientů s extrapulmonálními IMT dochází k rekurenci, vzdálené metastázy jsou velmi vzácné (30). Případy lokalizované v plicích, ale také v oblasti hlavy a krku, mají prognózu zvláště dobrou, rekurence jsou zde vzácnější (31-32).

Histologicky se jedná o nádor složený z vřetenitých myofibroblastů s eosinofilní cytoplazmou a převážně oválnými jádry s patrnými jadérky, součástí léze je též variabilně bohatý infiltrát nenádorových zánětlivých buněk: někdy může být přítomen jen nenápadný lymfocytární lem při okraji léze, v jiných případech je celý nádor prostoupen hojnými lymfocyty, plazmatickými buňkami a eosinofily. Některé nádorové buňky mohou nabývat vzhledu gangliových buněk s velkým jádrem a výrazným eosinofilním jadérkem, bývají též přítomny pseudoinkluze části cytoplazmy do jádra.

Lze rozlišit tři histologické subtypy IMT: v prvním z nich se jedná o relativně více celulární vřetenobuněčnou proliferaci ve storiformním a fascikulárním uspořádání s bohatým zánětlivým infiltrátem; pro druhý, méně celulární subtyp je charakteristické hojné hyalinizované stroma a nevýrazný zánětlivý infiltrát, třetí subtyp je rovněž hypocelulární, je přítomno myxoidní stroma, bohatá kapilární síť a četné nenádorové zánětlivé buňky, většinou však s fokálně zachovalými více celulárními fascikulárními či storiformními oblastmi s vřetenitými buňkami (4). Více než 90 % IMT imunohistochemicky exprimuje SMA (30).

Ačkoli byl IMT původně kvůli přítomnosti četných zánětlivých buněk považován za zánětlivý pseudotumor, v současnosti je klasifikován jako skutečná neoplastická léze vznikající ve většině případů na podkladě aberantní aktivity tyrosin-kinázy ALK, případně jiných kinázových proteinů (například ROS1, RET, NTRK3), k čemuž dochází

translokací příslušných genů do blízkosti rozličných transkripčně aktivních genových partnerů (33-34). Imunohistochemický průkaz exprese ALK lze využít jako zástupný marker přítomnosti translokace genu *ALK*, potvrdit ji lze pomocí FISH. Vzhledem k počtu možných fúzních partnerů a v případech IMT s aberacemi genů pro jiné kinázy je pro přesný popis přítomné aberace vhodnější využít RNA-seq.

1.3.3 Mesenchymální nádory s aberacemi genu *GLI1*

Tumory s alteracemi genu *GLI1* se mohou vyskytnout jak v měkkých tkáních končetin i trupu, tak v kostech a vnitřních orgánech, přičemž 40 % případů je lokalizováno v oblasti hlavy a krku (35). Postiženi bývají nejčastěji mladí dospělí pacienti, ale věkové rozmezí je velmi široké. Biologické chování je rovněž variabilní, většina tumorů je indolentní, přibližně ve 20 % případů ale může dojít k recidivě nebo vzniku vzdálených metastáz (35-36).

GLI1-rearanžované nádory mají nejistou histogenezi a nespecifický imunoprofil. Buňky jsou většinou oválné, epiteloidní až vřetenité, s eosinofilní či vodojasnou cytoplazmou a nápadně uniformními oválnými jádry s jemným chromatinem a drobnými jadérky, uspořádané obvykle v solidních hnízdech nebo trámcích (4, 35-36). Imunohistochemický průkaz proteinu GLI1 vykazuje vysokou specificitu a senzitivitu pro *GLI1*-rearanžované mesenchymální nádory, senzitivita je však neuspokojivá u plexiformního fibromyxomu (37). Dále lze imunohistochemicky v některých případech prokázat expresi markerů S100, SMA, CD56 a dalších, exprese jednotlivých markerů je ale nekonzistentní.

Ve dvou třetinách případů jsou v tumorech prokázány fúze genu *GLI1* zahrnující fúze *ACTB::GLI1*, *PTCH1::GLI1*, *MALAT1::GLI1* a *DERA::GLI1*, ve zbylých nádorech je detekována amplifikace genu *GLI1* (35-36, 38). V případě amplifikovaných *GLI1*-rearanžovaných tumorů je možná i koamplifikace genů *CDK4*, *MDM2* a *DDIT3*, které jsou lokalizovány v sousedících lokusech na dlouhém raménku 12. chromosomu (36). Pro detekci amplifikace genu *GLI1* se využívá FISH, v jedné době lze případně detekovat amplifikace i ostatních zmíněných sousedních genů; genové fúze se většinou detekují pomocí RNA-seq.

2 Cíle disertační práce

Cílem prací – case reportů bylo popsat extrémně raritní a diagnosticky obtížné případy, s kterými jsme se setkali během rutinní praxe i konzultační činnosti, a to včetně detailní molekulárně-genetické analýzy a širokého imunohistochemického panelu.

V publikacích založených na větších souborech nádorových jednotek bylo cílem přispět již větším množstvím dat ke zpřesňování nosologie již známých nádorových jednotek. V některých těchto studiích také definujeme jednotky nové, v jiných studiích naopak prezentujeme data podporující snahu některé současně rozdrobené jednotky sjednocovat.

V každé studii je kladen důraz na vhodnou imunohistochemickou i molekulárně-genetickou analýzu a možnosti náhrady molekulárně-genetického vyšetření nebo jeho části hodnocením imunohistochemickým.

V práci „Comprehensive clinicopathological, molecular, and methylation analysis of mesenchymal tumors with *NTRK* and other kinase gene aberrations" bylo jedním z cílů rovněž shromáždit data o využití cílené terapie v léčbě těchto vzácných měkkotkáňových tumorů.

3 Metody

Užité metody jsou detailně popsány v jednotlivých publikovaných pracích, pro redundanci zde nebudou znovu uváděny samostatně.

4 Komentované publikační výsledky

4.1 A minority of cases of acinic cell carcinoma of the salivary glands are driven by an *NR4A2* rearrangement: The diagnostic utility of the assessment of *NR4A2* and *NR4A3* alterations in salivary gland tumors

Studie předkládá výsledky klinicko-patologické a molekulárně-genetické analýzy 128 případů AciCC slinných žláz. Ve dvou případech se poprvé podařilo pomocí FISH detekovat zlom genu *NR4A2*.

Osmdesát čtyři případů představovalo klasický dobře diferencovaný AciCC, zatímco v 43 případech (34 %) se jednalo o AciCC s HGT, případně high-grade AciCC zcela bez zastižené low-grade komponenty. Věkové rozmezí bylo velmi široké, s mediánem 61 let, častěji byl tumor diagnostikován u žen. Ve více než 90 % případů se jednalo o primární tumory, ve studii bylo ale také zahrnuto 9 rekurentních a 3 metastatické nádory. Ve třech případech primárních tumorů nebyl tumor lokalizován v příušní žláze.

Nádory měly povětšinou solidně-mikrocystickou architekturu, téměř v jedné třetině případů byla ale také přítomna úprava cystopapilární. Světlobuněčná přeměna nádorových buněk byla pozorována v 33 případech (26 %). Imunohistochemické markery DOG1 a SOX10 byly pozitivní v 98 % a 99 % případů, nový specifický marker NR4A3 byl pozitivní v 82 % případů, přičemž někdy se touto protilátkou barvily jen části preparátů nebo bylo barvení značně slabé i při optimální vnější kontrole. V případě, že byl jeden z markerů negativní, byly vždy pozitivní zbývající dva markery, tato trojkombinace má tedy dle našich výsledků perfektní senzitivitu a může nahradit i molekulárně-genetické metody.

Jako zástupný marker translokace t(4;9) byl detekován zlom genu *NR4A3* pomocí FISH. Celkem byl zlom prokázán v 73 % testovaných případů, z NR4A3-imunopozitivních AciCC pak u 82 %. Diskrepance v počtu NR4A3-imunopozitivních případů a případů s úspěšnou detekcí zlomu genu *NR4A3* vzniká nejspíše tím, že FISH je v některých případech, kdy je zlom lokalizován značně upstream před samotným genem *NR4A3*, falešně negativní (7).

Všechny NR4A3-imunonegativní a 33 NR4A3-imunopozitivních případů bylo následně imunohistochemicky testováno s protilátkou proti NR4A2. Ve vzácných případech bez translokace t(4;9) způsobující overexpresi genu *NR4A3* byla v AciCC detekována upregulace genu *NR4A2*. Jedná se o paralogní geny kódující proteiny patřící do rodiny retinoidních receptorů steroidních-thyroidálních hormonů, které po aktivaci příslušnými ligandy působí jako transkripční faktory. Patogenetický proces u nádorů s přestavbou genu *NR4A2* je tedy pravděpodobně analogický enhancer hijackingu již dříve popsanému u AciCC s rearanžemi zahrnujícími gen *NR4A3* (7). Šest NR4A3-imunonegativních případů vykazovalo silnou nukleární pozitivitu při barvení s protilátkou NR4A2, zatímco všechny NR4A3-imunopozitivní případy byly negativní. Celkem 17 případů bylo imunohistochemicky negativních v průkazu NR4A3 i NR4A2. U dvou z těchto případů se následně podařilo prokázat zlom v oblasti genu *NR4A3* pomocí FISH.

Devět případů bylo finálně testováno pomocí break-apartové FISH sondy detekující zlom v oblasti genu *NR4A2*. Zlom se podařilo prokázat u dvou z těchto testovaných případů, oba byly zároveň pozitivní v imunohistochemickém průkazu NR4A2. Tato genetická aberace v AciCC byla poprvé popsána v naší práci.

ORIGINAL ARTICLE

A minority of cases of acinic cell carcinoma of the salivary glands are driven by an *NR4A2* rearrangement: the diagnostic utility of the assessment of *NR4A2* and *NR4A3* alterations in salivary gland tumors

Natálie Klubíčková[1,2,3] · Petr Grossmann[2] · Petr Šteiner[2] · Martina Baněčková[1,2] · Elaheh Mosaieby[1,2] ·
Olena Koshyk[4] · Michal Michal[1,2] · Ilmo Leivo[5,6] · Alena Skálová[1,2]

Abstract

Acinic cell carcinoma (AciCC) is a common salivary gland malignancy, typically composed of neoplastic acinic cells with zymogen granules. The vast majority of cases are driven by a t(4;9)(q13;q31) leading to enhancer hijacking and upregulation of the *NR4A3* gene. However, a minority of cases do not display *NR4A3* overexpression on immunohistochemical examination and are negative for the rearrangement involving the *NR4A3* gene when tested by FISH. Such cases overexpress *NR4A2*, and the protein product is detectable by immunohistochemistry. In this study, we aimed to assess the utility of NR4A2 and NR4A3 immunohistochemistry in the differential diagnosis of salivary gland tumors. Eighty-five cases of classic low-grade ACiCC, as well as 36 cases with high-grade transformation (HGT) and 7 high-grade AciCC cases were included in the analysis. NR4A3 was at least focally positive in 105/128 (82%) cases. Out of the 23 cases that were immunohistochemically negative for NR4A3, 6 displayed nuclear immunopositivity with the NR4A2 antibody. The *NR4A3* rearrangement was confirmed by FISH in 38/52 (73%) cases. In addition, this is the first report of an *NR4A2* rearrangement being detected by FISH in 2 AciCC cases that were negative for the *NR4A3* rearrangement. Our analysis confirms that the majority of AciCC, including high-grade cases and cases with HGT, are immunopositive for NR4A3, and suggests that NR4A3 immunohistochemistry is a powerful tool in the differential diagnosis of salivary gland tumors. However, its utility is limited in sub-optimally fixed samples which often display weaker and focal positivity. Our study also indicates that in a minority of cases, AciCC might be negative for NR4A3 immunostaining, because the pathogenic genetic event in these cases is instead a rearrangement involving the *NR4A2* gene.

Keyword Salivary gland · Acinic cell carcinoma · *NR4A3* · *NR4A2* · t(4 · 9)(q13 · q31) translocation · High-grade transformation

Introduction

Acinic cell carcinoma (AciCC) represents about 10% of malignant salivary gland tumors and is also the second most common pediatric salivary gland malignancy [1].

Middle-aged adults, more often female, are the most commonly affected, with the average age of about 50 years, but the age range is considerably wide. While the prognosis for patients with the classic low-grade AciCC is excellent, with 5-year and 10-year survival rates of 97% and 94%,

✉ Natálie Klubíčková
klubickova@biopticka.cz

1 Department of Pathology, Faculty of Medicine in Pilsen, Charles University, Pilsen, Czech Republic

2 Bioptical Laboratory, Ltd, Pilsen, Czech Republic

3 Biomedical Center, Faculty of Medicine in Pilsen, Charles University, Pilsen, Czech Republic

4 Medical Laboratory CSD, Kiev, Ukraine

5 Institute of Biomedicine, Pathology, University of Turku, Turku, Finland

6 Department of Pathology, Turku University Hospital, Turku, Finland

🖄 Springer

respectively [2], some cases display a transformation into high-grade, aggressively behaving neoplasms with unfavorable outcomes [3–5].

In typical low-grade cases, the neoplastic cells display a serous acinic differentiation with PAS-positive cytoplasmic granules. However, some neoplastic cells can also have eosinophilic, clear-cell or vacuolated cytoplasm. The most common architectural pattern is solid-microcystic, often with abundant lymphoid stroma, including well-formed lymphoid follicles with germ centers in some cases. Cribriform and cystic architecture is often associated with intratumoral hemorrhage. Follicular, tubular, and papillary growth patterns are less common and might pose a diagnostic challenge in some instances. Areas with transformation into high-grade carcinoma usually grow as solid nests, often with central comedonecrosis. Tumor cells are positive for SOX10 and DOG1, with the latter antibody usually showing an apical/canalicular pattern of staining. Conversely, p40, p63, and S100 markers are negative in AciCC. Even though the diagnostic process in acinic cell carcinoma is usually straight-forward, the immunohistochemical markers might be of benefit in challenging cases such as zymogen granule-poor and other rare morphological variants including clear-cell changes, tumors with high-grade transformation or unusually located tumors. In fine-needle aspiration cytology specimens, immunohistochemistry might aid to differentiate among zymogen granule-rich neoplastic cells of acinic cell carcinoma and normal acinic cells.

Genetically, the vast majority of AciCC are driven by t(4;9)(q13;q31), leading to the hijacking of strong enhancer regions from the secretory calcium-binding phosphoprotein cluster of genes (*SCPP*) to the proximity of *NR4A3* (*Nor1*) gene [6]. This causes the overexpression of *NR4A3* which might in turn detected by immunohistochemistry [7]. Rare cases that are negative for the translocation might display upregulation of another gene from the same group of nuclear receptors called *NR4A2* (*Nurr1*), located at chromosome band 2q24.1 [8]. Recently, immunohistochemical markers NR4A3 and, rarely, NR4A2 have been gaining importance in the differential diagnosis of salivary glands tumors, being highly specific and sensitive for AciCC [7–9].

Materials and methods

Case selection

For the current study, 128 AciCC cases were collected from institutional files of Biopticka laboratory. The diagnosis was confirmed by two pathologists (NK and AS) based on histomorphology and immunohistochemistry, in accordance with the current WHO classification of head and neck tumors [1]. Classic low-grade AciCC cases as well as cases with high-grade features or high-grade transformation (HGT) were included. Tumors with HGT were defined by the presence of a transformed area consisting of poorly differentiated carcinoma with high-grade features (with high mitotic activity and/or necrosis), within an otherwise well-defined, low-grade AciCC. The diagnosis of high-grade AciCC (without HGT) was rendered if areas with increased mitotic activity (> 5 mitotic figures/10 HPF (2.4 mm^2)) and/or necrosis were present in the tumor, without the presence of a classic low-grade area, in accordance with a grading system proposed by Xu et al. [3]. Similarly to previous studies [7], these high-grade cases were included based on the concordant immunohistochemistry and clinicopathological correlation, as most of the samples represented recurrent tumors, metastases, or probatory biopsy specimens.

Histology and immunohistochemistry

For conventional microscopy, the excised tissues were fixed in formalin, processed routinely, embedded in paraffin (FFPE), cut, and stained with hematoxylin & eosin. For the DOG1, SOX10, NR4A3, and NR4A2 immunohistochemistry, the 4-µm-thick sections cut from paraffin blocks were processed in accordance with institutional standard on BenchMark ULTRA (Ventana Medical Systems, Tucson, AZ). All primary antibodies with their respective epitope retrieval method used in this study are summarized in Table 1. Visualization was performed using the ultraView Universal DAB Detection Kit (Roche, Tucson, AZ) and ultraView Universal Alkaline Phosphatase Red Detection Kit (Roche, Tucson, AZ). The slides were counterstained with Mayer's hematoxylin. Appropriate controls were employed.

NR4A3 immunohistochemical examination was recognized as positive if moderate to strong nuclear staining was present at least focally (≥5% tumor cells). Cytoplasmic or membranous staining was considered non-specific and was not counted as positive. NR4A2 immunohistochemical stain displayed a strong background affinity to multiple, even non-neoplastic structures. Consequently, only strong diffuse nuclear staining was regarded as positive.

FISH

For the detection of *NR4A2* and *NR4A3* rearrangements, custom-design SureFISH *NR4A2* break-apart probe (SureFISH/Agilent Technologies, Santa Clara, CA, USA) and ZytoLight

Table 1 Antibodies used in the study

	Dilution	Clone	Source
DOG1	RTU	SP31	Ventana
NR4A2	1:100	N1404	Abcam
NR4A3	1:50	H-7	Santa Cruz
SOX10	RTU	SP267	Ventana

RTU, ready to use

SPEC *NR4A3* Dual Color Break Apart Probe (ZytoVision Gmbh, Bremerhaven, Germany) were used. Chromosomal locations (build Human Genome version hg19) used for custom *NR4A2* break-apart probe oligos were chr2:156,780,798–157,181,092 and chr2:157,198,713–157,599,007. The FISH procedure and interpretation of the results were performed as described previously [10].

Results

Demographic and clinical characteristics

The clinicopathological data for the 128 AciCC cases are summarized in Table 2. Eighty-five cases of low-grade AciCC, 7 cases of high-grade AciCC, and 36 cases with HGT were included in the study. The patients' age ranged from 11 to 86 years (mean = 56, median = 61). Patients with HGT and high-grade tumors were more than a decade older than patients with low-grade AciCC (mean = 65, median = 68 vs. mean = 52, median = 56). Whereas 72% of patients with low-grade AciCC were female, both sexes were affected almost equally in the HGT and high-grade groups. One hundred and sixteen cases were primary tumors, most commonly occurring in the parotid gland, while 1 case each originated from the sublingual gland, submandibular gland, and small salivary gland in the parapharyngeal space. Location was unknown in 1 case. In addition, 9 cases represented recurrences, and 3 metastases

Table 2 Clinical data and molecular-genetic features of the cases

128 AciCC cases			*n*	%
Clinical features				
	Sex			
		Female	84	66%
		Male	44	34%
	Age, median (range)		61 (11–86)	
	Primary tumor		116	91%
		Parotid gland	112	
		Submandibular gland	1	
		Sublingual gland	1	
		Minor salivary gland	1	
	Recurrence		9	7%
	Metastatic lesion		3	2%
Pathologic features				
	Size, median (range) (cm)		2.3 (0.4–9)	
	Mitotic figures/10 HPF (2.4 mm^2)			
		0–4	87	68%
		≥ 5	41	32%
	HG and HGT		43	34%
	Necrosis		41	32%
	Architecture			
		Solid-microcystic	115	90%
		Cystic/cystopapillary	39	30%
		Cribriform	16	13%
		Follicular	3	2%
	Clear-cell change		33	26%
	Eosinophilic/oncocytoid cytoplasm		2	2%
Immunohistochemistry				
	DOG1		126	98%
	SOX10		127	99%
	NR4A3		105	82%
***NR4A3* break-apart by FISH**				
	Total		38/52 analyzable cases	73%
	NR4A3-immunopositive cases		36/44 analyzable cases	82%
	NR4A3-immunonegative cases		2/8 analyzable cases	25%

AciCC, acinic cell carcinoma; *FISH*, fluorescence in situ hybridization; *HG*, high-grade; *HGT*, high-grade transformation; *HPF*, high-power field

in the lung, pleura, and omentum, respectively, were sampled. Tumor size ranged from 4 to 90 mm (mean 26.1, median 23).

Histopathologic and molecular-genetic features

Various architectural patterns were seen on microscopic examination, with the solid-microcystic pattern (Fig. 1A) being most prevalent ($n = 115$), commonly accompanied by abundant lymphoid stroma surrounding the neoplastic cell nests. Solid growth was present in 4% of low-grade AciCC cases ($n = 3$), while all cases with high-grade features contained at least minor parts with solid growth pattern. Occasionally, cystic or cystopapillary growth patterns were present ($n = 39$), often associated with intratumoral hemorrhage, with erythrocytes located in the lumina (Fig. 1B). Cribriform and follicular areas were revealed in 16 and 3 cases, respectively. Clear-cell change was frequent in both grade groups ($n = 33$), while oncocytoid or eosinophilic cytoplasm was observed in 2 cases with HGT. A collision with Warthin tumor was seen in 1 case of a parotid lesion of an 83-year-old female.

The high-grade cases and the high-grade areas in cases with HGT displayed moderate to high-grade cytologic atypia with larger round to oval, often vesicular nuclei, and well-visible nucleoli. The mitotic activity was moderate to high, reaching up to 69 mitotic figures/10 HPF (2.4 mm^2). In addition, necrotic areas were revealed in 95% of these cases ($n = 41$), usually in the form of comedo-type necrosis (Fig. 1C-D). In some cases, larger areas of geographic necrosis were revealed. Conversely, no necrotic foci were present and no more than 4 mitotic figures/10 HPF (2.4 mm^2) were counted in the low-grade cases.

One case with HGT revealed further sarcomatoid dedifferentiation. The tumor, arising in the parotid gland of a 78-year-old male, contained three components: a small typical low-grade solid-microcystic components, larger sarcomatoid component consisting of pleomorphic spindled cells growing in short fascicular and vaguely storiform patterns on the background of hyalinized fibrous stroma, and a tubular to cribriform adenocarcinoma-like component with high-grade nuclear atypia growing in nests inside the sarcomatoid area. The mitotic activity was similar in both the tubular and sarcomatoid regions, reaching 14 and 11 mitotic figures/10 HPF (2.4 mm^2), respectively, while no mitosis was revealed in the low-grade area. Small necrotic foci were present in the tubular component. On immunohistochemical examination, both the low-grade and the tubular-to-cribriform component were positive for NR4A3 but the sarcomatoid component was negative. FISH examination of an NR4A3 rearrangement was negative in all parts of the analyzed slide.

DOG1 immunomarker was positive in 126/128 (98%) cases (Fig. 2A), while SOX10 displayed nuclear positivity in 127/128 (99%) cases (Fig. 2B). NR4A3 was at least focally positive in 105/128 (82%) cases (Fig. 2C-D). A similar proportion (82% vs. 81% vs. 86%) of NR4A3-positive cases were revealed in the low-grade, HGT, and high-grade groups of AciCC.

Out of the 23 cases that were immunohistochemically negative for NR4A3 (Fig. 2E), all were positive for both DOG1 and SOX10. All NR4A3-negative and 33 NR4A3-positive cases were subsequently stained for NR4A2 ($n = 56$). Six of the NR4A3-immunonegative cases displayed unequivocal nuclear immunopositivity with the NR4A2 antibody (Fig. 2F), while all the 33 NR4A3-immunopositive cases tested negative for NR4A2 on immunohistochemistry (Table 3).

Fig. 1 Histomorphologic features of AciCC. **A** Neoplastic acinic cells with zymogen granules organized in a solid-microcystic pattern were the most common finding (case LG9). **B** Cystic-hemorrhagic pattern in low-grade AciCC (case LG15). **C** Clear cell change and necrotic foci in a case with HGT (case HGT9). **D** High-grade area with foci of comedonecrosis and high mitotic activity (case HGT3)
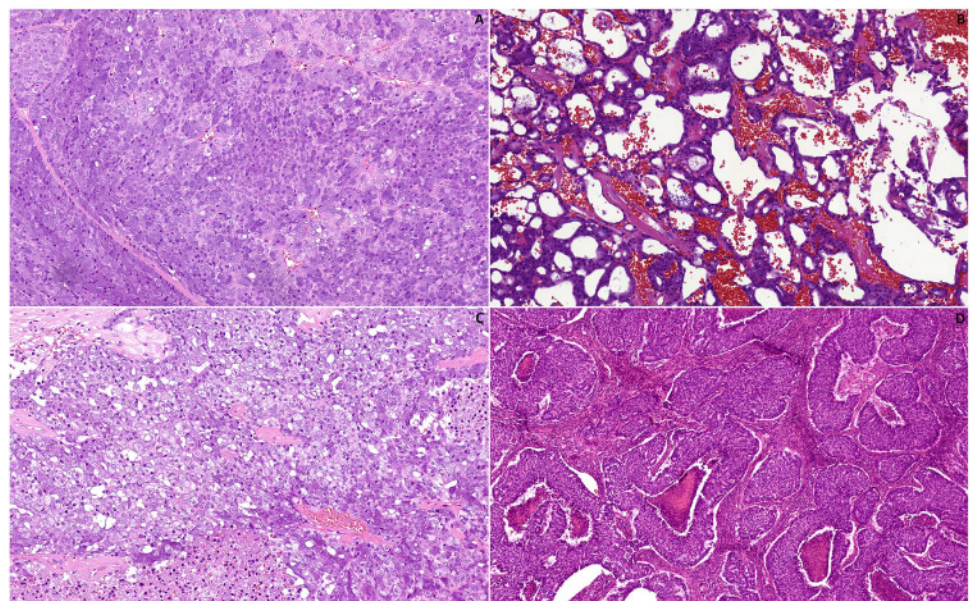
Fig. 2 Immunohistochemical findings Immunohistochemical staining for DOG1 (**A**) and SOX10 (**B**) was positive in 126/128 (98%) and 127/128 (99%) cases, respectively (case LG15). NR4A3 immunostaining revealed strong (**C**) (case LG10) to moderate (**D**) (case HGT9) nuclear positivity in 105/128 (82%) cases. Twenty-four cases did not stain for NR4A3 (**E**) (case LG13), six of which showed strong nuclear immunopositivity for NR4A2 (**F**) (case HGT23)
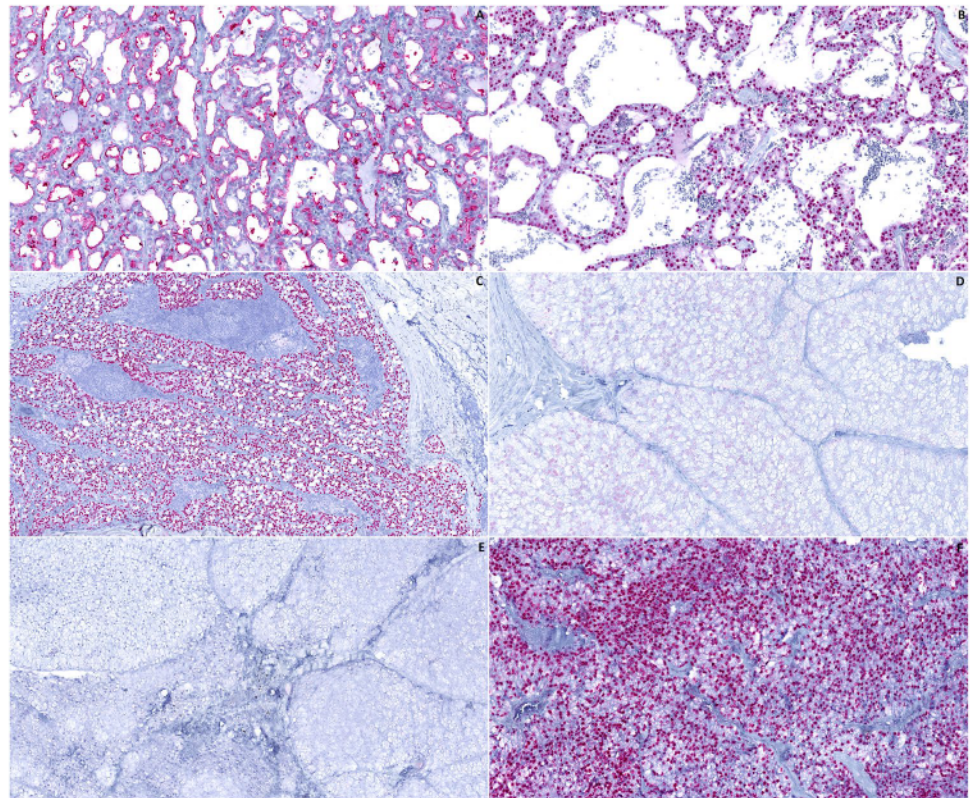
The *NR4A3* rearrangement was analyzed by FISH in 57 cases. Firstly, 47 NR4A3-immunopositive cases were tested. The rearrangement was verified in 23/28 (82%) low-grade AciCC cases, 11/14 (79%) cases with HGT, and 2/2 (100%) high-grade AciCC cases. In total, *NR4A3* rearrangement was confirmed by FISH in 36/44 (82%) NR4A3-immunopositive analyzable cases, while 8/44 (18%) cases were negative for the aberration. Secondly, 10 NR4A3-immunonegative cases were assessed, with 6/8 (75%) analyzable cases being negative on the FISH examination and 2/8 (25%) cases displaying a positive *NR4A3* split signal. Out of the whole cohort, 5 cases were not able to be analyzed by FISH.

Finally, we assessed the presence of a rearrangement involving *NR4A2* using a custom FISH break-apart probe (Table 3). In total, 9 cases were tested, including the 6 NR4A2-immunopositive cases and 3 cases that were negative for both NR4A2 and NR4A3 by immunohistochemistry. The *NR4A2* break-apart was confirmed in 2/8 (25%) analyzable cases, while 6/8 (75%) analyzable cases were negative and 1 case was not analyzable. Both cases with the *NR4A2* rearrangement confirmed by FISH were also positive for the NR4A2 immunohistochemical marker (Fig. 3B-C). The first case that harbored the break was an unusual low-grade AciCC affecting the parotid gland of a 19-year-old male. It displayed a solid-trabecular growth of uniform neoplastic cells with abundant eosinophilic and occasionally clear cytoplasm and was therefore originally diagnosed as oncocytoma

(Fig. 3A). FISH analysis of an *NR4A3* break-apart was negative in this case. The second case was a tumor with HGT occurring in a 61-year-old male. The low-grade areas with solid-microcystic architecture gradually devolved into high-grade solid tumor displaying a conspicuous cytoplasmic clearing, nuclear atypia, and central necrosis. The *NR4A3* rearrangement was not analyzable by FISH.

Overall, 17 cases were immunohistochemically negative for both NR4A3 and NR4A2 markers. Four of these were able to be tested for the NR4A3 rearrangement by FISH, and the break was confirmed in 2/4 (50%) cases. The NR4A2 break-apart was further analyzed by FISH in 3 of these cases, with a negative result in all of them.

Table 3 NR4A2 immunohistochemistry and FISH analysis in acinic cell carcinoma

	Number of positive cases	Number of analyzed cases
NR4A2 immunohistochemistry		
Total	6	56
NR4A3-immunonegative cases	6	23
NR4A3-immunopositive cases	0	33
NR4A2 break-apart by FISH	2	8

Fig. 3 *NR4A2*-rearranged case of AciCC (caseLG42). **A** The low-grade tumor was composed of uniform cells with eosinophilic cytoplasm organized in a solid-trabecular pattern. **B** Diffuse nuclear NR4A2 immunostaining. **C** FISH analysis utilizing a *NR4A2* break-apart probe was clearly positive
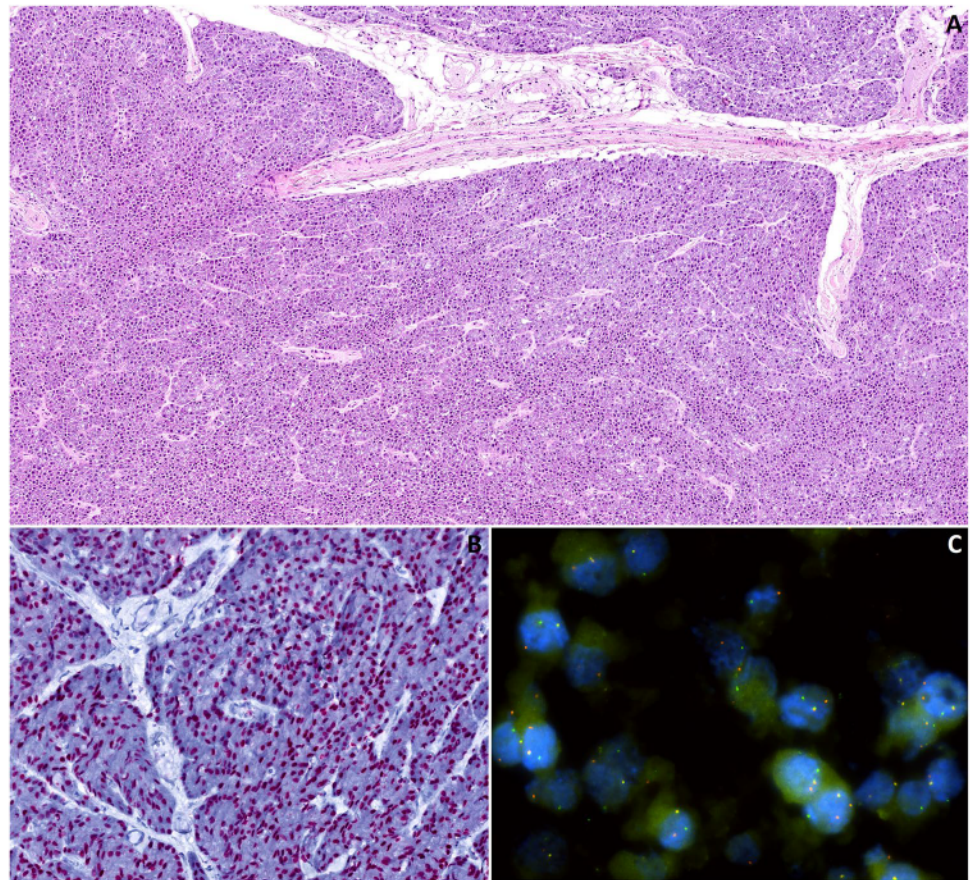
Discussion

In this study, we present an extensive analysis of the immunohistochemical and molecular genetic features of AciCC, a common malignant salivary gland tumor driven in most cases by t(4;9)(q13;q31) leading to upregulation of the *NR4A3* gene. NR4A3 immunostain is a powerful tool in differential diagnostics in AciCC cases. As much as 82% of cases were positive for NR4A3 in our series. However, previous reports documented an even higher proportion (up to 98%) of AciCC cases to be immunopositive for NR4A3 with a homogenous diffuse nuclear pattern [7, 9]. The discordance was likely caused by the inclusion of archival, sub-optimally fixed samples, which were slightly more prevalent in the low-grade cohort. The NR4A3 antigenicity was probably limited or completely lost in such cases, and the NR4A3 immunohistochemistry was apparently highly sensitive to sub-optimal processing in our laboratory. Although FISH analysis of the *NR4A3* rearrangement might be informative in some of these troublesome cases, a negative result of the molecular-genetic examination does not necessarily exclude the possibility of the t(4;9)(q13;q31) being present. As indicated by Haller et al. [7], some cases with chromosomal breakpoints of chromosome 9 located higher upstream from the *NR4A3* gene might show apparently normal, non-translocated fluorescence signals. Other methods might thereafter be employed to reveal the *NR4A3* overexpression (qRT-PCR) and the exact location of the chromosome breaks involved in the rearrangement, especially in rare cases with unusual morphology that might render the diagnostic process exceptionally difficult. Notably, since the mechanism of oncogenesis in acinic cell carcinoma is enhancer hijacking which upregulates *NR4A3*, and not a gene fusion that would code for an active fusion oncoprotein, no fusion transcript is detectable by RT-PCR or RNA-sequencing.

Importantly, both low-grade and high-grade (including cases with HGT) cases were able to be stained with the NR4A3 antibody. In cases with HGT, nuclear positivity for NR4A3 was observed in both low-grade and transformed areas. NR4A3 immunostaining might therefore be utilized in challenging cases, i.e., small samples containing poorly differentiated high-grade areas only, fine-needle aspiration cytology specimens [11, 12], tumors with unusual morphology etc.

In addition, AciCC might sporadically be driven by overexpression of *NR4A3* paralog *NR4A2*. Both genes code for proteins belonging to the steroid-thyroid hormone retinoid receptor family that act as transcription factors when activated by their respective ligands. The carcinogenetic process in tumors with the *NR4A2* rearrangement is therefore likely analogous to the enhancer hijacking described in *NR4A3*-rearranged acinic cell carcinomas. While *NR4A3*

locates to 9q31, *NR4A2* is found at 2q24. In this study, 6 NR4A3-immunonegative cases displayed a strong nuclear positivity with the NR4A2 antibody. NR4A2 immunoexpression was shown to correlate with *NR4A2* upregulation in AciCC in a recent study [8]. This is the first report of a rearrangement involving *NR4A2* being confirmed by FISH in 2 cases of AciCC. Interestingly, both cases displayed unusual morphologic features, with the first low-grade tumor resembling oncocytoma and the second tumor containing abundant clear-cell areas. Solid growth pattern was observed in both cases, similarly to the case reported by Haller et al. [8]. Further studies might contribute further evidence to clarify whether the *NR4A2* rearrangement occurs more frequently in AciCC cases with less usual morphology.

Lastly, a small cohort of our cases was negative for both NR4A2 and NR4A3 immunomarkers. FISH analysis of the *NR4A3* rearrangement proved more sensitive in two of these double-immunonegative cases, and they were finally classified as acinic cell carcinoma with an *NR4A3* rearrangement. However, rearrangements of *NR4A2* nor *NR4A3* were not detected by FISH in some of these double-immunonegative cases. Members of this group may represent cases where both detection methods used in this study failed, and the tumors in fact harbor *NR4A2* or *NR4A3* rearrangements. Some cases may nonetheless belong to a very minor group of AciCC cases whose pathogenesis is based on a different genetic aberration, whether it is, for example, the rearrangement of other genes from the nuclear receptor subfamily 4A, or another alteration of a completely unrelated gene.

In summary, we present a first report of an *NR4A2* rearrangement in a subset of acinic cell carcinoma cases. This genetic aberration was present in cases that were negative for the NR4A3 marker and positive for the NR4A2 marker on immunohistochemical examination. *NR4A2* and *NR4A3* code for highly similar, paralogous proteins; we therefore propose a similar pathogenetic process being involved in acinic cell carcinomas with the *NR4A2* rearrangement that has been proposed previously in tumors with the *NR4A3* break-apart. NR4A2 and NR4A3 are reliable immunohistochemical markers for acinic cell carcinoma whose importance is highlighted especially in challenging, less typical cases.

Declarations

Conflict of interest The authors declare no competing interests.

Informed consent Informed consent was not required for the study.

References

1. WHO classification of tumours editorial board (2022) Head and neck tumours, 5th edn. IARC Press, Lyon, France
2. Patel NR, Sanghvi S, Khan MN, Husain Q, Baredes S, Eloy JA (2014) Demographic trends and disease-specific survival in salivary acinic cell carcinoma: an analysis of 1129 cases. Laryngoscope 124(1):172–178
3. Xu B, Saliba M, Ho A, Viswanathan K, Alzumaili B, Dogan S, Ghossein R, Katabi N (2022) Head and Neck Acinic Cell Carcinoma: A New Grading System Proposal and Diagnostic Utility of NR4A3 Immunohistochemistry. Am J Surg Pathol 46(7):933–941
4. Thompson LD, Aslam MN, Stall JN, Udager AM, Chiosea S, McHugh JB (2016) Clinicopathologic and immunophenotypic characterization of 25 cases of acinic cell carcinoma with high-grade transformation. Head Neck Pathol 10(2):152–160
5. Skálová A, Sima R, Vanecek T et al (2009) Acinic cell carcinoma with high-grade transformation: a report of 9 cases with immunohistochemical study and analysis of TP53 and HER-2/neu genes. Am J Surg Pathol 33(8):1137–1145
6. Haller F, Bieg M, Will R et al (2019) Enhancer hijacking activates oncogenic transcription factor NR4A3 in acinic cell carcinomas of the salivary glands. Nat Commun 10(1):368
7. Haller F, Skálová A, Ihrler S et al (2019) Nuclear NR4A3 immunostaining is a specific and sensitive novel marker for acinic cell carcinoma of the salivary glands. Am J Surg Pathol 43(9):1264–1272
8. Haller F, Moskalev EA, Kuck S et al (2020) Nuclear NR4A2 (Nurr1) immunostaining is a novel marker for acinic cell carcinoma of the salivary glands lacking the classic NR4A3 (NOR-1) upregulation. Am J Surg Pathol 44(9):1290–1292
9. Wong KS, Mariño-Enriquez A, Hornick JL, Jo VY (2021) NR4A3 Immunohistochemistry reliably discriminates acinic cell carcinoma from mimics. Head Neck Pathol 15(2):425–432
10. Šteiner P, Andreasen S, Grossmann P et al (2018) Prognostic significance of 1p36 locus deletion in adenoid cystic carcinoma of the salivary glands. Virchows Arch 473(4):471–480
11. Millan N, Tjendra Y, Zuo Y, Jorda M, Garcia-Buitrago M, Velez-Torres JM, Gomez-Fernandez C (2022) Utility of NR4A3 on FNA cytology smears and liquid-based preparations of salivary gland. Cancer Cytopathol. https://doi.org/10.1002/cncy.22632. Online ahead of print.
12. Skaugen JM, Seethala RR, Chiosea SI, Landau MS (2021) Evaluation of NR4A3 immunohistochemistry (IHC) and fluorescence in situ hybridization and comparison with DOG1 IHC for FNA diagnosis of acinic cell carcinoma. Cancer Cytopathol 129(2):104–113

🖄 Springer

4.2   Sclerosing polycystic adenoma of salivary glands: A novel neoplasm characterized by PI3K-AKT pathway alterations – New insights into a challenging entity

Indexovým případem v této studii byl tumor 62letého muže léčeného inhibitory imunitních checkpointů pro dříve potvrzený metastazující světlobuněčný karcinom ledviny, nyní rovněž léčeného pro 9 měsíců trvající rezistenci v oblasti levostranné příušní žlázy. Tumor byl exstirpován a hodnocen jako apokrinní intraduktální karcinom dosahující do resekčních okrajů, proto byla následně provedena radikální parotidektomie a disekce krčních lymfatických uzlin. V resekátu byla prokázána léze složená ze tří komponent – konvenčního SPA, reziduálních struktur intraduktálního karcinomu se solidní, kribriformní a mikropapilární intraluminální proliferací mírně atypických buněk s apokrinní morfologií a fokusu invazivního salivárního duktálního karcinomu tvořeného nádorovými buňkami s high-grade atypiemi. Buňky intraduktálního karcinomu i salivárního duktálního karcinomu byly imunohistochemicky pozitivní v průkazu androgenních receptorů. Po operačním výkonu byl pacient při poslední kontrole 8 měsíců bez známek rekurence salivárního tumoru.

Ve studii bylo shromážděno a hodnoceno celkem 36 případů SPA, všechny vyrůstaly v oblasti parotis. Více než 2/3 pacientů byly ženy, věkové rozmezí bylo široké, a to od 11 do 79 let. V 5 případech byla zaznamenána rekurence nádoru, přičemž v jednom z těchto případů se jednalo o dvojnásobnou rekurenci, v dalším případě o rekurenci trojnásobnou, vyžadující nakonec provedení radikální parotidektomie s adjuvantní radioterapií. Ve všech případech byly histologicky potvrzeny typické znaky SPA (1.1.2) včetně cytomorfologické variability luminálních duktálních buněk (pěnitá, vakuolizovaná či vodojasná cytoplazma, onkocytická, dlaždicobuněčná a apokrinní metaplázie, hlenotvorba).

Ve všech případech byla přítomna méně nebo více abundantní ložiska intraluminální epiteliální proliferace s kribriformní, solidní či mikropapilární architekturou. V 35 případech měla tato ložiska charakter léze z buněk vmezeřených duktů, s imunohistochemickou pozitivitou S100 a SOX10. V 18 případech byla navíc přítomna i ložiska intraluminální proliferace druhého typu, tvořená buňkami apokrinního vzhledu, imunohistochemicky pozitivními v průkazu AR a negativními v průkazu markerů S100 a SOX10. V 17 případech navíc tyto intraluminální proliferace, ať už prvního nebo druhého typu, vykazovaly mírný až vysoký stupeň jaderných atypií, ložiskově pak nabývaly až vzhledu intraduktálního karcinomu. Invazivní high-grade salivární duktální karcinom byl přítomen v již popsaném indexovém případu.

U 11 případů byl dostupný materiál pro DNA-seq a RNA-seq. V 9 z těchto případů byly detekovány rekurentní, převážně bodové mutace v genech kódující proteiny signální dráhy PI3K, čímž byla potvrzena nádorová povaha léze. Mutace *PIK3CA* byly přítomny u 5 případů, somatická i germinální mutace *PTEN* pak u jednoho z těchto případů. Dva případy obsahovaly mutace genu *AKT1*, v jednom z nich byla dále prokázána mutace genu *HRAS*. Ta byla přítomna celkem u 4 případů.

Zatímco mutace *PIK3CA* byly prokázány u případů, které vykazovaly intraluminální proliferaci z buněk vmezeřených duktů, mutace *HRAS* byly ve všech 4 případech asociovány s apokrinní intraluminální proliferací. V indexovém případu byla

prokázána mutace *PIK3CA* v komponentách SPA i intraduktálního a salivárního duktálního karcinomu (tedy v komponentách s rysy jak vmezeřených duktů, tak apokrinními), zatímco mutace *HRAS* byla prokázána jen v komponentě apokrinního intraduktálního a salivárního duktálního karcinomu.

Sclerosing Polycystic Adenoma of Salivary Glands

A Novel Neoplasm Characterized by PI3K-AKT Pathway Alterations—New Insights Into a Challenging Entity

Alena Skálová, MD, PhD,*† Martina Baněčková, MD, PhD,*† Jan Laco, MD, PhD,‡
Silvana Di Palma, MD,§ Abbas Agaimy, MD,‖ Nikola Ptáková, MSc,¶
Valérie Costes-Martineau, MD, PhD,# Bengt F. Petersson, MD, PhD,**
Mari F.C.M. van den Hout, MD, PhD,†† Gisele de Rezende, MD,‡‡ Natálie Klubíčková, MD,*†
Miroslav Koblížek, MD,§§ Olena Koshyk, MD,‖‖ Tomáš Vaneček, PhD,¶
and Ilmo Leivo, MD, PhD¶¶

Abstract: Sclerosing polycystic adenoma (SPA) is a rare salivary gland neoplasm originally thought to represent a non-neoplastic lesion. Recently we have encountered an index case of apocrine intraductal carcinoma of parotid gland of 62-year-old man with invasive salivary duct carcinoma component arising from SPA, a combination of tumor entities that has never been published so far. Here, we further explore the nature of SPA by evaluating 36 cases that were identified from the authors' consultation files. The patients were 25 females and 11 males aged 11 to 79 years (mean, 47.8 y). All tumors originated from the parotid gland. Their size ranged from 11 to 70 mm (mean, 28 mm). Histologically, all cases revealed characteristic features of SPA, such as lobulated well-circumscribed growth, focal hyalinized sclerosis, presence of large acinar cells with abundant brightly eosinophilic intracytoplasmic granules, and ductal components with variable cytomorphologic characteristics, including foamy, vacuolated, apocrine, mucous, clear/ballooned, squamous, columnar and oncocyte-like cells. In all cases, there were foci of intraluminal solid and cribriform intercalated duct-like epithelial proliferations with variable dysplasia which were positive for S100 protein and SOX10, and fully enveloped by an intact layer of myoepithelial cells. In addition, 14/36 cases (39%) had focal intraductal cribriform and micropapillary apocrine-type dysplastic epithelial structures composed of cells positive for androgen receptors and negative for S100/SOX10. The intraductal proliferations of both types showed focal mild to severe dysplasia in 17 cases (17/36; 47%). Two cases showed overt malignant morphology ranging from high-grade intraductal carcinoma to invasive carcinoma with an apocrine ductal phenotype. Next generation sequencing using ArcherDX panel targeting RNA of 36 pan-cancer-related genes and/or a TruSight Oncology 170/500 Kit targeting a selection of DNA from 523 genes and RNA from 55 genes was performed. Tumor tissue was available for molecular analysis in 11 cases, and 9 (9/11; 82%) of them harbored genetic alterations in the PI3K pathway. Targeted sequencing revealed *HRAS* mutations c.37G > C, p.(Gly13Arg) (2 cases) and c.182A > G, p.(Gln61Arg) (2 cases), and *PIK3CA* mutations c.3140A > G, p.(His1047Arg) (3 cases), c.1633G > A, p.(Glu545Lys) (1 case), and c.1624G > A, p.(Glu542Lys) (1 case). Moreover, mutations in *AKT1* c.49G > A, p.(Glu17Lys) and c.51dup, p.(Tyr18ValfsTer15); c.49_50delinsAG, p.(Glu17Arg) (as a double hit) were found (2 cases). In addition, germinal and somatic mutation of *PTEN* c.1003C > T, p.(Arg335Ter); c.445C > T, p.(Gln149Ter), respectively, were detected. Gene fusions were absent in all cases. These prevalent molecular alterations converging on one major cancer-related pathway support the notion that SPA is a true neoplasm with a significant potential to develop intraluminal epithelial proliferation with apocrine and/or intercalated duct-like phenotype. The name SPA more correctly reflects the true neoplastic nature of this enigmatic lesion.

Key Words: sclerosing polycystic adenoma, sclerosing polycystic adenosis, salivary gland neoplasm, parotid gland, *PIK3CA-AKT* pathway

(Am J Surg Pathol 2022;46:268–280)

From the *Department of Pathology, Charles University, Faculty of Medicine in Plzen; †Bioptic Laboratory Ltd; ¶Molecular and Genetic Laboratory, Bioptic Laboratory Ltd, Plzen; ‡The Fingerland Department of Pathology, Charles University, Faculty of Medicine and University Hospital Hradec Kralove, Hradec Králové; §§Department of Pathology and Molecular Medicine, 2nd Faculty of Medicine in Prague, Prague, Charles University and Motol University Hospital, Prague, Czech Republic; §Department of Histopathology, Division of Clinical Medicine, University of Surrey, Royal Surrey County Hospital, Guildford, Surrey, UK; ‖Institute of Pathology, University Hospital Erlangen, Friedrich-Alexander University Erlangen-Nürnberg (FAU), Comprehensive Cancer Center (CCC) Erlangen-EMN, Erlangen, Germany; #Department of Pathology, CHU Gui de Chauliac, Montpellier, France; **Department of Pathology, National University Health System, Singapore, Singapore; ††Department of Pathology, Research Institute GROW, Maastricht University Medical Center, Maastricht, The Netherlands; ‡‡Department of Anatomic Histopathology and Cytogenetics, Department of Laboratory Medicine, Niguarda Cancer Center, Milan, Italy; ‖‖Medical Laboratory CSD, Kyiv, Ukraine; and ¶¶Institute of Biomedicine, Pathology, University of Turku, and Turku University Hospital, Turku, Finland.

Correspondence: Alena Skálová, MD, PhD, Sikl's Department of Pathology, Faculty of Medicine in Pilsen, Charles University, E. Benese 13, 305 99 Pilsen, Czech Republic (e-mail: skalova@fnplzen.cz).

Sclerosing polycystic adenoma (SPA) previously known as sclerosing polycystic adenosis, is a rare salivary gland neoplasm that was first described in 1996 by Smith et al.[1] SPA reveals a characteristic combination of histologic features, some of which are reminiscent of histopathologic changes that occur in the mammary gland, such as fibrocystic disease/sclerosing adenosis and intraductal epithelial proliferations of various types.[2] In their initial description of SPA, Smith et al[1] hypothesized that SPA represented a nonneoplastic, reactive lesion analogous to fibrocystic disease of the breast. However, SPA frequently harbors intraluminal epithelial solid and papillary proliferations that have been described earlier as dysplasia ranging from mild to severe/carcinoma in situ.[3–8] In addition, a single study utilizing polymorphisms of the human androgen receptor (AR) on 6 cases of SPA reported X-chromosome inactivation in all informative cases suggesting that SPA is a clonal neoplastic process.[9] In a recent study, Bishop et al[10] reported recurrent *PTEN* mutation and *PI3K* pathway alteration in 4 cases of SPA. Report of *PTEN* mutation and *PI3K* pathway alteration in additional 2 cases, and an association with Cowden syndrome in 1 patient[11] represents further evidence to support that these lesions are neoplastic and more appropriately referred to as "sclerosing polycystic adenoma" (SPA). This name has been proposed earlier[12] and it is used in this manuscript.

Recently, we have encountered an index case of parotid gland tumor composed of apocrine intraductal carcinoma (IC) and invasive salivary duct carcinoma (SDC) arising from conventional SPA, a combination of tumor entities that has never been published so far. IC is the current designation used by the World Health Organization (WHO) Classification of Head and Neck Tumors for a rare salivary gland neoplasm[13] that has previously also been referred to as "low-grade (LG) SDC" and "LG cribriform cystadenocarcinoma."[14] IC is conceptually believed to be similar to ductal carcinoma in situ (DCIS) of the breast. Although IC is one entity in the current WHO Classification of Head and Neck Tumors,[13] recent studies have suggested that at least 3 subtypes exist: a LG intercalated duct cell (IDC)-like variant with frequent *RET* rearrangements,[15–17] a LG apocrine and mixed IC with frequent *TRIM27-RET* fusion,[16–18] and an apocrine and mixed IC with SDC-like genetics.[19] Like SPA, apocrine IC may harbor molecular alterations similar to high-grade (HG) SDC with frequent *HRAS* and PI3K pathway mutations.[19] SDC is a highly aggressive carcinoma that recapitulates invasive ductal breast cancer and it constitutes up to 10% of all salivary gland carcinomas.[20] SDC is characterized by heterogenous molecular abnormalities involving predominantly inactivation of tumor suppressor genes, such as *TP53*, *PTEN*, and activation of genes of the PI3K/AKT/mTOR pathway (such as *PIK3CA*, *HRAS*, and *AKT1*).[21–24] It has been suggested earlier that apocrine IC and SPA may be related entities.[19] Here, we present an index case of apocrine IC of parotid gland with transformation to SDC arising from SPA. To further explore the nature of SPA and to learn how SPA, apocrine IC and SDC are associated, we decided to study molecular, immunohistochemical and histologic features of 36 cases of SPA, the largest series in the literature so far.

MATERIALS AND METHODS

Case Selection

Recently the authors (J.L. and A.S.) encountered an index case of a parotid gland tumor in a 62-year-old male patient with a unique combination of 3 components, SPA, apocrine IC, and invasive HG SDC. A total of 36 cases of SPA were selected from the authors' consultation files. All cases were reviewed by the corresponding author (A.S.) and another head and neck pathologist (M.B.), and were confirmed to meet the diagnostic criteria of SPA as described previously,[1,3,4] and detailed in the 2017 WHO Classification of Head and Neck Tumors.[2] Thirty-six cases were identified that met these inclusion criteria. Three and 12 of these SPA cases were included in 2 previous studies, Skalova et al[3] and Skalova et al,[9] respectively.

All available H&E sections from each case were reviewed, and the histologic features, including intraductal epithelial cribriform and papillary apocrine proliferations and the spectrum of dysplastic changes were tabulated. Focal epithelial proliferations were classified into 2 categories according to their histomorphology and immunophenotype as IDC-type composed of S100 protein/SOX10 positive and AR negative epithelial cells, and apocrine type composed of AR positive and S100 protein/SOX10 negative cells. LG dysplasia was defined by mild (G1) or moderate (G2) nuclear features and by a solid/tubular growth pattern with mild irregularities in cell shape and by occasional back-to-back arrangements with intraluminal protrusions (Figs. 1A, B). HG dysplasia was defined by moderate (G2) and severe (G3) atypical nuclear features and by a complex growth pattern characterized by solid/cribriform and intraluminal protrusions of micropapillary structures and rigid bridging (Figs. 1C, D).

Where available, clinical follow-up was obtained from the patients, their physicians, or referring pathologists.

Histology and Immunohistochemistry

For conventional microscopy, the excised tissues were fixed in formalin, processed routinely, embedded in paraffin (formalin fixed paraffin embedded), cut, and stained with hematoxylin and eosin.

For immunohistochemistry, 4-µm-thick sections were cut from paraffin blocks and mounted on positively charged slides (TOMO, Matsunami Glass IND, Osaka, Japan). Sections were processed on a BenchMark ULTRA (Ventana Medical Systems, Tucson, AZ), deparaffinized and subjected to heat-induced epitope retrieval by immersion in a CC1 solution (pH 8.6) at 95°C and for NOR1 antibody in a CC2 solution (pH 6.0) at 92°C. All primary antibodies used in this study are summarized in Table 1.

Visualization was performed using the ultraView Universal DAB Detection Kit (Roche, Tucson, AZ) and ultraView Universal Alkaline Phosphatase Red Detection Kit (Roche). The slides were counterstained with Mayer hematoxylin. Appropriate positive and negative controls were employed.
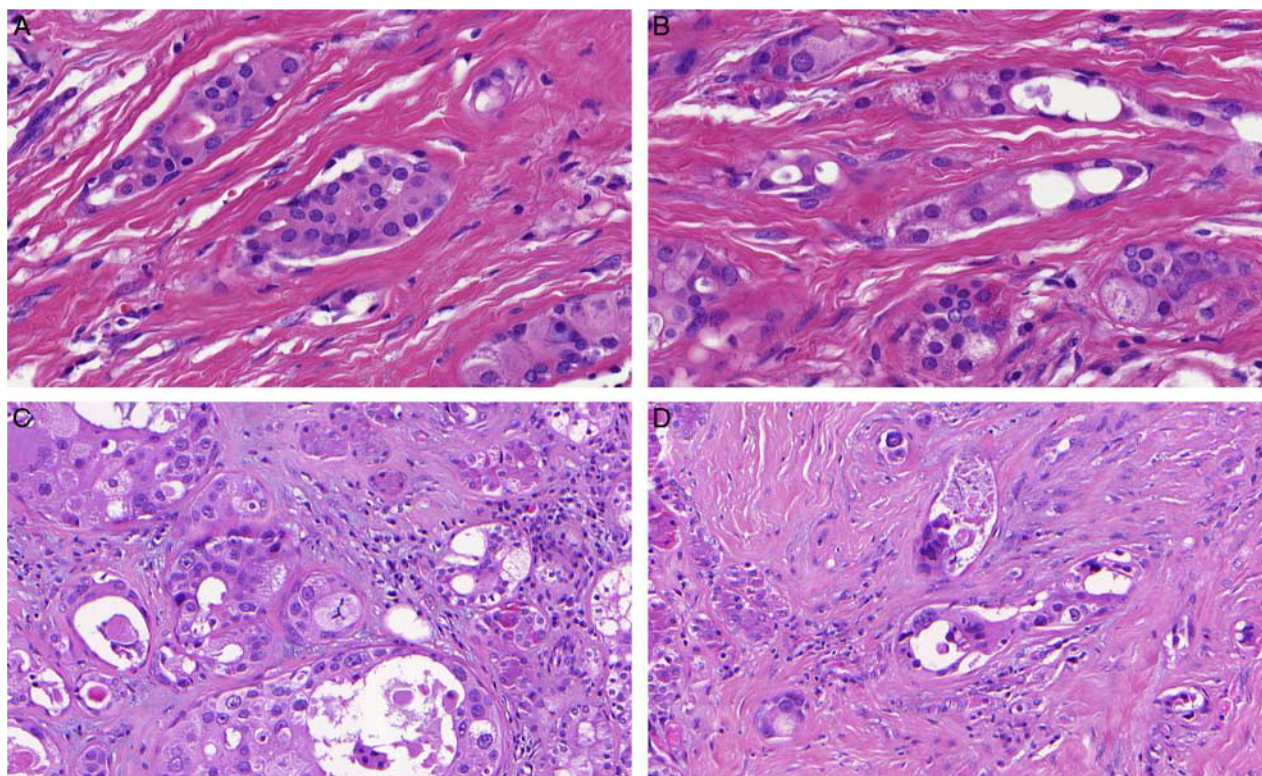
29

FIGURE 1. LG dysplasia was defined by mild (G1) or moderate (G2) nuclear features and by a solid/tubular growth pattern with mild irregularities in cell shape and by occasional back-to-back arrangements with intraluminal protrusions (A, B). HG dysplasia was defined by moderate (G2) and severe (G3) atypical nuclear features and by a complex growth pattern characterized by solid/cribriform and intraluminal protrusions of micropapillary structures and rigid bridging (C, D).

Molecular Studies: Next Generation Sequencing and Fluorescence in Situ Hybridization (FISH) Testing

Sample Preparation for Next Generation Sequencing

Two to 3 formalin fixed paraffin embedded sections (10 μm thick) were macrodissected to isolate tumor rich regions. Samples were extracted for total nucleic acid using Agencourt FormaPure Kit (Beckman Coulter, Brea, CA). Integrity of RNA was evaluated using PreSeq RNA QC Assay as previously described.[25]

Next Generation Sequencing and Analysis

Comprehensive Thyroid and Lung Kit

FusionPlex Comprehensive Thyroid and Lung Kit (ArcherDX Inc., Boulder, CO) was used to construct cDNA library for the detection of fusion transcripts and hotspot mutations in 36 genes. All steps were performed according to the manufacturer's protocol (version of the protocol LA135.G), and the library was sequenced on an Illumina platform as described previously.[25] Fusion and mutation detection was performed using the Archer Analysis software (v6.2; ArcherDX Inc.). Fusion parameters were set to a minimum of 5 valid fusion reads with a minimum of 3 unique start sites within the valid fusion reads.

TruSight Oncology 500 and 170 Kits

A DNA library was prepared using the TruSight Oncology 170/500 Kit (Illumina), targeting a selection of DNA from 523 genes of interest, and RNA from 55 genes, according to the manufacturer's protocol, except for the enzymatic fragmentation of DNA using KAPA FragKit (KAPA Biosystems, Washington, MA). Sequencing was performed on the NextSeq. 550 sequencer (Illumina) following the manufacturer's recommendations. Data analysis (DNA variant filtering and annotation) was performed using the Omnomics next generation sequencing (NGS) analysis software (Euformatics, Finland). Custom variant filter was set up including only nonsynonymous variants with coding consequences, read depth greater than 50, and benign variants according to the ClinVar database[26] were excluded. The remaining subset of variants was checked visually, and suspected artefactual variants were excluded.

Detection of PLAG1 Break by FISH

Briefly, a 4 μm thick section on a positively charged slide was routinely deparaffinized, incubated in the 1× Target Retrieval Solution Citrate pH 6 (Dako, Glostrup, Denmark) for 40 minutes at 95°C and digested in protease solution with Pepsin (0.5 mg/mL) (Sigma Aldrich, St. Louis, MO) in 0.01 M HCl at 37°C for 30 minutes. The slide was then dehydrated in a series of ethanol solutions (70%, 85%, 96%). Probe Sure FISH 8q12.1 PLAG1 Break

TABLE 1. Antibodies Used for The Immunohistochemical Study

Antibody	Clone	Dilution	Antigen Retrieval/Time	Source
p63	DAK-p63	RTU	EnVision low pH/30 min	Dako
AE1-AE3	AE1/AE3	RTU	EnVision high pH/30 min	Dako
CK7	OV-TL 12/30	RTU	EnVision high pH/30 min	Dako
Calponin	EP798Y	RTU	CC1/36 min	Ventana
S100 protein	Polyclonal	RTU	EnVision high pH/30 min	Dako
Mammaglobin	304-1A5	RTU	EnVision high pH/30 min	Dako
SOX10	SP267	RTU	CC1/64 min	Cell Marque
DOG1	SP31	RTU	CC1/36 min	Cell Marque
NOR-1	H-7	1:50	CC2/68 min	Ventana
PLAG1	3B7	1:100	CC1/64 min	Sigma Aldrich
AR	SP107	RTU	CC1/64 min	Cell Marque
Ki-67	MIB1	RTU	EnVision high pH/30 min	Dako
GATA3	L50-823	1:200	CC1/52 min	BioCareMedical

CC1 indicates EDTA buffer, pH 8.6, 95°C; CC2, citrate buffer, pH 6.0, 92°C; EnVision High pH, pH 9,0, 97°C; EnVision low pH, pH 6.0, 97°C; RTU, ready to use.

Apart Probe Kit (Agilent Technologies, Santa Clara, CA) was used for the detection of *PLAG1* rearrangement and was mixed of both probes (each color was delivered in a separated well), deionized water and LSI/WCP (Locus-Specific Identifier/Whole Chromosome Painting) hybridization buffer (Vysis/Abbott Molecular Diagnostics, Des Plaines, IL) in a 1:1:1:7 ratio, respectively. The slide with the applied probe was incubated in the ThermoBrite instrument (StatSpin/Iris Sample Processing, Westwood, MA) with codenaturation parameters at 85°C for 8 minutes and hybridization parameters at 37°C for 16 hours. After hybridization the slide was washed in a post-hybridization wash solution (2×SSC/0.3% NP-40) at 72°C for 2 minutes, air-dried in the dark, counterstained with 4′,6-diamidino-2-phenylindole DAPI (Vysis) and examined immediately.

The section was examined with an Olympus BX51 fluorescence microscope (Olympus Corporation, Tokyo, Japan) using a ×100 objective and filter sets Triple Band Pass (DAPI/SpectrumGreen/SpectrumOrange), Dual Band Pass (SpectrumGreen/SpectrumOrange) and Single Band Pass (SpectrumGreen and SpectrumOrange). One hundred randomly selected nonoverlapping tumor cell nuclei were examined for the presence of yellow (normal) or green and orange (chromosomal breakpoint) fluorescent signals. Cutoff value was set to >10% of nuclei with chromosomal breakpoint signals (mean+3 SD in normal non-neoplastic control tissues).

RESULTS

Demographic and Clinical Features

The clinicopathologic data for the 36 identified SPA cases are summarized in Table 2. The patients were 25 females and 11 males aged 11 to 79 years with a mean of 47.8 years. All tumors originated in the parotid gland. Tumor size ranged from 11 to 70 mm (mean 28 mm). Follow-up was available for 33 patients (33/36; 92%), however, patient information was lost in the cohorts (14/36; 39%) published earlier (Table 2). Complete follow-up information was available for a total of 19 cases (19/26; 53%) (range, 2 mo to 15 y; mean 42.7 mo).

Clinically, the tumors manifested as slowly growing and well-circumscribed, palpable masses with a duration of a few months to 10 years. Tenderness or intermittent pain was recorded in 3 patients.

Treatment was complete excision in all cases, performed with different surgical modalities (Table 2).

Five cases (5/36;14%) have recurred with a mean period before the first recurrence of 38 months. In 2 patients, there were multiple recurrences; in case 9, SPA recurred twice, at 6 and 13 years, and in case 19, SPA recurred 3 times at 6 and 18 months and at 13 years. The latter patient, at the age of 32, was treated by extended radical parotidectomy followed by radiotherapy. At follow-up of 13 years after the latest surgery, she was without evidence of disease, and was then lost to follow-up.

Two patients suffered from prior malignancy. In case 28, a 65-year-old female patient had a history of bone marrow transplantation for Hodgkin lymphoma 19 years before diagnosis of SPA. In case 32 (index case), a 62-year-old male patient who quit smoking 2 years before presented with a history of clear cell renal cell carcinoma. The kidney tumor was treated by left-sided nephrectomy. Ten months after surgery, the patient developed lung and liver metastases, and he was treated with PD-L1 immune checkpoint inhibitors. Four years after the kidney surgery, the patient presented with a slowly growing painless mass in the left parotideo-masseteric area of 9 months duration. On palpation, a mildly tender swelling was covered by skin with a violet discoloration. No symptoms of facial nerve paresis were observed. A tumor of the left parotid gland, 25 mm in diameter, was extirpated and a diagnosis of apocrine IC with a positive margin was rendered. Radical parotidectomy and lymph node dissection was performed, followed by radiotherapy. There was a well-circumscribed focus of SPA, measuring 21×20×12 mm, that extended into the resection margin. The parotidectomy specimen also included a small benign lymphoepithelial cyst, and residual structures of the apocrine IC with a focal invasive component of SDC close to the surgical margin (tumor-free resection margin was 0.6 mm). Perineural or lymphovascular invasions were not observed. The removed lymph nodes were negative (0/23). The patient is alive without evidence of any neoplastic disease 8 months after his latest surgery.

TABLE 2. Clinicopathologic Features of Current and Previously Reported SPAs

Case No.	Age/ Sex	Size (mm)	Presentation	IDC-like Proliferation (%)/Nuclear Grade	Apocrine Proliferation (%)/Nuclear Grade	Outcome (Follow-up) (mo, y)	Previously Published
1	27/female	45	Slowly growing painless mass	5	0	NED at 4 y, LOF	Skálová et al[3] case 2 Skálová et al[9] case 7
2	31/female	16	Slowly growing tender mass, 2 y	20	30/G3	NED at 3 y, LOF	Skálová et al[3] case 1 Skálová et al[9] case 8
3	35/female	22	Painless mass	5	0	NA	Skálová et al[9] case 1
4	24/female	25	Parotid mass suggestive of malignancy	5	5	NED at 2 y, LOF	Skálová et al[9] case 2
5	64/female	43	Parotid mass suggestive of malignancy	10	0	NA	Skálová et al[9] case 3
6	72/male	30	Parotid mass	40	0	NED at 3 y, LOF	Skálová et al[9] case 4
7	35/male	35	Slowly growing mass			NED at 3 y, LOF	Skálová et al[9] case 5
8	46/female	32	Firm circumscribed mass	<5	50/G3	NED at 5 y, LOF	Skálová et al[9] case 6
9	35/female	50	Mass for 18 mo, sometimes painful	<5	20	2 RE—at 6 y and at 13 y, LOF	Skálová et al[3] case 3 Skálová et al[9] case 9
10	33/female	20	Swelling of parotid gland, 2 mo	30	0	NED 2 y, LOF	Skálová et al[9] case 10
11	51/female	30	Parotid mass, features suggestive of neoplasm by FNA	<5	0	NED at 7 y, LOF	Skálová et al[9] case 11
12	58/male	15	Parotid mass	10	0	NED at 2 y, LOF	Skálová et al[9] case 12
13	60/female	18	Solid well-circumscribed mass of parotid with mucinous cysts	20	<5	NA	
14	26/female	48	Multinodular parotid mass with multiple satellite nodules	5	0	RE at 5 y; NED at 14 y	
15	57/male	30	Long lasting painless firm nodule of parotid removed by enucleation	20	0	NED at 13 y	
16	NA/male	NA	Multinodular well-defined nodule in parotid	30	5	NED at 15 y	
17	47/female	40	Slowly growing mass, 2 y	20/G2	20/G2	RE at 2 y, removed by conservative PE, NED at 15 y	
18	45/female	14	Well-demarcated solid nodule in parotid, removed by SPE	10/G3	10/G3	NED at 14 mo, LOF	
19	32/female	12	1st recurrence—diagnosed as PA 2nd—recurrence—conservative PE 3rd recurrence—extended RPE and RT	20/G2	0	3 RE—at 6 mo, 18 mo and 10 y NED at 13 y	Manojlović et al[6] case 1
20	33/female	40	8 y slowly growing mass suggestive of benign tumor; SPE	10	0	NED at 4 y, LOF	Manojlović et al[6] case 2
21	42/female	70	10 y slowly growing mass	30/G1	0	NED at 7 y	
22	71/male	30	Solitary nodule of hard consistency, 1 y	20	0	NED at 7 y	
23	69/female	22	2 y growing tough movable mass	20	15	NED at 6 y	
24	25/male	NA	5 y tough resistance	10	0	NED at 6 y	
25	36/female	NA	Solitary nodule of hard consistency	10/G1	0	NED at 5 y	
26	11/female	40	Slowly growing left-sided neck mass removed by SPE	20	0	NED at 10 mo; LOF	
27	51/female	22	6 mo swelling, feeling of pressure and intermittent pain below right ear	10	30/G3	NED 31 mo	
28	65/female	25	Slowly growing painless mass; SPE History of Hodgkin lymphoma 19 y ago	20/G2	0	NED at 3 y	
29	66/male	20	Palpable mass growing slowly for several months	0	30/G2	NED at 18 mo	

32

TABLE 2. (*continued*)

Case No.	Age/ Sex	Size (mm)	Presentation	IDC-like Proliferation (%)/Nuclear Grade	Apocrine Proliferation (%)/Nuclear Grade	Outcome (Follow-up) (mo, y)	Previously Published
30	64/female	24	12 mo painless mass, watering eye, lying ear; PPE	10/G2	< 5	NED at 12 mo	
31	48/male	11	Solitary nodule hard in consistency, palpable mass 1 y, total PE	40/G1	5	NED at 11 mo	
32	62/male	25	9 mo slowly growing painless mass treated by simple enucleation; Followed by RPE, LN dissection and RT History of CCRCC with lung and liver mets 3 y ago	15/G1	30/G1 apocrine IC invasive SDC	AWD at 12 mo	
33	63/female	25	RPE	20/G1	30/G1	NED at 8 mo	
34	52/female	13	24 mo preauricular edema, PE and LN dissection	30/G1	10	RE at 13 mo	
						NED at 43 mo	
			Recurrence treated by simple extirpation				
35	79/male	22	RPE and cervical dissection	40/G1	5	NED at 2 mo	
36	59/female	22	Solitary nodule, PE	5	40/G2	NED at 36 mo	

AWD indicates alive with disease; CCRCC, clear cell renal cell carcinoma; LN, lymph node; LOF, lost of follow-up; NA, not available; NED, no evidence of disease; PA, pleomorphic adenoma; PE, parotidectomy; PPE, partial parotidectomy; RE, recurrence; RPE, radical parotidectomy; RT, radiotherapy; SPE, superficial parotidectomy.

Histologic and Immunohistochemical Features

All 36 tumors in this series revealed characteristic diagnostic features of SPA, showing a circumscribed epithelial proliferations of ducts and acini, mostly arranged in nodular or multinodular patterns without capsule, but sometimes displaying an incomplete pseudocapsule. Most commonly, the cellular components in SPA were embedded in a sharply delineated, dense, sclerotic-collagenous stroma often with focal lymphoid aggregates (Fig. 2A). A highly characteristic feature of SPA was a lobular pattern of variably sized and shaped ducts lined by flattened, cylindrical, or apocrine epithelium separated by bands of hyalinized fibrous stroma. Frequently the ductal epithelium had a foamy cell appearance and sometimes the lumen of the ducts was filled by foamy cells (Fig. 2B). The epithelial component featured variably arranged and sized acini, tubules and ducts with heterogenous cytomorphologic characteristics of the lining epithelium, including foamy, vacuolated (sebaceous-like), apocrine, mucous, clear/"ballooned," squamous and oncocyte-like cells. The hallmark of SPA was the occurrence of numerous acini with abnormal acinar cells displaying brightly eosinophilic cytoplasmic granules/globules of varying sizes (Fig. 2C). The epithelial component of SPA was either cystic or solid. The cysts were often lined by a bilayered epithelium with luminal apocrine cells with apical snouts and an abluminal layer of myoepithelial cells (Fig. 2D). The ductal structures were in places surrounded by periductal concentric layers of hyalinized stroma (Fig. 2E). A less common feature was focal fibromyxoid (pleomorphic adenoma-like) stroma (Fig. 2F) sometimes intermixed with foci of mature adipose tissue.

SPA frequently harbored focal intraductal epithelial proliferations with foamy cell or oncocytic metaplasia vaguely resembling atypical ductal hyperplasia of the breast (Fig. 3A). These intraluminal epithelial ductal structures often displayed solid (Fig. 3B), cribriform (Fig. 3C), or micropapillary growth patterns with variable degrees of cytologic atypia.

Foci (< 5% to 40%, Table 2) of homogenous solid, micropapillary, and cribriform intraductal epithelial proliferations reminiscent of an IDC variant of IC were observed in most cases. The intraductal proliferations showed rigid bridging and cribriform patterns, and were composed of IDC-like epithelium positive for S100 protein, mammaglobin and SOX10 (Fig. 3D), and negative for AR (Fig. 3E). These structures were surrounded by a complete layer of myoepithelial cells decorated by positive staining for calponin (Fig. 3F). Less common findings were solid and cribriform intraductal epithelial proliferations with a pronounced apocrine morphology. The apocrine structures were present in 14/36 (39%) of cases ranging from small foci that made up <5% and up to 50% of the tumor (Table 2). In most cases of SPA, a variably prominent dilated ductal and cystic component was present (Fig. 4A). The cysts were divided by a prominent hyalinized stroma with focal lymphoid infiltrates. The cysts were lined by a cuboidal and/or attenuated epithelium with intercalated duct phenotype intermingled with foamy epithelial cells (Fig. 4B). Other dilated ducts were lined and partly filled by dysplastic epithelial proliferations with an apocrine morphology (Fig. 4C) and cells positive for AR (Fig. 4D).

In all cases, there were foci of homogenous intraductal solid and cribriform intercalated duct-like epithelial proliferations with variable degrees of dysplasia (Figs. 5A, B) and positivity for S100 protein and SOX10 (Fig. 5C), fully enveloped by an intact layer of myoepithelial cells. In addition, 9/36 cases (25%) had focal intraductal cribriform and micropapillary apocrine type variably dysplastic epithelial structures composed of cells positive for AR (Figs. 5D, E) and negative for S100/SOX10 (Fig. 5F). The
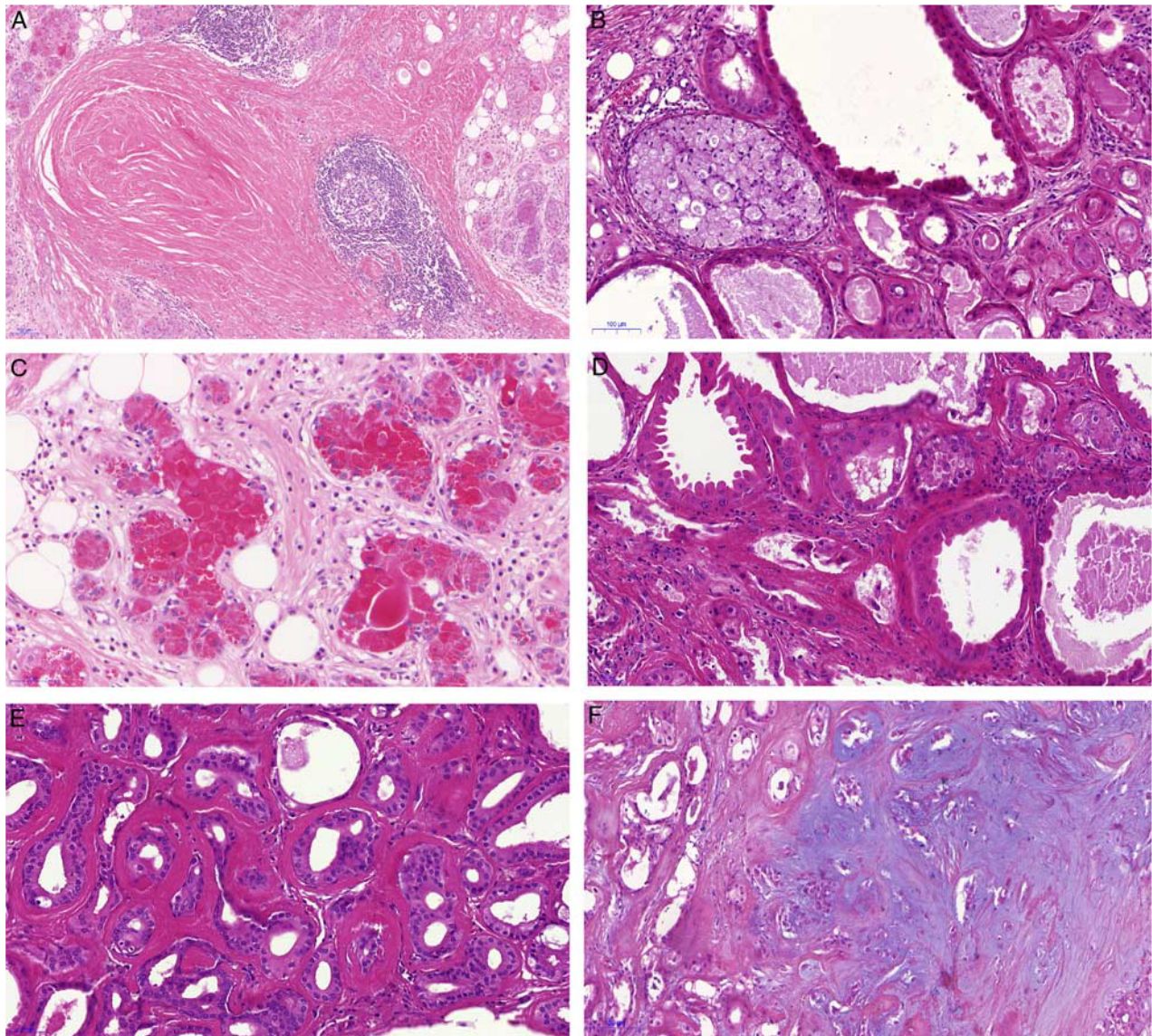
FIGURE 2. SPA is embedded in a sharply delineated, dense, sclerotic-collagenous stroma often with focal lymphoid aggregates (A). Frequently the lining ductal epithelium had a foamy cell appearance and sometimes the lumen of the ducts was completely filed by foamy cells (B). Acini were composed of abnormal acinar cells with brightly hyper-eosinophilic cytoplasmic granules/globules of varying size (C). The cysts were often lined by bilayered epithelium with inner luminal apocrine epithelium with apical snouts and abluminal myoepithelial layer (D). Ductal structures were surrounded by periductal concentric layers of stromal hyalinization (E). Less common feature was a focal presence of fibromyxoid (pleomorphic adenoma-like) stroma (F) sometimes intermixed with foci of mature adipose tissue.

intraductal proliferations showed focal mild to severe dysplasia in 17 cases (17/36; 47%). Two cases showed overt malignant morphologies ranging from HG IC to invasive carcinoma with apocrine ductal phenotype.

Index case: tumor of the left parotid gland, 25 mm in diameter, was composed of 3 closely associated components. The first lesion was a well-circumscribed predominantly poly-cystic tumor with features fully compatible with a diagnosis of SPA, conventional variant (Fig. 6A, right lower part of the picture), separated from the parotid gland by a fibrous pseudocapsule. The second lesion was composed of densely packed solid, cribriform (Fig. 6B), and intraluminal micropapillary epithelial proliferations. Tumor cysts were lined by large apocrine cells with cytoplasmic snouts (Fig. 6C). The cells had an apocrine morphology with abundant, granular eosinophilic cytoplasm, and large nuclei with mild polymorphism (Fig. 6D). The third lesion was found next to the apocrine IC and it was a frankly invasive SDC composed of HG tumor cells (Fig. 6E). By immuno-histochemistry, the apocrine neoplastic cells of both apocrine IC and invasive SDC were strongly and uniformly positive for AR (Fig. 6F).
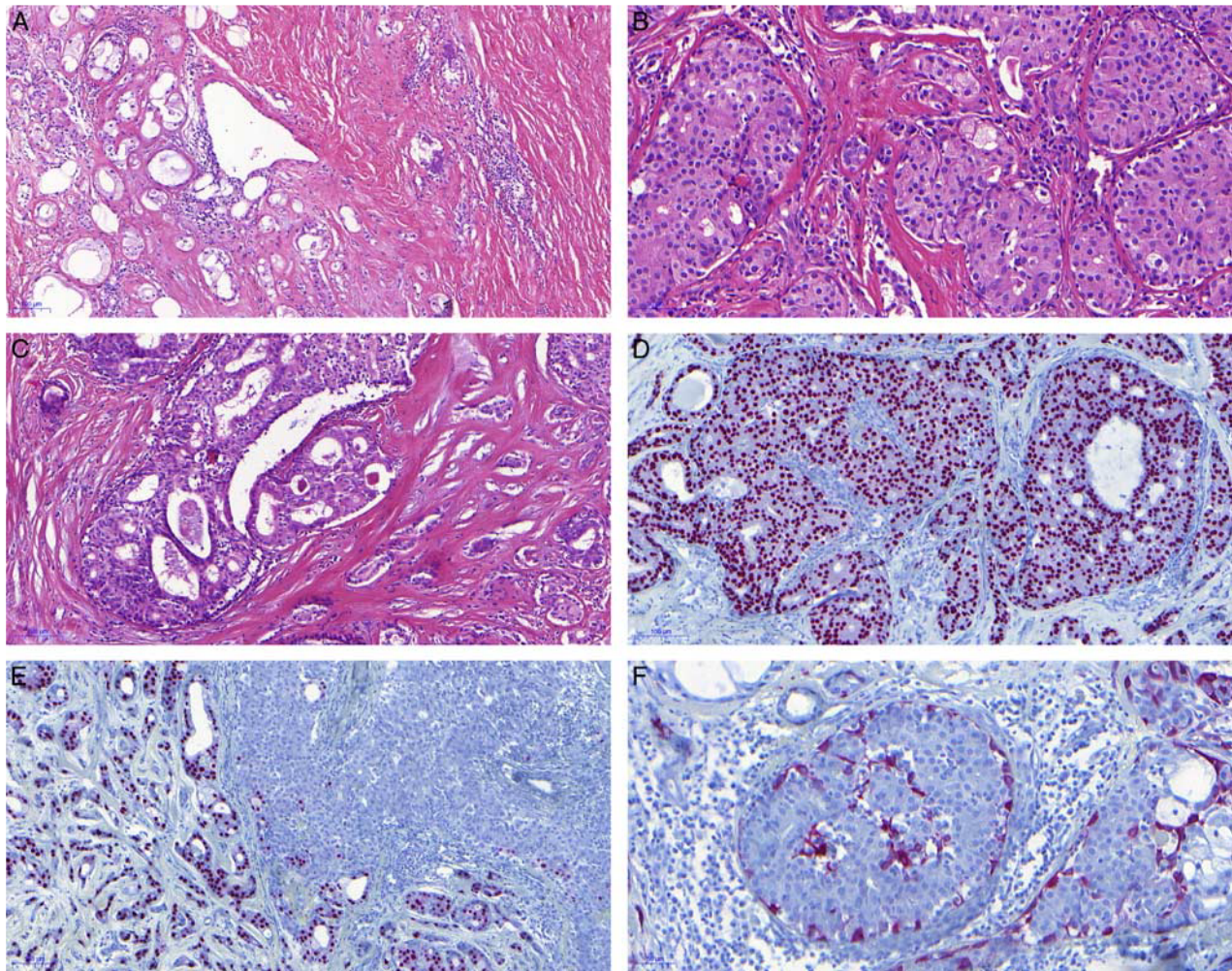
34

FIGURE 3. SPA frequently harbors intraductal epithelial proliferations with apocrine metaplasia and intraluminal proliferations resembling atypical ductal hyperplasia of the breast (A). These intraluminal epithelial ductal structures often display solid (B), cribriform (C), or micropapillary growth patterns with variable degree of cytologic atypia. The epithelial structures were composed of intercalated duct-like epithelium positive for S100 protein, mammaglobin and SOX10 (D) and negative for AR (E). These structures are surrounded by complete myoepithelial layer, here decorated by positive staining for calponin (F).

Immunohistochemistry

For purposes of this study, the immunohistochemical investigation was performed in 21 cases (21/36; 58%) in which tissue was available. Both ductal and acinar cells were positive for broad spectrum cytokeratins (AE1 to AE3) and cytokeratin CK7. The luminal epithelium in cystically dilated ducts was variably positive for S100, SOX10, and mammaglobin and negative for AR and GATA3, consistent with intercalated duct phenotype. In apocrine foci, in contrast, the luminal epithelium was stained with AR while it was negative for S100 and SOX10. In SPA, antibodies to p63, p40, and calponin variably decorated the abluminal myoepithelial cells in the periphery of the acini and ducts. Myoepithelial cells were also present occasionally and somewhat discontinuously around the solid, cribriform, and micropapillary intraductal and intracystic epithelial proliferations of both IC-like and apocrine types. Cell proliferation was predominantly low with an average MIB1

index of 3.2%. All cases were negative with DOG1, PLAG1, and NOR1 antibodies. HER2/neu overexpression and amplification was tested in 2 cases negative.

Molecular Testing

Results of targeted NGS are summarized in Table 3. A The Comprehensive Thyroid and Lung panel was used in 8 cases. In addition, TruSight Oncology 170/500 Kits were used in 7 cases (Table 3). Of 11 tumors with tissue available for molecular analysis, 9 (9/11; 82%) harbored genetic alterations in the PI3K pathway. One case was negative for mutation, one was unanalyzable due to low quality NGS data. The remaining 25 cases could not be sequenced due to inadequate DNA and RNA quality due to the age of the tissue blocks. In analyzable cases, targeted sequencing revealed HRAS mutations c.37G > C, p.(Gly13Arg) (2 cases) and c.182A > G, p.(Gln61Arg) (2 cases), and PIK3CA mutations c.3140A > G, p.(His1047Arg) (3 cases), c.1633G > A, p.(Glu545Lys) (1 case),
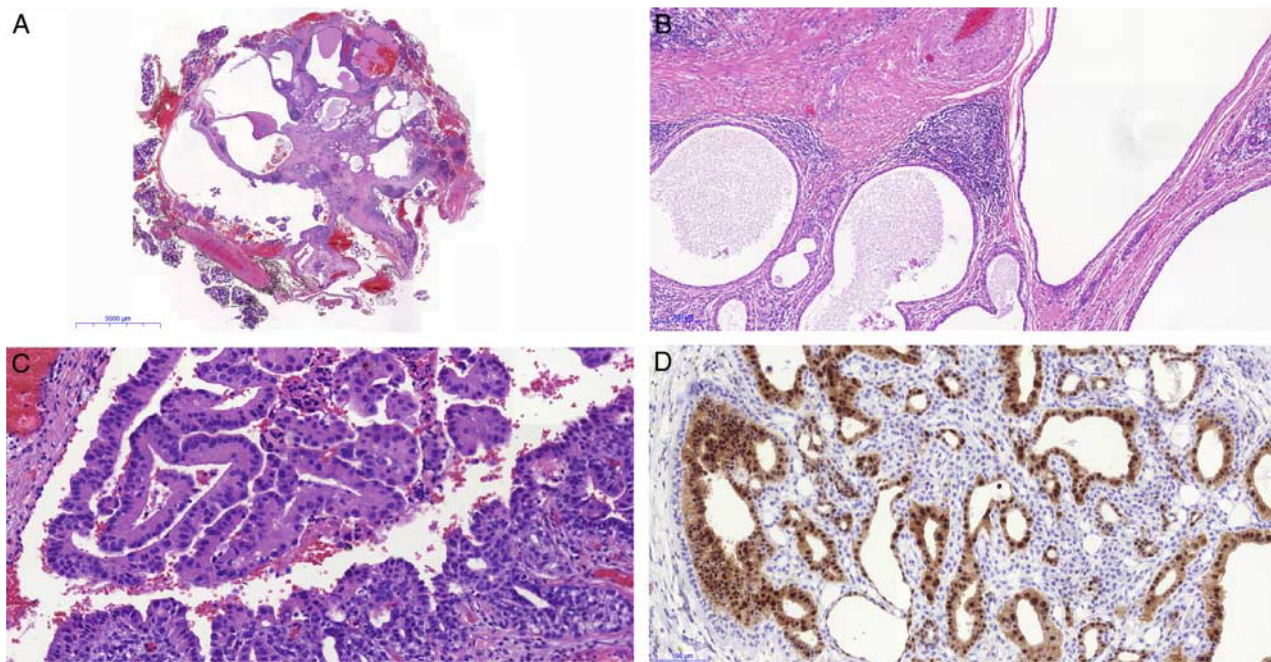
FIGURE 4. In most cases of SPA, a variably prominent, dilated ductal and cystic component is present (A). The cysts are divided by prominent hyalinized stroma with focal lymphoid infiltrate. Cyst are lined by cuboid and/or attenuated epithelium with intercalated duct phenotype intermingled with foamy epithelial cells (B). Other dilated duct in the same tumor are lined and partly filled by dysplastic epithelial proliferations with apocrine morphology (C) and lined by cells positive for AR (D).

and c.1624G > A, p.(Glu542Lys) (1 case). Moreover, mutations in AKT1 c.49G > A, p.(Glu17Lys) and c.51dup, p.(Tyr18ValfsTer15); c.49_50delinsAG, p.(Glu17Arg) (as a double hit) were found (2 cases). Additionally, germinal and somatic mutation of PTEN c.1003C > T, p.(Arg335Ter); c.445C > T, p.(Gln149Ter), respectively, were detected. Gene fusions were not found by RNA sequencing in any of the cases, in particular, genes *PLAG1* and *HMGA2* were found intact. All cases were negative for *PLAG1* alterations by FISH.

DISCUSSION

SPA is a rare benign salivary gland lesion that usually arises from the parotid gland. SPA has been an enigmatic entity since its initial description, and it was originally interpreted to be a non-neoplastic alteration of salivary glands analogous to fibrocystic disease of the breast.[1] In fact, it is still classified as such in the 2017 WHO Classification of Head and Neck Tumors.[2] Nevertheless, SPA has many characteristics that suggest that it is a genuine neoplasm. First, SPA often contains intraductal proliferation of apocrine ductal cells in solid and cribriform patterns surrounded by an intact or partially disrupted myoepithelial cell layer. These epithelial structures are composed of cells with a spectrum of nuclear atypia resembling that of the apocrine intraductal neoplasia of the breast and focally severe enough to fulfill the criteria of dysplasia or carcinoma in situ.[3] In addition, SPA is reported to have a significant risk of local recurrence (up to 20%).[7]

Recently, Bishop and colleagues analyzed 4 cases of SPA by targeted NGS and discovered mutations in genes that are well established drivers in human neoplasms. Such mutations were found in *PTEN* (4 of 4 cases), *PIK3CA* (2 of 4 cases) and *PIK3R1* (2 of 2 cases), all of which are members of the PI3K pathway of cell cycle regulation.[10] Hernandez-Prera et al[11] detected *PTEN* and *PIK3R1* mutations in additional 2 cases. Moreover, a patient with 2 different *PTEN* alterations had clinical stigmata of Cowden syndrome which was confirmed with germline genetic testing.[11]

In this study, we confirmed and expanded the observations of Bishop et al[10] and Hernandez-Prera et al.[11] In our series, we found that 92% of our SPA cases had a mutation in the PI3K/Akt pathway, in particular 1 of 2 mutations in *PIK3CA* gene c.3140A > G, p.(His1047Arg) or c.1624G > A, p.(Glu542Lys). All 5 tumors harboring *PIK3CA* mutation have shown focal solid and cribriform proliferation of epithelium with IDC-like phenotype and mild to moderate dysplasia. Interestingly, in contrast the 2 mutations in *HRAS* gene c.37G > C, p.(Gly13Arg) and c.182A > G, p.(Gln61Arg) were detected in 3 cases of SPA, all of them displaying intermediate to severe dysplastic changes of apocrine epithelial proliferations. In addition, the mutations of gene *AKT1* c.49G > A, p.(Glu17Lys) and *AKT1* c.51dup, p.(Tyr18ValfsTer15); AKT1 c.49_50delinsAG, p.(Glu17Arg) were discovered in 2 cases of SPA with extensive apocrine solid and cribriform dysplastic component. Our index case of apocrine IC with invasive SDC component arising from
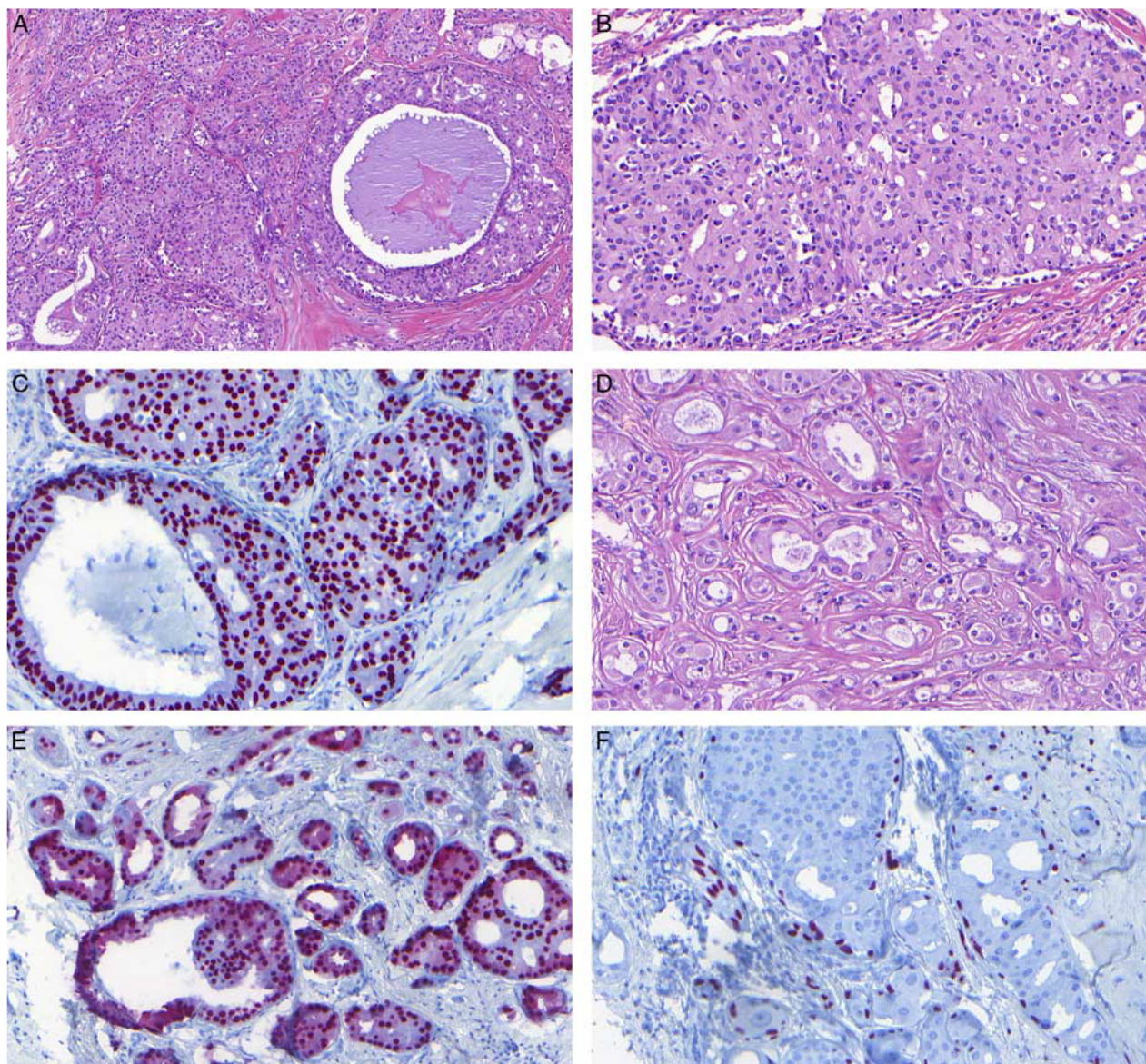
36

FIGURE 5. IDC-like dysplasia: complex solid and cribriform cystic epithelial proliferations (A); displaying mild nuclear atypia (B), SOX10 is positive (C) while AR negative. Apocrine dysplasia: closely attached solid, tubular and cribriform epithelial proliferations composed of the cells with mild nuclear atypia and finely granular cytoplasm (D), positive or AR (E), and negative for SOX10. Nuclear grade 3 (F).

SPA harbors an identical mutation in *PIK3CA* c.1624G > A, p.(Glu542Lys) in the conventional SPA component as well as in the malignant components of apocrine IC and invasive SDC. Moreover, when performing macrodissection we found a mutation in *HRAS* only in the malignant component. This is a novel finding as none of above mentioned mutations in *HRAS* and *AKT1* genes have been documented in SPA so far.

The PI3K/Akt pathway is involved in tumorigenesis, particularly influencing cell growth, cell cycle progression and cell survival. The aberrant activation of the PI3K pathway might be caused either by activating mutations in *AKT1*, *PIK3CA*, and *mTOR* genes or by inactivating mutations in

PTEN gene.[27] Somatic mutations in *AKT1* gene resulting in the substitution of glutamic acid with lysine at amino acid 17 (E17K) alter electrostatic interactions of a lipid-binding pocket in the plasma membrane forming a hydrogen bond with a phosphoinositide ligand stimulating downstream signaling and is responsible for oncogenic transformation.[27]

The alterations of *HRAS* and *PI3K* pathways in SPA with apocrine IC component are identical to alterations detected in SDC. Many studies imply important roles for PI3K/AKT/mTOR signaling in the tumorigenesis of SDC.[21–24,28,29] Mutation rates in SDC were estimated at 18% for *PIK3CA*, 16% for *HRAS* and 1.5% for *AKT1* gene.[28] Mutations in *PTEN* and *AKT1* in SDC have been
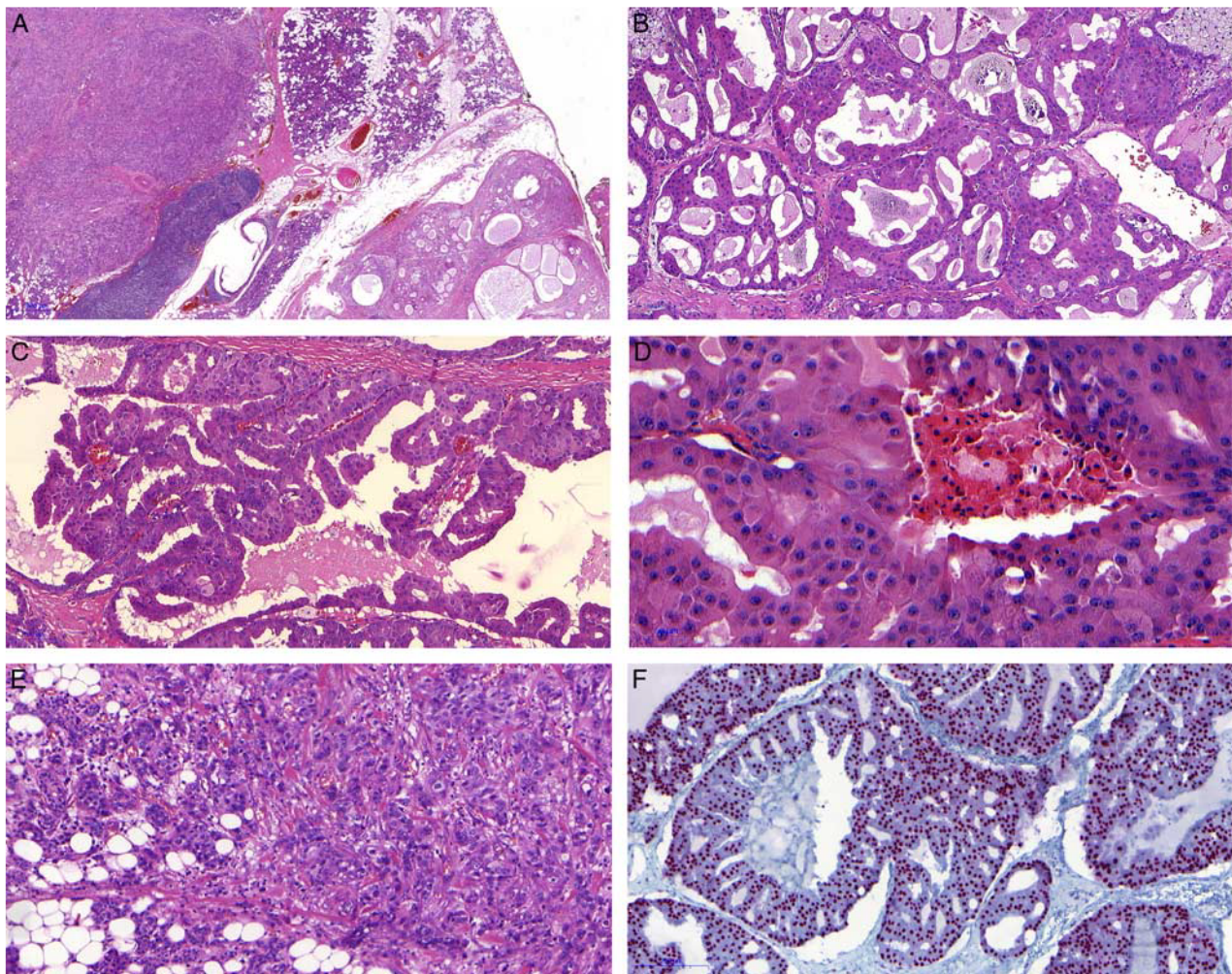
FIGURE 6. Index case: the tumor is composed of 3 closely related components. First lesion is a well-circumscribed predominantly polycystic SPA (A, right lower part of the picture) divided from parotid gland by fibrous pseudocapsule. The second component iss composed of densely packed solid, cribriform (B), and intraluminal micropapillary epithelial structures. The tumor cysts are lined by large apocrine cells with cytoplasmic snouts (C). The cells have apocrine morphology with abundant, granular eosinophilic cytoplasm and large nuclei with mild polymorphism (D). The third component found next to apocrine IC is frankly invasive SDC composed of HG cells (E). By immunohistochemistry, the apocrine neoplastic cells of both apocrine IC and invasive SDC are uniformly strongly positive for AR (F).

identified in other studies.[21–24] Interestingly, similar SDC-like genetic alterations of PI3K pathway including *PTEN*, *PIKCA*, and *PIK3R1* have been observed not only in SPA[10,11] but also in a subset of apocrine IC.[19]

SPA frequently harbors intraductal epithelial proliferations which may display atypia and morphologic features of DCIS.[3,9,30] Some degree of intraductal epithelial proliferations in SPA has been reported in at least 50% of SPA cases.[7] However, the proportion of cases of SPA with epithelial proliferations that reasonably fulfill the criteria for HG DCIS does not exceed 10% of reported cases.[7] Petersson[7] in his excellent review compared the intraductal epithelial proliferations in SPA with atypical ductal hyperplasia/DCIS of the mammary gland and concluded that "there is no reason to postulate that various categories of epithelial proliferations, for example, hyperplasia, atypical hyperplasia and LG DCIS are morphologically identical or biologically similar in SPA as those in the breast."[7] The authors of the current study agree with that conclusion. Here, we present for the first time diagnostic criteria for LG and HG dysplasia in the solid and cribriform epithelial proliferations in SPA. First, the IDC-type is characterized by mild to moderate dysplasia, S100 protein/SOX10 positive and AR negative immunophenotype harboring *PIK3CA* mutations. Second, the apocrine epithelial proliferations with intermediate to severe dysplasia, S100/SOX10 negative and AR positive immunophenotype harboring *HRAS* and *AKT1* mutations. It is important to emphasize that despite morphologic and immunohistochemical similarities with IC, none of our cases of SPA harbored any translocation.

Although no patient with SPA has developed metastases or died of disease, reports indicate that 2

TABLE 3. Molecular Genetic Findings in 11 Selected Cases of SPA (Using NGS Technologies)

Case No.	NGS Technology		*HRAS*	*PIK3CA*	*AKT1*	Other
21	Archer CTL; TS170			c.1633G > A, p. (Glu545Lys)		PTEN c.445C > T, p.(Gln149Ter) (somatic) PTEN c.1003C > T, p.(Arg335Ter) (germline)
23	TS500		NA	NA	NA	
27	Archer CTL		c.37G > C, p. (Gly13Arg)			
29	Archer CTL		c.182A > G, p. (Gln61Arg)		c.49G > A, p.(Glu17Lys)	
30	TS170; TS500 Archer CTL		Negative	Negative	Negative	
31	Archer CTL			c.3140A > G, p. (His1047Arg)		
32	TS170	SPA		c.1624G > A, p. (Glu542Lys)		
	TS500	IC apocrine/SDC invasive	c.37G > C, p. (Gly13Arg)	c.1624G > A, p. (Glu542Lys)		Isoform of the AR gene
33	Archer CTL			c.3140A > G, p. (His1047Arg)		
34	TS500			c.3140A > G, p. (His1047Arg)		
35	Archer CTL; TS500				c.51dup, p. (Tyr18ValfsTer15); c.49_50delinsAG, p. (Glu17Arg)	
36	Archer CTL; TS500		c.182A > G, p. (Gln61Arg)			

TS170, TruSight Oncology 1700 Panel; TS500, TruSight Oncology 500 Panel.

previous patients had invasive carcinoma with apocrine ductal phenotype arising from SPA.[11,30] Here, we present a unique case of a parotid gland tumor arising from SPA and composed of apocrine IC with transformation to SDC, and which harbored a mutation in PI3K/Akt pathway in all tumor components. This combination of tumor entities has not been published so far. Taken together, our findings not only strongly support that SPA is a neoplastic disease, but suggest a close relationship between SPA, apocrine IC and HG invasive SDC. SPA may represent a precursor lesion for the development of apocrine IC and sometimes even invasive SDC.

REFERENCES

1. Smith BC, Ellis GL, Slater LJ, et al. Sclerosing polycystic adenosis of major salivary glands: a clinicopathologic analysis of nine cases. *Am J Surg Pathol*. 1996;20:161–170.
2. Seethala R, Gnepp DR, Skálová A, et al. Sclerosing polycystic adenosis. In: El-Naggar AK, Chan JKC, Grandis JR, Takata T, Slootweg PJ, eds. *WHO Classification of Head and Neck Tumours*. Lyon, France: IARC Press; 2017:195.
3. Skalova A, Michal M, Simpson RHW, et al. Sclerosing polycystic adenosis of parotid gland with dysplasia and ductal carcinoma in situ: report of three cases with immunohistochemical and ultrastructural examination. *Virchows Arch*. 2002;440:29–35.
4. Gnepp DR, Wang LJ, Brandwein-Gensler M, et al. Sclerosing polycystic adenosis of the salivary gland. *Am J Surg Pathol*. 2006;30:154–164.
5. Fulciniti F, Losito NS, Ionna F, et al. Sclerosing polycystic adenosis of the parotid gland: report of one case diagnosed by fine-needle cytology with in situ malignant transformation. *Diagn Cytopathol*. 2010;38:368–373.
6. Manojlović S, Virag M, Milenović A, et al. Sclerosing polycystic adenosis of parotid gland: a unique report of two cases occurring in two sisters. *Pathol Res Pract*. 2014;210:342–345.
7. Petersson F. Sclerosing polycystic adenosis of salivary glands: a review with some emphasis on intraductal epithelial proliferations. *Head Neck Pathol*. 2013;7(suppl 1):S97–S106.
8. Petersson F, Tan PH, Hwang JSG. Sclerosing polycystic adenosis of parotid gland: report of a bifocal, paucicystic variant with ductal carcinoma in situ and pronounced stromal distortion mimicking stromal invasion. *Head Neck Pathol*. 2011;5:188–192.
9. Skalova A, Gnepp DR, Simpson RHW, et al. Clonal nature of sclerosing polycystic adenosis of salivary glands demonstrated by using the polymorphism of the human androgen receptor locus (HUMARA) as a marker. *Am J Surg Pathol*. 2006;30:939–944.
10. Bishop JA, Gagan J, Baumhoer D, et al. Sclerosing polycystic "adenosis" of salivary glands: a neoplasm characterized by PI3K pathway alterations more correctly named sclerosing polycystic adenoma. *Head Neck Pathol*. 2020;14:63–636.
11. Hernandez-Prera J, Heidarian A, Wenig B. Sclerosing polycystic adenoma: conclusive clinical and molecular evidence of its neoplastic nature. *Mod Pathol*. 2021;34(suppl 2):773–774.
12. Skalova A, Bishop J, Ferlito A, et al. Newly described entities in salivary gland pathology. *Am J Surg Pathol*. 2017;41:e33–e47.
13. Loening T, Leivo I, Simpson RHW, et al. Intraductal carcinoma. In: El-Naggar AK, Chan JKC, Grandis JR, Takata T, Slootweg PJ, eds. *WHO Classification of Head and Neck Tumours*. Lyon, France: IARC Press; 2017:170–171.
14. Brandwein-Gensler M, Gnepp DR. Low-grade cribriform cystadenocarcinoma. In: Barnes L, Eveson JW, Reichart P, Sidransky D, eds. *Pathology and Genetics of Head and Neck Tumours: World Health Organization Classification of Tumours*. Lyon, France: IARC; 2005:430.

15. Weinreb I, Bishop JA, Chiosea SI, et al. Recurrent *RET* gene rearrangements in intraductal carcinomas of salivary gland. *Am J Surg Pathol*. 2018;42:442–452.
16. Skalova A, Vanecek T, Uro-Coste E, et al. Molecular profiling of salivary gland intraductal carcinoma revealed a subset of tumor harboring *NCOA4-RET* and novel *TRIM27-RET* fusions: report of 17 cases. *Am J Surg Pathol*. 2018;42:1445–1455.
17. Skalova A, Ptáková N, Santana T, et al. *NCOA4-RET* and *TRIM27-RET* are characteristic gene fusions in salivary intraductal carcinoma, including invasive and metastatic tumors. Is "intraductal" correct? *Am J Surg Pathol*. 2019;43:1303–1313.
18. Lu H, Graham RP, Seethala R, et al. Intraductal carcinoma of salivary glands harboring *TRIM27-RET* fusion with mixed low grade and apocrine types. *Head Neck Pathol*. 2020;14:239–245.
19. Bishop JA, Gagan J, Krane JF, et al. Low-grade apocrine intraductal carcinoma: expanding the morphologic and molecular spectrum of an enigmatic salivary gland tumor. *Head Neck Pathol*. 2020;14:869–875.
20. Nagao T, Licitra L, Loening T, et al. Salivary duct carcinoma. In: El-Naggar AK, Chan JKC, Grandis JR, Takata T, Slootweg PJ, eds. *WHO Classification of Head and Neck Tumours*, 4th ed. Lyon, France: IARC Press; 2017:173–174.
21. Chiosea SI, Williams L, Griffith CC, et al. Molecular characterization of apocrine salivary duct carcinoma. *Am J Surg Pathol*. 2015;39:744–752.
22. Dalin MG, Desrichard A, Katabi N, et al. Comprehensive molecular characterization of salivary duct carcinoma reveals actionable targets and similarity to apocrine breast cancer. *Clin Cancer Res*. 2016;22:4623–4633.
23. Wang K, Russell JS, McDermott JD, et al. Profiling of 149 salivary duct carcinomas, carcinoma ex pleomorphic adenomas, and adenocarcinomas, not otherwise specified reveals actionable genomic alterations. *Clin Cancer Res*. 2016;22:6061–6068.
24. Santana T, Andrle P, Martinek P, et al. Biomarker immunoprofile and molecular characteristics in salivary duct carcinoma: clinicopathological and prognostic implications. *Hum Pathol*. 2019;93:37–47.
25. Skalova A, Vanecek T, Martinek P, et al. Molecular profiling of mammary analogue secretory carcinoma revealed a subset of tumors harboring a novel *ETV6-RET* translocation: report of 10 cases. *Am J Surg Pathol*. 2018;42:234–246.
26. Landrum MJ, Lee JM, Benson M, et al. ClinVar: improving access to variant interpretations and supporting evidence. *Nucleic Acids Res*. 2018;46:D1062–D1067.
27. Yang J, Nie J, Ma X, et al. Targeting PI3K in cancer: mechanisms and advances in clinical trials. *Mol Cancer*. 2019;18:1–28.
28. Shimura T, Yuichiro Tada Y, Hirai H, et al. Prognostic and histogenetic roles of gene alteration and the expression of key potentially actionable targets in salivary duct carcinomas. *Oncotarget*. 2018;9:1852–1867.
29. Griffith CC, Seethala RR, Luvison A, et al. *PIK3CA* mutations and *PTEN* loss in salivary duct carcinomas. *Am J Surg Pathol*. 2013;37:1201–1207.
30. Canas Marques R, Felix A. Invasive carcinoma arising from sclerosing polycystic adenosis of the salivary gland. *Virchows Arch*. 2014;464:621–625.

40

4.3   High-grade non-intestinal type sinonasal adenocarcinoma with *ETV6::NTRK3* fusion, distinct from secretory carcinoma by immunoprofile and morphology

V práci jsou popsány dva případy high-grade sinonasálního adenokarcinomu. Ačkoli se histomorfologicky i imunofenotypicky liší od sekrečního karcinomu slinných žláz, oba prezentované nádory s ním sdílejí fúzi *ETV6::NTRK3*. Práce podtrhává význam důsledné korelace výsledků molekulárně-genetické analýzy s histomorfologickým nálezem a imunoprofilem.

V obou případech bylo pacientům 39 let, nebyla pozorována pohlavní predilekce. V prvním případě tumor vyplňoval maxilární dutinu, prorůstal do dutiny nosní a infiltroval očnici. Po odběru probatorní biopsie následovala intenzivní léčba sestávající z neoadjuvantní chemoterapie, inkompletní chirurgické resekce a adjuvantní chemoradioterapie. Bylo dosaženo úplné remise, případ je však recentní. V druhém případě se pacient dostavil s opakovanou epistaxí způsobenou nádorovou masou v levostranné nosní dutině. Po odběru probatorní biopsie byla provedena kompletní ethmoidektomie, pacient dále podstoupil adjuvantní radioterapii a byl naživu bez známek onemocnění po 17 měsících.

Oba nádory byly výrazně hypercelulární, složené ze solidních a hustě buněčných kribriformních hnízd s četnými nekrózami v jejich centru. Ložiskově, především při okrajích tumoru byly pozorovány také formace papilární, mikrocystické a trabekulární, bez rozlišitelných známek sekrece či hlenotvorby. V případu 2 byla na periferii nádorových hnízd vrstva abluminálních buněk s cytoplazmatickým projasněním až zcela vodojasnou cytoplazmou. Jádra byla v obou případech zvětšená, překrývající se, s výraznými jadérky, četná jádra byla též vezikulární. Mitotická aktivita byla vysoká a přítomna byla také četná apoptotická tělíska, proliferační index Ki-67 dosahoval až 51 %.

Nádorové buňky byly imunohistochemicky pozitivní v průkazu markerů S100 a SOX10, cytokeratinů 7, 18 a 19 a GATA3, zatímco průkaz mammaglobinu byl negativní. Markery p40 a p63 barvily jádra abluminálních buněk s vakuolizovanou či vodojasnou cytoplazmou v případu 2, zatímco v případu 1 byla pozitivita p40 a p63 převážně náhodná, rozmístěná rovnoměrně v nádorových hnízdech. PanTrk vykazoval difúzní nukleární pozitivitu v obou případech. Testované komponenty SWI/SNF měly expresi imunohistochemicky zachovalou, markery AR a Her2 byly negativní.

Nádory byly sekvenovány pomocí DNA a RNA panelu TruSight Oncology 500. Zatímco DNA část panelu nepřinesla žádný nález, RNA-seq odhalila v obou případech přítomnost shodné fúze *ET6::NTRK3* mezi exonem 5 genu *ETV6* a exonem 15 genu *NTRK3*.

V kontextu nádorů slinných žláz je fúze *ETV6::NTRK3* specifická pro sekreční karcinom (39). V typických případech je sekreční karcinom tvořený jen mírně atypickými nádorovými buňkami uspořádanými v solidně-mikrocystických, tubulárních, folikulárních nebo papilárně-cystických nádorových lobulech. Typický je namodralý PAS-pozitivní sekret přítomný v mezibuněčných luminech. Imunohistochemicky lze prokázat expresi S100 a mammaglobinu, zatímco markery p40 a p63 jsou negativní. Sekreční karcinom byl vzácně prokázán i v sinonasální oblasti (40). Stejně jako u jiných salivárních nádorů je možná HGT sekrečního karcinomu, definovaná jako přítomnost

špatně diferencovaného high-grade karcinomu nebo adenokarcinomu na pozadí původního low-grade tumoru (41). V high-grade případech popisovaných ve zde uvedené studii však nebyla žádná komponenta low-grade salivárního nádoru identifikována, diskordantní je též imunofenotyp: negativita mammaglobinu a pozitivita p40/p63.

Nádory proto byly na základě zjištěných charakteristik klasifikovány jako subtyp sinonasálního non-ITAC s fúzí *ETV6::NTRK3*. Již dříve byly popsány případy low-grade sinonasálních non-ITAC se stejnou fúzí, v jenom případě byl namísto genu *NTRK3* rearanžován gen pro podobnou kinázu – RET (fúze *ETV6::RET*) (42-43). Kromě toho byl popsán jeden případ tracheálního adenokarcinomu s morfologií sinonasálního low-grade non-ITAC a fúzí *ETV6::NTRK3* (44). Kromě genetického pozadí a do jisté místy konkordantní morfologie tumory sdílejí některé imunohistochemické charakteristiky: markery CK7, S100 a SOX10 jsou pozitivní, zatímco mammaglobin je negativní.

ORIGINAL ARTICLE

High-grade non-intestinal type sinonasal adenocarcinoma with *ETV6::NTRK3* fusion, distinct from secretory carcinoma by immunoprofile and morphology

Natálie Klubíčková[1,2] · Elaheh Mosaieby[1,3] · Nikola Ptáková[3,4] · Aude Trinquet[5] · Marick Laé[6] · Valérie Costes-Martineau[5] · Alena Skálová[1,2]

Abstract

We report 2 cases of high-grade sinonasal adenocarcinoma with a distinct morphological and immunohistochemical phenotype. Albeit histologically different from secretory carcinoma of the salivary glands, both tumors presented here share an *ETV6::NTRK3* fusion. The highly cellular tumors were composed of solid and dense cribriform nests, often with comedo-like necroses in the center, and minor areas with papillary, microcystic, and trabecular formations without secretions, mostly located at the periphery of the lesion. The cells displayed high-grade features, with enlarged, crowded, and often vesicular nuclei with conspicuous nucleoli and brisk mitotic activity. The tumor cells were immunonegative for mammaglobin while showing immunopositivity for p40/p63, S100, SOX10, and GATA3, as well as for cytokeratins 7, 18, and 19. For the first time, we describe 2 cases of primary high-grade non-intestinal type adenocarcinomas of the nasal cavity, distinct from secretory carcinoma by morphology and immunoprofile, harboring the *ETV6::NTRK3* fusion.

Keywords Sinonasal · Nasal cavity · non-intestinal-type adenocarcinoma · *ETV6::NTRK3* · Secretory carcinoma · Salivary duct carcinoma

Introduction

Primary sinonasal adenocarcinomas are rare tumors encompassing a wide morphological spectrum, divided into two groups: intestinal-type sinonasal adenocarcinoma (ITAC) and non-intestinal-type sinonasal adenocarcinoma (non-ITAC) subtypes [1]. While ITACs resemble gastrointestinal primary adenocarcinomas, with columnar epithelial structures and interspersed goblet cells, forming papillae, glands, cribriform structures or, in less differentiated cases, solid nests, as well as occasional mucin lakes, non-ITACs show even wider morphological spectrum. Columnar cells forming variable non-gastrointestinal-like glandular structures are seen in low-grade (LG) cases, whereas high-grade (HG) cases usually consist of solid nests with only a few glands and commonly with central comedo-like necrosis, or individual mucin-producing cells infiltrating into the surrounding stroma. Clear-cell change, endowing an appearance of clear-cell renal cell carcinoma, can be observed in some cases of non-ITAC. In addition, SMARCB1-deficient adenocarcinoma was recently recognized and included in the

Alena Skálová and Valérie Costes-Martineau contributed equally to this work and are considered co-senior authors.

✉ Natálie Klubíčková
  klubickova@biopticka.cz

1 Department of Pathology, Faculty of Medicine in Pilsen and University Hospital Plzen,, Charles University, Alej Svobody 80, 323 00 Pilsen, Czech Republic

2 Bioptical Laboratory, Pilsen, Czech Republic

3 Molecular-Genetic Laboratory, Bioptical Laboratory, Pilsen, Czech Republic

4 Department of Biology and Medical Genetics, Second Faculty of Medicine, Charles University and Motol University Hospital, Prague, Czech Republic

5 Department of Pathology, Hopital Gui de Chauliac, Montpellier, France

6 Department of Pathology, Centre Henri Becquerel, Rouen, France

⚫ Springer

WHO Classification of Tumours [1] as a subtype of "SWI/SNF complex-deficient sinonasal carcinoma."

With excessive solid areas, the differentiation between HG sinonasal non-ITAC and other poorly differentiated epithelial neoplasms of the salivary gland and non-salivary gland origin might pose a problem. Recent molecular-genetic findings had aided in the subclassification of primary sinonasal carcinomas, prompting the inclusion of a number of new entities in the 5th edition of the WHO Classification of Head and Neck Tumours [1]. The aggressive SWI/SNF complex-deficient sinonasal carcinomas lack the expression of SMARCA4 or SMARCB1 proteins while displaying relatively monomorphic rhabdoid, plasmacytoid, or epithelioid morphology and infiltrative growth into the surrounding tissue [2]. NUT carcinoma is another novel entity with a very poor prognosis, composed of undifferentiated primitive cells with irregular overlapping nuclei and prominent nucleoli, and defined by pathogenic fusions of the *NUTM* gene, most commonly *NUTM::BRD4* [3]. The diagnosis of exclusion of sinonasal undifferentiated carcinoma (SNUC) should be rendered in cases of a high-grade appearing proliferation of relatively monomorphic, sometimes basaloid-looking tumor cells with the evidence of epithelial origin (cytokeratin immunostaining) and absence of any features pointing toward other possible entities, including but not limited to tumors specific for the sinonasal tract as well as neuroendocrine and neuroepithelial neoplasms, melanoma and salivary gland tumors. Up to 80% of SNUC cases were reported to harbor hotspot mutations of the *IDH2* gene [4, 5], while only rare cases displayed *IDH1* gene mutations [5].

Salivary gland tumors might rarely arise from the minor salivary glands located in the sinonasal tract, representing 5–10% of all sinonasal adenocarcinoma cases [6]. Multiple entities in this group are defined by recurrent genetic alterations, such as *MYB::NFIB* and *MYBL1::NFIB* in adenoid cystic carcinoma [7, 8], *MAML2* fusions in mucoepidermoid carcinoma [9], *NR4A3* upregulation by enhancer hijacking in acinic cell carcinoma [10], or *ETV6::NTRK3* in secretory carcinoma [11, 12].

In the context of salivary gland tumors, *ETV6::NTRK3* fusion is specific for secretory carcinoma (SC) [11]. In typical cases, SC is a circumscribed unencapsulated proliferation of lobules separated by fibrous septa, composed of tumor cells with only mild atypia and low-grade nuclear features, growing in solid-microcystic, solid, tubular, follicular, or papillary-cystic patterns, with bluish PASd-positive luminal secretions and low mitotic activity, positive for S100 and mammaglobin while being negative for DOG1 (except for occasional minor staining), p40, and p63 on immunohistochemical examination [11]. High-grade transformation (HGT) of the low-grade SC, albeit rare, is possible, conveying a more aggressive clinical course and poorer outcomes to the patients affected by such tumors [13, 14]. Similar to other salivary gland tumors, SC might rarely arise in the sinonasal location, retaining the typical morphological features described above [12].

In the nasal cavity, three cases of low-grade non-ITAC were reported to harbor the *ETV6::NTRK3* fusion, as well as one case with a less common *ETV6::RET* fusion [15–17]. In addition, one case of tracheal adenocarcinoma with the morphology of sinonasal low-grade non-ITAC and an *ETV6::NTRK3* fusion was reported [18]. Lastly, the fusion has recently been documented in two high-grade salivary gland adenocarcinomas lacking the typical low-grade morphological features of SC [19, 20].

In this report, we present for the first time two cases of primary high-grade sinonasal adenocarcinomas that were initially classified as high-grade sinonasal non-ITAC. Using RNA sequencing, an *ETV6::NTRK3* fusion was detected in both cases. We aim to contribute to unraveling the position of this neoplasm in the classification of head and neck tumors.

Materials and methods

Histological and immunohistochemical studies

For conventional microscopy, excised tissues were fixed in formalin, processed routinely, embedded in paraffin (FFPE), cut, and stained with hematoxylin and eosin. Immunohistochemical staining was routinely performed using an automated Ventana BenchMark ULTRA system (Ventana Medical Systems Inc., Tucson, AZ, USA). The primary antibodies used are summarized in Table 1.

Next-generation sequencing

For mutation analysis, TruSight Oncology 500 panel, a comprehensive NGS assay on FFPE samples that identifies fusion transcripts, somatic variants, copy number changes, tumor mutational burden, and microsatellite instability was used. NA libraries were created using the TruSight Oncology 500 Kit (Illumina) following the manufacturer's instructions (KAPA Biosystems, Washington, MA), although we used KAPA FragKit (KAPA Biosystems, Washington, MA) for DNA enzymatic fragmentation. Following the manufacturer's guidelines, sequencing was conducted using an Illumina NovaSeq6000 sequencer. The OmnomicsNGS analysis program was used for data analysis (DNA variant filtering and annotation) (Euformatics, Finland). Reported variants were filtered retaining variations with coding effects, read depths greater than 50, and variants with allelic frequency >10%, with the removal of benign variants according to the ClinVar database. The remaining collection of variations was visually verified in raw data, and probable artifactual

Table 1 Immunohistochemical examination

Marker	Clone	Company	Dilution	Case 1	Case 2
AR	SP107	Ventana	RTU	–	–
CDX2	DAK-CDX2	Dako	RTU	ND	–
CK14	SP53	Cell Marque	RTU	ND	+
CK18	CD10	Dako	RTU	+	+
CK19	A53-B/A2.26	Ventana	RTU	+	+
CK5/6	D5/16 B4	Dako	1:100	–	–
CK7	OV-TL 12/30	Dako	1:800	+	+
CK8	35βH11	Ventana	RTU	F+	F+
DOG1	SP31	Ventana	RTU	F+	–
GATA3	L50-823	Biocare Medical	1:100	+	+
Her2	HercepTest	Dako	RTU	–	–
Ki-67	MIB-1	Dako	RTU	42%	51%
Mammaglobin	304-1A5	Dako	RTU	–	–
MUC4	1G8	Santa Cruz Biotech	1:100	–	+
NOR1	H-7	Santa Cruz Biotech	1:50	ND	–
p16	R15-A	DB Biotech	1:100	ND	–
p40	DAK-p40	Dako	RTU	F+	+
p63	DAKp63	Dako	RTU	F+	+
PanTrk	EPR17341	Abcam	1:50	+	+
S100	polyclonal	Dako	RTU	+	+
SALL4	6E3	Sigma	1:800	–	ND
SMA	1A4	Dako	RTU	–	–
SMARCA2	polyclonal	Atlas Antibodies	1:100	N	N
SMARCA4	EPNCIR111A	Abcam	1:1000	N	N
SMARCB1	MRQ-27	Ventana	RTU	N	N
SOX10	SP267	Ventana	RTU	+	+
STAT6	YE361	Abcam	1:1000	ND	–
TTF1	SPT24	Biocare Medical	1:50	–	ND

Abbreviations: *F*, focally; *N*, normal expression; *ND*, not done; *RTU*, ready-to-use; +, positive; –, negative

variants were eliminated. The list of genes covered by this panel is available at the product website (https://www.illumina.com/products/by-type/clinical-research-products/trusight-oncology-500.html). In addition, the samples were analyzed using the NGS-based ligation-dependent multiplex RT-PCR assay as described previously [21].

Case presentation

Clinical features

In case 1, a 39-year-old female patient presented with nasal obstruction. The tumor filled the left maxillary sinus, extended into the nasal cavity, and infiltrated into the left orbit (Fig. 1). The lesion was staged clinically as cT4a and was inoperable without orbital exenteration. After a diagnostic biopsy, the patient received three cycles of neoadjuvant chemotherapy with docetaxel, carboplatin, and fluorouracil, achieving significant regression of the tumor. Four months after the first diagnosis, the patient underwent a conservative surgical removal of the residual lesion, with a positive posterior surgical margin, prompting the administration of adjuvant proton therapy and chemotherapy with cisplatin. After finishing the treatment, the patient had no signs of disease on clinical examination; however, a CT scan was not yet performed because the case is recent.

A 39-year-old male presented with epistaxis in case 2, caused by a mass in the left nasal cavity, measuring 18 mm in the greatest dimension. After a preliminary biopsy was taken and diagnosed, complementary ethmoidectomy was performed with clear surgical margins. Consequently, the patient received radiotherapy. The patient was alive with no evidence of disease 17 months after the first diagnosis.

Histopathological features

The tumors widely infiltrated into the submucosa of the nasal cavity. Both tumors displayed high-grade features, growing mostly in hypercellular solid and dense cribriform nests, often
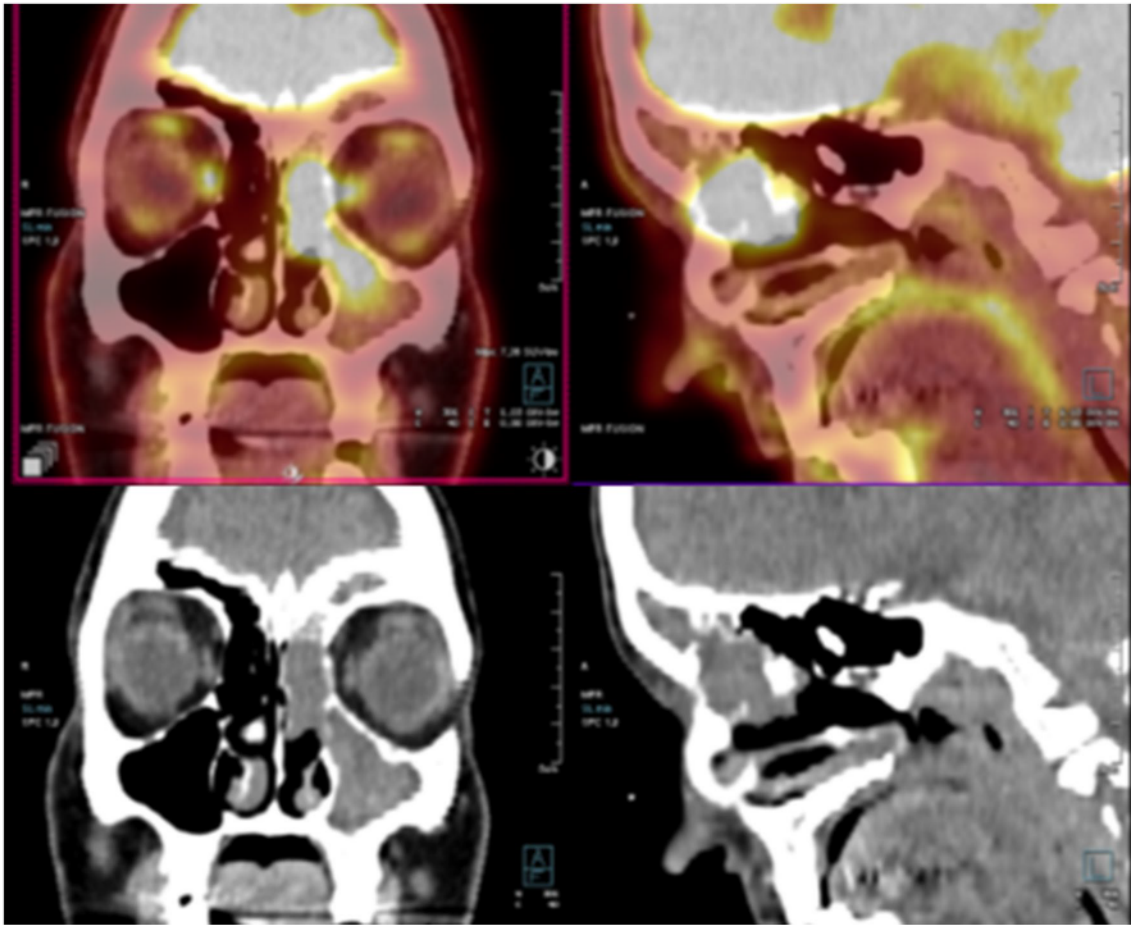
🌐 Springer

Fig. 1 PET/CT imaging study performed in case 1. The tumor filled the left maxillary sinus, extended into the nasal cavity, and infiltrated into the left orbit

with central necrosis (Figs. 2A-B, 3A-B). Minor parts, usually located at the periphery of the lesion, were less dense and showed irregular papillary, microcystic, or trabecular patterns but still displayed high-grade cytological features (Figs. 2A, 3C–D). Crowding of large, oval-to-round, and often vesicular nuclei with prominent eosinophilic nucleoli was observed in both cases. In case 1, the cells contained small or moderate amounts of pale eosinophilic cytoplasm (Fig. 2C–D). In case 2, lining the tumor nests were abluminal cells displaying clear cytoplasmic vacuoles or frank clear-cell change, while the population of luminal cells had pale to moderately eosinophilic cytoplasm (Fig. 3A–B). Numerous apoptotic bodies and brisk mitotic activity (26 and 17 mitotic figures/2.4 mm^2 in cases 1 and 2, respectively) were observed. Minimal nonneoplastic lymphoplasmacytic infiltration was present in the background in case 1, while case 2 showed more prominent stromal chronic inflammation.

On immunohistochemical examination (Table 1), markers p40 and p63 highlighted the abluminal cells in case 2 (Fig. 3E), similar to cytokeratin 14. These cells corresponded to the abluminal cells with clear intracytoplasmic vacuoles or complete cytoplasmic clearing on H&E slides. In case 1, p63 had the same pattern with nuclear positivity in the abluminal cells lining the tumor nests only in one focus, while in other areas, both p40 and p63 showed randomly scattered nuclear positivity (Fig. 2E). On H&E slides, these cells did not appear different from the p40/p63-negative tumor cells. The tumor cells were diffusely positive for S100, SOX10, and cytokeratins 7, 18, and 19, in both the luminal and abluminal cells. Cytokeratin 8 was only focally positive, while cytokeratin 5/6 was completely negative. PanTrk (Fig. 2F) and GATA3 were diffusely positive in the nuclei of the tumor cells; mammaglobin, however, was negative in both cases. MUC4 was negative in case 1, but it displayed a peculiar pattern of immunostaining in case 2, being positive at the membranes lining the lumina of the small cystic or cribriform formations, as well as a focal membranous positivity in the solid areas of the tumor (Fig. 3F). DOG1 stained the cytoplasmic membranes in 10% of tumor cells in case 1 and was completely negative in case 2 (even after
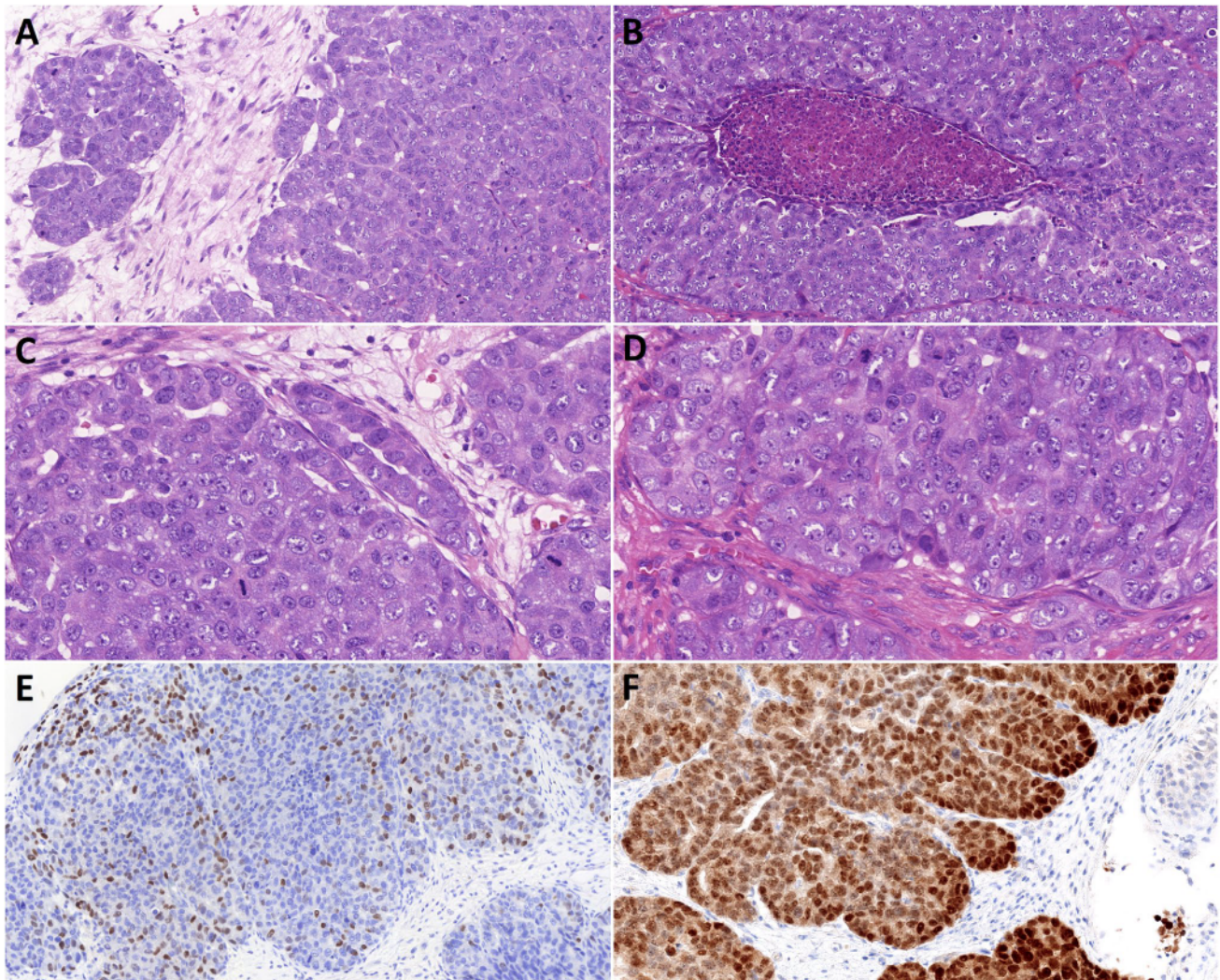
Fig. 2 Histopathological features of case 1. **A–B** The tumor grew mostly in solid or dense cribriform nests with central necrosis, displaying high-grade nuclear features and brisk mitotic activity. Focally, especially at the periphery of the tumor, tubular and cribri- form formations were observed. **C–D** High-grade cytologic atypia was observed in the tumor cells. **E** Scattered nuclear p63 immunopo- sitivity. **F** Diffuse nuclear PanTrk immunostaining

repeated staining). Both tumors showed high proliferative activity, with Ki-67 indices reaching 42% and 51% in cases 1 and 2, respectively.

SMARCB1, SMARCA2, and SMARCA4 immunoexpression was retained in both cases. Smooth muscle actin, androgen receptor, and Her2 were negative in both cases. Furthermore, case 1 did not stain with the SALL4 and TTF1 antibodies, while case 2 was additionally negative for p16, NOR1, CDX2, and STAT6.

Molecular genetic findings

An identical *ETV6::NTRK3* fusion involving exon 5 of the *ETV6* gene and exon 15 of the *NTRK3* gene was detected by RNA-sequencing in both cases (Fig. 4). The reference transcript sequences used for describing *ETV6* and *NTRK3* have accession numbers NM_001987.5 and NM_001012338.3, respectively; the chromosomal position is described using the reference genome GRCh37 (hg19), with breakpoints at chr12:12022900 and chr15:88483984. The NGS-based ligation-dependent multiplex RT-PCR assay corroborated these results. No pathogenic genetic alterations were revealed by the DNA part of the TruSight Oncology 500 panel.

Discussion

Based on the high-grade morphology with solid, cribri- form, and papillary architecture, distinctive immunoprofile with p40/p63, S100, SOX10, and GATA3 positivity, and
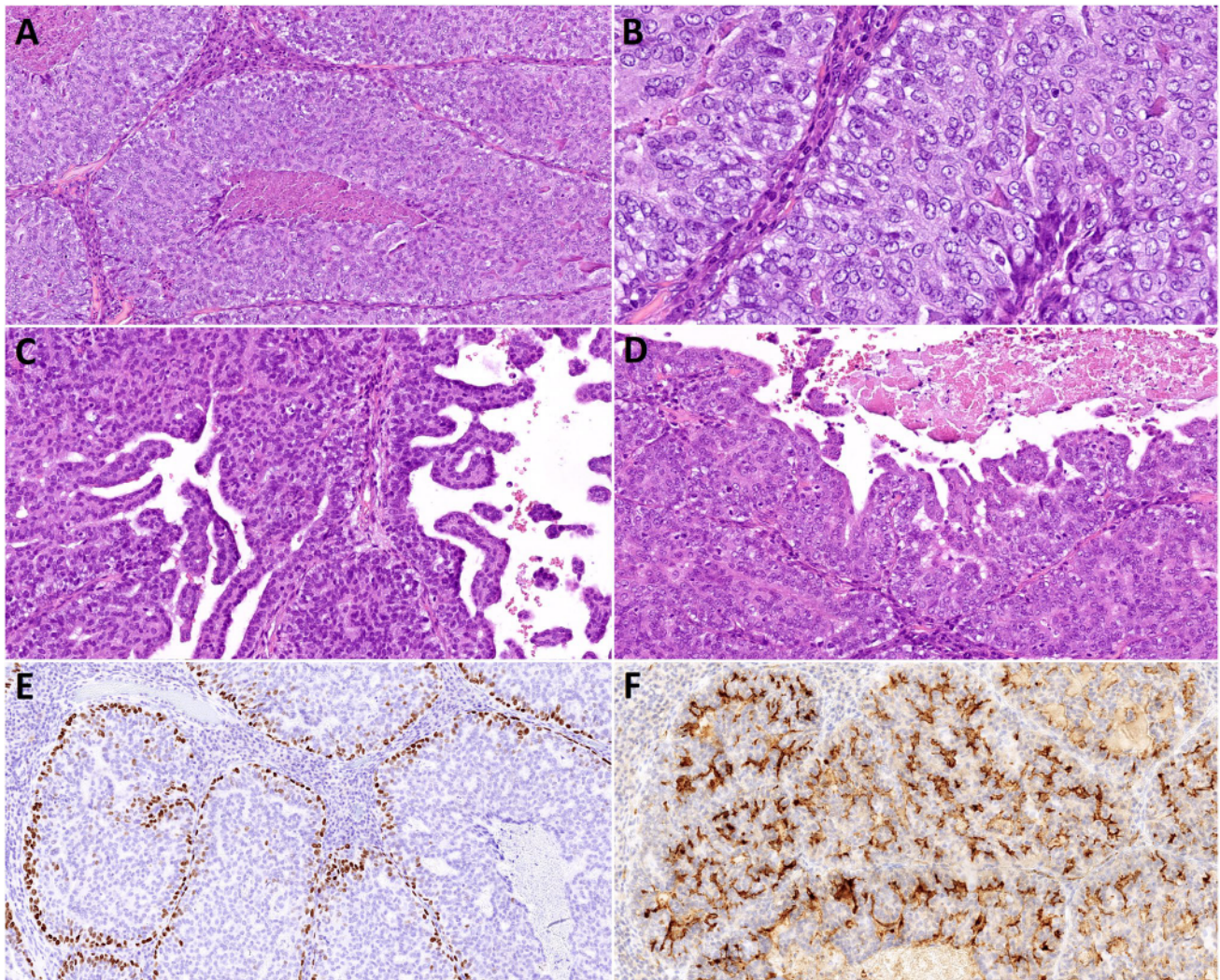
Fig. 3 Histopathological features of case 2. **A** The tumor showed features similar to case 1, growing in solid nests with necrotic debris in their centers. **B** Abluminal cells with clear cytoplasm at the periphery of the tumor nests, displaying high-grade cytologic atypia, similar to the luminal tumor cells. **C–D** Cystopapillary, papillary and trabecular architecture was present focally. **E** p63 immunopositivity in the nuclei of the abluminal cells. **F** MUC4 highlighted the membranes of the tumor cells
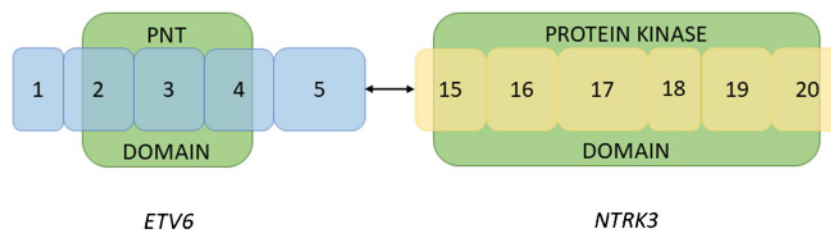
Fig. 4 Exon 5 of *ETV6* is fused to exon 15 of *NTRK3*. The fusion product retains the PNT domain of *ETV6*, which enables homodimerization or heterodimerization with other proteins containing the domain, e.g., ETS family proteins. The tyrosine-protein kinase domain of *NTRK3* is also present in the fusion product. This leads to dysregulated activation and constitutive activity of the kinase domain of the fusion protein and, in turn, carcinogenesis

a complete lack of mammaglobin staining, together with the *ETV6::NTRK3* fusion, we propose the tumors reported herein might represent a subtype of high-grade non-ITAC, distinct from SC.

The major consideration in the differential diagnosis should be a HGT of SC, which was described previously in salivary gland SCs [13]. HGT is defined as the presence of a transformed area lacking the original line of differentiation, consisting of poorly differentiated adenocarcinoma or carcinoma with high-grade features (high mitotic activity and/or necrosis), within an otherwise well-defined, conventional low-grade component characterized by specific microscopic and immunohistochemical features of the particular salivary gland tumor [14]. In contrast to the HGT of SC, no areas with typical SC morphology were identified in our cases. Even though a complete overgrowth of the typical low-grade SC areas by the component with high-grade morphology is possible, this interpretation is unlikely because of the p40/p63 immunoexpression which is not a feature of the high-grade component of SC with HGT. It is therefore more plausible to classify the two cases presented herein as sinonasal high-grade non-ITAC with *ETV6::NTRK3* fusion, analogous to the previously characterized low-grade non-ITACs with this genetic aberration [15–17]. In addition to the analogous morphology and genetic background, these tumors also show a similar immunohistochemical profile. The low-grade tumors are positive for both S-100 and SOX10 or at least one of these markers in the case reported by Rooper et al. [16]. Cytokeratin 7 was positive in all cases. In addition, mammaglobin was negative or showed only focal staining, while GATA3 displayed focal staining in 1/3 cases tested. Conversely, some differences between the low-grade cases reported previously and the high-grade cases presented herein were noted: DOG1 was positive in all of the low-grade cases, but in our study, it showed only limited positivity in one of the two high-grade cases. GATA3 was negative in 2/3 analyzed cases. The markers p40/p63 were tested in only one low-grade case and were negative [16].

Notably, given the tubular and/or cystopapillary architecture and the immunoprofile with S-100, SOX10, and limited DOG1 positivity, origin in the minor salivary glands of the sinonasal tract could be considered in the cases presented herein, as well as the low-grade non-ITAC cases with *ETV6* rearrangement reported previously [15–17], and the tumors could instead be designated "seromucinous salivary gland adenocarcinoma," perhaps specific for the sinonasal tract. However, such an entity was not included in the current WHO Classification of Tumors, while at present, our cases correspond to the recognized entity of non-ITAC [1]. Further studies may contribute to defining this unit and separating it from the group of non-ITAC.

High-grade adenocarcinoma with similar morphology and an *ETV6::NTRK3* fusion, arising in the parotid gland of a 22-year-old male patient, was reported recently [19]. The tumor exhibited infiltrative solid-papillary and focally glomeruloid patterns of growth, consisting of large, atypical cells with high mitotic activity and areas of necrosis. Similar to our cases, the tumor cells were diffusely positive for MUC4 and GATA3, while exhibiting focal S100 and panTrk staining. The cell nests were focally lined with CK5/6 and p40 immunopositive abluminal cells. In addition, single cells were positive for androgen receptors, whereas mammaglobin and Her2 were negative. After undergoing surgical removal of the tumor and neck lymph node dissection, the short follow-up period of the patient was uneventful. Even though the morphological features and sparse AR immunopositivity were suggestive of salivary duct carcinoma, the tumor was finally diagnosed as high-grade secretory carcinoma, given its localization in the parotid gland, MUC4 and S100 expression, papillary-cystic morphology, and molecular profile [19].

In the same line, a high-grade salivary gland tumor composed of expansile, centrally necrotic nests composed of AR-positive and S100-negative apocrine-type cells with an *ETV6::NTRK3* fusion was recently interpreted as salivary duct carcinoma with an unusual genetic background [20]. This finding is clinically highly relevant, given the poor prognosis and limited treatment options for the entity.

In addition, tumors of a similar morphology, with solid, focally necrotic, as well as micropapillary and cribriform areas, can be noted in previous works that did not include molecular-genetic analysis [22, 23]. However, the morphologically similar tumors showing the poorly differentiated/undifferentiated phenotype reported by Stelow et al. [23] had an immunophenotype somewhat different from our cases: S-100 was negative, and only one of the two tested tumors was positive for CK7, while p63 expression was not tested in this study. Interestingly, some of the high-grade cases reported by Purgina et al. [22] showed a so-called seromucinous immunophenotype, i.e., the expression of at least one of the markers S-100, SOX10, and DOG1, thus approaching the subgroup of *ETV6*-rearranged non-ITACs discussed above.

In summary, we report 2 cases of a high-grade tumor diagnosed as non-ITAC of the sinonasal region, characterized by overt hypercellularity, largely solid growth pattern with comedo-like necrosis, immunohistochemical positivity for p40/p63, S100, SOX10, and GATA3, with a recurrent *ETV6::NTRK3* fusion. Even though they share a common *ETV6::NTRK3* fusion, these high-grade adenocarcinomas might represent a neoplasm distinct from SC by morphology and immunoprofile.

Data Availability Data supporting the findings of this study are available within the article. The complete datasets generated during and/or analyzed during the current study are available from the corresponding author upon reasonable request.

Code availability Not applicable.

Declarations

Ethics approval The study was approved by the Institutional Review Board of the Faculty of Medicine in Pilsen, Charles University. The procedures used in this study adhere to the tenets of the Declaration of Helsinki.

Consent to participate No patient consent was required for this study.

Conflict of interest The authors declare no competing interests.

References

1. Thompson LDR, Loney EL, Bishop JA et al (2022) Chapter 2: Nasal, paranasal, and skull base tumours. In: WHO Classification of Tumours Editorial Board. Head and neck tumours. [Internet; beta version ahead of print]. International Agency for Research on Cancer, Lyon (France) [cited 2023 May 8]. (WHO classification of tumours series, 5th ed.; vol. 9). Available from: https://tumourclassification.iarc.who.int/chapters/52/1

2. Agaimy A (2023) SWI/SNF-deficient sinonasal carcinomas. Adv Anat Pathol 30(2):95–103

3. French CA (2010) NUT midline carcinoma. Cancer Genet Cytogenet 203(1):16–20

4. Dogan S, Chute DJ, Xu B et al (2017) Frequent IDH2 R172 mutations in undifferentiated and poorly-differentiated sinonasal carcinomas. J Pathol 242(4):400–408

5. Mito JK, Bishop JA, Sadow PM et al (2018) Immunohistochemical detection and molecular characterization of IDH-mutant sinonasal undifferentiated carcinomas. Am J Surg Pathol 42(8):1067–1075

6. Leivo I (2007) Update on sinonasal adenocarcinoma: classification and advances in immunophenotype and molecular genetic make-up. Head Neck Pathol 1(1):38–43

7. Brayer KJ, Frerich CA, Kang H, Ness SA (2016) Recurrent fusions in MYB and MYBL1 define a common, transcription factor-driven oncogenic pathway in salivary gland adenoid cystic carcinoma. Cancer Discov 6(2):176–187

8. Mitani Y, Liu B, Rao PH et al (2016) Novel MYBL1 gene rearrangements with recurrent MYBL1-NFIB fusions in salivary adenoid cystic carcinomas lacking t(6;9) translocations. Clin Cancer Res 22(3):725–733

9. Okumura Y, Nakano S, Murase T et al (2020) Prognostic impact of CRTC1/3-MAML2 fusions in salivary gland mucoepidermoid carcinoma: a multiinstitutional retrospective study. Cancer Sci 111(11):4195–4204

10. Haller F, Bieg M, Will R et al (2019) Enhancer hijacking activates oncogenic transcription factor NR4A3 in acinic cell carcinomas of the salivary glands. Nat Commun 10(1):368

11. Skálová A, Vanecek T, Sima R et al (2010) Mammary analogue secretory carcinoma of salivary glands, containing the ETV6-NTRK3 fusion gene: a hitherto undescribed salivary gland tumor entity. Am J Surg Pathol 34(5):599–608

12. Baneckova M, Agaimy A, Andreasen S et al (2018) Mammary analog secretory carcinoma of the nasal cavity: characterization of 2 cases and their distinction from other low-grade sinonasal adenocarcinomas. Am J Surg Pathol 42(6):735–743

13. Skálová A, Vanecek T, Majewska H et al (2014) Mammary analogue secretory carcinoma of salivary glands with high-grade transformation: report of 3 cases with the ETV6-NTRK3 gene fusion and analysis of TP53, β-catenin, EGFR, and CCND1 genes. Am J Surg Pathol 38(1):23–33

14. Skalova A, Leivo I, Hellquist H et al (2021) High-grade transformation/dedifferentiation in salivary gland carcinomas: occurrence across subtypes and clinical significance. Adv Anat Pathol 28(3):107–118

15. Andreasen S, Skálová A, Agaimy A et al (2017) ETV6 gene rearrangements characterize a morphologically distinct subset of sinonasal low-grade non-intestinal-type adenocarcinoma: a novel translocation-associated carcinoma restricted to the sinonasal tract. Am J Surg Pathol 41(11):1552–1560

16. Rooper LM, Thompson LDR, Gagan J et al (2022) Low-grade non-intestinal-type sinonasal adenocarcinoma: a histologically distinctive but molecularly heterogeneous entity. Mod Pathol 35(9):1160–1167

17. Andreasen S, Kiss K, Melchior LC, Laco J (2018) The ETV6-RET gene fusion is found in ETV6-rearranged low-grade sinonasal adenocarcinoma without NTRK3 involvement. Am J Surg Pathol 42(7):985–988

18. Kishikawa S, Hayashi T, Shimizu J et al (2022) Low-grade tracheal adenocarcinoma with ETV6::NTRK3 fusion: unique morphology akin to subsets of sinonasal low-grade non-intestinal-type adenocarcinoma. Virchows Arch 481(5):793–797

19. Rupp NJ, Nemes C, Rushing EJ, Huber GF, Freiberger SN (2021) High-grade salivary gland adenocarcinoma harboring ETV6-NTRK3 fusion: defined by morphology or molecular aberration? Head Neck Pathol 15(3):1082–1084

20. Todorovic E, Dickson BC, Weinreb I (2020) Salivary gland cancer in the era of routine next-generation sequencing. Head Neck Pathol 14:311–320

21. Lanic MD, Guérin R, Wassef M et al (2023) Detection of salivary gland and sinonasal fusions by a next-generation sequencing based, ligation-dependent, multiplex RT-PCR assay [published online ahead of print, 2023 Jun 22]. Histopathology. https://doi.org/10.1111/his.14971

22. Purgina B, Bastaki JM, Duvvuri U, Seethala RR (2015) A subset of sinonasal non-intestinal type adenocarcinomas are truly seromucinous adenocarcinomas: a morphologic and immunophenotypic assessment and description of a novel pitfall. Head Neck Pathol 9(4):436–446

23. Stelow EB, Jo VY, Mills SE, Carlson DL (2011) A histologic and immunohistochemical study describing the diversity of tumors classified as sinonasal high-grade nonintestinal adenocarcinomas. Am J Surg Pathol 35(7):971–980

🖄 Springer

4.4 SMARCB1-deficient sinonasal adenocarcinoma: a rare variant of SWI/SNF-deficient malignancy often misclassified as high-grade non-intestinal-type sinonasal adenocarcinoma or myoepithelialcarcinoma

SMARCB1-deficientní sinonasální adenokarcinom je velmi vzácný vysoce agresivní tumor, řazený v současné WHO klasifikaci nádorů hlavy a krku mezi karcinomy s deficitem funkce chromatin-remodelujícího proteinového komplexu SWI/SNF (4). V práci je předložena podrobná analýza 14 případů SMARCB1-deficientního adenokarcinomu.

Pacienti byli dospělí středního až vyššího věku. Nádory byly v 7 případech lokalizovány v dutině nosní, v 6 případech rostly primárně v paranasálních sinusech, v 1 případě nebyla lokalizace blíže specifikována. Ve většině případů měli pacienti v době diagnózy lokálně značně pokročilé onemocnění (T4), někdy s infiltrací orbity a baze lební, jeden pacient měl již vzdálené metastázy. V 11 případech byli postiženi pacienti mužského pohlaví. Ačkoli byli pacienti léčeni intenzivními léčebnými režimy sestávajícími z variabilně rozsáhlého chirurgického zákroku a chemoradioterapie, u žádného z pacientů s dostupnými daty nebylo dosaženo remise onemocnění, 62,5 % pacientů zemřelo v důsledku lokálně pokročilého a/nebo metastazujícího tumoru, většina do 1 roku od diagnózy.

Nádory vykazovaly převážně solidní trabekulární a alveolární architekturu, ve všech případech byly přítomny variabilně početné žlázové struktury s mikroglandulární, acinární, trabekulární, kribriformní a insulární úpravou. V 6 případech byla pozorována diferenciace připomínající tumor ze žloutkového váčku s retikulární a mikrocystickou architekturou a strukturami odpovídajícími Schiller-Duvalovým tělískům. Nádorové buňky měly většinou plasmacytoidní, rhabdoidní a onkocytoidní vzhled s relativně bohatou eosinofilní cytoplazmou, ve dvou případech nabývaly spíše basaloidního vzhledu. Fokálně byla v případě 3 pozorována morfologie buněk pečetního prstene.

Všechny případy vykazovaly úplnou ztrátu imunohistochemické exprese SMARCB1, v případě 14 byla navíc detekována ztráta imunoexprese SMARCA2. Dále byly nádory pozitivní v průkazu širokospektrých cytokeratinů a CK7, v 5 případech byla pozorována fokální pozitivita p63, ve třech případech slabá fokální pozitivita synaptofyzinu a ve dvou případech slabá fokální pozitivita CDX2. V případech s morfologií tumoru ze žloutkového váčku byly pozitivní markery SALL4 nebo glypican-3.

Tumory byly dále molekulárně-geneticky vyšetřeny pomocí targetované sekvenace za použití panelů TruSight Oncology 500 a VariantPlex, delece *SMARCB1* byla rovněž v 6 případech analyzována pomocí FISH. V 9 případech se některou z použitých metod podařilo prokázat delece nebo nonsense mutace v genu *SMARCB1*. V jednom případě se nepodařilo prokázat žádné patogenní genetické změny, v jednom případě bez detekované aberace genu *SMARCB1* byla přítomna nonsense mutace genu *PAX3*.

ORIGINAL ARTICLE

SMARCB1-deficient sinonasal adenocarcinoma: a rare variant of SWI/SNF-deficient malignancy often misclassified as high-grade non-intestinal-type sinonasal adenocarcinoma or myoepithelial carcinoma

Alena Skálová[1,2] · Touraj Taheri[3] · Martina Bradová[1,2] · Tomáš Vaněček[4] · Alessandro Franchi[5] · David Slouka[6] · Tomáš Kostlivý[6] · Gisele de Rezende[7] · Jaroslav Michálek[8] · Natálie Klubíčková[1,2] · Nicola Ptáková[4] · Antónia Nemcová[9] · Michal Michal[1,2] · Abbas Agaimy[10] · Ilmo Leivo[11]

Abstract

SMARCB1-deficient sinonasal adenocarcinoma is a rare variant of SWI/SNF-deficient malignancies with SMARCB1 loss and adenocarcinoma features. More than 200 high-grade epithelial sinonasal malignancies were retrieved. A total of 14 cases exhibited complete SMARCB1 (INI1) loss and glandular differentiation. SMARCA2 and SMARCA4 were normal, except for one case with a loss of SMARCA2. Next-generation sequencing (NGS) and/or fluorescence in situ hybridization (FISH) revealed an alteration in the *SMARCB1* gene in 9/13 cases, while 2/13 were negative. Two tumors harbored *SMARCB1* mutations in c.157C > T p.(Arg53Ter) and c.842G > A p.(Trp281Ter). One harbored *ARID1B* mutations in c.1469G > A p.(Trp490Ter) and *MGA* c.3724C > T p.(Arg1242Ter). Seven tumors had a *SMARCB1* deletion. One carried an *ESR1* mutation in *c.644-2A > T*, and another carried a *POLE* mutation in c.352_374del p.(Ser118GlyfsTer78). One case had a *PAX3* mutation in c.44del p.(Gly15AlafsTer95). Histomorphology of SMARCB1-deficient adenocarcinoma was oncocytoid/rhabdoid and glandular, solid, or trabecular in 9/14 cases. Two had basaloid/blue cytoplasm and one showed focal signet ring cells. Yolk sac tumor-like differentiation with Schiller-Duval-like bodies was seen in 6/14 cases, with 2 cases showing exclusively reticular-microcystic yolk sac pattern. Follow-up of a maximum of 26 months (median 10 months) was available for 8/14 patients. Distant metastasis to the lung, liver, mediastinum, bone, and/or retroperitoneum was seen in 4/8 cases. Locoregional failure was seen in 75% of patients, with 6/8 local recurrences and 3 cervical lymph node metastases. At the last follow-up, 5 of 8 (62%) patients had died of their disease 2 to 20 months after diagnosis (median 8.2 months), and 3 were alive with the disease. The original diagnosis was usually high-grade non-intestinal-type adenocarcinoma or high-grade myoepithelial carcinoma. A correct diagnosis of these aggressive tumors could lead to improved targeted therapies with potentially better overall disease-specific survival.

Keywords SWI/SNF complex · SMARCB1-deficient adenocarcinoma · Sinonasal · Head and neck · Rhabdoid · Yolk sac-like · Next-generation sequencing

Introduction

Poorly differentiated or undifferentiated sinonasal carcinomas represent a challenging area in head and neck pathology. Over the recent years, advances in molecular techniques have led to significant progress in understanding the molecular underpinnings of sinonasal malignancies, with significant developments in the histological and pathogenetic classification of entities included in the historical spectrum of "sinonasal undifferentiated carcinoma (SNUC)" and poorly differentiated unclassified carcinoma [1]. SNUC, a diagnosis of exclusion, should be made only in cases of relatively monomorphic, sometimes basaloid-looking, high-grade/poorly differentiated tumor cells with evidence of epithelial origin and the absence

---

Abbas Agaimy and Ilmo Leivo are senior authors of this manuscript and contributed equally to this work.

Extended author information available on the last page of the article

🖂 Springer

of features pointing toward other entities. Recently, up to 80% of SNUC cases were reported to harbor hotspot mutations in the *IDH2* gene [2, 3], while mutations in the *IDH1* gene have been reported only rarely [3]. Another novel entity with a very poor prognosis is NUT carcinoma, composed of undifferentiated primitive cells with irregular overlapping nuclei with prominent nucleoli and defined by pathogenic fusions of the *NUTM1* gene, most commonly *NUTM1::BRD4* [4].

Recent molecular-genetic findings have aided in subclassifying primary sinonasal carcinomas, prompting the inclusion of several new entities in the 5th edition of the *WHO Classification of Head and Neck Tumors* [5]. A major change has been the recognition of subtypes of carcinomas defined by genetic defects leading to the inactivation of different protein subunits in the switch/sucrose nonfermentable (SWI/SNF) chromatin remodeling complex [6]. This led to the identification of 4 sinonasal entities driven by SWI/SNF deficiency complexes: SMARCB1 (INI1)-deficient sinonasal carcinoma (lacking gland formation and frequently displaying a non-descript basaloid and less frequently eosinophilic/oncocytoid morphology), SMARCB1-deficient sinonasal adenocarcinoma with unequivocal glands or yolk sac-like pattern, SMARCA4-deficient carcinoma lacking glandular or squamous immunophenotypes, and SMARCA4-deficient subset (~ 80%) of sinonasal teratocarcinosarcoma [6]. The most common of these four, the SMARCB1 (INI-1)-deficient sinonasal carcinoma, is an aggressive tumor that was first reported in 2014 independently by two research groups [7, 8]. It is a rare form of cancer arising in the nasal cavity and paranasal sinuses, and it is characterized by the loss or inactivation of the SWI/SNF-complex genes that play crucial roles in the regulation of cell growth and division [9].

Primary sinonasal adenocarcinomas (SNAC) are rare tumors encompassing a wide morphological spectrum. They are divided into three groups: intestinal-type sinonasal adenocarcinoma (ITAC), non-intestinal-type sinonasal adenocarcinoma (non-ITAC), and adenocarcinomas of salivary gland subtypes [10]. The classification of SNAC has developed in the last two decades [11]. High-grade non-intestinal SNACs are particularly heterogeneous, with highly variable morphology [12] including several molecularly defined new entities [13, 14].

SMARCB1-deficient sinonasal adenocarcinoma is a rare SWI/SNF-deficient malignancy defined by the presence of unequivocal glandular differentiation and/or by the presence of other features of adenocarcinoma [15]. Glandular differentiation has been very rarely reported in SMARCB1 (INI-1)-deficient sinonasal carcinomas, although it is possible that this feature has been underrecognized [16–19]. The tumors are usually composed of oncocytoid/plasmacytoid tumor cells in rounded nests, trabeculae, reticular, microcystic, and glandular patterns and could be misdiagnosed as high-grade non-intestinal adenocarcinoma, myoepithelial carcinoma, or even metastatic yolk sac tumor [20].

The use of next-generation sequencing platforms in clinical practice has allowed for further subclassification of tumors previously grouped together. The discovery of a subset of tumors with several unique molecular features has opened up the door to potential therapeutic targets [21]. These targetable subsets include not only NUT carcinoma [22] and SNUC with a novel isocitrate dehydrogenase (IDH) mutation [23] but also SWI/SNF-deficient sinonasal malignancies [24]. We aim to summarize our experience with a subset of SWI/SNF-deficient sinonasal adenocarcinomas diagnosed in three major consult centers in head and neck pathology (AS, AA, and AF).

Materials and methods

Case selection

In their consultation practice, two of the authors (AA and AS) encountered cases of sinonasal undifferentiated malignancies reminiscent of salivary myoepithelial carcinoma or high-grade sinonasal non-ITAC that showed a complete loss of *SMARCB1* immunoexpression. Indeed, some of these cases were submitted for consultation with a diagnosis of sinonasal myoepithelial carcinoma or high-grade sinonasal non-ITAC, and a diagnosis of SMARCB1-deficient adenocarcinoma was not raised by the primary pathologist. These consult cases prompted us to perform a computer search of our routine and consult files for high-grade sinonasal non-ITAC carcinomas and SNUCs. Seventy-five and one hundred thirty high-grade malignant tumors of sinonasal localization with epithelial features and available tissue material were retrieved from the authors' files, respectively (AS and AA). All cases were evaluated morphologically and examined immunohistochemically (IHC) by cytokeratin cocktail AE1-AE3 antibodies and antibodies to CK7, CK5/6, p63/p40, SOX10, S100, SALL4, glypican-3, and SWI/SNF proteins (Table 1). Next-generation sequencing (NGS) using the Illumina Oncology TS500 and TST170 DNA panels was performed in 44 cases, including 9 cases that demonstrated loss of SWI/SNF proteins by immunohistochemistry (AS) and 4 cases (AA). The latter cases were subjected to selected immunohistochemical and molecular studies (Table 2).

Histological and immunohistochemical studies

For conventional microscopy, the excised tissues were fixed in formalin, processed routinely, embedded in paraffin (FFPE), cut, and stained with hematoxylin and eosin.

For immunohistochemistry, 4-µm-thick sections were cut from paraffin blocks and mounted on positively charged

Table 1 Antibodies used for immunohistochemical study

Antibody specificity	Clone	Dilution	Antigen retrieval/time	Source
AE1/3	AE1/AE3 + PCK26	RTU	CC1/20 min	Ventana
CK7	OV-TL 12/30	RTU	EnVision High pH/30 min	Dako
CK5/6	D5/16B4	1:50	EnVision High pH/30 min	Dako
p63	DAK-p63	RTU	EnVision Low pH/30 min	Dako
p40	BC28	RTU	CC1/52 min	Biocare Medical
SOX 10	SP267	RTU	CC1/64 min	Cell Marque
S100	Polyclonal	RTU	EnVision High pH/30 min	Dako
CDX2	EPR2764Y	RTU	CC1/64 min	Cell Marque
CK20	Ks20.8	1:100	CC1/36 min	DakoCytomation
MIB1	30–9	RTU	CC1/64 min	Ventana
SALL4	6E3	1:800	CC1/64 min	Sigma-Aldrich
Glypican-3	GC33	RTU	CC1/52 min	Ventana
SMARCA2	Polyclonal	1:200	CC2/56 min	Atlas Antibodies AB
SMARCA4	EPNCIR111A	1:1000	CC1/52 min	Abcam
SMARCB1	MRQ-27	RTU	CC1/52 min	Ventana

RTU, ready to use; *CC1*, EDTA buffer pH 8.6 at 95 °C; *EnVision High*, pH 9.0 at 97 °C; *EnVision Low*, pH 6.0 at 97 °C; *min*, minutes

slides (TOMO, Matsunami Glass IND, Osaka, Japan). Sections were processed on a BenchMark ULTRA (Ventana Medical Systems, Tucson, AZ), deparaffinized, and subjected to heat-induced epitope retrieval by immersion in a CC1 solution (pH 8.6) at 95 °C. All primary antibodies used in this study are summarized in Table 1.

Visualization was performed using the ultraView Universal DAB Detection Kit (Roche, Tucson, AZ) and the ultraView Universal Alkaline Phosphatase Red Detection Kit (Roche, Tucson, AZ). The slides were counterstained with Mayer's hematoxylin. Appropriate positive and negative controls were employed.

Molecular studies

TruSight Oncology 500 Kit (TS500)

Mutation analysis and fusion transcript detection were performed using the TruSight Oncology 500 Kit (Illumina, San Diego, CA). RNA was extracted using the Maxwell RSC DNA FFPE Kit and the Maxwell RSC Instrument (Promega, Madison, WI) according to the manufacturer's instructions and quantified using the Qubit HS RNA Assay Kit (Thermo Fisher Scientific, Waltham, MA). DNA was extracted using the QIAsymphony DSP DNA mini (Qiagen, Hilden, Germany) and quantified using the Qubit BR DNA Assay Kit (Thermo Fisher Scientific, Waltham, MA). The quality of DNA was assessed using the FFPE QC kit (Illumina) and the quality of RNA using the Agilent RNA ScreenTape Assay (Agilent, Santa Clara, CA). DNA samples with Cq < 5 and RNA samples with DV200 ≥ 20 were used for further analysis. After DNA enzymatic fragmentation

with the KAPAFrag Kit (KAPA Biosystems, Wilmington, MA), DNA and RNA libraries were prepared with the TruSight Oncology 500 Kit (Illumina) according to the manufacturer's protocol. Sequencing was performed on the NovaSeq 6000 sequencer (Illumina) following the manufacturer's recommendations. Data analysis was performed using the TruSight Oncology 500 v2.2 Local App (Illumina). Variant annotation and filtering were performed using the Omnomics NGS analysis software (Euformatics, Espoo, Finland). A custom variant filter was set up including only non-synonymous variants with coding consequences, read depth greater than 50, and benign variants according to the ClinVar database [25] were also excluded. The remaining subset of variants was checked visually, and suspected artefactual variants were excluded.

VariantPlex Kit (VST)

DNA was extracted using the Qiasymphony DSP DNA mini (Qiagen, Hilden, Germany), and input DNA clean-up was performed using the Archer PreSeq™ DNA QC Assay Protocol. DNA was quantified using the Qubit HS DNA Assay Kit (Thermo Fisher Scientific, Waltham, MA, USA). The Archer VariantPlex Solid Tumor Kit was used (VST, ArcherDX Inc., Boulder, CO). Library preparation was performed following the Archer VariantPlex™ Protocol for Illumina (ArcherDx) and the product Insert VariantPlex™ Solid Tumor Panel. Final libraries were diluted 1:100,000 and quantified following the Library Quantification for Illumina (KAPA Biosystems, Wilmington, MA), normalized, and pooled. The libraries were sequenced on NovaSeq 6000 (Illumina) following the manufacturer's recommendations. Variant annotation and

Table 2 Clinicopathological and molecular features of SMARCB1-deficient sinonasal adenocarcinomas, Pilsen (case 1–9); Erlangen (cases 10–14)

No	Age/sex	Site	Original diagnosis	Glandular pattern (% of glandular component)	Non-glandular pattern; predominant histology	IHC +	IHC −	Molecular analysis
1	66M	Nasal cavity	Squamous cell carcinoma; HGT of acinic cell carcinoma	Oncocytoid, plasmacytoid, clear cells, abortive glandular (20%), tubular (10%)	Eosinophilic, oncocytoid; solid alveolar	AE1/AE3, CK7, EMA	CK20, CDX2, SOX10, S100, GATA3, NUT, p16 Glypican-3; SALL4	TSO500: SMARCB1 c.157C>T p.(Arg53Ter), ARID1B c.1469G>A p.(Trp490Ter), MGA c.3724C>T p.(Arg1242Ter) FISH SMARCB1: not done
2	62M	Ethmoid sinus	SNUC; HG non-ITAC	Abortive glandular (70%)	Rhabdoid, oncocytoid; solid alveolar	AE1/AE3, CK7, EMA	CK20, CDX2, SOX10, S100, GATA3, NUT, AR, desmin, MyoD1 Glypican-3; SALL4	TSO500: SMARCB1 c.842G>A, p.(Trp281Ter) FISH SMARCB1: not done
3	39M	Nasal cavity	SNUC; HG myoepithelial ca	Dyscohesive pattern, signet ring cell, large eosinophilic oncocytoid (60%)	Rhabdoid, solid alveolar	AE1/AE3, CK7, CK19, EMA, wk. p63	CK20, CDX2, AR, SOX10, S100, synaptophysin Glypican-3; SALL4	Not analyzable*
4	55M	Nasal cavity	HG myoepithelial ca	Oncocytoid glandular (10%)	Eosinophilic, solid	AE1/AE3, OSCAR, CK7, wk. synaptophysin Glypican-3	CK14, CK20, CDX2, S100; SALL4 Chromogranin, CK5/6, p16, myogenin, MyoD1, SOX10, CD56, CD99	Not analyzable*
5	66M	Nasal cavity	SMARCB1-deficient adenocarcinoma	Yolk sac-like structures with Schiller-Duval-like bodies (90%)	Basaloid to eosinophilic, solid	Glypican-3, wk. CDX2, AE1-AE3, OSCAR, CAM.5.2	SALL4, NUT, p16	TSO500: SMARCB1 heterozygous deletion, ESR1 c.644-2A>T FISH SMARCB1: heterozygous deletion**
6	36M	Nasal cavity	HG ITAC	Yolk sac-like structures with Schiller-Duval-like bodies (85%), abortive glandular (5%)	Eosinophilic, solid	Glypican-3; SALL-4; AE1-AE3; wk. CDX2	CK7; CK20	TSO500: SMARCB1 heterozygous deletion FISH SMARCB1: homozygous deletion***
7	Xx/M	Nasal cavity	Unclassified carcinoma; HG myoepithelial ca	Oncocytoid; glandular (10%), abortive glandular (60%)	Eosinophilic, rhabdoid, oncocytoid; solid trabecular, clear cell	AE1/AE3, OSCAR, CK7, CK19, p63	Glypican-3; SALL4; p40, p16, SOX10	TSO500: negative FISH SMARCB1: negative
8	46M	Maxillary sinus	SMARCB1-deficient adenocarcinoma	Yolk sac-like structures with Schiller-Duval-like bodies (70%), glandular (10%)	Basaloid, rhabdoid, solid alveolar	P63, OSCAR, CK5/6, CK7, glypican-3	S100, desmin, synaptophysin, NUT, SOX10, p16, SALL-4	VST: SMARCB1 heterozygous deletion FISH SMARCB1: not analyzable

Table 2 (continued)

No	Age/sex	Site	Original diagnosis	Glandular pattern (% of glandular component)	Non-glandular pattern; predominant histology	IHC +	IHC −	Molecular analysis
9	52/M	Nasal cavity	SNUC; HG myoepithelial ca	Cribriform with minor lumens (20%)	Oncocytoid, eosinophilic, solid, clear cell	CK7, wk. p63, AE1-AE3,	S100, CK14, SOX10, p16, NUT, glypican-3; SALL4; INSM1, CD56	TSO500: not analyzable FISH SMARCB1: heterozygous deletion
10	62/M	Sinonasal site NOS	Carcinoma with INi1 loss	Abortive glandular with mucin	Eosinophilic, oncocytoid; solid areas	AE1/AE3, CK7, wk. synaptophysin	CK5/6, SALL4, S100, SOX10, AFP HepPar1, glypican-3, CK20, CDX2, p40	TS500: PAX3 c.44del p.(Gly15AlafsTer95) FISH SMARCB1: not done
11	76/F	Paranasal sinus right	Unclassified carcinoma	Pure reticular-microcystic yolk sac pattern		AE1/AE3, SALL4 & glypican-3 diffuse, focal p63, CK7, EMA & AFP	CD34, CD117, ERG, ALK, NUT, SOX10	TS500: SMARCB1 homozygous deletion, POLE c.352_374del p.(Ser118GlyfsTer78) FISH SMARCB1: not done
12	59/M	Sinuses left	SNUC or NUT carcinoma	Oncocytoid abortive glandular	Eosinophilic, trabecular	p63, AE1/AE3, focal CK5/6, wk. synaptophysin	CD34, CD117, CK7, CDX2, CD56, NUT, SOX10	TS500: SMARCB1 homozygous deletion FISH SMARCB1: homozygous deletion
13	NA	Sinonasal site NOS	HG non-ITAC	Abortive glandular	Solid, large cells	AE1/AE3 diffuse, CK7 variable, p63 focal	AR, S100, SOX10	TS500: not done FISH SMARCB1: not done
14	55/F	Nasal cavity + sinuses	Unclassified carcinoma	Reticular-myxoid, cribriform		AE1/AE3, SALL4	AFP	TS500: SMARCB1 homozygous deletion FISH SMARCB1: homozygous deletion

Ca, carcinoma; F, female; FISH, fluorescence in situ hybridization; HG, high grade; HGT, high-grade transformation; ITAC, intestinal type adenocarcinoma; M, male; meta, metastasis; mo, month; NA, not analyzable; ND, not done; NED, no evidence of disease; NOS, nor otherwise specified; SNUC, sinonasal undifferentiated carcinoma; wk, weak and/or focal staining; TSO500, TruSight Oncology 500; VST, VariantPlex Solid Tumor Panel; FISH—SMARCB1 enumeration

*Not analyzable by all mentioned methods. **Atypical FISH pattern—susp. partial deletion of SMARCB1 gene. ***Mix of tumor and non-tumor tissue (FISH counted in tumor tissue)

filtering were performed using Archer Analysis software v7 (ArcherDx) with the parameters mentioned above.

Fluorescent in situ hybridization (FISH)

For the detection of *SMARCB1* deletion, ZytoLight® SPEC SMARCB1/22q12 Dual Color Probe was used (ZytoVision GmbH, Bremerhaven, Germany). The FISH procedure was performed as described elsewhere [26]. The heterozygous deletion was defined as one green signal (SMARCB1) compared to two orange control signals (KREMEN1), and the homozygous deletion as zero green signals (SMARCB1) compared to at least one orange control signal (KREMEN1).

Results

Demographic and clinical features

A total of 14 cases demonstrated clear morphologic evidence of glandular differentiation and loss of SMARCB1 immunoexpression, and these were included in the study (Table 2). They occurred in 11 men and 2 women with ages ranging from 36 to 92 years (mean 59 years). Clinical data were not available for one patient. The tumors arose in the nasal cavity (7), maxillary sinus (1), ethmoid sinus (1), paranasal sinus NOS (4), and sinonasal tract NOS (1). Imaging revealed extensive involvement of the paranasal sinuses with or without the involvement of the nasal cavity and frequent involvement of the skull base (Fig. 1a, b).

Of eight patients with detailed tumor staging information, six (75%) presented with stage T4 disease with extensive involvement of the bony confinements of the sinonasal cavities and variable infiltration into periorbital or skull base tissues. Synchronous regional lymph node involvement and distant metastases were detected in one patient (Table 3).

Treatment consisted of radical surgical resection combined with chemotherapy and/or radiation in eight patients.

One patient received only supportive (palliative) care after a diagnostic biopsy. For the remaining six patients, detailed information regarding therapy was not available (Table 3).

Follow-up data were available for 8 patients, and the follow-up period ranged from shortly after diagnosis to 26 months (median, 10). Distant metastases were recorded in 4 of 8 cases (50%). The sites of distant metastases included the lungs ($n=2$), the liver ($n=1$), the mediastinum ($n=2$), the bones ($n=1$), and the retroperitoneum ($n=1$). They occurred from presentation to 24 months after diagnosis (median, 10 months). Regional failure was seen in 75% of patients, with 6/8 local recurrences and 3 regional recurrences to cervical lymph nodes. At the last follow-up, 5 of 8 (62%) patients had died of their disease 2 to 20 months after diagnosis (median, 8.2 months), and 3 were alive with the disease (Table 3).

Histopathological and immunohistochemical finding

In most of the cases, tumor histomorphology was predominantly solid, with trabecular and alveolar growth patterns. The tumor cells were large with eosinophilic, oncocytoid, plasmacytoid, and/or rhabdoid appearance. In nine cases (9/14, 64%), the dominant cell morphology was oncocytoid/rhabdoid (Fig. 2a–c). However, in two cases a basaloid/blue cytoplasm was observed (Table 2 and Fig. 2d). All cases demonstrated varying proportions of glandular changes, including alveolar/acinar with abortive microglandular differentiation, trabecular, and solid/cribriform/insular patterns. A focal signet-ring cell pattern was noted in one case (Table 2 and Fig. 3a, b). Variable luminal and stromal mucin-like secretion was noted in some cases, one case with prominent myxoid stroma. Areas with yolk sac tumor-like differentiation with Schiller-Duval body-like structures were found in six cases (6/14; 43%) with two cases showing exclusively reticular-microcystic yolk sac pattern (Table 2 and Fig. 3c–e). Seven cases with high-grade malignant histomorphology and two cases with intermediate-grade
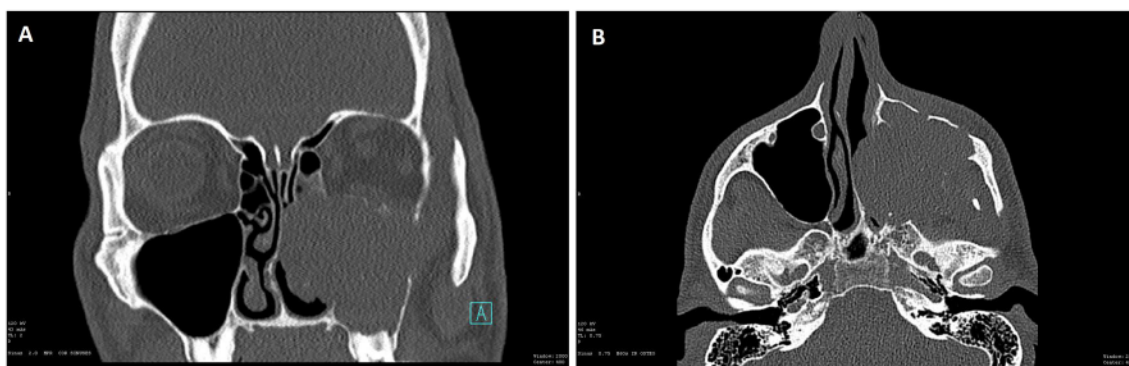

Fig. 1 SMARCB1-deficient sinonasal adenocarcinoma T3N0M0: coronal noncontrast CT scan (A) and axial noncontrast CT scan (B)

Table 3 Clinical course and follow-up of SMARCB1-deficient sinonasal adenocarcinomas, Pilsen (cases 1–9); Erlangen (cases 10–14)

No	Age/sex	Initial stage	Treatment	Clinical course (months)	Outcome/ follow-up (months)
1	66/M	pT4a, cN0, cM0	Radical surgery, CT	Recurrence (6) Cervical LN meta (6)	DOD (10)
2	62/M	pT4, cN0, cM0	No surgery, palliative RT, CT	Meta lungs (12)	DOD (20)
3	39/M	pT4, cN2, cM2	Surgery, RT, CT	Meta liver, LN, skeleton, retroperitoneum (2)	DOD (2)
4	55/M	Unknown	Unknown	Unknown	Unknown
5	66/M	pT4a, cN0, M0	Radical surgery, RT	Recurrent tumor (7)	AWD (7)
6	36/M	pT4a, cN0, M0	Surgery, RT, CT		AWD (6)
7	92/M	pT3, cN0, M0	Surgery, RT	Recurrent tumor (6)	DOD (6)
8	46/M	pT3, cN0, M0	Surgery, RT, proton	Recurrent tumor, meta lungs and mediastinum (24)	AWD (26)
9	52/M	cT4a, cNX, MX	Surgery, RT, CT	Recurrent tumor, meta cervical LN	DOD (3)
10	62/M	*	*	*	*
11	76/F	*	*	*	*
12	59/M	*	*	*	*
13	NA	*	*	*	*
14	55/F	*	*	*	*

AWD, alive with disease; *DOD*, died of disease; *CT*, chemotherapy; *F*, female; *LN*, lymph node; *M*, male; *meta*, metastasis; *NA*, not available; *NED*, no evidence of disease

*Clinical and follow-up data for cases 10–14 are not available

Fig. 2 SMARCB1-deficient sinonasal adenocarcinoma is characterized by the presence of oncocytoid/plasmacytoid cell morphology, with variable but unequivocal gland formation (**A**–**C**) defined by open glandular structures (**A**), abortive microglandular differentiation (**B**), and small nests (**C**). Less common pattern is basaloid/ blue phenotype with uniformly high-grade cytomorphology (**D**)
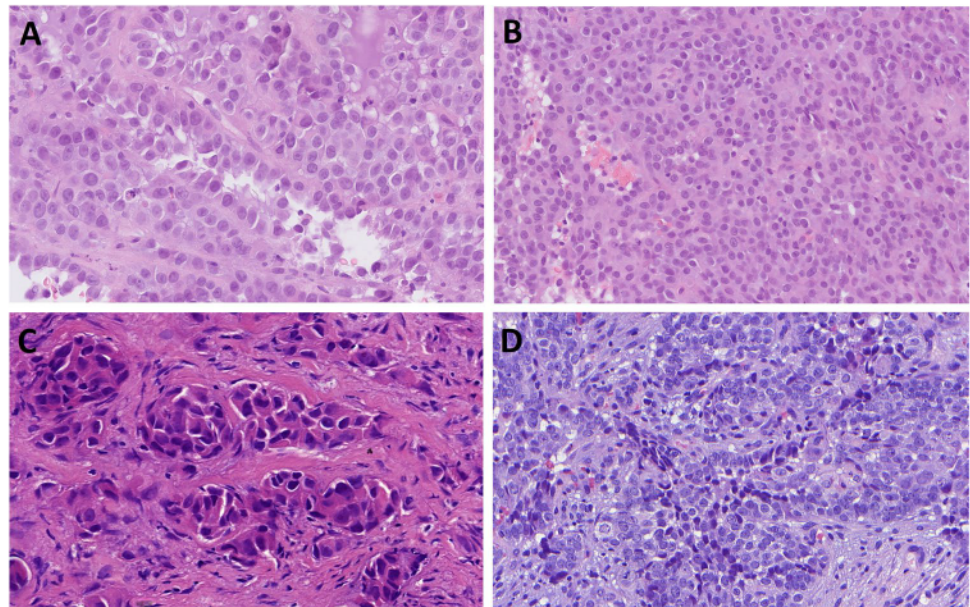
malignant histomorphology were observed (Table 2). In all cases, the Ki-67 index was high (> 40%).

In immunohistochemical stainings, all cases were completely negative for SMARCB1 (INI-1) proteins (Fig. 4a). SMARCA2 and SMARCA4 had normal patterns of expression (retained) except for case 14, which has shown SMARCA2 loss. In all cases, the neoplastic cells showed strong staining for cytokeratins AE1/AE3 and/or OSCAR (9/9), CK7 (9/9), and EMA (4/4), while S100,

SOX10, CK20, CDX2, p63, p40, GATA3, NUT, and AR were mostly negative. Proliferative activity was high, with the Ki-67 index reaching 40–80% (mean 56%) (Fig. 4b). Focal p63 staining was seen in 5 cases, CDX2 staining in 2 cases, and weak focal synaptophysin in 3 cases. Immunohistochemical markers for yolk sac tumor (SALL4 or glypican-3) decorated 6 cases (Fig. 4c–d), corresponding to their yolk sac tumor-like histologies.

Springer

Fig. 3 Cribriform structures may be present in solid areas (**A**), and focal signet-ring cell pattern was noted in one case (**B**). Fibrous stroma with intermingled glands with a sieve-like morphology or floating tumor cell strips embedded within mucoid stroma was present in two cases (**C**) along with structures resembling the Schiller-Duval bodies. (**D**) Two cases showing exclusively reticular-microcystic yolk sac pattern (**E**) positive for SALL4 (inset)
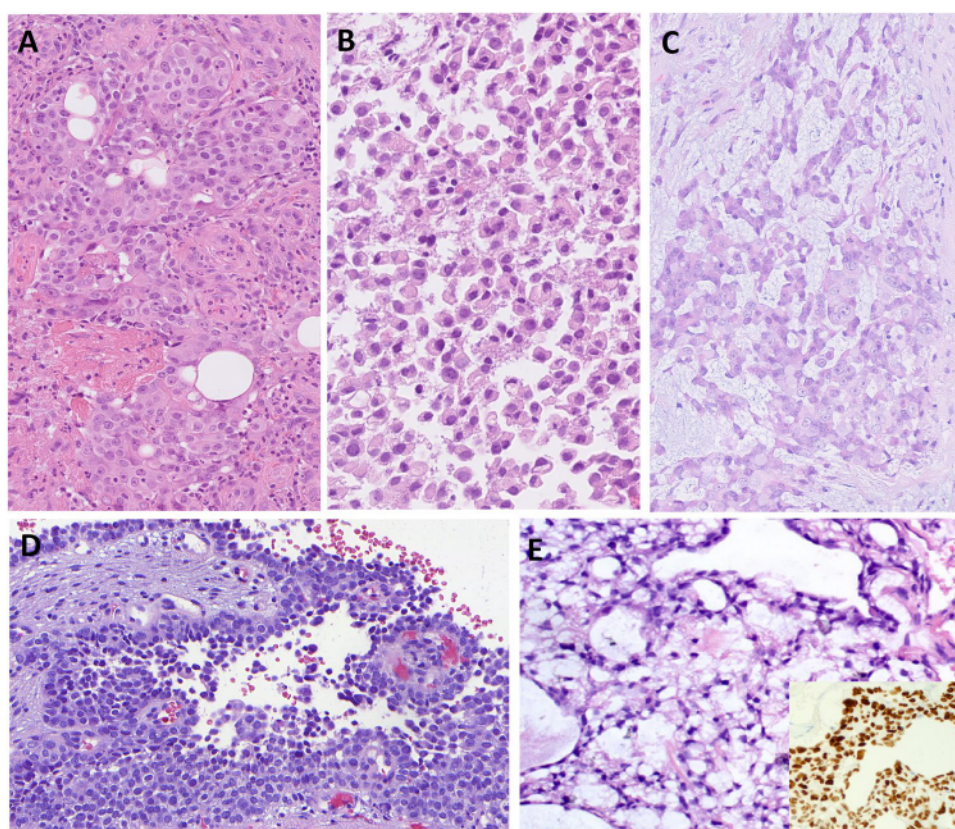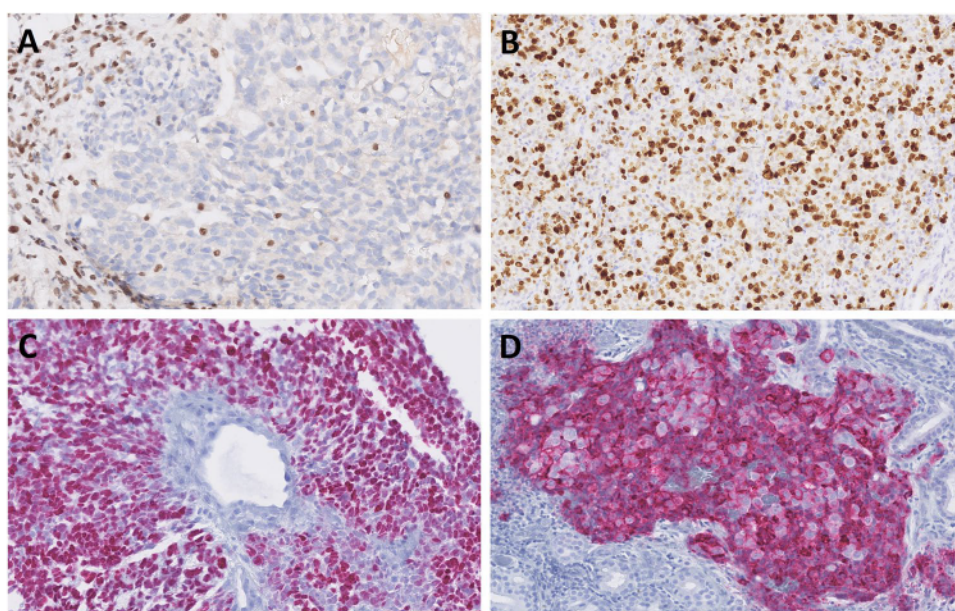

Fig. 4 Representative example of complete loss of SMARCB1 immunohistochemistry in tumor cells with positive internal control in lymphocytes and fibroblasts (**A**). Proliferative activity was high with Ki-67 > 40% (**B**). Germ cell markers of yolk sac-like differentiation, SALL4 (**C**) and glypican-3 (**D**) highlighted 6 cases

Molecular findings

Next-generation sequencing (NGS) and/or fluorescence in situ hybridization (FISH) revealed alteration in the *SMARCB1* gene in nine cases (9/13, 69%), while two cases were negative and two cases were not analyzable. In one case, molecular analysis was not done. (Table 2). Among the positive cases, two had nonsense mutations truncating the *SMARCB1* gene, namely *SMARCB1* c.157C > T p.(Arg53Ter) and c.842G > A, p.(Trp281Ter). Seven cases had deletions in the *SMARCB1* gene detected by NGS or FISH. One case was negative for both SNV and CNV

analysis by NGS and also negative for *SMARCB1* deletion by FISH. Another one was negative for SNV and CNV by NGS only. In addition, one of these tumors harbored mutations in genes *ARID1B* c.1469G > A p.(Trp490Ter) and *MGA* c.3724C > T p.(Arg1242Ter); another case had a splicing mutation in the *ESR1* gene c.644-2A > T and the other had a mutation in gene *POLE* c.352_374del p.(Ser118GlyfsTer78). In addition, in one case, there was a mutation in the gene *PAX3* c.44del p.(Gly15AlafsTer95). The complete results of molecular testing are illustrated in Table 2.

Discussion

SWI/SNF (switching/sucrose non-fermentable) genes were first described in *Saccharomyces* yeast in 1984 as genes required to enable mating-type switching and sucrose metabolism [27]. In the process of evolution from yeast to mammals, the SWI/SNF complex (aka BAF complex) has evolved into a large ATP-dependent chromatin remodeling complex with many subunits encoded by a variety of genes with a markedly heterogeneous structure and function. Due to the tumor suppressor role of this complex, somatic mutations in SWI/SNF genes are involved in the tumorigenesis of multiple human neoplasms [28, 29]. Other tumor suppressor genes, such as *RB1*, *TP53*, *MYC*, and *BRCA1*, are known to interact with the SWI/SNF complex, and therefore mutations in these partner genes can affect its function and increase cell proliferation [28–31]. Up to 25% of human cancers carry mutations in at least one of nine SWI/SNF subunit genes including *SMARCA1* and *2*, *SMARCB1*, *ARID1A/B*, *PBRM1*, and *ARID2* [32].

SMARCB1 (SWI/SNF-related, matrix-associated, actin-dependent regulator of chromatin, subfamily b, member 1) is also known as INI1 (for integrase interactor 1) and SNF5, the latter of which was initially named based on a conserved region of this protein in the SWI/SNF complex in yeast [33]. *SMARCB1*, located on chromosome 22q11.2, functions as a tumor suppressor gene. Mutations in the *SMARCB1* gene were first described in rhabdoid tumors in 1998, evidencing for the first time the link between the SWI/SNF complex and human cancer [33]. *SMARCB1* mutations have been implicated in the pathogenesis of several malignancies, including atypical teratoid rhabdoid tumor, malignant rhabdoid tumor, epithelioid sarcoma, renal medullary carcinoma, myoepithelial carcinoma, epithelioid malignant peripheral nerve sheath tumor, and extraskeletal myxoid chondrosarcoma [8]. Although these diverse neoplasms exhibit many distinct clinicopathologic features, they all tend to share the presence of "rhabdoid" cells, defined as large cells with abundant eosinophilic cytoplasm and eccentrically placed nuclei with open chromatin and prominent nucleoli. A meta-analysis of 10,849 patients from 15 studies found that 5% of

human cancers had alterations in SMARCB1 [34, 35, 36]. Such tumors mostly but not exclusively comprise rare, high-grade lethal cancers [32, 34].

Since the first description of malignant rhabdoid tumors in pediatric patients, various histological patterns in SWI/SNF-mutated tumors have been reported. Such tumors comprise, but are not limited to, rhabdoid eosinophilic cells, blue-basaloid cells, small cells, and clear cells, as well as glandular, sarcomatoid, yolk sac-like, and mixed histological patterns [15, 37]. A rare histologic subgroup of SWI/SNF-deficient neoplasms and the subject of our investigation is SMARCB1-deficient sinonasal adenocarcinoma defined by glandular features. In our limited series, we found that a majority of SMARCB1-deficient sinonasal adenocarcinomas exhibited a dominant eosinophilic pattern with an oncocytoid/rhabdoid appearance, followed by a solid blue-basophilic cell pattern. Glandular structures including tubular, microglandular, cribriform, solid, and signet-ring patterns were identified in all our cases, comparable to other published series also showing intracytoplasmic and intraluminal mucin confirmed by mucin staining [15]. Of interest is the finding of yolk sac tumor-like differentiation with Schiller-Duval body-like structures in 34% of our cases, with both basophilic and non-pink cell appearances.

Three potential pitfalls can be expected in the diagnosis of SMARCB1-deficient sinonasal adenocarcinoma. First, the common eosinophilic-glandular pattern of this tumor could be misclassified as a high-grade non-ITAC. Loss of immunohistochemical SMARCB1 staining, which was uniformly observed in all our cases, is an essential criterion to avoid this diagnostic error. A second differential diagnostic error could be due to the basophilic/blue glands with endometrioid/yolk sac-like structures that might be interpreted as features of ITAC. Although this misinterpretation is more likely due to the focal CK20 and CDX2 positivity seen in these cases, there was a lack of diffuse CK20/CDX2 staining, which, along with the loss of SMARCB1 staining and focal positivity for glypican-3 and/or SALL4, helped in differentiating these entities. Shah et al. also highlighted other differential diagnoses in this setting, such as extragonadal or metastatic yolk sac tumor and metastatic hepatocellular carcinoma [15]. These diagnoses could be inferred from positive staining for glypican-3 and SALL4; however, these entities are extremely rare in the sinonasal tract. Moreover, negative SMARCB1 and other germ cell markers would rule out these diagnoses. Third, the microglandular/cribriform and eosinophilic appearance of cells with focal p63 staining can be interpreted as myoepithelial differentiation. Our cases were entirely negative for S100 and SOX10, which, in combination with SMARCB1, negativity excludes myoepithelial carcinoma.

SWI/SNF-deficient malignancies pursue a highly aggressive clinical course, resulting in widespread disease dissemination either at the time of diagnosis or soon afterwards and causing the death of the patient soon after diagnosis, despite an apparently curative therapeutic intent. Systemic chemotherapy has shown no success so far [23]. To date, satisfactory systemic chemotherapy has not been established for these patients. This disappointing finding underlines the urgent need for effective systemic therapy to allow sufficient intermediate to long-term disease control. However, there are a number of scientific investigations aimed at deciphering the vulnerable molecular sites secondary to SWI/SNF mutation in these tumors [38]. Gene sequencing and molecular subgrouping of each SWI/SNF-mutated tumor will help identify a target suitable for tailored therapy [35]. Recently, SWI/SNF-deficiency has increasingly emerged as pivotal in cancer immunogenicity and hence a promising biomarker when predicting response to immune-checkpoint inhibition therapy utilizing several recently established drugs [23]. Immunotherapy targeting PDL1 [35, 39], employing the PRC2 (EZH2 subunit) inhibitor tazemetostat [15], as well as inhibitors acting against protein kinases, MYC, MDM2/4, and the proteasome are major examples of these efforts [32, 35].

Summary

In this limited series, it appears that SMARCB1-deficient SNACs show a predilection for male patients, and in contrast to non-glandular tumors, may occur with greater frequency in the nasal cavity. The original diagnosis in most cases of SMARCB1-deficient SNAC was HG non-ITAC and less frequently HG myoepithelial carcinoma or HG ITAC. Differential diagnosis is challenging, but the availability of immunohistochemical antibodies against SWI/SNF proteins represents an emerging effective tool for screening these neoplasms. For the first time, we have shown an NGS-detectable mutation in the *SMARCB1* gene in a subset of cases. Recent advances in molecular profiling have led to major updates and revisions in the classification of high-grade sinonasal carcinomas. Although the majority of these tumors are characterized by aggressive biologic behavior, the identification of these mutations could potentially lead to improved targeted therapeutic options and improved overall disease-specific survival.

Data availability Data supporting the findings of this study are available within the article. The complete datasets generated during and/or analyzed during the current study are available from the corresponding author upon reasonable request.

Code availability Not applicable.

Declarations

Ethics approval The study was approved by the institutional review board of the Faculty of Medicine in Pilsen, Charles University. The procedures used in this study adhere to the tenets of the Declaration of Helsinki.

Informed consent No patient consent was required for this study.

Conflict of interest The authors declare no competing interests.

References

1. Agaimy A, Franchi A, Lund VJ, Skálová A, Bishop JA, Triantafyllou A, Andreasen S, Gnepp DR, Hellquist H, Thompson LDR, Rinaldo A, Ferlito A (2020) Sinonasal undifferentiated carcinoma (SNUC): from an entity to morphologic pattern and back again-a historical perspective. Adv Anat Pathol 27(2):51–60

2. Dogan S, Chute DJ, Xu B et al (2017) Frequent IDH2 R172 mutations in undifferentiated and poorly-differentiated sinonasal carcinomas. J Pathol 242(4):400–408

3. Mito JK, Bishop JA, Sadow PM et al (2018) Immunohistochemical detection and molecular characterization of IDH-mutant sinonasal undifferentiated carcinomas. Am J Surg Pathol 42(8):1067–1075

4. French CA (2010) NUT midline carcinoma. Cancer Genet Cytogenet 203(1):16–20

5. Bishop JA, Thompson LDR, Loney EL (eds) (2022) Chapter 2: nasal, paranasal, and skull base tumours. In: WHO classification of tumours editorial board. Head and neck tumours. [Internet; beta version ahead of print]. Lyon (France): International Agency for Research on Cancer; [cited 2023 May 8]. (WHO classification of tumours series, 5th ed.; vol. 9). Available from: https://tumourclassification.iarc.who.int/chapters/52/1

6. Agaimy A (2023) SWI/SNF-deficient sinonasal carcinomas. Adv Anat Pathol 30(2):95–103

7. Agaimy A, Koch M, Lell M et al (2014) SMARCB1(INI1)-deficient sinonasal basaloid carcinoma: a novel member of the expanding family of SMARCB1-deficient neoplasms. Am J Surg Pathol 38:1274–1281

8. Bishop JA, Antonescu CR, Westra WH (2014) SMARCB1 (INI-1)-deficient carcinomas of the sinonasal tract. Am J Surg Pathol 38:1282–1289

9. Agaimy A, Hartmann A, Antonescu CR et al (2017) SMARCB1 (INI-1)-deficient sinonasal carcinoma: a series of 39 cases expanding the morphologic and clinicopathologic spectrum of a recently described entity. Am J Surg Pathol 41:458–471

10. Leivo I (2016) Sinonasal adenocarcinoma: update on classifcation, immunophenotype and molecular features. Head Neck Pathol 10:68–74

11. Leivo I (2007) Update on sinonasal adenocarcinoma: classification and advances in immunophenotype and molecular genetic make-up. Head Neck Pathol 1(1):38–43

12. Stelow EB, Jo VY, Mills SE et al (2011) A histologic and immunohistochemical study describing the diversity of tumors classifed as sinonasal high-grade nonintestinal adenocarcinomas. Am J Surg Pathol 35:971–980

13. Baneckova M, Agaimy A, Andreasen S et al (2018) Mammary analog secretory carcinoma of the nasal cavity: characterization of 2 cases and their distinction from other low-grade sinonasal adenocarcinomas. Am J Surg Pathol 42(6):735–743

14. Klubíčková N, Mosaieby E, Ptáková N et al (n.d.) High-grade nonintestinal type sinonasal adenocarcinoma with ETV6::NTRK3 fusion, distinct from secretory carcinoma by immunoprofile and morphology. Virchows Arch 2023 in press

15. Shah AA, Jain D, Ababneh E, Agaimy A, Hoschar AP, Griffith CC, Magliocca KR, Wenig BM, Rooper LM, Bishop JA (2020) SMARCB1 (INI-1)-deficient adenocarcinoma of the sinonasal tract: a potentially under-recognized form of sinonasal adenocarcinoma with occasional yolk sac tumor-like features. Head Neck Pathol 14(2):465–472

16. Zamecnik M, Rychnovsky J, Syrovatka J (2018) Sinonasal SMARCB1 (INI1) deficient carcinoma with yolk sac tumor diferentiation: report of a case and comparison with INI1 expression in gonadal germ cell tumors. Int J Surg Pathol 26:245–249

17. Li CY, Han YM, Xu K et al (2021) Case report: SMARCB1 (INI-1)-deficient carcinoma of the nasal cavity with pure yolk sac tumor differentiation and elevated serum AFP levels. Onco Targets Ther 14:2227–2233

18. Hazir B, Şímsek B, Erdemír A et al (2022) Sinonasal SMARCB1 (INI1) deficient carcinoma with yolk sac tumor differentiation: a case report and treatment options. Head Neck Pathol 16:596–601

19. Ng JKM, Chan JYK, Li JJX et al (2022) SMARCB1 (INI1)-deficient sinonasal carcinoma with yolk sac differentiation showing co-loss of SMARCA4 immunostaining- a case report and literature review. Head Neck Pathol 16:934–941

20. Skalova A, Agaimy, A, Vaněček T, Klubíčková N, Kiss, K, Baneckova M, Michal M (2023) SMARCB1-deficient sinonasal adenocarcinoma: rare variant of SWI/SNF-deficient malignancy often misclassified as high-grade non-intestinal adenocarcinoma or myoepithelial carcinoma. *Laboratory Investigation*, (USCAP 2022 Abstracts: Head and Neck Pathology (1014–1081)), 1072–1073. https://doi.org/10.1016/j.labinv.2023.100092

21. Reiersen DA, Pahilan ME, Devaiah AK (2012) Meta-analysis of treatment outcomes for sinonasal undifferentiated carcinoma. Otolaryngol Head Neck Surg 147:7–14

22. French CA (2013) The importance of diagnosing NUT midline carcinoma. Head Neck Pathol 7(1):11–16

23. Alzumaili B, Sadow PM (2023) IDH2 -Mutated sinonasal tumors: a review. Adv Anat Pathol 30(2):104–111

24. Agaimy A (2023) SWI/SNF-deficient Malignancies: optimal candidates for immune-oncological therapy? Adv Anat Pathol 30(3):211–217

25. Landrum MJ, Lee JM, Benson M, Brown GR, Chao C, Chitipiralla S, Gu B, Hart J, Hoffman D, Jang W, Karapetyan K, Katz K, Liu C, Maddipatla Z, Malheiro A, McDaniel K, Ovetsky M, Riley G, Zhou G, Holmes JB, Kattman BL, Maglott DR (2018) ClinVar: improving access to variant interpretations and supporting evidence. Nucleic Acids Res 46(D1):D1062–D1067. https://doi.org/10.1093/nar/gkx1153

26. Šteiner P, Andreasen S, Grossmann P et al (2018) Prognostic significance of 1p36 locus deletion in adenoid cystic carcinoma of the salivary glands. Virchows Arch 473(4):471–480. https://doi.org/10.1007/s00428-018-2349-6

27. Stern M, Jensen R, Herskowitz I (1984) Five SWI genes are required for expression of the HO gene in yeast. J Mol Biol 178(4):853–68

28. Reddy D, Bhattacharya S, Workman JL (2023) (mis)-Targeting of SWI/SNF complex(es) in cancer. Cancer Metastasis Rev. https://doi.org/10.1007/s10555-023-10102-5

29. Li Z, Zhao J, Tang Y (2023) Advances in the role of SWI/SNF complexes in tumours. J Cell Mol Med 27:1023–1031

30. Bochar DA, Wang L, Beniya H, Kinev A, Xue Y, Lane WS, Wang W, Kashanchi F, Shiekhattar R (2000) BRCA1 is associated with a human SWI/SNF-related complex: linking chromatin remodeling to breast cancer. Cell 102(2):257–65

31. Lee D, Kim JW, Seo T, Hwang SG, Choi EJ, Choe J (2002) SWI/SNF complex interacts with tumor suppressor p53 and is necessary for the activation of p53-mediated transcription. J Biol Chem 277(25):22330–22337

32. Mittal P, Roberts CWM (2020) The SWI/SNF complex in cancer - biology, biomarkers and therapy. Nat Rev Clin Oncol 17:435–448

33. Brzeski J, Podstolski W, Olczak K, Jerzmanowski A (1999) Identification and analysis of the Arabidopsis thaliana BSH gene, a member of the SNF5 gene family. Nucleic Acids Res 27(11):2393–2399

34. Versteege I, Sévenet N, Lange J et al (1998) Truncating mutations of hSNF5/INI1 in aggressive paediatric cancer. Nature 394:203–206

35. Cooper GW, Hong AL (2022) SMARCB1-Deficient cancers: novel molecular insights and therapeutic vulnerabilities. Cancers (Basel) 14(15):3645

36. Wang N, Qin Y, Du F, Wang X, Song C (2022) Prevalence of SWI/SNF genomic alterations in cancer and association with the response to immune checkpoint inhibitors: a systematic review and meta-analysis. Gene 5(834):146638

37. Agaimy A (2022) Proceedings of the North American Society of Head and Neck Pathology, Los Angeles, CA, March 20, 2022: SWI/SNF-deficient Sinonasal Neoplasms: An Overview. Head Neck Pathol 16(1):168–178

38. Carugo A, Minelli R, Sapio L, Soeung M, Carbone F, Robinson FS, Tepper J, Chen Z, Lovisa S, Svelto M, Amin S, Srinivasan S, Del Poggetto E, Loponte S, Puca F, Dey P, Malouf GG, Su X, Li L, Lopez-Terrada D, Rakheja D, Lazar AJ, Netto GJ, Rao P, Sgambato A, Maitra A, Tripathi DN, Walker CL, Karam JA, Heffernan TP, Viale A, Roberts CWM, Msaouel P, Tannir NM, Draetta GF, Genovese G (2019) p53 is a master regulator of proteostasis in SMARCB1-deficient malignant rhabdoid tumors. Cancer Cell 35(2):204-220.e9

39. Ngo C, Postel-Vinay S (2022) Immunotherapy for SMARCB1-deficient sarcomas: current evidence and future developments. Biomedicines 10(3):650

⚫ Springer

Authors and Affiliations

Alena Skálová[1,2] · Touraj Taheri[3] · Martina Bradová[1,2] · Tomáš Vaněček[4] · Alessandro Franchi[5] · David Slouka[6] · Tomáš Kostlivý[6] · Gisele de Rezende[7] · Jaroslav Michálek[8] · Natálie Klubíčková[1,2] · Nicola Ptáková[4] · Antónia Nemcová[9] · Michal Michal[1,2] · Abbas Agaimy[10] · Ilmo Leivo[11]

✉ Alena Skálová
skalova@biopticka.cz

1 Department of Pathology, Faculty of Medicine in Pilsen, Charles University, E. Benese 13, 305 99 Pilsen, Czech Republic

2 Bioptic Laboratory, Ltd., Pilsen, Czech Republic

3 Department of Anatomical Pathology, Queensland Health, Royal Brisbane and Women Hospital, University of Queensland, Brisbane, Australia

4 Molecular and Genetic Laboratory, Bioptic Laboratory, Ltd, Pilsen, Czech Republic

5 Department of Translational Research, School of Medicine, University of Pisa, Pisa, Italy

6 Department of Otorhinolaryngology, University Hospital in Pilsen, Faculty of Medicine in Pilsen, Charles University, Pilsen, Czech Republic

7 Department of Anatomic Histopathology and Cytogenetics, Department of Laboratory Medicine, Niguarda Cancer Center, Milan, Italy

8 Department of Clinical and Molecular Pathology, University Hospital and Medical Faculty of Palacky University, Olomouc, Czech Republic

9 Pathological Laboratories, Medicyt, Ltd., Košice, Slovak Republic

10 Institute of Pathology, University Hospital Erlangen, Friedrich-Alexander University Erlangen-Nürnberg (FAU), Erlangen, Germany

11 Institute of Biomedicine, Pathology, University of Turku and Department of Pathology, Turku University Hospital, Turku, Finland

4.5 Biphenotypic sinonasal sarcoma with *PAX3::MAML3* fusion transforming into high-grade rhabdomyosarcoma: Report of an emerging rare phenomenon

V tomto case reportu popisujeme případ 67letého pacienta s BSNS dediferencujícím do high-grade rhabdomyosarkomu. Ačkoli naprostá většina BSNS má indolentní biologické chování a tedy dobrou prognózu, tato práce upozorňuje na raritní možnost transformace ve vysoce agresivní tumor.

Pacient anamnesticky prodělal 3 roky před diagnózou septoplastiku, v době jeho diagnózy klinické projevy spočívaly v obstrukci nosní dutiny a nadměrné slzivosti. Endoskopické vyšetření a MR prokázaly přítomnost infiltrativního procesu postihujícího pravostrannou dutinu nosní, frontální, ethmoidální a maxilární paranasální sinusy a očnici stejné strany. Po probatorní biopsii, která byla hodnocena jako embryonální rhabdomyosarkom, byl pacient léčen neoadjuvantní chemoterapií (vinkristin-daktinomycin-cytoxan), při které však nádor progredoval. Následně byl tumor resekován, adjuvantně byla provedena radioterapie, po 4 měsících však zobrazovací metody prokázaly rekurenci. Efekt neměla ani další podaná chemoterapie (vinkristin-irinotekan-temozolamid), nádor dále progredoval a pacient zemřel 15 měsíců po první diagnóze.

Resekát byl histologicky tvořen středně až vysoce celulární proliferací uniformních vřetenitých buněk místy uspořádaných v rozpoznatelných provazcích, bez signifikantních atypií a mitotické aktivity. Imunohistochemické vyšetření prokázalo difúzní pozitivitu PAX7, S100 a variabilně vyjádřenou pozitivitu SMA. Četné buňky rovněž exprimovaly marker kosterně-svalové diferenciace MyoD1, desmin a další marker kosterní svaloviny myogenin však byly negativní.

V některých řezech tyto blandní oblasti odpovídající BSNS abruptně přecházely do high-grade neoplázie tvořené atypickými a mitoticky aktivními rhabdoidními buňkami. Tyto oblasti byly imunohistochemicky difúzně pozitivní v průkazu desminu, MyoD1 a myogeninu, nádor byl tudíž hodnocen jako high-grade rhabdomyosarkom. Markery S100 a SMA byly negativní, imunoexprese PAX7 byla v těchto transformovaných oblastech prokázána jen v několika fokusech. Jak PAX7, tak MyoD1 regulují časnější stadia myogeneze u savců než myogenin a všechny tyto tři transkripční faktory jsou v myogenezi exprimovány významně dříve než strukturální protein desmin (45-46). To naznačuje, že buňky BSNS jsou zastaveny v dřívějších fázích myogeneze, což je též konkordantní s nálezem častější imunoexprese MyoD1 ve srovnání s imunoexpresí myogeninu a desminu v předchozích studiích (18, 20). Buňky v komponentě high-grade rhabdomyosarkomu v námi prezentovaném případu byly pak zjevně schopny diferencovat dále směrem myogenního fenotypu.

RNA-seq prokázala přítomnost fúze *PAX3::MAML3*. Výsledek byl následně potvrzen pomocí FISH, přičemž zlomy genů *PAX3* a *MAML3* byly nalezeny jak v komponentě odpovídající BSNS, tak v high-grade rhabdomyosarkomu.

High-grade transformace BSNS byla již popsána ve dvou předchozích studiích (47-48). V obou případech vykazovaly high-grade komponenty vřetenobuněčnou morfologii s výraznými atypiemi, bez rhabdoidních znaků. Jeden případ s prokázanou fúzí *PAX3::MAML3* nebyl imunohistochemicky testován na expresi myogenních markerů; druhý případ, v kterém byl pomocí FISH potvrzen zlom genu *PAX3*, vykazoval

v high-grade komponentě fokální imunoexpresi myogeninu a desminu, marker MyoD1 však testován nebyl (47-48). Riziko transformace je u BSNS zřejmě velmi malé, má nicméně závažné klinické důsledky, rozsáhlý sampling resekovaného materiálu je u BSNS tudíž nutností. V klinické praxi je pak u pacientů s BSNS vhodná důsledná dispenzarizace.

BRIEF REPORT

Biphenotypic sinonasal sarcoma with *PAX3::MAML3* fusion transforming into high-grade rhabdomyosarcoma: report of an emerging rare phenomenon

Anders Meyer[1] · Natálie Klubíčková[2,3] · Elaheh Mosaieby[2,3] · Petr Grossmann[3] · Antonina Kalmykova[2,4] · Olena Koshyk[2,4] · Michael Michal[2,3]

Abstract

We report a case of a 67-year-old male patient with a sinonasal tumor that showed areas of classic biphenotypic sinonasal sarcoma (BSNS) which in some sections sharply transitioned into high-grade rhabdomyosarcoma. Immunohistochemically, the conventional BSNS parts showed S100 protein, SMA, PAX7, and focal MyoD1 expression, whereas desmin and myogenin were negative. In contrast, the cells in high-grade areas expressed desmin, MyoD1, myogenin, and PAX7, while being negative for S100 protein and SMA. Using the Archer FusionPlex assay, the classical *PAX3::MAML3* gene fusion was detected. FISH for *PAX3* and *MAML3* confirmed a break of these genes in both components. Despite aggressive therapy, the tumor progression resulted in the patient's death. The herein presented case, together with 2 previously published cases of BSNS with high-grade transformation, helps to better understand this novel phenomenon. Although the risk for such transformation appears low, it has important clinical and diagnostic implications which are discussed.

Keywords Biphenotypic sinonasal sarcoma · Rhabdomyosarcoma · High-grade transformation · PAX3::MAML3

Introduction

Biphenotypic sinonasal sarcoma (BSNS) was initially described by Lewis et al. in 2012 as a low-grade sarcoma with neural and myogenic features [1]. Clinically, these tumors usually follow an indolent course with frequent recurrences but no reported metastases and only exceptional disease-related mortality [1–4]. Morphologically, BSNS typically consists of an infiltrative hypercellular proliferation of uniform spindle cells arranged in fascicles, often with a herringbone pattern and frequent invaginations of hyperplastic surface mucosa. Mitotic activity is usually minimal. The vast majority of cases co-express smooth muscle actin (SMA) and S100 protein, while a minority of cases may also exhibit morphological and/or immunohistochemical signs of skeletal muscle differentiation [1, 3–5]. Fusions of *PAX3* gene are the molecular hallmark of BSNS, with *MAML3* being the fusion partner in the majority of cases [3, 4, 6]. Herein, we present a unique case of high-grade rhabdomyosarcoma (RMS) emerging from a typical BSNS with an aggressive clinical course.

Case presentation

The patient was a 67-year-old male with Parkinson's disease and a history of septoplasty, bilateral frontal sinusotomy, and removal of right middle turbinate concha bullosa 3 years before presenting with nasal congestion and epiphora. MRI showed a soft tissue mass involving the right ethmoid, maxillary, and frontal sinuses and invading the extraconal orbit causing mild asymmetric right-sided ocular proptosis (Fig. 1A,B). Endoscopic evaluation revealed a soft tissue mass measuring 4.4 × 3.4 × 2.2 cm which obscured the nasal airway and centered around the

✉ Michael Michal
michael.michal@biopticka.cz

1 Department of Pathology, University of Kansas, KS, Kansas City, USA

2 Department of Pathology, Faculty of Medicine, Charles University, Medical Faculty and Charles University Hospital Plzen, Alej Svobody 80, 323 00, Plzen, Czech Republic

3 Bioptical Laboratory, Ltd., Plzen, Czech Republic

4 Medical Laboratory CSD Health Care, Ltd., Kyiv, Ukraine

Fig. 1 MRI on axial flair (**A**) and on coronal T2 short tau inversion recovery (**B**) showed a soft tissue mass involving the right ethmoid, maxillary, and frontal sinuses and invading the extraconal orbit causing mild asymmetric right-sided ocular proptosis
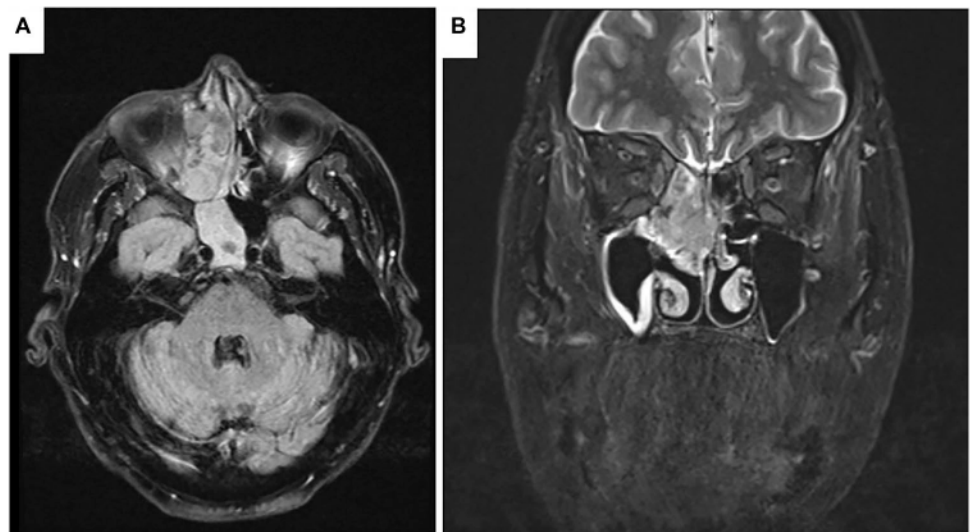
middle turbinate. Biopsy revealed a high-grade sarcoma with myogenic differentiation by immunohistochemistry, diagnosed as embryonal RMS. Staging PET was negative for metastatic disease. The patient initiated neoadjuvant chemotherapy with vincristine-dactinomycin-cytoxan. Repeated imaging after three cycles showed local progression and increased FDG avidity without metastatic disease.

The resection specimen showed a proliferation of uniform spindled cells with moderate to high cellularity, occasional fascicular arrangement, minimal atypia, and no mitotic activity (Fig. 2B). In some areas, invaginations of the hyperplastic surface mucosa were enveloped by the tumor cells (Fig. 2A). No rhabdoid differentiation was noted by morphological examination in this area. However, in some sections, this typical BSNS morphology sharply transitioned

Fig. 2 The resection specimen showed a proliferation of uniform spindled cells with moderate to high cellularity, occasional fascicular arrangement, minimal atypia and no mitotic activity (**B**). In some areas, invaginations of the hyperplastic surface mucosa were enveloped by the tumor cells (**A**). Immunohistochemically, the conventional BSNS areas showed patchy SMA (**C**) and diffuse S100 protein (**D**) expression. There was also a diffuse strong positivity with PAX7 (**E**) and patchy expression of MyoD1 (**F**)
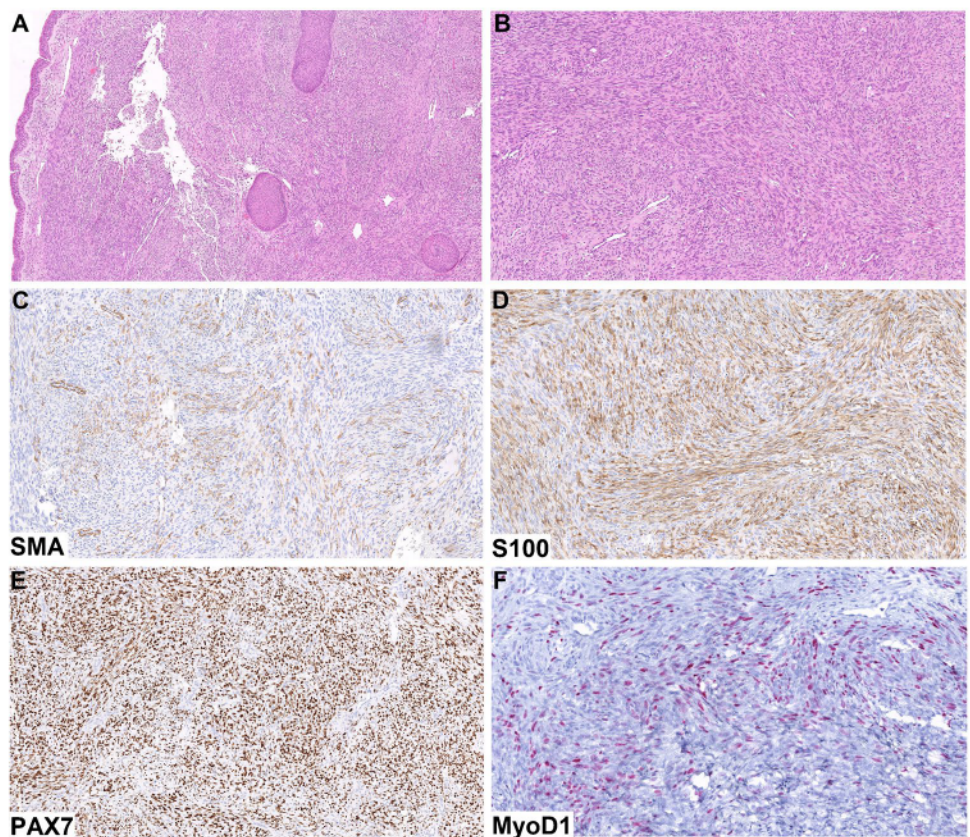
to a high-grade sarcoma with rhabdoid features, very high mitotic activity, and areas of necrosis (Fig. 3A,B).

Immunohistochemically, the conventional BSNS areas showed patchy SMA (Fig. 2C) and diffuse S100 protein (Fig. 2D) expression. There was also a diffuse strong positivity with PAX7 (Fig. 2E) and patchy expression of MyoD1 (Fig. 2F), while desmin and myogenin were completely negative. In contrast, the high-grade areas were completely negative for S100 protein and SMA, and there was only patchy positivity with PAX7 (Fig. 3D), whereas the expression of desmin (Fig. 3C), MyoD1 (Fig. 3E), and myogenin (Fig. 3F) was diffuse in these parts.

Based on the presence of the typical BSNS areas, molecular studies were performed using Archer FusionPlex assay as described previously [7]. This analysis revealed *PAX3*(exon7)*::MAML3*(exon2) fusion which was confirmed by FISH, using *MAML3* (4q31.1) and *PAX3* (2q36.1) break-apart probes (both from SureFISH, Agilent). Of note, the FISH analysis confirmed the presence of the rearrangement (with a cut-off defined as at least 10% cells with a break) in both the conventional and high-grade components.

Postoperatively, the patient received 5040 cGy in 28 fractions. Imaging studies 4 months after resection demonstrated recurrence along the right medial orbital wall and orbital floor. He was initiated on vincristine-urinotecan-temozolamide. Imaging after three cycles again showed local progression. Clinically, the tumor caused total vision loss in the right eye and started to protrude from the right nare. Due to continued progression on maximal therapy, the patient transitioned to hospice and died 15 months after his initial diagnosis.

Discussion

BSNS with morphologically evident rhabdomyoblastic differentiation has been described in approximately 10% of cases [1–3, 5]. However, as the 2 largest studies have shown, at least focal immunohistochemical expression of desmin or MyoD1 is common, with the percentage of immunopositive cases ranging from 35 to 66% and 26 to 91%, respectively. Myogenin expression is the least frequent and is encountered in only 20% of cases [3, 4]. PAX7 expression in BSNS has not been extensively studied but was noted previously as well [8]. The skeletal muscle phenotype of BSNS is in line with its molecular background, which is most commonly characterized by fusions of *PAX3* with either *MAML3* or (less commonly) with *FOXO1* or *NCOA1*. Very rarely, other fusions partners may be involved, including *RREB::MRTFB* (*MKL2*) [3–6, 9–11]. However, the nosological classification of the latter as BSNS is somewhat controversial as identical gene fusions have been described in other head and

Fig. 3 In some sections, this typical BSNS morphology sharply transitioned to a high-grade sarcoma with rhabdoid features, very high mitotic activity, and areas of necrosis (**A, B**). There was only patchy positivity with PAX7 (**D**), whereas the expression of desmin (**C**), MyoD1 (**E**), and myogenin (**F**) was diffused in these parts
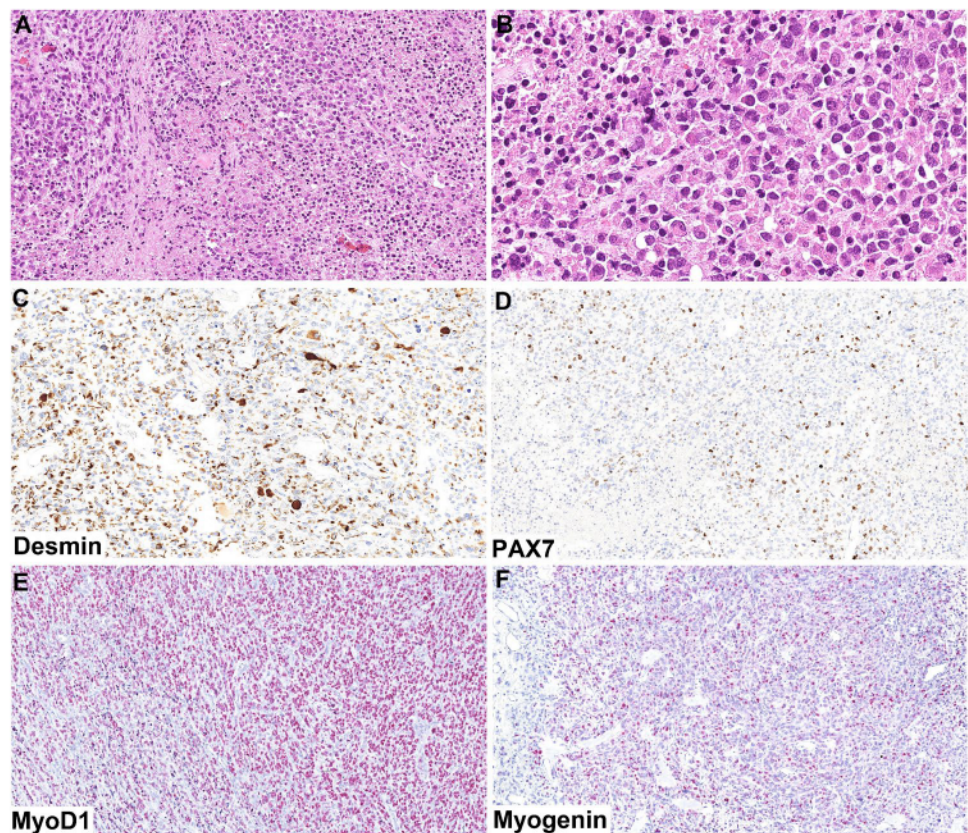
neck mesenchymal tumors [10–12]. During development, PAX3 determines the cell fate of melanocytic, neuronal, and skeletal muscle differentiation and regulates normal myogenesis and postnatal muscular regeneration [5, 6, 13], while MAML3 has been shown to function as a potent transactivator of PAX3 response elements [6]. Gene expression profiling of BSNS with *PAX3::MAML3* fusion also showed altered expression of several genes and signaling networks involved in neural crest, skeletal system, and general embryonic development, including the myogenic genes *MYOCD* and *MYOD1* [6]. Interestingly, the *PAX3::FOXO1* and *PAX3::NCOA1* fusions were also described in rare cases of alveolar RMS [5]. It has been speculated that the differences in clinicopathological features between BSNS and alveolar RMS are probably determined by the cell of origin and cellular environment and by additional genetic aberrations [4].

Nevertheless, the case we are presenting herein shows that a very small subset of BSNS may progress towards a high-grade RMS. After review of the literature, we found 2 recently reported cases of molecularly confirmed BSNS with high-grade transformation, their clinicopathological features together with our case are summarized in Table 1. From the available description and figures, it seems that both cases showed a high-grade spindle cell morphology without the rhabdoid features detected in our case. Unfortunately, the first case was not tested for skeletal muscle markers at all [14], and the other was tested only for desmin and myogenin, both of which were focally positive in the high-grade areas of this case, suggesting differentiation into spindle cell RMS [15].

The differential diagnosis of ordinary BSNS includes a list of other neoplasms with uniform spindle cell morphology occurring in this anatomic area such as malignant peripheral nerve sheath tumor (including malignant Triton tumor when rhabdomyoblastic differentiation is present), cellular schwannoma, monophasic fibrous synovial sarcoma, sinonasal glomangiopericytoma, and solitary fibrous tumor. However, the distinction is usually possible using a carefully selected panel of immunohistochemical stains [1–4]. In contrast, the rhabdomyosarcomatous component in our case could be mistaken for embryonal RMS or pleomorphic RMS. If this area is sampled without the conventional BSNS component (as happened in the initial probatory biopsy in our case), the distinction is impossible without molecular genetic methods. Since the clinical behavior and/or response to treatment of embryonal and pleomorphic RMS might differ from RMS arising from BSNS, we believe it is reasonable that molecular investigation of such cases in the sinonasal area with either *PAX3* FISH probe or preferably using an adequate RNA-sequencing panel is carried out. Significant prognostic differences have already been noted between several molecular subgroups of spindle cell RMS. For example,

Table 1. Clinicopathological features of BSNS cases with high-grade progression

	Case 1 (Bell D et al[11])	Case 2 (Hasnie S et al[12])	Current case
Age/sex	66/M	72/F	67/M
Size (cm)	3.0 × 2.4 × 2.0	NA	4.4 × 3.4 × 2.2
Course of disease	BSNS recurring as high-grade sarcoma in superior extraconal orbit with intracranial extension 15 years later.	2-year history of progressive nasal obstruction with epistaxis and headaches. Resection of a "polyp" which was diagnosed as BSNS. Then resection of a skull base lesion encompassing the entirety of both sinonasal cavities.	History of septoplasty, bilateral frontal sinusotomy, and removal of right middle turbinate concha bullosa 3 years before presenting with nasal congestion and epiphora. MRI showed a soft tissue mass involving the right ethmoid, maxillary, and frontal sinuses and invading the extraconal orbit causing mild asymmetric right-sided ocular proptosis
Treatment and outcome	Primary tumor – resection, radiotherapy, chemotherapy. Recurrence – resection, irradiation. No evidence of disease (10 months)	Resection. Died on complications related to surgery 4.5 months after the resection with no signs of tumor recurrence	Neoadjuvant chemotherapy, resection, irradiation. Died 15 months after diagnosis on tumor progression
Morphology	High-grade spindle cell sarcoma	High-grade spindle cell sarcoma	High-grade rhabdomyosarcoma
IHC of the high-grade areas	Patchy SMA and S100 expression, myogenic markers not tested	Focal desmin and myogenin	Desmin, PAX7, MyoD1, Myogenin positive
Molecular genetics	*PAX3::MAML3* fusion	*PAX3* gene break, copy number alterations of 9p and 22	*PAX3::MAML3* fusion

spindle cell RMS with *VGLL2* and *VGLL3* fusions has a relatively favorable prognosis which is in contrast to the very aggressive subset harboring *MYOD1* mutations [16]. Importantly, spindle cell RMS with *VGLL3* fusions and *MYOD1* mutations has a predilection for the head and neck area [16]. As the other published case of BSNS with high-grade transformation featured spindle cell RMS pattern, a comprehensive molecular investigation for this morphological variant of RMS is warranted as well. Lastly, the herein presented case emphasizes the importance of careful follow-up of patients with BSNS and a throughout sampling of every case to prevent a delayed detection of high-grade transformation.

With regard to the case presented herein, it is interesting to note the significantly different expression of skeletal muscle markers in the conventional BSNS areas compared to the high-grade areas. Even though the former areas were diffusely positive for PAX7 and MyoD1, they were completely negative for desmin and myogenin. In contrast, the high-grade areas were moderately to diffusely positive for all these markers. Both PAX7 and MyoD1 regulate earlier stages of mammalian myogenesis than myogenin [17], and all these 3 transcriptional factors are expressed significantly earlier in myogenesis than the structural protein desmin [18]. This suggests that the cells in conventional BSNS areas were arrested at earlier stages of myogenesis which would be also in line with a generally more frequent expression of MyoD1 compared to the expression of desmin and myogenin in the previous studies [3, 4]. In contrast, possibly due to additional molecular aberrations, the cells in the high-grade areas, although being highly anaplastic, were apparently able to differentiate further along the myogenic pathway as also evidenced by their rhabdoid morphology.

In conclusion, we presented a unique case of BSNS with transformation into high-grade RMS which together with 2 previously published cases of BSNS with high-grade transformation helps to better understand this novel phenomenon. Although the risk for high-grade transformation of BSNS appears low, it has important clinical and diagnostic implications. Besides advocating for a careful follow-up of patients with BSNS and a throughout sampling of every case, we believe that molecular profiling of sinonasal RMS of any type is warranted.

Declarations

References

1. Lewis JT, Oliveira AM, Nascimento AG, Schembri-Wismayer D, Moore EA, Olsen KD et al (2012) Low-grade sinonasal sarcoma with neural and myogenic features: a clinicopathologic analysis of 28 cases. Am J Surg Pathol 36:517–525

2. Carter CS, East EG, McHugh JB (2018) Biphenotypic sinonasal sarcoma: a review and update. Arch Pathol Lab Med 142:1196–1201

3. Le Loarer F, Laffont S, Lesluyes T, Tirode F, Antonescu C, Baglin AC et al (2019) Clinicopathologic and molecular features of a series of 41 biphenotypic sinonasal sarcomas expanding their molecular spectrum. Am J Surg Pathol 43:747–754

4. Fritchie KJ, Jin L, Wang X, Graham RP, Torbenson MS, Lewis JE et al (2016) Fusion gene profile of biphenotypic sinonasal sarcoma: an analysis of 44 cases. Histopathology 69:930–936

5. Huang SC, Ghossein RA, Bishop JA, Zhang L, Chen TC, Huang HY et al (2016) Novel PAX3-NCOA1 fusions in biphenotypic sinonasal sarcoma with focal rhabdomyoblastic differentiation. Am J Surg Pathol 40:51–59

6. Wang X, Bledsoe KL, Graham RP, Asmann YW, Viswanatha DS, Lewis JE et al (2014) Recurrent PAX3-MAML3 fusion in biphenotypic sinonasal sarcoma. Nat Genet 46:666–668

7. Michal M, Rubin BP, Kazakov DV, Michalova K, Steiner P, Grossmann P et al (2020) Inflammatory leiomyosarcoma shows frequent co-expression of smooth and skeletal muscle markers supporting a primitive myogenic phenotype: a report of 9 cases with a proposal for reclassification as low-grade inflammatory myogenic tumor. Virchows Arch 477:219–230

8. Georgantzoglou N, Green D, Stephen SA, Kerr DA, Linos K (2022) Biphenotypic sinonasal sarcoma with PAX7 expression. Int J Surg Pathol 30:642–645

Springer

9. Nichols MM, Alruwaii F, Chaaban M, Cheng YW, Griffith CC (2022) Biphenotypic sinonasal sarcoma with a novel PAX3::FOXO6 fusion: a case report and review of the literature. Head Neck Pathol. https://doi.org/10.1007/s12105-022-01479-w

10. Mechtersheimer G, Andrulis M, Delank KW, Volckmar AL, Zhang L, von Winterfeld M et al (2021) RREB1-MKL2 fusion in a spindle cell sinonasal sarcoma: biphenotypic sinonasal sarcoma or ectomesenchymal chondromyxoid tumor in an unusual site? Genes Chromosom Cancer 60:565–570

11. Siegfried A, Romary C, Escudie F, Nicaise Y, Grand D, Rochaix P et al (2018) RREB1-MKL2 fusion in biphenotypic "oropharyngeal" sarcoma: new entity or part of the spectrum of biphenotypic sinonasal sarcomas? Genes Chromosom Cancer 57:203–210

12. Agaimy A, Din NU, Dermawan JK, Haller F, Melzer K, Denz A et al (2023) RREB1::MRTFB fusion-positive extra-glossal mesenchymal neoplasms: a series of five cases expanding their anatomic distribution and highlighting significant morphological and phenotypic diversity. Genes Chromosom Cancer 62:5–16

13. Buckingham M, Relaix F (2007) The role of Pax genes in the development of tissues and organs: Pax3 and Pax7 regulate muscle progenitor cell functions. Annu Rev Cell Dev Biol 23:645–673

14. Bell D, Phan J, DeMonte F, Hanna EY (2022) High-grade transformation of low-grade biphenotypic sinonasal sarcoma: radiological, morphophenotypic variation and confirmatory molecular analysis. Ann Diagn Pathol 57:151889

15. Hasnie S, Glenn C, Peterson JEG, El Rassi ET, McKinney KA (2022) High-grade biphenotypic sinonasal sarcoma: a case report. J Neurol Surg Rep 83:e105–e109

16. Agaimy A, Dermawan JK, Leong I, Stoehr R, Swanson D, Weinreb I et al (2022) Recurrent VGLL3 fusions define a distinctive subset of spindle cell rhabdomyosarcoma with an indolent clinical course and striking predilection for the head and neck. Genes Chromosom Cancer 61:701–709

17. Charville GW, Varma S, Forgo E, Dumont SN, Zambrano E, Trent JC et al (2016) PAX7 Expression in rhabdomyosarcoma, related soft tissue tumors, and small round blue cell neoplasms. Am J Surg Pathol 40:1305–1315

18. Folpe AL (2002) MyoD1 and myogenin expression in human neoplasia: a review and update. Adv Anat Pathol 9:198–203

4.6   _EWSR1::POU2AF3(COLCA2)_   sarcoma: An aggressive, polyphenotypic sarcoma with a head and neck predilection

V publikaci jsou předloženy další poznatky o nově, molekulárně-geneticky definované jednotce – sarkomu s fúzí _EWSR1(/FUS)::POU2AF3_, která byla recentně vyčleněna ze skupiny nediferencovaných sarkomů z kulatých až vřetenitých buněk (21-22).

Ve studii bylo zahrnuto 8 případů postihujících 5 pacientů mužského a 3 pacienty ženského pohlaví, jednalo se o dospělé středního a vyššího věku (medián 60 let). Ve 4 případech byly nádory lokalizovány v oblasti hlavy a krku: ve dvou případech v sinonasálním traktu, v 1 případě v nasopharyngu a v 1 případě se jednalo o lytickou lézi čelní kosti. Ve zbylých případech nádory rostly v měkkých tkáních hrudníku a stehna, v plíci a ve fibule. Ačkoli byli pacienti léčeni intenzivní multimodální onkologickou terapií, pouze dva pacienti neměli při poslední kontrole provedené 33,5 měsíců, respektive 53,5 měsíců po diagnóze známky onemocnění. Jeden pacient zemřel z neurčené příčiny, přičemž však u něj byla potvrzena lokální rekurence a vysloveno podezření na přítomnost vzdálené metastázy. Ostatní pacienti byli v rozmezí 4–122 měsíců naživu, avšak se vzdálenými metastázami a/nebo lokálními rekurencemi.

Na základě histologického vyšetření byly vytyčeny dvě morfologické podskupiny. První z nich obsahovala dva případy, jednalo se o méně celulární nádory tvořené vřetenitými a hvězdicovitými buňkami s maximálně středně těžkými jadernými atypiemi a nízkou mitotickou aktivitou, nádory měly fibrotické či fibromyxoidní stroma. Spíše ojediněle byly zastiženy drobné fokusy se zvýšenou celularitou a zakulacenými nádorovými buňkami. Druhá podskupina čítala 6 případů, nádory zde měly jasně maligní, high-grade morfologii s vysokou celularitou, vyšší mitotickou aktivitou a ve dvou případech též přítomností nekrotických ložisek. Nádory měly bifázickou strukturu: hnízda kulatých buněk s jádry s jemně zrnitých chromatinem a prominentními jadérky (připomínající buňky neuroendokrinních neoplázií) byla obklopena proliferací vřetenitých nádorových buněk. Jednotlivé případy v této podskupině vykazovaly glandulární, osteogenní a rhabdomyoblastickou diferenciaci.

Imunohistochemicky byly ve více než polovině případů exprimovány markery CD56 (4/4 případů), GFAP (5/8), širokospektré keratiny (5/8), S100 (4/7) a SATB2 (4/6). V některých případech byla dále potvrzena imunoexprese neuroendokrinních markerů synaptofyzinu, chromograninu a INSM1. Nejvyšší intenzity dosahovala imunohistochemická barvení ve výše popsaných kulatobuněčných hnízdech s neuroendokrinními rysy.

Ve všech případech byla pomocí RNA-seq identifikována fúze _EWSR1::POU2AF3_, zlom genu _EWSR1_ byla dále potvrzen pomocí FISH v 5 případech. V 9/12 dosud popsaných tumorů pocházejících z oblasti hlavy a krku byl zlom genu _EWSR1_ lokalizován v exonech 12 až 17, ve zbylých případech byl lokalizován v exonech 9 či 10. Naopak ve všech případech pocházejících z jiných oblastí byl zlom přítomen v exonech 9 nebo 10. Příčinou může být odlišná cesta vzniku fúze, ovlivněná například specifickým mikroprotředím v oblasti hlavy a krku. Exony 12 až 14 obsahují motiv RRM,

který se podílí na interakci s RNA a DNA. Vazba nukleových kyselin či ribonukleoproteinů může mít vliv na funkci fúzního genu *EWSR1::POU2AF3*.

MODERN PATHOLOGY

Research Article

EWSR1::POU2AF3(COLCA2) Sarcoma: An Aggressive, Polyphenotypic Sarcoma With a Head and Neck Predilection

Olena Koshyk[a,b], Carina A. Dehner[c,d], Mari F.C.M. van den Hout[e], Isabelle Vanden Bempt[f], Raf Sciot[g], Hsuan-Ying Huang[h], Abbas Agaimy[i], Nasir Ud Din[j], Natálie Klubíčková[a,k], Elaheh Mosaieby[a,k], Alena Skálová[a,k], Květoslava Michalová[a,k], Patrick Schöffski[l,m], Andre M. Oliveira[c], Kevin C. Halling[c], Sounak Gupta[c], John M. Gross[n], Johanna W.M. Nin[o], Michal Michal[a,k], Andrew L. Folpe[c], Kemal Kosemehmetoglu[p], Jorge Torres-Mora[c], Michael Michal[a,k,*]

[a] *Department of Pathology, Charles University, Faculty of Medicine in Plzeň, Czech Republic;* [b] *Medical Laboratory CSD, Ltd, Kyiv, Ukraine;* [c] *Department of Laboratory Medicine and Pathology, Mayo Clinic, Rochester, Minnesota;* [d] *Department of Pathology, Indiana University School of Medicine, Indianapolis, Indiana;* [e] *Department of Pathology, GROW School for Oncology and Developmental Biology, Maastricht University Medical Center, Maastricht, The Netherlands;* [f] *Department for Human Genetics, University Hospitals Leuven, KU Leuven, Leuven, Belgium;* [g] *Department of Pathology, University Hospitals Leuven, KU Leuven, Leuven, Belgium;* [h] *Department of Anatomical Pathology, Kaohsiung Chang Gung Memorial Hospital and Chang Gung University College of Medicine, Kaohsiung City, Taiwan;* [i] *Institute of Pathology, Friedrich-Alexander University Erlangen-Nürnberg, University Hospital, Erlangen, Germany;* [j] *Section of Histopathology, Department of Pathology and Laboratory Medicine, Aga Khan University Hospital, Karachi, Pakistan;* [k] *Bioptical Laboratory, Ltd, Plzeň, Czech Republic;* [l] *Department of General Medical Oncology, University Hospitals Leuven, Leuven Cancer Institute, Leuven, Belgium;* [m] *Department of Oncology, KU Leuven, Laboratory of Experimental Oncology, Leuven, Belgium;* [n] *Department of Pathology, The Johns Hopkins Medical Institutions, Baltimore, Maryland;* [o] *Department of Internal Medicine, Maastricht University Medical Center, Maastricht, The Netherlands;* [p] *Department of Pathology, Hacettepe University, Ankara, Turkey*

ARTICLE INFO

ABSTRACT

EWSR1::POU2AF3 (*COLCA2*) sarcomas are a recently identified group of undifferentiated round/spindle cell neoplasms with a predilection for the head and neck region. Herein, we report our experience with 8 cases, occurring in 5 men and 3 women (age range, 37-74 years; median, 60 years). Tumors involved the head/neck (4 cases), and one each the thigh, thoracic wall, fibula, and lung. Seven patients received multimodal therapy; 1 patient was treated only with surgery. Clinical follow-up (8 patients; range, 4-122 months; median, 32 months) showed 5 patients with metastases (often multifocal, with a latency ranging from 7 to 119 months), and 3 of them also with local recurrence. The median local recurrence–free and metastasis-free survival rates were 24 months and 29 months, respectively. Of the 8 patients, 1 died of an unknown cause, 4 were alive with metastatic disease, 1 was alive with unresectable local disease, and 2 were without disease. The tumors were composed of 2 morphologic subgroups: (1) relatively bland tumors consisting of spindled to stellate cells with varying cellularity and fibromyxoid stroma (2 cases) and (2) overtly malignant tumors composed of nests of "neuroendocrine-appearing" round cells surrounded by spindled cells (6 cases). Individual cases in the second group showed glandular, osteogenic, or rhabdomyoblastic differentiation. Immunohistochemical results included CD56 (4/4 cases), GFAP (5/8), SATB2 (4/6), keratin (AE1/AE3) (5/8), and S100 protein (4/7). RNA sequencing identified *EWSR1::POU2AF3* gene fusion in all cases. *EWSR1* gene rearrangement was confirmed by fluorescence in situ hybridization in 5 cases. Our findings confirm the head/neck predilection and

aggressive clinical behavior of *EWSR1::POU2AF3* sarcomas and widen the morphologic spectrum of these rare lesions to include relatively bland spindle cell tumors and tumors with divergent differentiation.

Introduction

With the widespread application by pathologists of sophisticated molecular genetic techniques such as next-generation sequencing, an ever-increasing number of new, distinctive entities are now recognized within the group of undifferentiated round and/or spindle cell sarcomas. One of the most recently identified categories comprises aggressive, histologically undifferentiated spindle cell/round cell sarcomas harboring *EWSR1/FUS::POU2AF3(COLCA2)* gene fusions, first reported by Agaimy et al[1] in a series of 5 sinonasal tumors and more recently reported by Hiemenz et al[2] in a series of 6 cases predominantly (but not exclusively) involving soft tissue and bone locations in the head/neck. Herein, we present our experience with 8 additional examples of *EWSR1/FUS::POU2AF3* sarcoma, further expanding the clinical, morphologic, and immunohistochemical spectrum of these rare malignant neoplasms.

Materials and Methods

Review of our collective consultation archives identified 8 cases known to harbor *EWSR1/FUS::POU2AF3* fusions. Clinical information was obtained from the medical records. Statistical analysis, including survival analyses, was performed with Bluesky Statistics software (version 7.40, BlueSky Statistics, LLC).

Immunohistochemistry for each case was performed at several different laboratories based on the original differential diagnostic considerations (staining protocols and antibody sources are available upon request). Some markers (ie, GFAP, SATB2, and neuroendocrine markers) were added in selected cases for the purposes of this study. In cases 1 and 6, both the primary and recurrent or metastatic tumors, respectively, were available for analysis. RNA sequencing in cases 1, 3, 4, 6, and 7 was performed using various customized versions of FusionPlex assay (Archer, Inc). Case 2 was analyzed using TruSight RNA Fusion panel (Illumina Inc), while DNA and RNA sequencing in case 8 was performed using the TruSight Oncology 500 kit (Illumina Inc). Cases 5 and 6 were sequenced using a targeted, custom-designed, amplicon-based panel using QIAGEN's QIAseq chemistry. In 6 cases, an *EWSR1* fluorescence in situ hybridization break-apart probe was used for confirmation of gene rearrangement. All methods have been described in more detail previously.[3-7]. Molecular data from case 5 have been previously reported.[7]

Results

Clinical Findings

The clinical features are summarized in Table 1. There were 5 male and 3 female patients aged 37 to 74 years (median, 60 years; mean, 57 years). The head and neck area was involved in 4 cases (frontal bone, nasopharynx, and 2 cases in the sinonasal area); 1 case each affected the thigh, thoracic wall, fibula, and lung.

Imaging studies were available for 4 patients (cases 1-3 and 8). Computed tomography (CT) scan in case 1 revealed a tumor

involving left ethmoidal and frontal sinuses with a soft tissue component and with destruction of bilateral cribriform plates and left sphenoidal ala. Magnetic resonance imaging revealed a T1 isointense and T2 hyperintense mass with contrast enhancement and diffusion restriction involving the left ethmoid sinus, left sphenoid wing, and bilateral frontal sinuses. CT scan in case 2 showed a lytic tumor in the right frontal bone (Fig. 1D), while an infiltrative, variably calcified lesion of soft tissue density involving the right nasal cavity and frontal, ethmoid, and maxillary sinuses was found in case 3 (Fig. 2A). The initial tumor in case 8 affected the left part of the thoracic wall around fifth rib with lytic bone involvement on CT scan.

All patients underwent surgical resection of their primary tumors with R0, R1, or R2 margins (for details, see Table 1). One patient received neoadjuvant chemotherapy/radiotherapy; adjuvant chemotherapy and radiation therapy were administered to 4 and 6 patients, respectively. One patient (case 6) was treated with surgery only. Clinical follow-up (8 patients; range, 4-122 months; median, 32 months; mean, 39 months) showed 5 patients with metastases (unconfirmed by biopsy in case 1), and 3 of them also exhibited local recurrence. Of the 8 patients, 1 died of an unknown cause, 4 were alive with metastatic disease, 1 was alive with unresectable local disease, and 2 were without disease. The metastases occurred with a latency ranging from 7 to 119 months, were often multifocal, and involved bone (n = 3) and pleura, base of the skull and lymph nodes (1 case each). The median local recurrence−free and metastasis-free survival rates were 24 months and 29 months, respectively.

Submitting diagnostic considerations from referring pathologists included Ewing-like sarcoma (2×), osteosarcoma (2×), "spindle cell sarcoma," ossifying fibromyxoid tumor (OFMT), desmoplastic fibroma, intranodal palisaded myofibroblastoma, atypical carcinoid, synovial sarcoma, myoepithelial tumor, and neuroendocrine carcinoma.

Morphologic Findings

Microscopically, 6 cases grew in an infiltrative fashion into surrounding soft tissue and bone, whereas cases 5 and 6 appeared relatively well circumscribed. Although all tumors consisted of relatively uniform spindled to round cells, 2 distinct morphologic groups could be discerned. The first of these, illustrated by cases 1 and 2, displayed variable cellularity and consisted of relatively bland, spindled to stellate cells in a fibromyxoid stroma; nuclear atypia was mild to moderate, mitotic activity was low, not exceeding 2 mitoses per 10 high-power fields, and necrosis was absent (Fig. 1). In case 1, the primary tumor showed predominantly low cellularity (Fig. 1A), with only a small focus having more cellular, round cell features (Fig. 1B); the recurrent tumor consisted chiefly of more cellular spindled proliferation (Fig. 1C). Similarly, case 2 was predominantly hypocellular (Fig. 1E), with scattered small to medium-sized nests having a more cellular, round cell appearance (Fig. 1E-G). The initial tumor in case 1 had a striking arborizing capillary vasculature (Fig. 1A), whereas small hyalinized vessels predominated in the recurrence and in case 2 (Fig. 1E).

Table 1
Clinical features of *EWSR1::POU2AF3* tumors

Case no.	Age (y)/sex	Tumor site	Size	Prior diagnosis	Treatment	Local recurrence/ distant mets (mo after diagnosis)	Status at the last follow-up	Overall survival (mo)
1	65/M	Sinonasal area (destructive lesion of ethmoidal and frontal sinuses)	2.9	Ossifying fibromyxoid tumor	Resection (R2) and adjuvant RT	Recurrence and lytic lesion in the left ilium on PET-CT suspicious for mets (not biopsied) in 24 mo	Died of an unknown cause	24
2	60/F	Frontal bone (lytic bone lesion)	5.2 × 4.5 × 2.5	Desmoplastic fibroma, Spindle cell sarcoma grade 2, dedifferentiated osteosarcoma	Resection (no residual disease on CT); CHT initiated after mets detected	Multiple lytic mets in bilateral frontal bones and at the base of the skull 7 mo after surgery	AWD	7
3	43/F	Sinonasal area (nasal cavity, frontal, ethmoid, and maxillary sinuses)	NA	Osteosarcoma	Functional endoscopic sinus resection (R1), adjuvant proton RT	No	AWD	4
4	46/M	Nasopharynx	NA	Ewing(-like) sarcoma; synovial sarcoma, myoepithelial tumor	Resection (R0), adjuvant RT, and CHT	Multifocal bone mets (119)	AWD	122
5	72/M	L thigh	3.9	Intranodal palisaded myofibroblastoma	Resection (R0); adjuvant CHT and RT	No	NED	33.5
6	60/M	Lung (intraparenchymal)	4.2	Atypical carcinoid	Resection (R0), mets resected	Local recurrence/ multifocal pleural mets (22 and 38)	AWD	41.5
7	74/F	R proximal fibula (bone)	NA	Ewing(-like) sarcoma	Resection (R0) neoadjuvant and adjuvant RT and CHT	No	NED	53.5
8	37/M	Thoracic wall (soft tissue lesion with adjacent lytic rib involvement; no other tumor located elsewhere)	NA	Neuroendocrine carcinoma	Resection (R1) with RT (60 Gy) and CHT (EP); mets treated with CHT (VAC)	Multifocal locoregional recurrence with pleural, pericardial, diaphragmatic and lymph node mets found in 24 mo	AWD	30

AWD, alive with disease; CHT, chemotherapy; CT, computed tomography; EP, cysplatinum/etoposide; F, female; L, left; M, male; mets, metastases; NA, not available; NED, no evidence of disease; PET, positron emission tomography; R, right; RT, radiotherapy; VAC, vincristine-D-actinomycine-cyclofosfamide.

The second, larger subgroup consisted predominantly of highly cellular sheets and fascicles of overtly malignant-appearing spindled and round cells, with somewhat biphasic architecture (Figs. 2-5). Mitotic activity ranged from 4 to 24 mitoses per 10 high-power fields, and small areas of necrosis were identified in 2 cases. Stroma was relatively scarce in cases 3, 4, 6, and 7 (Fig. 3B), whereas cases 4 and 5 contained foci with abundant myxoid stroma, in which the tumor cells grew in cord-like, pseudopapillary, pseudoglandular, and cribriform formations (Fig. 3A, C, E). Relatively hypocellular zones with hyalinized collagen were variably present (Figs. 3D and 5A-C). Some cases contained numerous hyalinized small vessels (Fig. 3A, B), whereas others had an inconspicuous vasculature.

Perhaps, the most distinctive feature of this second subgroup (found in 4 cases) was the presence of nests or loose dispersed sheets of round cells with basophilic nuclei with finely stippled chromatin ("neuroendocrine"), sometimes with peripheral palisading, surrounded by zones with more spindled cells having lighter and more evenly dispersed chromatin (Figs. 3D; 4B, C, G; and 5A-C). One prominent pinpoint nucleolus was typically present in both types of cells (Figs. 2D and 5C).

Unusual features, noted in individual cases, included keratin 7−positive glands containing Alcian blue−positive mucin (case 8) (Fig. 5D), clear cells (cases 7 and 8) (Fig. 4H), osteogenic differentiation with production of osteoid matrix (case 3) (Fig. 2E), and rhabdomyoblastic differentiation including

rhabdomyoblasts with visible cross-striations (case 6) (Fig. 4D). Interestingly, rhabdomyoblasts were absent in the metastasis from this tumor.

Scanned whole slide images for most cases are available online at the hyperlinks listed in Supplementary File S1. No correlation was found between any of the histologic features studied and the clinical course of the disease.

Immunohistochemical Findings

The immunohistochemical results are summarized in Table 2. The most commonly expressed markers were GFAP (5/8 cases; 63%) (Fig. 5F), SATB2 (4/6 cases; 67%) (Fig. 2F and 4F), keratins (AE1/AE3) (5/8 cases; 63%) (Fig. 5G), and S100 protein (4/7 cases; 57%) (Fig. 5E). In general, expression of these markers was more pronounced in the round cell nodules, compared with the spindled cells (Figs. 4F and 5E-G). Expression of CD56 (4/4 cases) (Fig. 3F), synaptophysin, chromogranin, and INSM1 (collectively 3/7; 43%) also tended to be restricted to these round cell areas (Fig. 5H, I). As expected, more robust SATB2 expression was seen in case 3 with overt osteoblastic differentiation as compared with undifferentiated spindle cell zones in other cases (Figs. 2F and 4F). In case 6, markers of rhabdomyoblastic differentiation (eg, desmin, myogenin, and MyoD1) were seen in differentiating rhabdomyoblasts as well as in morphologically undifferentiated cells (Fig. 4E). More limited expression of these markers was present in the metastasis as well. A wide variety of other markers, tested on
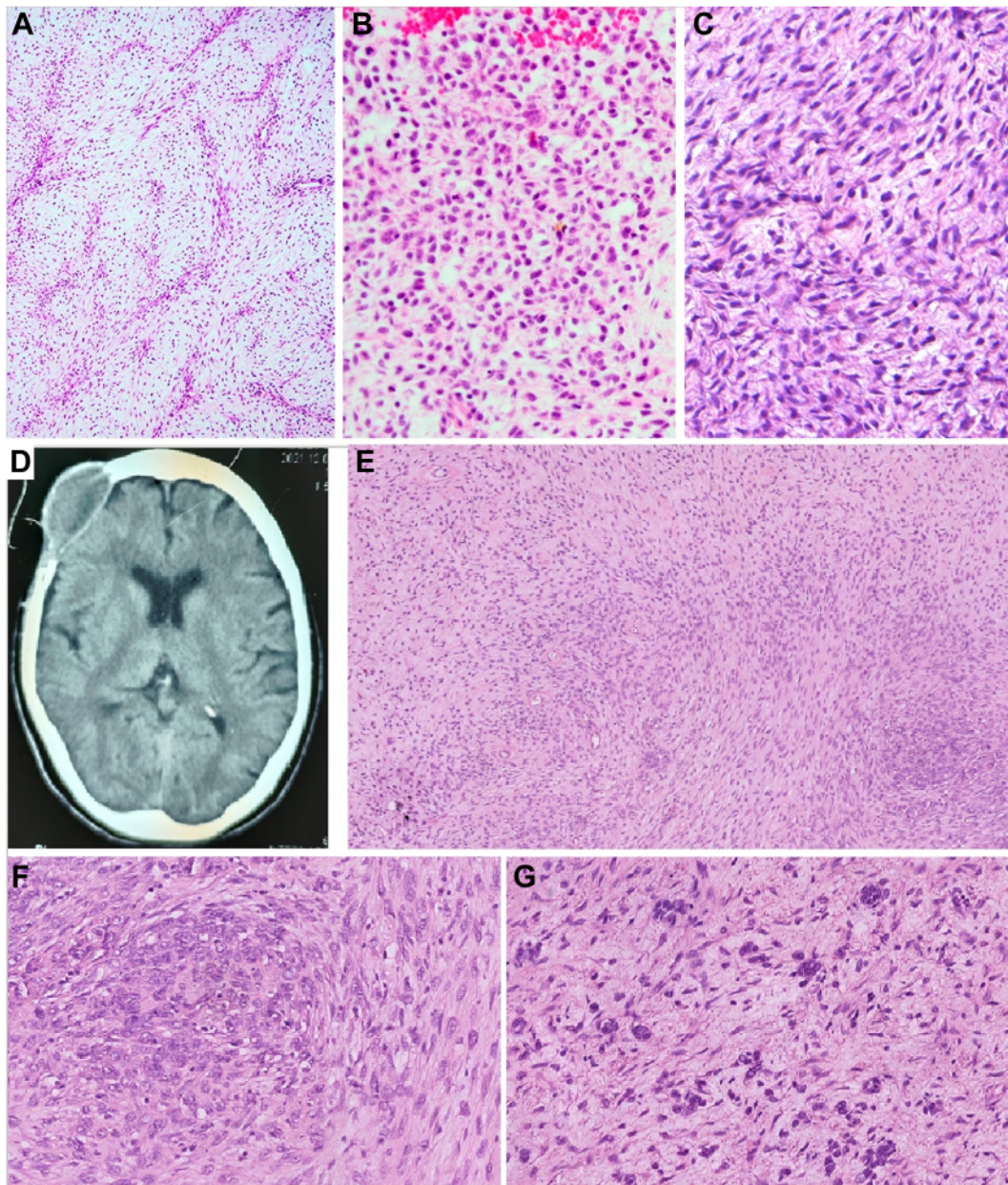
Figure 1.
(A-C) Case 1. The tumor in case 1 consisted of spindle to stellate cells with mild to moderate atypia and fibromyxoid stroma. (A) The primary tumor showed a striking arborizing vasculature and predominantly low cellularity, (B) with only a small focus having more cellular, round cell features. (C) The recurrent tumor consisted chiefly of more cellular spindled proliferation. (D-G) Case 2. (D) Computed tomography scan in case 2 showed a lytic tumor in the right frontal bone. This case was also hypocellular with scattered small-to medium-sized nests having a more cellular, round cell appearance. (E) Small, hyalinized vessels predominated. (F) High-power view of one of the larger nests with more round cell appearance. (G) High-power view of one of the small round cell aggregates.

an ad hoc basis in individual cases, were negative or noncontributory (listed in Table 2).

Molecular Genetic Findings

The molecular genetic data are summarized in Table 2. Fusions with genomic breakpoints in exons 9, 10, 14, 15, and 16 of *EWSR1* were noted across the cohort, while breakpoints in only exon 2 of *POU2AF3* gene were detected. Case 2 showed 3 coexisting breakpoint-defined subclones affecting adjacent exons 14 to 16 of *EWSR1*. Notably, the *EWSR1* genomic breakpoints in all 4 sinonasal cases were located in exons 14 to 16, while all extrasinonasal cases had breakpoints in exons 9 or 10. In cases 1 to 3, 5, 7, and 8, a break of *EWSR1* was confirmed by fluorescence in situ hybridization. In case 8, DNA sequencing did not detect any pathogenic mutations, and the tumor mutation burden was low (3.9/Mb). No case harbored *FUS* rearrangement.

Discussion

Including the original description by Agaimy et al,[1] followed by the series by Hiemenz et al,[2] and our current cases, a total of 19
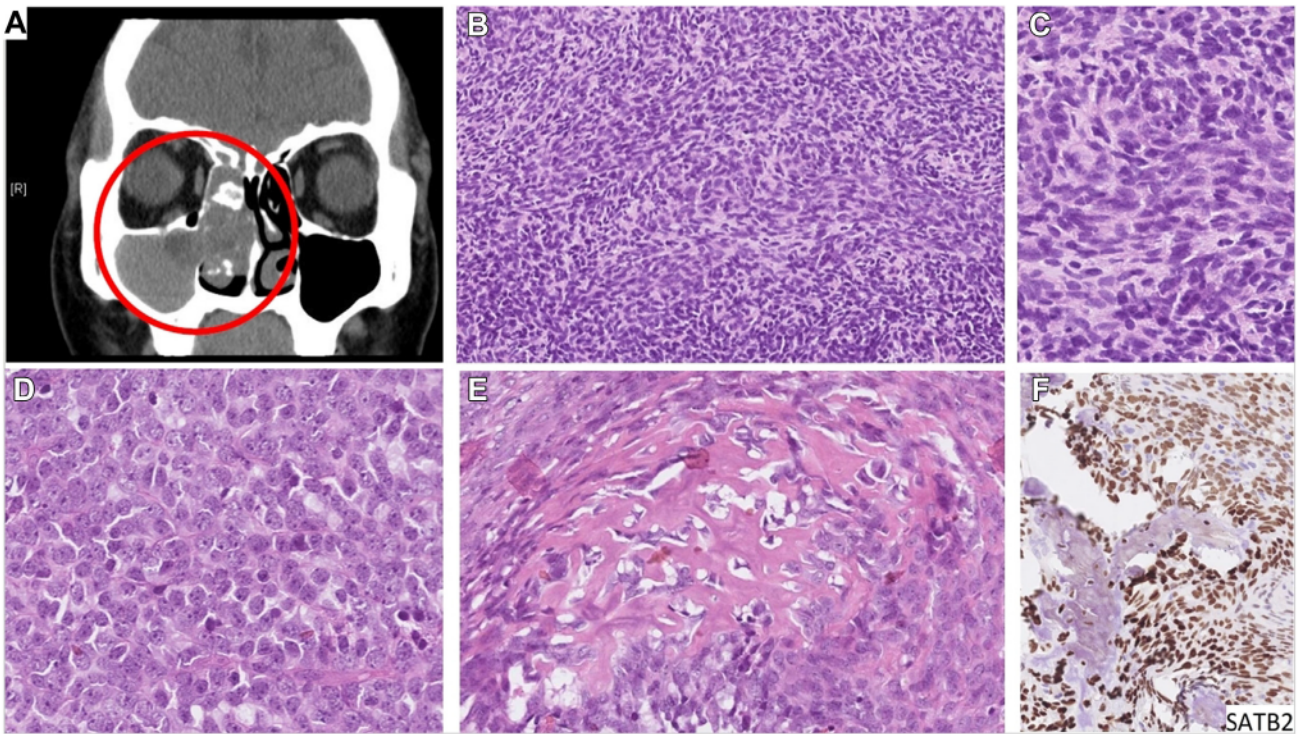
Figure 2.
Case 3. (A) Computed tomography scan revealed an infiltrative lesion of soft tissue density (red circle), involving the right nasal cavity and frontal, ethmoid, and maxillary sinuses with multifocal calcifications. (B, C) The tumor consisted of highly cellular sheets and fascicles of spindled cells and occasional round cells with little intervening stroma. (D) Foci with round cells featuring more basophilic nuclei with finely stippled chromatin and typically 1 prominent pinpoint nucleolus. (E) Some of the tumor cells showed osteogenic differentiation with production of osteoid matrix. (F) In line with the observed osteogenic properties, the tumor cells showed a diffuse strong expression of SATB2.

neoplasms carrying the *EWSR1/FUS::POU2AF3* (formerly *COLCA2*) fusion have been well documented (clinicopathological features of all cases are summarized in the Supplementary Table S1). A single case mentioned in one fusion detection methodological study (included in the current study as case 5) lacked any clinical or anatomical data.[7]

Clinically, these tumors show a striking predilection for the head and neck area (13/19 cases), particularly for the sinonasal tract (9/19 cases), but they may occur at other sites, including soft tissue and bone. They affect predominantly middle-aged to older adults without sex predilection. *EWSR1/POU2AF3*-rearranged neoplasms reported so far mostly behaved as high-grade sarcomas irrespective of their morphology. Half of the published cases (9/18) developed metastases (as late as 10 and 23 years after diagnosis, hence warranting a lifelong follow-up) with or without recurrence and additional 3 patients experienced either recurrence or progressive tumor growth. The 5-year local recurrence–free survival and metastasis-free survival were 48% and 54%, respectively, after combining the available clinical data from these 3 studies. While only 1 of 18 patients died of disseminated disease, most remaining patients were alive with disease despite multimodal therapy. However, 5 patients were without evidence of disease at the last follow-up, and all 4 with available treatment information received a multimodal therapy.

The previously emphasized morphologic features, including the presence of undifferentiated round and spindled cells with fine chromatin and prominent nucleoli[1,2] and frequent biphasic arrangement of spindled and round/epithelioid cells, often mimicking synovial sarcoma,[2] were observed in our cases as well. The reported cases did not exhibit any consistent morphologic evidence of epithelial, mesenchymal, or other specific lines of differentiation, apart from single cases in our study exhibiting glandular, osteoblastic, and rhabdomyoblastic differentiation, respectively. However, they seem to display an unusual immunophenotype with frequent expression of markers associated with epithelial (pankeratins and/or EMA expression) or neuroendocrine differentiation.[1,2]

New findings in our study include the presence of 2 morphologically different subgroups. The first consisted of relatively uncharacteristic low-grade–appearing spindle cell tumors with mild to moderate atypia and variable cellularity with occasional foci showing round cells, while the second encompassed hypercellular neoplasms with predominantly high-grade round and spindle cell morphology. A very characteristic and frequent microscopic feature of this latter group was the presence of distinctly biphasic arrangement of the tumor cells with the formation of round cell nests on a predominantly spindle cell background reminiscent of biphasic synovial sarcoma but lacking true gland formation (apart from a single case). The round cells often contained more basophilic staining nuclei with more stippled chromatin, imparting a neuroendocrine appearance. Notably, it was these round cells that preferentially showed expression of keratins and the various neuroendocrine markers we tested. Novel findings also included the identification of true glands with mucin production and rhabdomyoblastic and osteogenic differentiation found in one case each.

The exact nosology of these neoplasms remains to be further delineated. Data from these 19 reported cases are in line with a sarcoma showing polyphenotypic (ambiguous) immunoprofile. Their morphologic heterogeneity precludes putting them into any of the defined epithelial or mesenchymal neoplastic categories despite their focal overlap with basaloid epithelial or
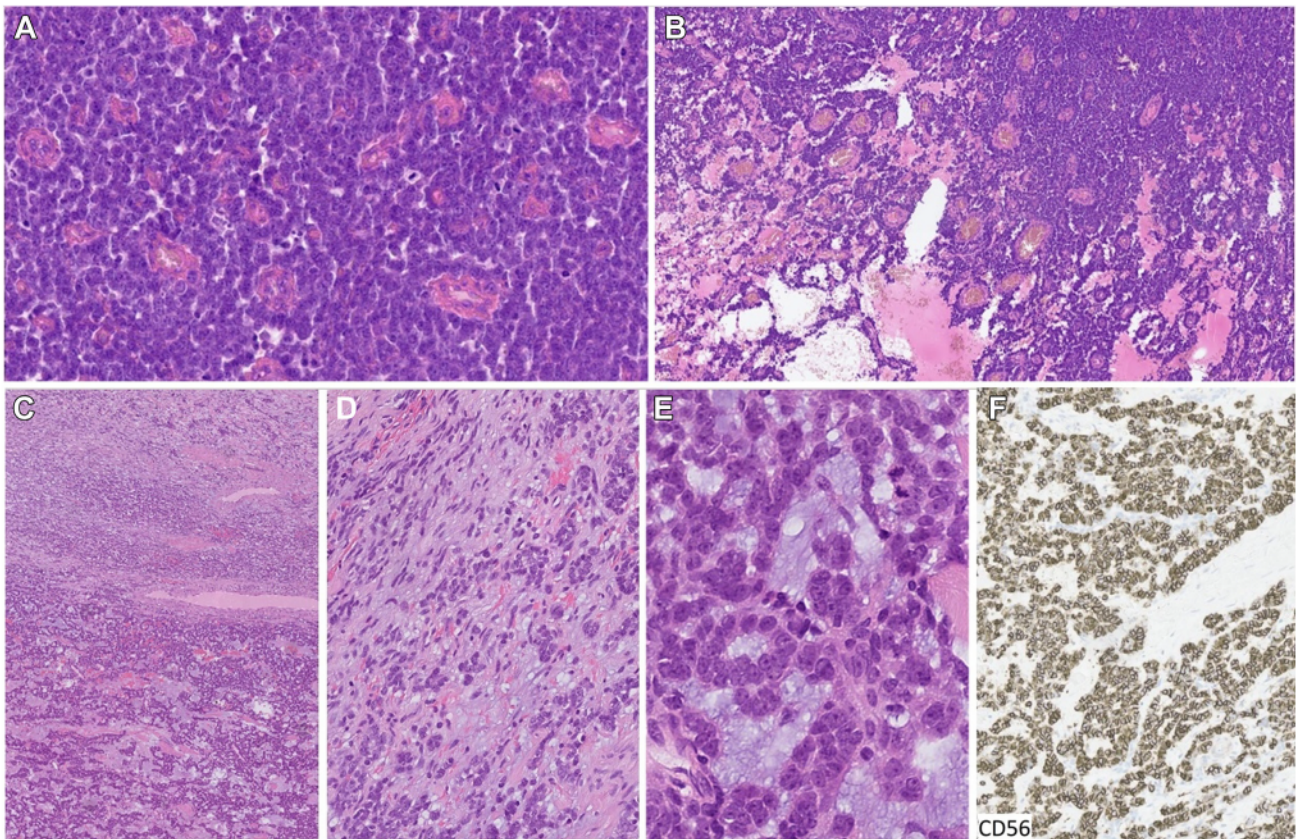
Figure 3.
(A, B) Case 4. This case consisted purely of nests or loose dispersed sheets of round cells with basophilic nuclei with finely stippled neuroendocrine-like chromatin. It contained (A) abundant small hyalinized vessels and (B) areas with myxoid stromal matrix, which imparted a cord-like and pseudopapillary architecture. (C-F) Case 5. (C) Case 5 showed a prominent biphasic arrangement consisting of predominantly spindle cell periphery (top), whereas toward the center (bottom), it contained round cells with neuroendocrine features with cord-like, pseudopapillary, and pseudoglandular arrangement within a myxoid stroma. (D) Transitional areas with round cells within the predominantly spindle cell background occasioning a resemblance to similar areas in case 2. (E) High-power view of round cells with neuroendocrine features forming pseudoglandular structures. (F) Diffuse strong expression of CD56.

neuroendocrine neoplasms in a subset of cases. While some may superficially mimic biphasic synovial sarcomas based on subtle biphasic arrangements of plump rounded and spindled cells, their morphology (variable spindle and round cell features) and polyphenotypic immunoprofile (variable expression of epithelial, rhabdomyogenic, and neurogenic markers such as S100, GFAP, and others) are partially reminiscent of the recently reported category of *EWSR1::PATZ1* fusion sarcomas.[8] Their capacity for multilineage immunophenotypic differentiation is in line with derangement of cellular differentiation pathways downstream of the fusion transcript.

The observed morphologic differences between both subgroups obviously raise the question of whether all tumors presented in this study belong to the same entity or represent 2 fundamentally different neoplasms sharing the same genetic event, the *EWSR1/FUS::POU2AF3* fusion. We believe that several cases in our study offered a strong clue in support of a single entity with a wide morphologic spectrum. Notably, the significant variation in cell shape and cellularity within the same tumors and between primary tumors and their recurrences suggests the presence of a bland-looking spindled morphology at one end and a highly cellular undifferentiated round cell morphology at the other end of the spectrum with a lot of transitional morphologies on the spectrum in-between. A similar morphologic spectrum of morphologically low-grade–appearing

sarcomas with low cellularity on one end and frankly high-grade neoplasms with significantly different appearance on the other is commonplace in several other soft tissue entities such as low-grade fibromyxoid sarcoma (LGFMS)/sclerosing epithelioid fibrosarcoma, low-grade/high-grade myxoid liposarcoma, or more recently within the spectrum of *EWSR1::PATZ1*-rearranged sarcomas.[8-10]

The differential diagnosis of these tumors is defined by the predominant pattern seen in a given case and is also influenced by the anatomical site and immunohistochemical findings. The low-grade spindle cell tumors might be reminiscent of other spindle cell sarcomas with fibromyxoid stroma such as OFMT and LGFMS. Features arguing against the diagnosis of OFMT were the wide infiltrative growth and lack of pseudocapsule and ossification (in the vast majority of cases).[11] The absence of abrupt transitions between collagenized and myxoid stroma and the lack of MUC4 expression (caveat: only 2 cases tested) argue against LGFMS.[12] Low-grade myxofibrosarcoma or, in case of a primary bone tumor, various forms of osteosarcoma may enter the differential as well (see later discussion). The high-grade round and spindle cell tumors may be difficult to distinguish from Ewing sarcoma, *CIC*-rearranged sarcoma, and other sarcomas with this morphology which can be achieved using histology; immunohistochemistry; and, if necessary, molecular methods.[13] While *EWSR1/FUS::POU2AF3* sarcomas can be added to a long list of mimickers of
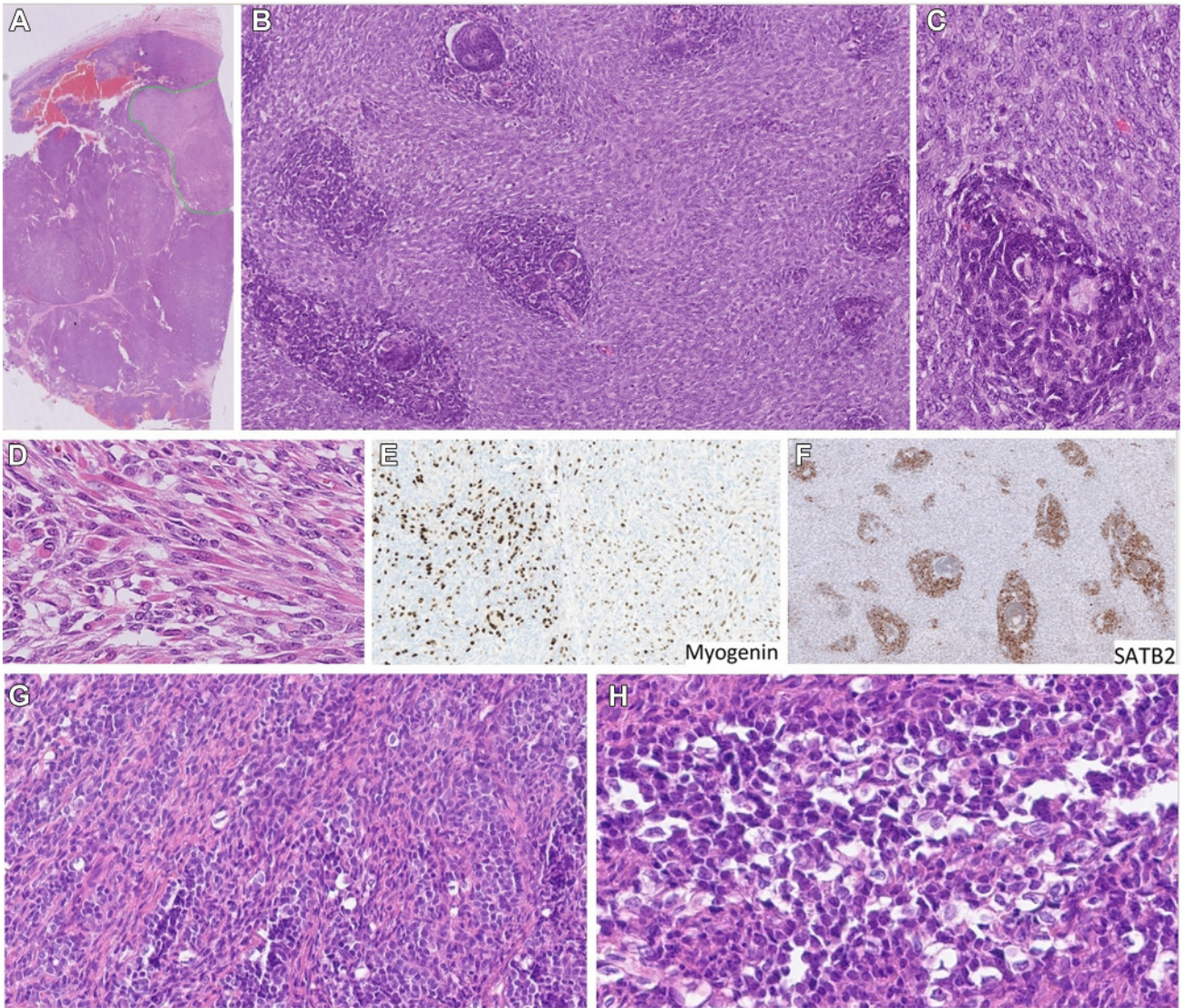
Figure 4.
(A–F) Case 6. (A) Case 6 contained a sharply demarcated rhabdomyoblastic nodule (green line). (B, C) Most parts showed a biphasic arrangement and consisted of round cell nests with predominantly neuroendocrine nuclear features on a background of more ovoid to spindled cells having lighter chromatin. (D) High-power view of the focus containing strap cells and rhabdomyoblasts with cross-striations. (E) Markers of rhabdomyoblastic differentiation including myogenin were positive throughout the tumor. (F) SATB2 expression was found almost exclusively in the round cell nests. (G, H) Case 7. (G) The tumor also showed a biphasic arrangement, with most parts of the tumor consisting of more loosely dispersed sheets of round cells with neuroendocrine features admixed with spindle cells. (H) Numerous clear cells were present.

neuroendocrine neoplasms,[14] the latter typically exhibit more diffuse expression of epithelial and neuroendocrine markers (typically coexpression of synaptophysin, chromogranin, and/or INSM1), and in most cases, a primary lesion can be identified clinically. As already emphasized by Hiemenz et al,[2] these tumors are in many aspects highly reminiscent of synovial sarcoma, particularly of those with predominantly spindle cell morphology, and a confident distinction purely on morphologic grounds is unreliable. However, with the use of novel highly specific and sensitive immunohistochemical markers that are becoming available at many institutions, synovial sarcoma can most likely be excluded (caveat: only 1 case tested for SS18::SSX antibody).[15] Nevertheless, while we believe that, when present, some of the more recurrent histopathological features of *EWSR1/FUS::-POU2AF3* tumors may raise suspicion for the diagnosis, high-throughput genetic assays such as RNA sequencing represent

the only way to reliably diagnose these tumors at this point. In addition, some cases lack the more characteristic histologic traits, and they cannot be distinguished from morphologically highly overlapping differential diagnostic entities that lack specific immunohistochemical markers such as low-grade myxofi-brosarcoma, osteosarcoma, or various myoepithelial or basaloid epithelial neoplasms without appropriate molecular studies.

Regarding the molecular background, among the 19 reported cases, 17 carried the *EWSR1::POU2AF3* fusion, while 2 cases had *FUS* as the 5′ fusion partner instead of *EWSR1*. While the number of published cases is low and the following observation might thus be merely coincidental, it is interesting to note that in 14 of 17 cases with *EWSR1::POU2AF3* fusion, the locations of genomic breakpoints seemed to follow an anatomical site−dependent pattern. Namely, 9 of 12 head and neck cases had genomic breakpoints located in exons 12 to 17 and only 3 cases in exons 9
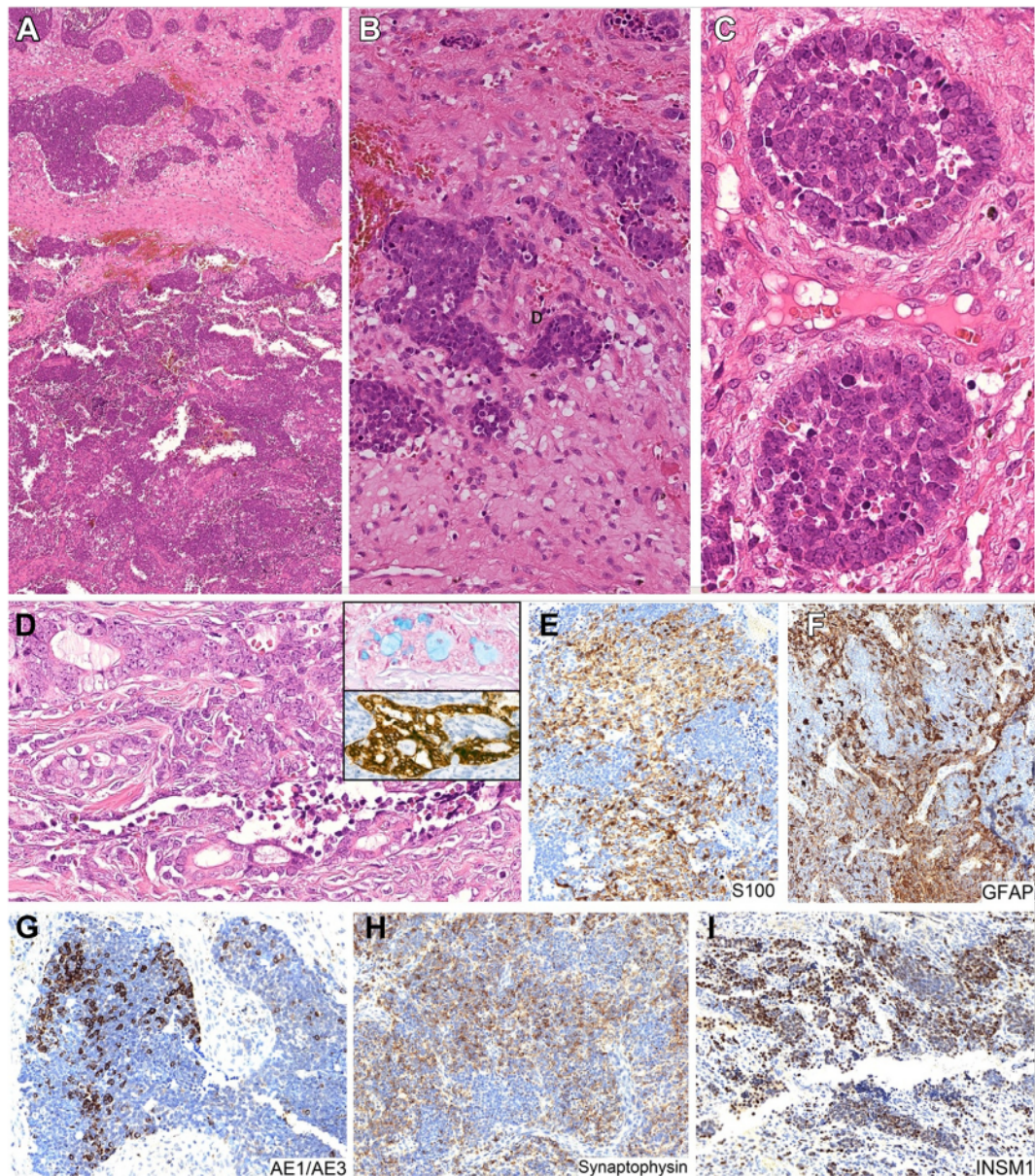
Figure 5.
Case 8. (A) Cellular stroma−poor areas (bottom) alternated with more hyalinized spindle cell regions containing scattered round cell nests (top). (B) Nests of round cells with neuroendocrine features on the hypocellular background featuring spindle to stellate shaped cells with little atypia were reminiscent of similar areas in cases 1 and 2. (C) Peripheral palisading of the round cells was present in some nests. (D) A small focus with keratin 7−positive glands (lower inset) containing Alcian blue−positive mucin (upper inset). (E-I) Multifocal expression of S100, GFAP, AE1/AE3, synaptophysin, and INSM1 preferentially found within the round cell areas.

or 10 of *EWSR1* gene. In contrast, all 5 cases located outside the head and neck area had breakpoints localized in exons 9 or 10. Exons 12 to 14 contain a central RNA recognition motif (RRM), which is involved in RNA and DNA binding (Fig. 6). Similar to Ewing sarcoma and many other *EWSR1*-rearranged tumors that usually have genomic breakpoints located in exons 6 to 8, the RRM is lost in non−head and neck cases.[16-18] In contrast, most of the reported head and neck cases retained the RRM domain. The binding of regulatory nucleic acids or ribonucleoproteins may potentially affect the function of the fusion protein. A difference in the pathogenesis of the translocation, including the specific microenvironment of the head and neck area, might potentially be causative, while the exact significance and molecular basis remain unclear.

POU class 2 homeobox associating factor 3 (POU2AF3) gene [formerly named *colorectal cancer associated 2 (COLCA2)*] located on chromosome 11q23.1 has been associated with increased colorectal cancer risk in a genome-wide association study. The pattern of expression of the POU2AF3 protein in neoplastic, stromal, and immune cells in patients with higher-risk alleles for colorectal cancer suggested a tumor suppressor role.[19] However, the exact mechanism through which the POU2AF3 protein is deregulated remains unclear.[1] Moreover, *POU2AF3* codes for a transcriptional coactivator protein that through its OCA domain (Fig. 6) binds with the transcription factor POU2F3, which is critical for the development of tuft cells, a rare chemosensory lineage that coordinates immune and neural responses to foreign pathogens in mucosal tissues.

Table 2
Histologic, immunohistochemical, and molecular features of EWSR1::POU2AF3 tumors

Case no.	Mits/10 HPF and necrosis	AE1/AE3	EMA	S100	GFAP	NE markers (all available)	SAT-B2	Other positive IHC	Other negative IHC	EWSR1 breakpoint	POU2AF3 breakpoint
1	2/10 Absent	-	-	-	-	ND	-	SMA+; CD10+	Desmin; SOX10; MUC4, CDX2	Ex 14	Ex 2
2	2/10 Absent	+	ND	-	-	SYN-	++	ND	MUC4; ALK; NUT; Pan-Trk; STAT6; Desmin; SOX10; SMA; Myo-D1; Myogenin; CD34; Beta-Catenin, CDX2	Ex 14-16	Ex 2
3	6/10 Present (10%)	-	-	-	+	SYN- CD56+	+++	ND	CD99; NKX2.2; SOX10; H3k27me3 retained; SS18::SSX; TLE1; Desmin; myogenin; STAT6	Ex 15	Ex 2
4	10/10 Present (10%)	++	+	+	++	SYN- CHROMO- CD56+	ND	CD99+++	Desmin; Myogenin; SMA	EX 14	Ex 2
5	9/10 Absent	-	-	++	++	SYN+ CHROMO- CD56+++	+	SMA+	OSCAR; Desmin; MyoD1; myogenin; SOX10; TLE1; BRAF; CD34; panTRK; CD99; CDX2	EX 9	Ex 2
6	4/10 Absent	++	-	+	+	SYN+ CHROMO+ CD56+++	++	Desmin/MyoD1/ Myogenin ++; SMA+; membranous CD99+; MyoD1+; Myogenin+	BCOR; WT1; TLE1; CDX2; SOX10	EX 9	Ex 2
7	8/10 Absent	++	-	ND	-	SYN- CHROMO-	ND	ND	Desmin; Myogenin; SMA; CD99	EX 9	Ex 2
8	24/10 Absent	+	+	++	++	SYN++ CHROMO++ INSM1+	-	CK5+; CK7+; SMA+	CD99; SOX10; TTF1; CDX2; CD34; p63; CK20; MC polyomavirus; calponin; WT1; ERG; CyclinD1 and ALK; Rb and INI1 retained; TP53 wt	EX 10	Ex 2
		5/8 (63%)	2/7 (29%)	4/7 (57%)	5/8 (63%)	CD56: 4/4 Any other: 3/7 (43%)					

CHROMO, chromogranin; Ex, exon; IHC, immunohistochemistry; mits/10 HPF, mitoses per 10 high-power fields; ND, not done; NE, neuroendocrine; SMA, smooth muscle actin; SYN, synaptophysin.
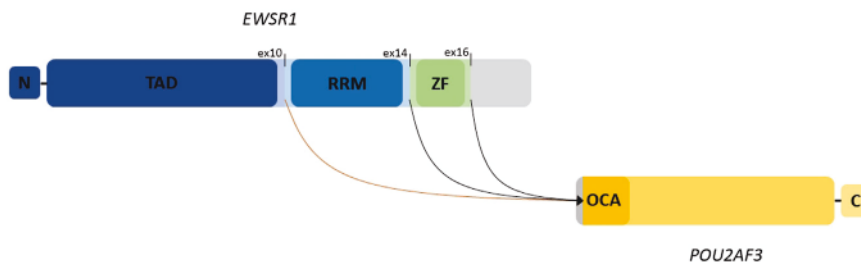
Figure 6.
Schematic depiction of the *EWSR1::POU2AF3* fusion. Dark blue, blue, green, and yellow parts of the respective genes represent the regions that are retained in the fusion products, while the gray parts are lost. In non–head and neck cases, only the transactivation domain (TAD) (dark blue) of *EWSR1* is retained. In contrast, the head and neck cases contain both TAD and the RNA recognition motif (RRM) (blue) of *EWSR1*; in addition, some head and neck cases also retain the RanBP2 type zinc finger (ZF) (green). The OCA domain of POU2AF3 (yellow), which enables binding to POU domain–containing transcription factors, is almost completely retained in the fusion gene. ex, exon.

Recent studies have also revealed tuft-cell–like human tumors, particularly as a variant of small cell lung cancer.[20]

In conclusion, we reported 8 additional cases of *EWSR1:: POU2AF3* sarcomas, further defining their clinicopathological features and, for the first time, emphasizing their potential for heterologous differentiation. Many cases exhibit relatively characteristic biphasic morphologic features, whereas others may show epithelial, rhabdomyosarcomatous, or osteosarcomatous differentiation or present as nondescript spindle and/or round cell sarcomas. Although further studies are needed to confirm whether all tumors with *EWSR1::POU2AF3* fusion represent a single entity, we believe that some of the partially overlapping clinicopathological features in our cases lend support to this notion. Because most of these tumors follow an aggressive clinical course and, in some cases, their low-grade morphology may be deceiving, the use of high-throughput molecular methods is recommended to achieve early detection, enabling optimal treatment.

Author Contributionsnt

O.K., C.A.D., J.T.-M., and Michael Michal designed the study, analyzed the data, and drafted and edited the manuscript. A.A. and A.L.F. edited the manuscript. A.M.O. performed the statistical analysis. All other authors contributed cases, provided clinical information, or performed molecular testing. All authors approved the final version of the manuscript.

Data Availability

Data that support the findings of this study are available from the corresponding author on reasonable request.

Declaration of Competing Interest

The authors have no conflict of interest to disclose.

Ethics Approval and Consent to Participate

The study was conducted following the rules set by the Faculty Hospital in Pilsen Ethics Committee. Informed consent was not required for the study.

Supplementary Material

The online version contains supplementary material available at https://doi.org/10.1016/j.modpat.2023.100337

References

1. Agaimy A, Baněčková M, De Almeida J, et al. Recurrent EWSR1::COLCA2 fusions define a novel sarcoma with spindle/round cell morphology and strong predilection for the sinonasal tract. *Am J Surg Pathol.* 2023;47(3):361–369. https://doi.org/10.1097/PAS.0000000000002000
2. Hiemenz MC, Kaur J, Kuang Z, et al. POU2AF3-rearranged sarcomas: a novel tumor defined by fusions of EWSR1 or FUS to a gene formerly designated COLCA2. *Genes Chromosomes Cancer.* 2023;62(8):460–470. https://doi.org/10.1002/gcc.23136
3. Michal M, Rubin BP, Kazakov DV, et al. Inflammatory leiomyosarcoma shows frequent co-expression of smooth and skeletal muscle markers supporting a primitive myogenic phenotype: a report of 9 cases with a proposal for reclassification as low-grade inflammatory myogenic tumor. *Virchows Arch.* 2020;477(2):219–230.
4. Michal M, Berry RS, Rubin BP, et al. EWSR1-SMAD3-rearranged fibroblastic tumor: an emerging entity in an increasingly more complex group of fibroblastic/myofibroblastic neoplasms. *Am J Surg Pathol.* 2018;42(10):1325–1333.
5. Skálová A, Baněčková M, Laco J, et al. Sclerosing polycystic adenoma of salivary glands: a novel neoplasm characterized by PI3K-AKT pathway alterations-new insights into a challenging entity. *Am J Surg Pathol.* 2022;46(2):268–280.
6. Agaimy A, Tögel L, Haller F, Zenk J, Hornung J, Märkl B. YAP1-NUTM1 Gene fusion in porocarcinoma of the external auditory canal. *Head Neck Pathol.* 2020;14(4):982–990.
7. Balan J, Jenkinson G, Nair A, et al. SeekFusion—a clinically validated fusion transcript detection pipeline for PCR-based next-generation sequencing of RNA. *Front Genet.* 2021;12:739054.
8. Michal M, Rubin BP, Agaimy A, et al. EWSR1-PATZ1-rearranged sarcoma: a report of nine cases of spindle and round cell neoplasms with predilection for thoracoabdominal soft tissues and frequent expression of neural and skeletal muscle markers. *Mod Pathol.* 2021;34(4):770–785.
9. Evans HL. Low-grade fibromyxoid sarcoma: a clinicopathologic study of 33 cases with long-term follow-up. *Am J Surg Pathol.* 2011;35(10):1450–1462.

10. Smith TA, Easley KA, Goldblum JR. Myxoid/round cell liposarcoma of the extremities. A clinicopathologic study of 29 cases with particular attention to extent of round cell liposarcoma. *Am J Surg Pathol*. 1996;20(2):171−180.
11. Miettinen M, Finnell V, Fetsch JF. Ossifying fibromyxoid tumor of soft parts—a clinicopathologic and immunohistochemical study of 104 cases with long-term follow-up and a critical review of the literature. *Am J Surg Pathol*. 2008;32(7):996−1005.
12. Doyle LA, Möller E, Dal Cin P, Fletcher CD, Mertens F, Hornick JL. MUC4 is a highly sensitive and specific marker for low-grade fibromyxoid sarcoma. *Am J Surg Pathol*. 2011;35(5):733−741.
13. Le Loarer F, Baud J, Azmani R, Michot A, Karanian M, Pissaloux D. Advances in the classification of round cell sarcomas. *Histopathology*. 2022;80(1):33−53.
14. Kasajima A, Konukiewitz B, Schlitter AM, et al. Mesenchymal/non-epithelial mimickers of neuroendocrine neoplasms with a focus on fusion gene-associated and SWI/SNF-deficient tumors. *Virchows Arch*. 2021;479(6):1209−1219.
15. Baranov E, McBride MJ, Bellizzi AM, et al. A novel SS18-SSX fusion-specific antibody for the diagnosis of synovial sarcoma. *Am J Surg Pathol*. 2020;44(7):922−933.
16. Wang X, Schwartz JC, Cech TR. Nucleic acid-binding specificity of human FUS protein. *Nucleic Acids Res*. 2015;43(15):7535−7543.
17. Sankar S, Lessnick SL. Promiscuous partnerships in Ewing's sarcoma. *Cancer Genet*. 2011;204(7):351−365.
18. Bridge JA, Fidler ME, Neff JR, et al. Adamantinoma-like Ewing's sarcoma: genomic confirmation, phenotypic drift. *Am J Surg Pathol*. 1999;23(2):159−165.
19. Peltekova VD, Lemire M, Qazi AM, et al. Identification of genes expressed by immune cells of the colon that are regulated by colorectal cancer-associated variants. *Int J Cancer*. 2014;134(10):2330−2341.
20. Wu XS, He XY, Ipsaro JJ, et al. OCA-T1 and OCA-T2 are coactivators of POU2F3 in the tuft cell lineage. *Nature*. 2022;607(7917):169−175.

4.7 Comprehensive clinicopathological, molecular, and methylation analysis of mesenchymal tumors with *NTRK* and other kinase gene aberrations

V práci vydané v Journal of Pathology (IF 7,3) uvádíme extenzivní analýzu 22 vřetenobuněčných mesenchymálních tumorů s aberacemi genů pro proteinové kinázy. Je uveden detailní histologický rozbor s rozdělením těchto tumorů do tří morfologických tříd. Pomocí metylačního profilování bylo možné dokázat, že 8/9 testovaných tumorů se v nesupervizovaném clusterování řadilo k metylační třídě infantilního fibrosarkomu. Toto zjištění potvrzuje hypotézu, že všechny tyto tumory patří do společné skupiny, jednotlivé případy se pak pohybují na morfologickém spektru od low-grade indolentních lézí po lokálně agresivně se chovající a potenciálně metastazující high-grade sarkomy.

V studovaném souboru bylo shromážděno celkem 22 případů, v 14 z nich se jednalo o pediatrické pacienty (medián věku 5,5 měsíců), ve zbylých případech byli pacienti dospělí (medián věku 44,5 let), nebyla pozorována predilekce pohlaví. Nádory vyrůstaly v měkkých tkáních končetin a trupu i ve viscerálních orgánech, 5 případů bylo lokalizováno v oblasti hlavy a krku. V 15 případech byly tumory resekovány, v 6 případech byla léčba doplněna chemoterapií a/nebo cílenou terapií inhibitory NTRK nebo RET. Ve třech případech byly nádory léčeny kombinací chemoterapie a cílené léčby. V 19 % případů byly zaznamenány rekurence, vzdálené metastázy byly přítomny v 6 % případů, jednalo se o jednoho tříletého pacienta, který po resekci nádoru měkkých tkání obličeje doplněné chemoterapií vyvinul mediastinální metastázy a zemřel 30 měsíců po diagnóze. Užitím cílené terapie se podařilo dosáhnout úplné remise nebo významné regrese nádorů v 5/6 případů. Ve zbylém případě musela být terapie NTRK inhibitorem larotrektinibem přerušena kvůli vedlejším účinkům.

Tři morfologické třídy užívané v práci byly definovány následujícím způsobem: low-grade skupinu čítající v této studii 6 případů tvořily blandní vřetenobuněčné nádory s nízkou celularitou, nenápadnými jadernými atypiemi a minimálními mitotickou aktivitou. V této skupině byly pozorovány různé morfologické vzory a jejich kombinace v jednotlivých případech, jednalo se například o léze připomínající neurální tumor podobný lipofibromatóze (lipofibromatosis-like neural tumor), léze s výraznou stromální a perivaskulární hyalinizací či léze připomínající hemangiopericytom. Do high-grade skupiny čítající 11 případů byly řazeny tumory s vysokou buněčností a výraznou mitotickou aktivitou (více než 11 mitotických figur na 2,4 mm^2), morfologicky odpovídající infantilnímu či adultnímu fibrosarkomu nebo připomínající high-grade maligní tumor z pochev periferních nervů. Dále byla zavedena skupina intermediate-grade tumorů tvořená 4 případy, kam spadaly léze nezařaditelné ani do jedné z výše popsaných kategorií. Intermediate-grade tumory vykazovaly morfologické vzory podobné low-grade tumorům, avšak se zvýšenou celularitou a mírně vyšší mitotickou aktivitou (do 6 mitotických figur na 2,4 mm^2), případně připomínaly low-grade maligní tumor z pochev periferních nervů. Dále byl v studii zahrnut případ, který v separátních histologických blocích obsahoval jak stuktury low-grade tumoru s výraznou stromální a perivaskulární hyalinizací, tak struktury velmi hypercelulárního infantilního fibrosarkomu.

Imunohistochemické markery S100 a CD34 byly pozitivní v 12/22 a 14/22 případů, koexprese obou markerů byla prokázána u 10/22 případů. Všechny tumory

s fúzemi genu *NTRK1/3* byly pozitivní v imunohistochemickém průkazu exprese markeru panTrk, lze ho tedy využít pro screening případů, u nichž by dále měla být vyšetřena přítomnost aberace těchto genů.

Pomocí RNA-seq byly ve 4 případech detekovány dosud nepopsané fúze kinázových genů – *PWWP2A::RET*, *NUMA1::RET*, *CAPZA2::MET* a *ITSN1::RAF1*. DNA-seq prokázala v jednom případu cervikálního tumoru, v kterém nebyla cílenou RNA-seq detekována žádná fúze, mutace v genech *BRAF* a *EGFR* (*BRAF* delins p.V600K a *EGFR* duplikace p.S768_D770dup), jedná se ve skupině těchto nádorů o první popsaný případ s mutacemi jinými než fúzemi.

Ve výše zmíněném případu s low-grade a high-grade komponentou byla pomocí FISH rozpoznána homozygotní ztráta genu *CDKN2A*, a to pouze v high-grade komponentě, mohlo se tedy jednat o mutaci, který způsobila progresi onemocnění s rozvojem agresivní high-grade nádorové subpopulace.

Metylační profilování bylo úspěšné u 9 případů. Nesupervizované clusterování metylačních profilů přiřadilo 8/9 tumorů do metylační třídy infantilního fibrosarkomu, jednalo se o tumory celého výše popsaného morfologického spektra, s fúzemi jinými než *ETV6::NTRK3*, a o případ bez fúzí, s mutacemi *BRAF* a *EGFR*. Zbylý případ byl zařazen do metylační třídy inflamatorního myofibroblastického tumoru, nejspíše kvůli přítomnosti hojného nenádorového zánětlivého infiltrátu. Výsledky byly potvrzeny též hierarchickým clusterováním.

Byly rovněž porovnány profily genomových copy-number variant (CNV). Byla pozorována dobrá shoda mezi plochým profilem CNV a low-grade a intermediate-grade morfologií. Naproti tomu byly u high-grade případů zjištěny mnohonásobné zisky a ztráty genetického materiálu. Ve skupině high-grade nádorů mělo variantní počty kopií přibližně 25 % genomu, ve skupině low-grade a intermediate-grade pak přibližně 7 % genomu.

ORIGINAL ARTICLE

Comprehensive clinicopathological, molecular, and methylation analysis of mesenchymal tumors with *NTRK* and other kinase gene aberrations

Natálie Klubíčková[1,2*†], Josephine K Dermawan[3†], Elaheh Mosaieby[1,2], Petr Martínek[2], Tomáš Vaněček[2], Veronika Hájková[2], Nikola Ptáková[2,4], Petr Grossmann[2], Petr Šteiner[2], Marián Švajdler[1,2], Zdeněk Kinkor[2], Květoslava Michalová[1,2], Peter Szepe[5], Lukáš Plank[5], Stanislava Hederová[6], Alexandra Kolenová[6], Neofit Juriev Spasov[7], Kemal Kosemehmetoglu[8], Leo Pažanin[9], Zuzana Špůrková[10], Martin Baník[11], Luděk Baumruk[12], Anders Meyer[13], Antonina Kalmykova[14], Olena Koshyk[14], Michal Michal[1,2] and Michael Michal[1,2]

1   *Department of Pathology, Faculty of Medicine in Pilsen, Charles University, Pilsen, Czech Republic*
2   *Bioptical Laboratory Ltd, Pilsen, Czech Republic*
3   *Robert J. Tomsich Pathology and Laboratory Medicine Institute, Cleveland Clinic, Cleveland, OH, USA*
4   *Department of Biology and Medical Genetics, Second Faculty of Medicine, Charles University and Motol University Hospital, Prague, Czech Republic*
5   *Institute of Pathological Anatomy, Jessenius Faculty of Medicine in Martin, Comenius University, Martin, Slovakia*
6   *Department of Pediatric Hematology and Oncology, National Institute of Children's Diseases and Medical Faculty, Comenius University, Bratislava, Slovakia*
7   *Department of Pediatrics and Medical Genetics, Oncohematology Unit, Medical University Plovdiv, University Hospital Sveti Georgi, Plovdiv, Bulgaria*
8   *Department of Pathology, Hacettepe University, Ankara, Turkey*
9   *Department of Pathology, Sestre Milosrdnice University Hospital Center, Zagreb, Croatia*
10 *Department of Pathology, Na Bulovce Hospital, Prague, Czech Republic*
11 *Department of Pathology, Regional Hospital Karlovy Vary, Karlovy Vary, Czech Republic*
12 *Department of Pathology, Regional Hospital Příbram, Příbram, Czech Republic*
13 *Department of Pathology, University of Kansas, Kansas City, KS, USA*
14 *Medical Laboratory CSD Health Care Ltd, Kyiv, Ukraine*

Correspondence to: N Klubíčková, Department of Pathology, Medical Faculty and University Hospital Plzeň, Charles University, Alej Svobody 80, 323 00 Pilsen, Czech Republic. E-mail: klubickova@biopticka.cz

†These authors contributed equally to this study.

Abstract

Alterations in kinase genes such as *NTRK1/2/3*, *RET*, and *BRAF* underlie infantile fibrosarcoma (IFS), the emerging entity 'NTRK-rearranged spindle cell neoplasms' included in the latest WHO classification, and a growing set of tumors with overlapping clinical and pathological features. In this study, we conducted a comprehensive clinicopathological and molecular analysis of 22 cases of IFS and other kinase gene–altered spindle cell neoplasms affecting both pediatric and adult patients. Follow-up periods for 16 patients ranged in length from 10 to 130 months (mean 38 months). Six patients were treated with targeted therapy, achieving a partial or complete response in five cases. Overall, three cases recurred and one metastasized. Eight patients were free of disease, five were alive with disease, and two patients died. All cases showed previously reported morphological patterns. Based on the cellularity and level of atypia, cases were divided into three morphological grade groups. S100 protein and CD34 were at least focally positive in 12/22 and 14/22 cases, respectively. Novel *PWWP2A::RET*, *NUMA1::RET*, *ITSN1::RAF1*, and *CAPZA2::MET* fusions, which we report herein in mesenchymal tumors for the first time, were detected by RNA sequencing. Additionally, the first uterine case with *BRAF* and *EGFR* mutations and CD34 and S100 co-expression is described. DNA sequencing performed in 13 cases uncovered very rare additional genetic aberrations. The CNV profiles showed that high-grade tumors demonstrate a significantly higher percentage of copy number gains and losses across the genome compared with low- and intermediate-grade tumors. Unsupervised clustering of the tumors' methylation profiles revealed that in 8/9 cases, the methylation profiles clustered with the IFS methylation class, irrespective of their clinicopathological or molecular features.
© 2024 The Authors. *The Journal of Pathology* published by John Wiley & Sons Ltd on behalf of The Pathological Society of Great Britain and Ireland.

Introduction

Soft tissue tumors with kinase gene alterations comprise a heterogeneous group of mesenchymal neoplasms which includes, besides others, dermatofibrosarcoma protuberans (DFSP), inflammatory myofibroblastic tumor (IMT), and infantile fibrosarcoma (IFS) [1]. In addition to the canonical *ETV6::NTRK3* fusion described in IFS more than two decades ago [2,3], the recent widespread adoption of RNA sequencing (RNA-seq) has led to the description of several alternative gene rearrangements such as those of *NTRK1/2/3*, *BRAF*, *MET*, and others [1,4–7]. It has also led to the emergence of a novel and not yet fully defined group of mesenchymal tumors with kinase gene alterations that partially overlaps with IFS. It is currently included in the WHO classification as 'NTRK-rearranged spindle cell neoplasms' (*NTRK*-SCN) [8,9]. It includes spindle cell tumors of both children and adults that form a continuous morphological spectrum which, based on cellularity and degree of atypia, can be roughly divided into three morphological subgroups.

The first subgroup consists of bland spindle cell lesions exhibiting low cellularity, minimal atypia, and very few mitoses [further referred to as the low-grade (LG) group], while the second contains lesions with high cellularity, high mitotic activity, and a high level of atypia [high-grade (HG) group]. In addition, some cases are difficult to assign to one of these categories as they fall somewhere in-between [intermediate-grade (IG) group]. The LG group may exhibit one of several often co-occurring morphological patterns such as a lipofibromatosis-like neural tumor (LNT) pattern [10], a prominent stromal and perivascular hyalinization (SPH) pattern [11], a myopericytic/hemangiopericytic pattern [12], and others [9,13]. Tumors in the IG group may retain similar patterns, or they may vaguely resemble LG malignant peripheral nerve sheath tumors (LG-MPNSTs) [9,14]. Tumors from the HG group morphologically overlap with IFS, adult fibrosarcoma, and/or HG-MPNSTs (due to significant overlap, these will be collectively referred to as the IFS pattern) [1,9,14].

Many tumors across the morphological spectrum of *NTRK*-SCN exhibit immunohistochemical co-expression of CD34 and S100 protein, and their molecular background is characterized by various gene fusions of, and less often mutations in, kinase genes such as *NTRK1/2/3*, *BRAF*, *RAF1*, *RET*, *MET*, and others [9,14–22], all of which lead to the activation of the MAP kinase signaling pathway [1]. However, very little is known regarding their methylation and copy number variation (CNV) profiles and potential secondary genetic alterations. In this clinicopathological study, we focused on their comprehensive molecular characterization using FISH, DNA sequencing (DNA-seq), and RNA-seq, as well as CNV and methylation profiling.

Materials and methods

Compliance with ethical standards

The study was conducted following the rules set by the Faculty Hospital in Pilsen Ethics Committee. Informed consent was not required for the study.

Case selection

Twenty-two cases falling within the morphological and molecular spectrum of the so-called *NTRK*-SCN and IFS were retrieved from our institutional tumor registry. All but one were received in consultation, which explains the low incidence of conventional *ETV6::NTRK3*-fused IFS in our cohort. Cases 11, 16, and 18 were reported previously by our group but were now subjected to a more extensive molecular-genetic analysis [19,20,23]. In case 6, LG and HG areas were present in two different sections, which enabled us to analyze both parts separately. Based on cellularity (defined as no overlapping, partial overlapping, or consistent overlapping of tumor cells) and level of atypia (classified based on uniformity of tumor cells, nuclear to cytoplasmic ratio, and hyperchromatism of nuclei), the cases were divided into three morphological grade groups as outlined in the Introduction. Importantly, this division was based purely on morphological features and is not meant to imply clinical behavior of grade 3 (or HG) sarcomas.

Immunohistochemistry

All cases were immunohistochemically stained using a Ventana BenchMark ULTRA (Ventana Medical System, Inc., Tucson, AZ, USA) for S100 protein and CD34. Additionally, 12 cases that harbored *NTRK1/3* rearrangements were tested with a panTrk antibody. Details regarding antibody dilutions and clones are provided in supplementary material, Table S1.

Molecular genetic studies

All molecular methods in this section are described in more detail in Supplementary materials and methods.

FISH

For the detection of *CDKN2A* loss using FISH, factory premixed ZytoLight SPEC *CDKN2A/CEN9* Dual Color Probe (ZytoVision GmbH, Bremerhaven, Germany) was used. The FISH procedure was performed as described previously [24].

Next-generation sequencing (NGS)

The customized Sarcoma FusionPlex kit (ArcherDX Inc., Boulder, CO, USA) was used, which detects fusion transcripts of selected exons of 88 genes, and mutations in hotspots of 14 genes, respectively. For further mutation analysis, we used the commercially available TruSight Oncology 500 panel (Illumina, San Diego, CA, USA), a comprehensive NGS assay on FFPE samples that

identifies somatic variants, copy number changes, tumor mutational burden (TMB), and microsatellite instability (MSI). Only tumor tissue was analyzed, except for case 18 where a peripheral blood sample was available.

Methylation analysis

Eleven kinase-rearranged tumors were tested by methylation profiling (cases 1, 3, 4, 6, 11, 13, 15, 18, 19, 21, and 22). Two specimens failed quality control (cases 4 and 15). Genomic DNA was extracted from paraffin blocks and 250 ng of genomic DNA was subjected to bisulfite conversion and processed on the Illumina Infinium MethylationEPIC/850k platform (Illumina) with over 850,000 methylation sites according to the manufacturer's instructions.

Additionally, we obtained raw idat files for 247 samples from the Heidelberg sarcoma methylation classifier reference cohort (Gene Expression Omnibus study accession number GSE140668). Idat processing and data analysis on all 256 samples were performed using R software (version 4.1.0) (R Foundation for Statistical Computing, Vienna, Austria) and the 'minfi' R package (version 1.38.0) (Bioconductor, Boston, MA, USA).

For unsupervised clustering, dimensionality reduction was performed by the t-distributed stochastic neighborhood embedding (t-SNE) method. After normalizing the input data matrix (centering the mean of each column to zero), the top 10,000 most variable CpG sites by variance were analyzed using the 'Rtsne' R package (version 0.15) (https://CRAN.R-project.org/package=Rtsne, last accessed 8 June 2023) with the following nondefault parameters: perplexity = 10, max_iter = 5,000, and $\theta = 0$. Additionally, unsupervised hierarchical clustering was performed on the top 1,000 most variable CpG sites by variance using the 'pheatmap' R package (version 1.0.12) (https://CRAN.R-project.org/package=pheatmap, last accessed 8 June 2023) with Ward.D2's linkage and Euclidean distance for clustering.

For CNV analysis, the Mset files after idat files preprocessing were processed by the 'conumee' R package (version 1.32.0) (Bioconductor). CNV was considered present if the absolute segmentation mean was greater than or equal to 0.3. The fraction of CNV across the genome was calculated by dividing the sum of all segments with CNV by the sum of all segments across the genome. Additionally, the idat raw data files were uploaded to a DNA methylation-based classification tool, Sarcoma classifier (version 10.1) [25,26], available via https://www.molecularneuropathology.org/ (last accessed 8 June 2023).

Results

Clinical data

Clinicopathological data are summarized in Table 1. There were 11 female and 11 male patients, including 14 children ranging in age from newborns to 13 years (mean 24 months; median 5.5 months). The eight adult patients were aged 26–72 years (mean 47 years; median 44.5 years). Various superficial and deep sites were affected including the duodenal wall ($n = 1$) or the uterus ($n = 2$). The size ranged from 1.3 to 30 cm (mean 8.5 cm, median 5 cm).

Histological findings

Microscopically, the tumors were usually uncircumscribed, and some widely infiltrated into the surrounding tissues. The 22 cases exhibited various and often multiple morphological patterns and morphological grades. In this situation, the highest grade was assigned.

Five cases at the LG end of the morphological spectrum exhibited SPH and LNT patterns and were composed of uniform bland non-overlapping spindle cells that were dispersed in abundant stroma. The mitotic activity did not exceed two mitoses per 10 high-power fields (HPF; 2.4 mm^2). The tumor cells grew in sheets or cords around thick hyalinized vessels in the case of SPH or widely infiltrated into subcutaneous adipose tissue in the case of LNT (Figure 1A). Case 11 showed a myxoid SPH pattern composed mostly of epithelioid cells with abundant eosinophilic cytoplasm (Figure 1B) [23].

Three IG cases showed more polymorphism, hyperchromasia, and occasional overlapping of tumor cells, which were arranged haphazardly or in short fascicles. The cases resembled LG-MPNST (Figure 1C) or had an SPH (Figure 1D) or a myopericytomatous pattern (case 19). The latter case was composed of myoid spindle cells arranged in haphazard fascicles punctuated by prominent vasculature (Figure 1E,F). The mitotic activity was higher than in the LG group but did not exceed 6 mitoses/10 HPF (Figure 1F); necrosis was absent.

All 12 cases classified as HG had a scarce stroma and were composed of hypercellular, largely overlapping cell population with a high nuclear to cytoplasmic ratio, hyperchromatic nuclei, and significant variability in cell shape. The cases were arranged in a herringbone pattern, vague fascicles, or solid sheets (Figure 2A,B). The mitotic activity ranged from 11 to 56 mitoses/10 HPF and small areas of necrosis were often present. In case 17, the tumor exhibited epithelioid to rhabdoid tumor cells (Figure 2C). Case 18 showed areas with unusual LG triphasic morphology resembling fibrous hamartoma of infancy (Figure 3A) that transformed into HG-IFS in some foci (Figure 3B) [20]. A typical LG-SPH pattern (Figure 3C) with progression to HG-IFS (Figure 3D) was present in case 6. Case 1 had the typical IFS morphology and contained a rich non-neoplastic inflammatory infiltrate (Figure 3E).

Immunohistochemical findings

The immunohistochemical results are summarized in Table 1. CD34 (Figures 3F,H and 4C) and S100 protein (Figures 3G,I and 4D) were at least focally positive in

Table 1. Main clinicopathological and molecular data.

Case No.	Age/sex	Localization	Max. dim. (cm)	Grade	Morphology review	S100	CD34	panTrk	Fusions detected by RNA-seq	Additional pathogenic mutations by DNA-seq	CDKN2A enumeration by FISH and/or methylation profiling	MSI/TMB (mut/Mb)	Methylation class by t-SNE clustering	Treatment	Outcome/length (months)
1	3 y/F	Lower eyelid	NA	HG	IFS	+	+++	+++	LMNA::NTRK1	–	Normal	NA/low	IMT	S + TT-E	2 × LR before our diagnosis; NED/13
2	37 y/F	Instep	1.3	LG	LNT	+	+++	++	LMNA::NTRK1	–	Normal	NA	ND	S	NED/35
3	43 y/M	Hip	6.3	IG	SPH	++	+++	+++	LMNA::NTRK1	–	Loss[†]	Low/low	IFS	S	NED/10
4	1 d/M	Duodenum	NA	HG	IFS	–	–	+++	TPM3::NTRK1	–	Normal	NA	NA	CHT + TT-L	AWD/20
5	10 mo/M	Lower leg	NA	LG	LNT	+	–	+++	TPM3::NTRK1	NA	Normal	NA	ND	NA	NA
6*	3 y/M	Upper lip and orbit	NA	HG	IFS	+++	+++	+++	EML4::NTRK3	NA	Loss[‡]	Low/high (17.7)	IFS	S + CHT	Mediastinal MTS; DOD/30
7	4 mo/M	Forearm	NA	LG	SPH	++	+++	+++	ETV6::NTRK3	–	Normal	NA	ND	S + CHT + TT-L	NED/27
8	5 mo/M	Cheek	NA	HG	IFS	–	+	++	ETV6::NTRK3	–	ND	Low/low	ND	S + CHT	AWD/121
9	6 mo/F	Foot	NA	HG	IFS	–	++	++	ETV6::NTRK3	NA	ND	NA	ND	CHT + TT-L	NED/21
10	1 mo/M	Scalp, intracranial propagation	4.7	HG	IFS	–	+	+++	ETV6::NTRK3	–	Normal	Low/low	ND	S	NA
11	26 y/F	Uterus	22.7	LG	Myxoid SPH with epithelioid/rhabdoid cells	+++	+++	+++	STRN::NTRK3	–	Normal	NA	IFS	S	NA
12	13 y/F	Retroperitoneum	NA	LG	SPH	+	+++	+++	RBPMS::NTRK3	ND	ND	ND	ND	NA	LR; AWD/NA
13	14 d/F	Coccygeal region	1.5	HG	IFS	–	–	–	PWWP2A::RET	NA	Normal	NA	IFS	CHT + TT-S	AWD/22
14	10 mo/M	Nuchal region	4	IG	LG-MPNST-like	–	–	–	CCDC6::RET	NA	Normal	NA	ND	S	NA
15	6 y/M	Orbit	2	IG	SPH	++	+	–	MYH10::RET	NA	Loss[‡]	Low/low	NA	S + CHT + TT-S	AWD/22
16	34 y/M	Forearm	NA	LG	LNT/SPH	+++	+++	–	NCOA4::RET	NA	NA	Low/low	ND	S (R1)	LR/48; later LFU
17	62 y/F	Thigh	13	HG	Epithelioid/rhabdoid cells	–	–	ND	NUMA1::RET	ND	ND	ND	ND	NA	Recent case
18	1 d/F	Back	18	HG	Triphasic/IFS	++	+++	–	TFG::MET	MYC gain[†]	Normal	Low/high (35.4)	IFS	S	NED/130
19	72 y/F	Retroperitoneum	30	IG	MP	–	–	ND	CAPZA2::MET	NA	Loss[†]	NA	IFS	None	DU/NA
20	56 y/M	Knee	1.5	HG	IFS	–	+++	–	ITSN1::RAF1	–	ND	Low/low	ND	S	NED/10
21	5 mo/M	Retroperitoneum	5	HG	IFS	+++	–	–	OSBP::BRAF	–	Normal	NA	IFS	S + CHT	NED/29
22	46 y/F	Cervix	0.8	LG	SPH	+++	+++	–	–	BRAF delins; EGFR dup	Normal	NA	IFS	S	NA

*LG and HG areas present in two different blocks and analyzed separately.

[†]Confirmed by CNV analysis.

[‡]Homozygous loss confirmed by FISH.

+, 1–33% positive cells; ++, 34–66%; +++, 67–100%.

amp, amplification; AWD, alive with disease; CHT, chemotherapy; d, day; del, deletion; delins, deletion–insertion; dup, duplication; DOD, died of disease; DU, died, undetermined cause of death; HG, high grade; IFS, infantile fibrosarcoma pattern; IG, intermediate grade; ins, insertion; LFU, lost to follow-up; LG, low grade; LNT, lipofibromatosis-like neural tumor pattern; LR, local recurrence; m, months; MP, myopericytoma-like tumor pattern; MTS, metastasis; NA, not available; ND, not done; NED, no evidence of disease; pm, point mutation; S, surgery; TT-E, targeted therapy, entrectinib; TT-L, targeted therapy, larotrectinib; TT-S, targeted therapy, selpercatinib.
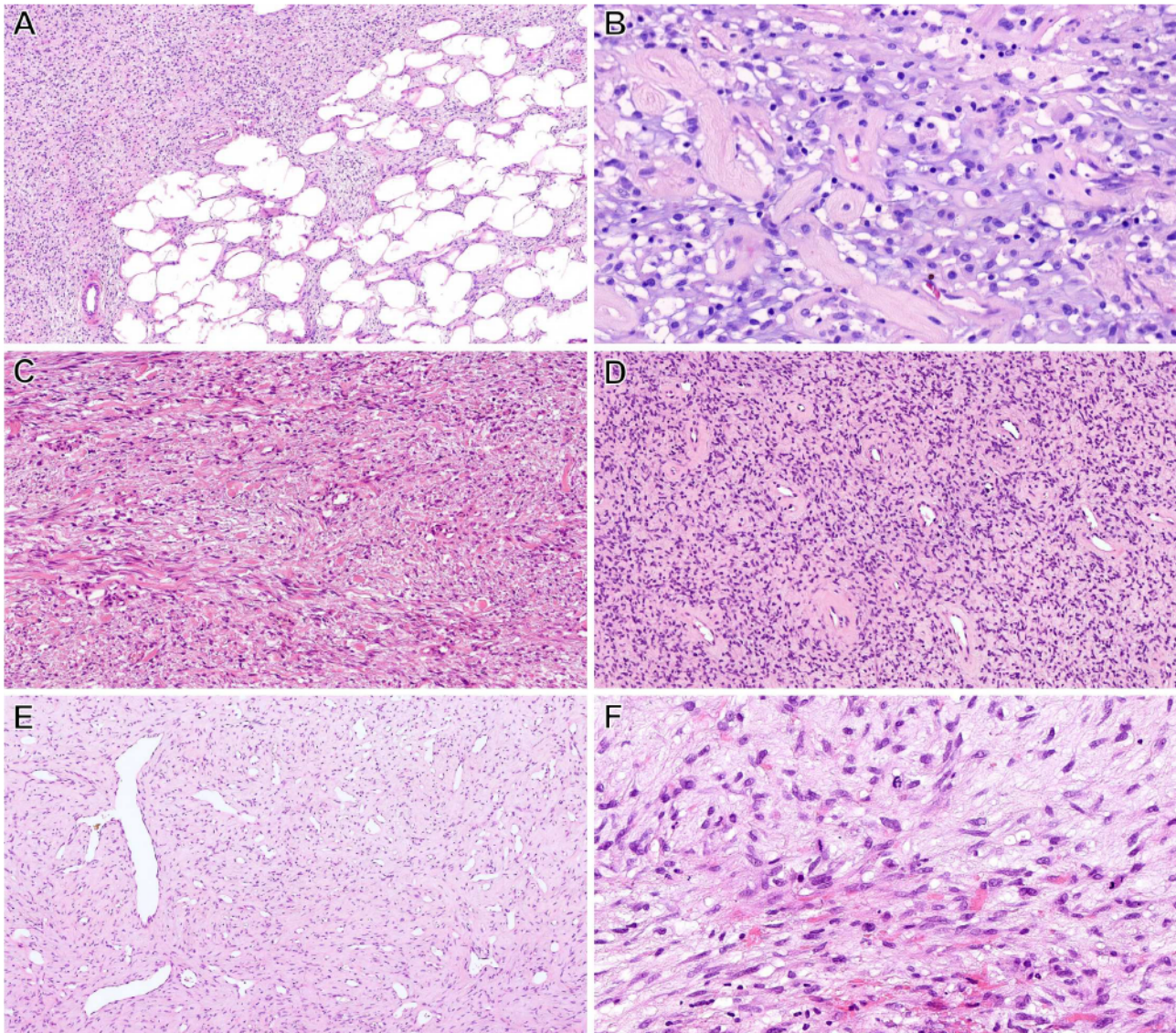
Figure 1. (A) Case 5 showed a prototypical LNT pattern with wide infiltration into subcutaneous adipose tissue. (B) Case 11 showed a myxoid SPH pattern composed mostly of epithelioid cells with abundant eosinophilic cytoplasm. (C and D) Cases 14 and 15 exhibited increased cellularity and were classified as IG. The former case had an LG-MPNST pattern (C), while the latter showed IG-SPH morphology (D). (E) Case 19 had a myopericytomatous pattern, and the tumor was composed of myoid spindle cells with low to moderate cellularity arranged in haphazard fascicles punctuated by abundant thin–walled vessels, some of which had a staghorn shape. Some areas had increased cellularity and mitotic activity (F).

14/22 (64%) and 12/22 (55%) cases, respectively, with both markers being expressed in 10/22 (45%) cases. All 12 cases with *NTRK* fusions were positive for panTrk (Figure 3J).

Molecular genetic findings

RNA and DNA sequencing

The main molecular-genetic results are presented in Table 1, and more detailed summaries are available in supplementary material, Tables S2 and S3.

NTRK1/3 fusions were revealed by RNA-seq in 12 cases, including four cases with IFS morphology and *ETV6::NTRK3* fusion. Case 6 with *EML4::NTRK3* was composed of LG-SPH areas transforming into IFS (Figure 3C,D). A uterine case with *STRN::NTRK3*

showed an extraordinary, highly myxoid LG-SPH pattern (Figure 1B) [23], while case 12 with *RBPMS:: NTRK3* fusion exhibited the LG-SPH pattern. The five *NTRK1*-fused tumors spanned the entire morphological spectrum, showing LG-LNT (*n* = 2), IG-SPH (*n* = 1), and HG-IFS (*n* = 2) patterns.

Tumors with *RET* fusions (*n* = 5) also spanned the entire spectrum from LG to HG lesions and showed various morphologies including the IFS pattern encountered in case 13 with a novel *PWWP2A::RET* fusion (Figure 2B). A novel *NUMA1::RET* fusion was detected in case 17 which showed epithelioid/rhabdoid morphology (Figure 2C). Both cases with *MET* fusion were unusual. Case 18 with *TFG::MET* fusion displayed a unique LG triphasic morphology (Figure 3A) combined with HG-IFS areas (Figure 3B) [20], while case 19 with
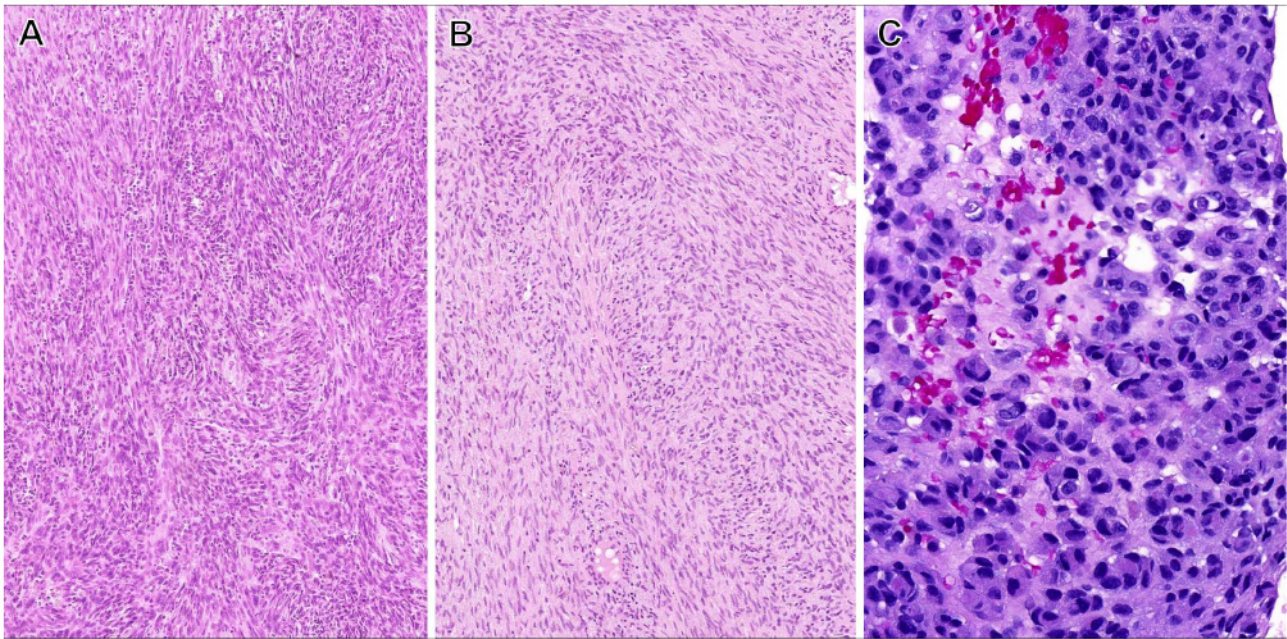
Figure 2. (A) Case 20 with a novel *ITSN1::RAF1* fusion and IFS morphology. (B) IFS morphology was also encountered in case 13, which harbored a novel *PWWP2A::RET* fusion. (C) Case 17 revealed epithelioid to rhabdoid tumor cells with HG atypia.

the *CAPZA2::MET* fusion had an IG myopericytomatous appearance (Figure 1E,F).

Both cases with *RAF1* ($n = 1$) and *BRAF* ($n = 1$) fusion showed IFS morphology (Figure 2A). Case 22 with an LG-SPH pattern (Figure 4A,B) lacked fusions but harbored a pathogenic *BRAF* delins p.V600K and an *EGFR* p.S768_D770dup.

DNA-seq was successful in 13 cases and uncovered rare additional genetic aberrations, mostly variants of unknown significance, with only two exceptions: likely pathogenic mutations of *PALB2* (case 11) and *ROS1* (case 18) of suspected and confirmed germline origin, respectively (supplementary material, Table S3). Additionally, in case 18, a CNV (duplication) of *MYC* was revealed by DNA-seq and confirmed by the methylation profiling CNV plot. A high TMB was detected in 2/8 tested cases (cases 6 and 18, 17.7 and 35.4 mut/Mb, respectively). All seven tested cases had low MSI.

Methylation profiling

Methylation profiling was successful in 9/11 cases. Case 13 with IFS morphology harboring the novel *PWWP2A::RET* fusion matched to the DKFZ sarcoma methylation class of infantile fibrosarcoma with a calibrated score of 0.98. No other match was found. However, in cases 3, 6, and 22, the classifier suggested a methylation class sarcoma, MPNST-like with low calibrated scores (0.73, 0.8, and 0.31, respectively). The other suggested methylation classes were DFSP for case 11 (score 0.57) and rhabdomyosarcoma-like in case 21 (score 0.43). No methylation class was suggested in three cases.

Unsupervised clustering of methylation profiles by t-SNE showed that the eight kinase-rearranged cases

(cases 3, 6, 11, 13, 18, 19, 21, and 22) that passed quality control clustered together with the IFS methylation class and were distinct from 15 other soft tissue tumor types and control reactive tissue, including nerve sheath tumors, myofibroblastic tumors, and undifferentiated sarcomas (Figure 5A). Case 1, which contained a significant proportion of admixed inflammatory cells (Figure 3E), was the only case that clustered with IMT. This finding was further confirmed by hierarchical clustering. Figure 5B presents a heatmap showing the top 1,000 most variable CpG sites and similar methylation profiles between the eight kinase-rearranged tumors and the IFS methylation class, regardless of the underlying kinase fusion. Based on unsupervised hierarchical clustering, the MPNST-like methylation class showed the second most closely related methylation profile to the kinase-rearranged cases, while the MPNST methylation class showed a very distinct and different methylation signature.

Next, we analyzed and compared the percentages of genome-wide copy number alterations in the kinase-rearranged cases, comparing morphologically LG/IG with HG tumors. The HG cases (cases 6, 13, 18, 21) showed frequent copy number gains and losses, non-recurrently involving gains in *CCND1* (case 13), *MDM2/CDK4* (cases 6 and 18), and *CDK6* (case 21), and losses in *CDKN2A/B* (case 6) (Figure 6A), compared with the relatively flat copy number profile in LG cases (cases 3, 11, 19, 22) (Figure 6B). However, *CDKN2A/B* loss was also present in two LG cases (cases 3 and 19). Of note, the clinicopathological features of the two cases with *MDM2* gain were not in keeping with a diagnosis of dedifferentiated liposarcoma or intimal sarcoma with kinase gene fusions as recently reported [27]. Overall, the percentage of the genome involved by
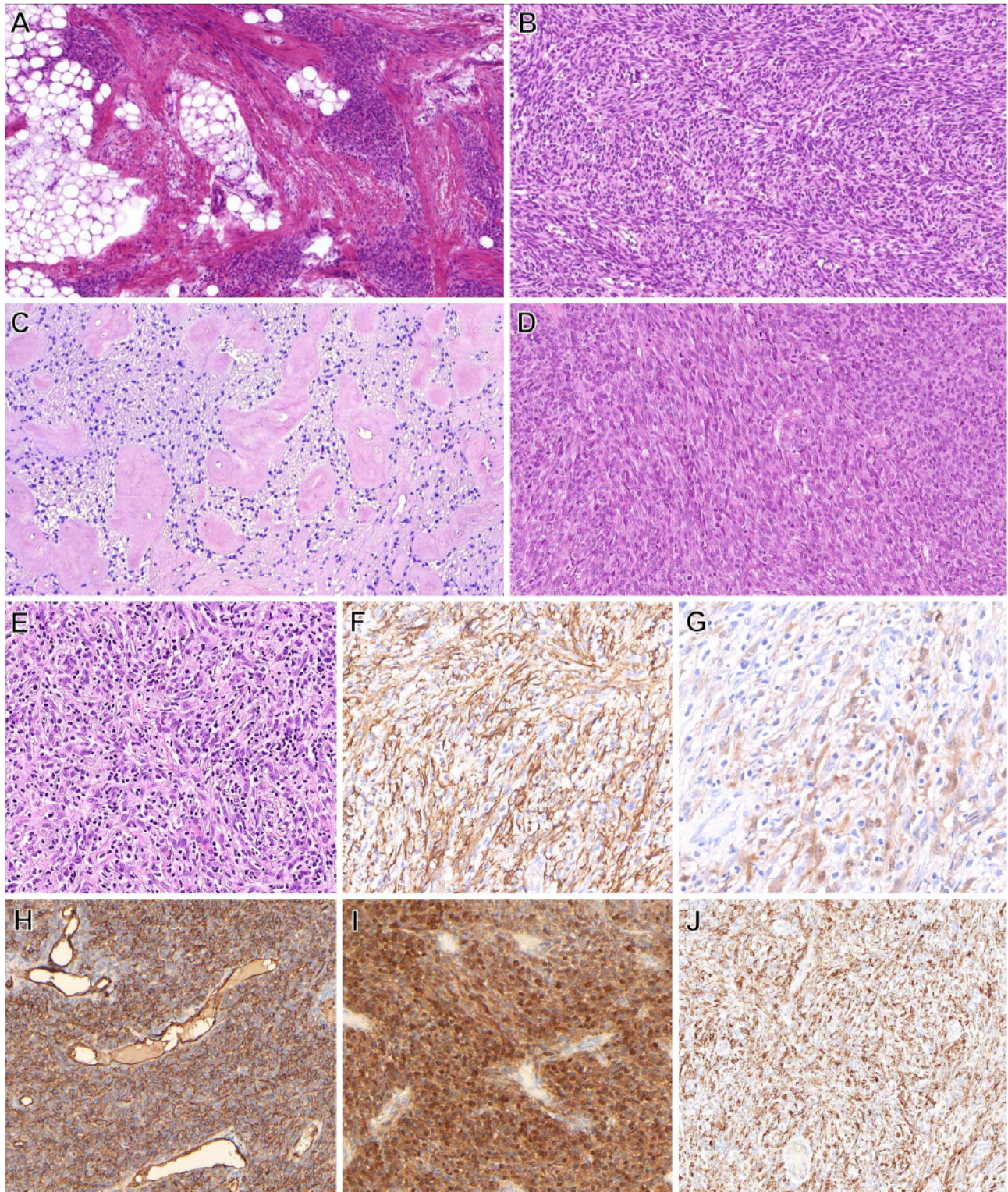
Figure 3. (A) Case 18 showed areas with unusual LG triphasic morphology resembling fibrous hamartoma of infancy, which in some areas transformed into IFS areas (B). (C and D) Case 6 with *EML4::NTRK3* was composed of LG-SPH areas (C) transforming into an HG-IFS morphology (D). (E) Case 1 with *LMNA::NTRK1* contained a significant inflammatory infiltrate and clustered with the IMT methylation class. Both CD34 (F) and S100 (G) were positive. (H and I) The tumor in case 6 co-expressed both CD34 (H) and S100 protein (I). In addition, diffuse panTrk expression was present (J).

CNVs, serving as a surrogate for genomic complexity, in HG cases was significantly higher than those in LG–IG tumors (mean % CNV: 24.7% versus 7.0%, Student-*t* $p < 0.036$) (Figure 6C).

FISH

In addition, the loss of the *CDKN2A* gene locus was analyzed using FISH, confirming homozygous loss in cases 6 and 15. In case 6, loss of *CDKN2A* was present
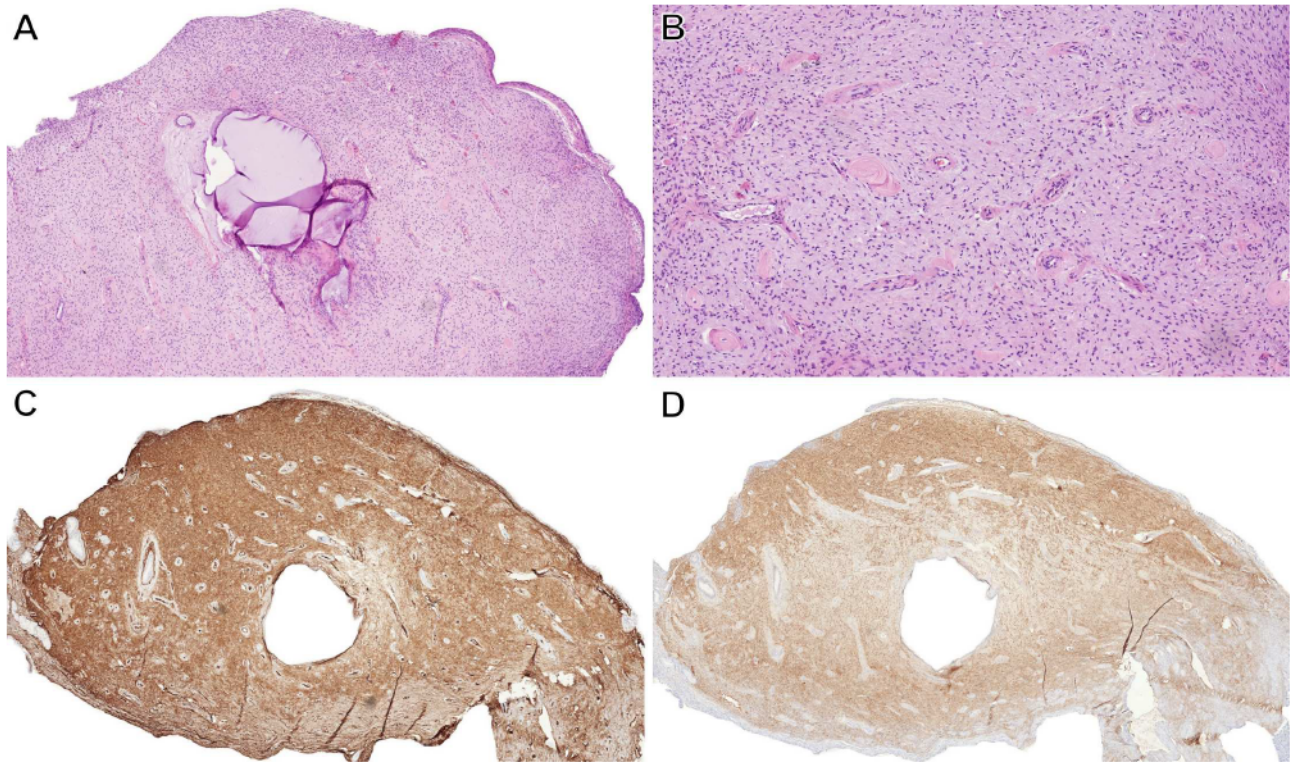
Figure 4. (A–D) No fusion was found in case 22 with an LG-SPH pattern (A and B), which instead harbored a pathogenic *BRAF* delins p.V600K and a pathogenic in-frame duplication in *EGFR* p.S768_D770dup. The tumor co-expressed CD34 (C) and S100 protein (D).

only in the IFS-like component (independently confirmed by a CNV plot), while the LG-SPH areas analyzed separately by FISH had both copies intact.

Treatment and follow-up data

Treatment and follow-up data as summarized in Table 1 were available for 19 and 16 patients, respectively. Follow-up length ranged from 10 to 130 months (mean 38 months; median 24.5 months). Overall, the recurrence and metastatic rates in our study were 19% and 6%, respectively. The only tumor that metastasized and eventually had a fatal outcome (case 6) showed HG-IFS morphology. In case 19, the patient had a large inoperable retroperitoneal tumor and died of an unknown cause.

In 12/19 cases, including eight cases with follow-up data, the patients were treated by surgery with ($n = 3$) or without ($n = 9$) chemotherapy. The status of surgical margins was mostly unknown. Overall, five patients had no evidence of disease (NED) with follow-up length ranging from 10 to 130 months; one case recurred 48 months after an R1 excision; and one patient was alive with disease (AWD). The patient in case 6 experienced distant metastasis and eventually died of the tumor in 30 months.

Six patients were treated with targeted therapy combined with surgery and/or chemotherapy. The eyelid tumor in case 1 had repeatedly recurred before being diagnosed as an *NTRK1*-rearranged tumor. The patient was then started on entrectinib and 13 months later had

NED. In case 7, the incompletely excised tumor was further treated with chemotherapy and larotrectinib, leading to complete response (NED, 27 months). The patient in case 15 was initially treated with surgery and chemotherapy. Selpercatinib was then administered, leading to significant regression of the residual tumor within 2 months (AWD, 22 months). Complete response with chemotherapy and larotrectinib was achieved in case 9 (NED, 21 months). Minimal response to chemotherapy but almost complete response to selpercatinib was observed in case 13 (minimal residual tumor, 22 months). Larotrectinib was discontinued due to severe side effects in case 4 (AWD, 20 months).

Discussion

The distinction between IFS and *NTRK*-SCN as currently defined by the WHO is mostly straightforward as they usually occur at different ages. However, due to a significant overlap in diagnostic criteria, a subset of cases could be assigned to both groups, particularly infantile cases with alternative kinase fusions and IFS morphology that co-express CD34 and/or S100 protein. In fact, some studies speculated that all pediatric *NTRK*-rearranged mesenchymal tumors including IFS may represent a single disease [13]. While the inability for precise classification does not currently affect the patients' management, gaining this ability might eventually prove to be of prognostic or therapeutic relevance.
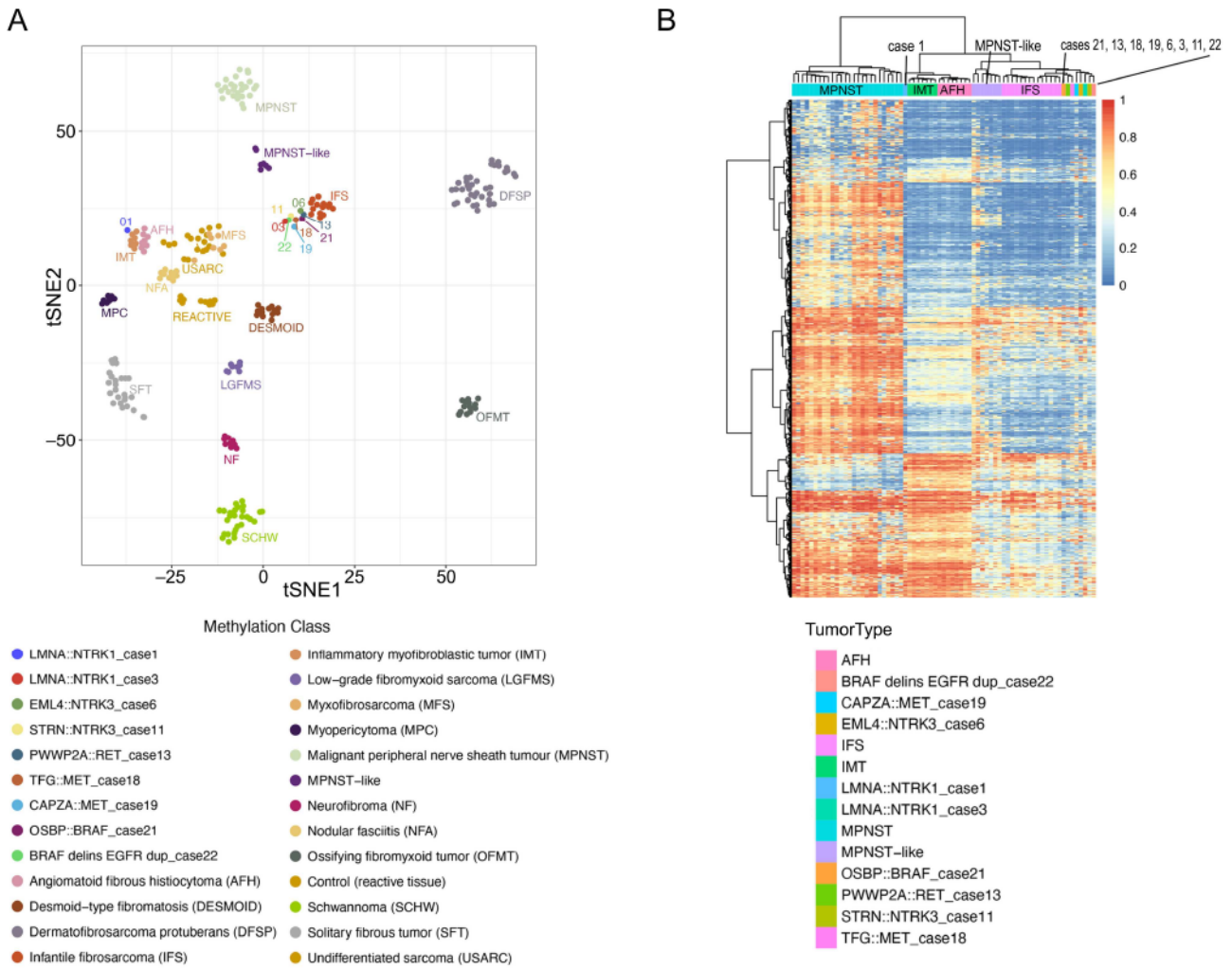
Figure 5. (A) Unsupervised clustering of methylation profiles by t-SNE compared with 247 miscellaneous soft tissue methylation classes showed that eight cases (cases 3, 6, 11, 13, 18, 19, 21, and 22) clustered together with the IFS methylation class and one case (case 1) clustered with IMT. (B) Unsupervised hierarchical clustering of methylation profiles comparing these nine cases of kinase-rearranged tumors with IFS, IMT, MPNST, and MPNST-like cases demonstrated similar findings.

Given the relatively short median follow-up and multiple factors influencing prognosis (margin status, selected therapy, etc.), of which some are unknown in our study, any comparison of clinical behavior between NTRK-SCN and IFS would be inaccurate based on our data. However, the only case in our study that metastasized and eventually led to the patient's death was case 6 with HG morphology, which supports the previously mentioned assumption [9] that at least in adult patients [1] the metastatic potential of NTRK-SCN seems to partially correlate with histologic grade, as tumors with low cellularity, atypia, and mitotic activity generally tend to follow an indolent clinical course [14,28]. However, rare exceptions may occur [29]. From the therapeutic perspective, our study further confirms the effectiveness of targeted therapy with NTRK and RET inhibitors [30,31], leading to a complete or near-complete response in 5/6 cases.

Very interesting novel data regarding the relationship between NTRK-SCN and IFS were recently published by Tauzière-Espariat et al [29]. Using unsupervised whole RNA-seq clustering analysis, they showed that almost all infantile and adult cases with NTRK fusions (and one MET-rearranged case) including ETV6::NTRK3-fused IFS cluster closely together independently of their clinicopathological features. Moreover, using DNA methylation-based DKFZ brain tumor and sarcoma classifiers [25,26], 9/16 cases were significantly classified (calibrated scores ≥ 0.9) either as sarcoma, MPNST-like (n = 6) or as IFS (n = 3). Then, on t-SNE analysis of the methylation data, their cohort segregated into three different subgroups. While four tumors (4/16, 25%) occurring in infants aged 0–1 year, with IFS morphology, CD34 and S100-negative immunoprofile, and ETV6::NTRK3 fusion classified within the IFS cluster, the largest fraction (11/16, 69%) formed a possibly novel cluster very close to the existing methylation class sarcoma, MPNST-like. Six out of the 11 cases (54.5%) had a CDKN2A deletion, an aberration not found in other tumors in the study. This methylation cluster included tumors irrespective of age that were initially diagnosed by histopathology either as NTRK-SCN or as adult-type
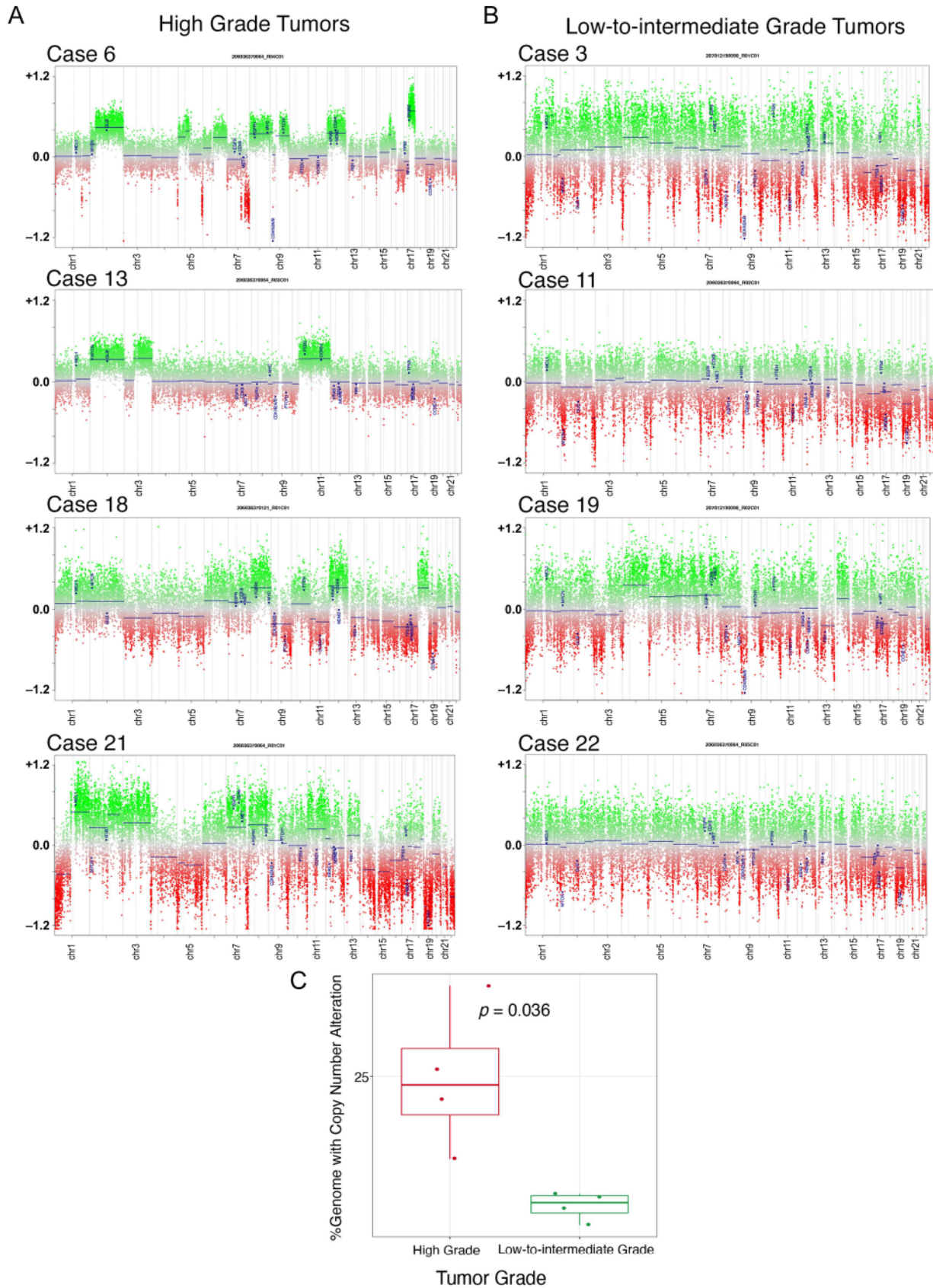
Figure 6. Percentage of genome CNAs in low to intermediate- and high-grade cases. Genome-wide CNA obtained from the methylation profile using the conumee R package. (A and B) Copy number profiles of high-grade (A) and low to intermediate-grade cases (B) across the genome with copy number segments computed over genomic regions with gains or losses. Each dot represents a CpG probe. (C) Copy number alterations: the center line corresponds to the median; lower and upper hinges correspond to the 25th and 75th percentiles; upper and lower whiskers correspond to 1.5 × interquartile range. Each dot represents an individual case. *p* value from Student's *t*-analysis.

fibrosarcomas; all showed CD34 and S100 co-expression, and all had either *NTRK* or *MET* fusions [29].

In contrast to these findings [29], our results show that irrespective of their clinical, morphological, or genetic features, the methylation profiles of the eight kinase-rearranged cases clustered together with the IFS methylation class, while being distinct from 15 other soft tissue tumor types (including the MPNST-like group) and control reactive tissue. This finding was further confirmed by hierarchical clustering. Interestingly, the MPNST-like methylation class represented the second most closely related methylation profile, while the MPNST methylation class showed a very distinct and different methylation signature. Notably, case 1 with a rich inflammatory background clustered together with the IMT methylation class, a common phenomenon observed in tumors with abundant inflammatory cells. The disagreement between the two studies is difficult to explain but might be caused by differences in study cohorts or different methylation classes being included in the unsupervised clustering analysis. Nevertheless, it is important to note that the MPNST-like methylation class is currently not very well characterized and is supposed to include cases with MPNST-like morphology, retained expression of the H3K27 trimethylation marker, and a high frequency of *CDKN2A/B* homozygous deletions [26]. Therefore, this group may include a heterogeneous mixture of tumors, including some with kinase fusions, possibly explaining the close relationship of cases in our study as well as in the study by Tauziède-Espariat *et al* [29]. More studies are still needed to elucidate the exact link between *NTRK*-SCN and IFS.

On the other hand, when we attempted tumor classification using the DKFZ sarcoma methylation classifier, only the congenital case 13 with *PWWP2A::RET* fusion significantly classified (score 0.98) with the methylation class IFS. To the best of our knowledge, this is the first reported case assigned to this methylation class within this classifier that harbors a fusion different from *ETV6::NTRK3*. An additional three cases were assigned to the methylation class sarcoma, MPNST-like, but with low calibrated scores. Such inconsistent and highly variable results likely reflect the fact that the original training and validation cohort in the sarcoma classifier lacked a well-characterized cohort of *NTRK*-SCN, and thus is inadequate in this tumor class.

CNV plots were generated in all cases where methylation profiling was possible. This allowed us to correlate the CNV profiles of each case with their morphological features. Our results indicate a relatively good concordance between a flat CNV profile and LG/IG morphology. In contrast, multiple gains and losses were usually found in HG cases. Specifically, about 25% of the genome in the HG group was involved by non-recurrent copy number gains and losses, compared with only 7% in the LG and IG group. *CDKN2A/B* loss is a non-recurrent feature of tumors in the latter group, which was also shown in the study by Tauziède-Espariat *et al* [29]. Additionally, we also observed non-recurrent copy number gains in *CDKNA2A/B*, *CCND1*, *MDM2/CDK4*, and *CDK6* among our HG cases. Short follow-up data for most of our cases hindered a reliable comparison of CNV profiles with prognosis but the only case with a fatal outcome (case 6) had a highly complex CNV profile, which is in keeping with a previous study on this topic [32].

Our study also presented four gene fusions that are novel in soft tissue tumors, namely *PWWP2A::RET*, *NUMA1::RET*, *CAPZA2::MET*, and *ITSN1::RAF1*. The *PWWP2A* gene, which encodes a protein involved in histone acetylation [33], was previously identified as a fusion partner to *ROS1* in Spitz tumors [34,35]. *NUMA1* fusions, whose product, NuMA, plays an important role in mitotic spindle assembly and function [36], were reported in acute promyelocytic leukemia [37], as well as in rare cases of IMT [38] and aneurysmal fibrous histiocytoma [39]. *CAPZA2*, encoding an actin-binding protein, CapZ [40], was previously detected as a *MET* fusion partner in non-small cell lung cancer [41]. To the best of our knowledge, no fusions or other alterations of the *ITSN1* gene (encoding a vesicle scaffolding protein, intersectin-1 [42]) have been reported to date. Overall, the pathogenic effects of all these novel fusions most likely derive from the fusion partner containing the tyrosine or serine/threonine kinase domain, i.e. *NTRK1/3*, *RET*, *RAF1*, or *MET*. Proteins encoded by these genes are all part of the ubiquitous MAP kinase signaling cascade, and the general mechanism by which they lead to oncogenesis has been thoroughly described [1,34]. Of these four novel fusions, the most interesting is *CAPZA2::MET* as only five *MET*-rearranged mesenchymal tumors have been described in the literature [5,9,20,35]. Our case is distinct from them both morphologically and clinically since it is the first such case reported in an adult.

This study also included two uterine cases. While the first harbored an *NTRK3* fusion [23], which is well known to occur in uterine mesenchymal tumors [43–45], the latter (case 22) was extraordinary. It had the typical morphology and immunoprofile of *NTRK*-SCN but instead of a fusion, it harbored pathogenic aberrations of *BRAF* and *EGFR*, which has not been seen previously in this context. However, *BRAF* as well as *EGFR* aberrations were recently reported in congenital mesoblastic nephroma, i.e. a tumor with a significant morphologic overlap with IFS and *NTRK*-SCN [21,22,46,47].

Despite rapidly increasing knowledge regarding the various driving molecular aberrations detected in kinase fusion mesenchymal tumors, larger-scale studies analyzing other potential molecular aberrations that could be responsible for therapy resistance or tumor progression were missing [48]. We used a large DNA panel to analyze 13 cases and found only rare secondary genetic aberrations with unclear significance.

In summary, we report a comprehensive clinicopathological and molecular genetic analysis of 22 cases of both pediatric and adult mesenchymal tumors with kinase gene aberrations. We detected four novel fusions not previously reported in these neoplasms, including

the first adult *MET*-rearranged case, as well as the first uterine case of this type lacking a fusion but harboring *BRAF* and *EGFR* mutations. In the methylation profiling analysis, 8/9 of our cases clustered together with the IFS methylation class, suggesting that they represent a closely related entity.

Acknowledgements

Author contributions statement

All authors contributed to the study conception and edited the manuscript. Material preparation, final data collection and analysis were performed by NK and Michael M. JKD performed the methylation and CNV analysis. The first draft of the manuscript was written by NK, with a significant contribution from Michael M. All authors commented on previous versions of the manuscript. All authors read and approved the final manuscript.

Data availability statement

Data supporting the findings of this study are available within the article. The complete datasets generated during and/or analyzed during the current study are available from the corresponding author upon reasonable request.

References

1. Davis JL, Al-Ibraheemi A, Rudzinski ER, *et al*. Mesenchymal neoplasms with NTRK and other kinase gene alterations. *Histopathology* 2022; **80:** 4–18.

2. Knezevich SR, Garnett MJ, Pysher TJ, *et al*. ETV6-NTRK3 gene fusions and trisomy 11 establish a histogenetic link between mesoblastic nephroma and congenital fibrosarcoma. *Cancer Res* 1998; **58:** 5046–5048.

3. Rubin BP, Chen CJ, Morgan TW, *et al*. Congenital mesoblastic nephroma t(12;15) is associated with ETV6-NTRK3 gene fusion: cytogenetic and molecular relationship to congenital (infantile) fibrosarcoma. *Am J Pathol* 1998; **153:** 1451–1458.

4. Kao YC, Fletcher CDM, Alaggio R, *et al*. Recurrent BRAF gene fusions in a subset of pediatric spindle cell sarcomas – expanding the genetic spectrum of tumors with overlapping features with infantile fibrosarcoma. *Am J Surg Pathol* 2018; **42:** 28–38.

5. Flucke U, van Noesel MM, Wijnen M, *et al*. TFG-MET fusion in an infantile spindle cell sarcoma with neural features. *Genes Chromosomes Cancer* 2017; **56:** 663–667.

6. Church AJ, Calicchio ML, Nardi V, *et al*. Recurrent EML4–NTRK3 fusions in infantile fibrosarcoma and congenital mesoblastic nephroma suggest a revised testing strategy. *Mod Pathol* 2018; **31:** 463–473.

7. Tan SY, Al-Ibraheemi A, Ahrens WA, *et al*. ALK rearrangements in infantile fibrosarcoma-like spindle cell tumours of soft tissue and kidney. *Histopathology* 2022; **80:** 698–707.

8. Kallen ME, Hornick JL. The 2020 WHO classification: what's new in soft tissue tumor pathology? *Am J Surg Pathol* 2021; **45:** e1–e23.

9. Antonescu CR. Emerging soft tissue tumors with kinase fusions: an overview of the recent literature with an emphasis on diagnostic criteria. *Genes Chromosomes Cancer* 2020; **59:** 437–444.

10. Agaram NP, Zhang L, Sung YS, *et al*. Recurrent NTRK1 gene fusions define a novel subset of locally aggressive lipofibromatosis-like neural tumors. *Am J Surg Pathol* 2016; **40:** 1407–1416.

11. Suurmeijer AJH, Kao YC, Antonescu CR. New advances in the molecular classification of pediatric mesenchymal tumors. *Genes Chromosomes Cancer* 2019; **58:** 100–110.

12. Haller F, Knopf J, Ackermann A, *et al*. Paediatric and adult soft tissue sarcomas with NTRK1 gene fusions: a subset of spindle cell sarcomas unified by a prominent myopericytic/haemangiopericytic pattern. *J Pathol* 2016; **238:** 700–710.

13. Davis JL, Lockwood CM, Stohr B, *et al*. Expanding the spectrum of pediatric NTRK-rearranged mesenchymal tumors. *Am J Surg Pathol* 2019; **43:** 435–445.

14. Suurmeijer AJH, Dickson BC, Swanson D, *et al*. A novel group of spindle cell tumors defined by S100 and CD34 co-expression shows recurrent fusions involving RAF1, BRAF, and NTRK1/2 genes. *Genes Chromosomes Cancer* 2018; **57:** 611–621.

15. Antonescu CR, Dickson BC, Swanson D, *et al*. Spindle cell tumors with RET gene fusions exhibit a morphologic spectrum akin to tumors with NTRK gene fusions. *Am J Surg Pathol* 2019; **43:** 1384–1391.

16. Davis JL, Vargas SO, Rudzinski ER, *et al*. Recurrent RET gene fusions in paediatric spindle mesenchymal neoplasms. *Histopathology* 2020; **76:** 1032–1041.

17. Dermawan JK, Azzato EM, Goldblum JR, *et al*. Superficial ALK-rearranged myxoid spindle cell neoplasm: a cutaneous soft tissue tumor with distinctive morphology and immunophenotypic profile. *Mod Pathol* 2021; **34:** 1710–1718.

18. Choo F, Rakheja D, Davis LE, *et al*. GAB1-ABL1 fusions in tumors that have histologic overlap with NTRK-rearranged spindle cell tumors. *Genes Chromosomes Cancer* 2021; **60:** 623–630.

19. Michal M, Ptáková N, Martínek P, *et al*. S100 and CD34 positive spindle cell tumor with prominent perivascular hyalinization and a novel NCOA4-RET fusion. *Genes Chromosomes Cancer* 2019; **58:** 680–685.

20. Michal M, Ud Din N, Švajdler M, *et al*. TFG::MET-rearranged soft tissue tumor: a rare infantile neoplasm with a distinct low-grade triphasic morphology. *Genes Chromosomes Cancer* 2022; **62:** 290–296.

21. Penning AJ, Al-Ibraheemi A, Michal M, *et al*. Novel BRAF gene fusions and activating point mutations in spindle cell sarcomas with histologic overlap with infantile fibrosarcoma. *Mod Pathol* 2021; **34:** 1530–1540.

22. Wegert J, Vokuhl C, Collord G, *et al*. Recurrent intragenic rearrangements of EGFR and BRAF in soft tissue tumors of infants. *Nat Commun* 2018; **9:** 2378.

23. Michal M, Hájková V, Skálová A, *et al*. STRN-NTRK3-rearranged mesenchymal tumor of the uterus: expanding the morphologic spectrum of tumors with NTRK fusions. *Am J Surg Pathol* 2019; **43:** 1152–1154.

24. Gerami P, Li G, Pouryazdanparast P, *et al*. A highly specific and discriminatory FISH assay for distinguishing between benign and malignant melanocytic neoplasms. *Am J Surg Pathol* 2012; **36:** 808–817.

25. Capper D, Jones DTW, Sill M, *et al*. DNA methylation-based classification of central nervous system tumours. *Nature* 2018; **555:** 469–474.

26. Koelsche C, Schrimpf D, Stichel D, *et al*. Sarcoma classification by DNA methylation profiling. *Nat Commun* 2021; **12**: 498.

27. Brahmi M, Dufresne A, Verret B, *et al*. NTRK fusion in soft tissue sarcomas harboring MDM2/CDK4 amplification: three case reports. *Ann Oncol* 2021; **32**: 813–814.

28. Kao YC, Suurmeijer AJH, Argani P, *et al*. Soft tissue tumors characterized by a wide spectrum of kinase fusions share a lipofibromatosis-like neural tumor pattern. *Genes Chromosomes Cancer* 2020; **59**: 575–583.

29. Tauziède-Espariat A, Duchesne M, Baud J, *et al*. NTRK-rearranged spindle cell neoplasms are ubiquitous tumours of myofibroblastic lineage with a distinct methylation class. *Histopathology* 2022; **82**: 596–607.

30. Ortiz MV, Gerdemann U, Raju SG, *et al*. Activity of the highly specific RET inhibitor selpercatinib (LOXO-292) in pediatric patients with tumors harboring *RET* gene alterations. *JCO Precis Oncol* 2020; **4**: PO.19.00401.

31. Laetsch TW, DuBois SG, Mascarenhas L, *et al*. Larotrectinib for paediatric solid tumours harbouring NTRK gene fusions: phase 1 results from a multicentre, open-label, phase 1/2 study. *Lancet Oncol* 2018; **19**: 705–714.

32. Vargas AC, Ardakani NM, Wong DD, *et al*. Chromosomal imbalances detected in *NTRK*-rearranged sarcomas by the use of comparative genomic hybridisation. *Histopathology* 2021; **78**: 932–942.

33. Link S, Spitzer RMM, Sana M, *et al*. PWWP2A binds distinct chromatin moieties and interacts with an MTA1-specific core NuRD complex. *Nat Commun* 2018; **9**: 4300.

34. Donati M, Kastnerova L, Martinek P, *et al*. Spitz tumors with *ROS1* fusions: a clinicopathological study of 6 cases, including FISH for chromosomal copy number alterations and mutation analysis using next-generation sequencing. *Am J Dermatopathol* 2020; **42**: 92–102.

35. Wiesner T, He J, Yelensky R, *et al*. Kinase fusions are frequent in Spitz tumours and spitzoid melanomas. *Nat Commun* 2014; **5**: 3116.

36. Chu X, Chen X, Wan Q, *et al*. Nuclear mitotic apparatus (NuMA) interacts with and regulates astrin at the mitotic spindle. *J Biol Chem* 2016; **291**: 20055–20067.

37. Wells RA, Catzavelos C, Kamel-Reid S. Fusion of retinoic acid receptor alpha to NuMA, the nuclear mitotic apparatus protein, by a variant translocation in acute promyelocytic leukaemia. *Nat Genet* 1997; **17**: 109–113.

38. Rao N, Iwenofu H, Tang B, *et al*. Inflammatory myofibroblastic tumor driven by novel *NUMA1-ALK* fusion responds to ALK inhibition. *J Natl Compr Canc Netw* 2018; **16**: 115–121.

39. Panagopoulos I, Gorunova L, Bjerkehagen B, *et al*. *LAMTOR1-PRKCD* and *NUMA1-SFMBT1* fusion genes identified by RNA sequencing in aneurysmal benign fibrous histiocytoma with t(3;11)(p21;q13). *Cancer Genet* 2015; **208**: 545–551.

40. dos Remedios CG, Chhabra D, Kekic M, *et al*. Actin binding proteins: regulation of cytoskeletal microfilaments. *Physiol Rev* 2003; **83**: 433–473.

41. Riedel R, Fassunke J, Scheel AH, *et al*. *MET* fusions in NSCLC: clinicopathologic features and response to MET inhibition. *J Thorac Oncol* 2023; **19**: 160–165.

42. Herrero-Garcia E, O'Bryan JP. Intersectin scaffold proteins and their role in cell signaling and endocytosis. *Biochim Biophys Acta Mol Cell Res* 2017; **1864**: 23–30.

43. Chiang S, Cotzia P, Hyman DM, *et al*. *NTRK* fusions define a novel uterine sarcoma subtype with features of fibrosarcoma. *Am J Surg Pathol* 2018; **42**: 791–798.

44. Croce S, Hostein I, Longacre TA, *et al*. Uterine and vaginal sarcomas resembling fibrosarcoma: a clinicopathological and molecular analysis of 13 cases showing common *NTRK*-rearrangements and the description of a *COL1A1-PDGFB* fusion novel to uterine neoplasms. *Mod Pathol* 2019; **32**: 1008–1022.

45. Costigan DC, Nucci MR, Dickson BC, *et al*. *NTRK*-rearranged uterine sarcomas: clinicopathologic features of 15 cases, literature review, and risk stratification. *Am J Surg Pathol* 2022; **46**: 1415–1429.

46. Zhao M, Yin M, Kuick CH, *et al*. Congenital mesoblastic nephroma is characterised by kinase mutations including *EGFR* internal tandem duplications, the *ETV6-NTRK3* fusion, and the rare *KLHL7-BRAF* fusion. *Histopathology* 2020; **77**: 611–621.

47. Koo SC, Schieffer KM, Lee K, *et al*. *EGFR* internal tandem duplications in fusion-negative congenital and neonatal spindle cell tumors. *Genes Chromosomes Cancer* 2023; **62**: 17–26.

48. Thorwarth A, Haase K, Roefzaad C, *et al*. Genomic evolution and personalized therapy of an infantile fibrosarcoma harboring an *NTRK* oncogenic fusion. *JCO Precis Oncol* 2022; **6**: e2100283.

4.8 *TIMP3::ALK* fusions characterize a distinctive myxoid fibroblastic tumor of the vocal cords: a report of 7 cases

Ve studii popisujeme 7 případů unikátního indolentního, variabilně myxoidního nádoru hlasivek. Je diskutován vztah této nově navržené nádorové jednotky a IMT.

Šest pacientů ve věku od 15 do 65 let bylo mužského pohlaví, sedmým pacientem byla 54letá žena. U jednoho pacienta došlo nejspíše kvůli inkompletní excizi primárního tumoru k recidivě. Všichni pacienti s dostupnými daty neměli při následných kontrolách známky onemocnění.

Nádory obsahovaly střídající se kompaktnější oblasti a oblasti s myxoidním stromatem. V myxoidních oblastech byly nádorové buňky volně rozptýleny ve stromatu, někdy s nahodilým růstovým vzorem podobným tkáňové kultuře připomínajícím proliferativní fasciitidu, zatímco v kompaktnějších oblastech byly přítomny krátké nepravidelné svazky vřetenitých buněk. Fascikulární nebo storiformní růstový vzor relativně uniformních vřetenitých buněk typický pro IMT nebyl přítomen. V nádorech byla přítomna jemná síť větvících se kapilár s nevýraznou perivaskulární kondenzací nádorových buněk, ve třech případech byly patrné nápadně „kudrnaté", zakřivené cévy. Řídký, většinou perivaskulární nenádorový zánětlivý infiltrát tvořený polymorfonukleárními leukocyty, lymfocyty a plazmatickými buňkami byl přítomen v 6 případech, v 1 případě byly v nádorové tkáni rozptýleny pouze občasné lymfocyty a hustší lymfoplazmocelulární infiltrát byl přítomen jen při okraji nádoru.

Cytomorfologicky měly nádorové buňky vysoce variabilní a atypický vzhled. Zatímco některé buňky byly nevýrazné, oválného až vřetenitého nebo hvězdicového tvaru, se středně velkými, lehce bazofilními jádry a nenápadnou, mírně eosinofilní cytoplazmou, typickým znakem těchto nádorů byla přítomnost velkých atypických buněk s výraznými jadérky, často s jednou nebo více intranukleárními a cytoplazmatickými vakuolami, popřípadě intranukleárními cytoplazmatickými pseudoinkluzemi. Některé z těchto velkých buněk měly tmavá bazofilní jádra s rozmazanými okraji. Dále byly přítomny buňky vzhledu buněk gangliových, se světlou objemnou cytoplazmou, středně velkými jádry s jemným chromatinem a živě eosinofilními meganukleoly. Některé atypické buňky vykazovaly dlouhé bipolární nebo multipolární dendritické výběžky, čímž se podobaly Purkyňovým buňkám nebo tzv. tadpole rhabdomyoblastům. I přes tyto výrazné atypie však chyběla signifikantní mitotická aktivita, atypické mitózy a nekróza.

Imunohistochemická detekce ALK byla pozitivní ve všech případech, zatímco průkaz hladkosvalového markeru SMA byl zcela negativní v 5 případech, ve dvou případech byla detekována slabá variabilní exprese. RNA-seq odhalila ve všech analyzovatelných případech identickou fúzi *TIMP3::ALK* mezi exonem 1 genu *TIMP3* a exonem 12 genu *ALK*.

Zatímco buňky vzhledu buněk gangliových jsou běžnou součástí IMT (31), prominentní velké buňky s intranukleárními a cytoplazmatickými vakuolami nebo intranukleárními cytoplazmatickými pseudoinkluzemi nejsou typickým rysem IMT. Většina IMT se vyznačuje bohatým a difúzním zánětlivým infiltrátem, ve zde prezentovaných případech byl však zánětlivý infiltrát spíše řídký. Imunohistochemicky nebyl navíc prokázán myofibroblastický fenotyp (negativita SMA), myofilamenta nebyla

pozorována ani ultrastrukturálně (49). Všechny analyzovatelné případy sdílely identickou fúzi *TIMP3::ALK*. Jedná se tedy o tumor vymezený unikátními genetickými, morfologickými a klinickými znaky, představující specifický subtyp IMT nebo samostatnou jednotku.

ORIGINAL ARTICLE

TIMP3::ALK fusions characterize a distinctive myxoid fibroblastic tumor of the vocal cords: a report of 7 cases

Natálie Klubíčková[1,2] · Michael Michal[1,2] · Abbas Agaimy[3] · Nina Zidar[4] · Michal Pavlovský[5] · Kenji Yorita[6] · Petr Grossmann[2] · Veronika Hájková[2] · Nikola Ptáková[2] · Petr Šteiner[2] · Michal Michal[1,2]

Abstract

We report 7 cases of an indolent, variably myxoid tumor of the vocal cords, characterized by overt cellular atypia with large cells containing intranuclear and intracytoplasmic vacuoles, delicate curvilinear vessels, and sparse inflammatory infiltrate. Six patients were male, aged 15 to 65 years, and 1 patient was a 54-year-old female. All tumors were located in the superficial portion of the vocal cord. One patient suffered a recurrence that was completely resected; all patients with available follow-up data currently have no evidence of disease. The tumors contained alternating areas with myxoid stroma and more compacted regions with tumor cells organized in short fascicles, interwoven with delicate curvilinear vasculature. Overt cellular atypia with large cells containing intranuclear and intracytoplasmic vacuoles or resembling ganglion cells was present in all cases but mitoses and necrosis were absent. ALK immunostaining was positive in all cases, while most tumors were negative for smooth muscle actin. Targeted RNA-sequencing revealed an identical *TIMP3::ALK* fusion with exon 1 of *TIMP3* gene being fused with exon 12 of *ALK* gene in all analyzable cases. For various reasons discussed, it remains unclear whether this tumor represents a mere subtype of IMT or a separate entity. Nevertheless, it is a morphologically distinct and diagnostically challenging lesion that needs to be recognized by surgical pathologists in order to prevent overdiagnosis in this clinically very delicate area.

Keywords Soft tissues · Myxoid fibroblastic tumor · Inflammatory myofibroblastic tumor · *TIMP3::ALK* · Vocal cords · Larynx

✉ Natálie Klubíčková
klubickova@biopticka.cz

1 Department of Pathology, Charles University, Faculty of Medicine in Pilsen, Alej Svobody 80, 323 00 Pilsen, Czech Republic

2 Bioptical Laboratory, Ltd., Pilsen, Czech Republic

3 Institute of Pathology, Friedrich-Alexander University Erlangen-Nürnberg, University Hospital Erlangen (UKER), Erlangen, Germany

4 Institute of Pathology, Faculty of Medicine, University of Ljubljana, Ljubljana, Slovenia

5 Department of Pathology, Regional Hospital Most, Most, Czech Republic

6 Department of Diagnostic Pathology, Japanese Red Cross Kochi Hospital, Kochi, Japan

Introduction

Inflammatory myofibroblastic tumor (IMT) is defined as a rarely metastasizing low-grade neoplasm composed of fibroblastic and myofibroblastic spindle cells admixed with inflammatory infiltrate consisting of plasma cells, lymphocytes, and/or eosinophils [1]. Though initially considered to represent a reactive inflammatory pseudotumor, IMT is currently accepted as a true neoplasm driven in the majority of cases by constitutionally active ALK or, less frequently, other receptor tyrosine kinase proteins [2–4], achieved by translocation of the respective genes to transcriptionally active gene partners. Younger adults and children are typically affected, but the disease may occur over a wide age range. The most common site of occurrence is the lung, followed by mesentery, omentum, and the urinary tract. About 15% of IMT cases arise in the head and neck region and the upper respiratory tract [5]. In this localization, IMT has a particularly favorable prognosis: most tumors have been

 Springer

completely treated by a single excision, while only 1 of the 13 cases analyzed by Kerr et al. [6] developed a local recurrence 3 years after the initial treatment. Three main histological patterns are recognized in IMT: cellular spindle cell pattern with a predominantly fascicular arrangement of tumor cells and rich inflammatory infiltrate; hypocellular fibrous pattern with abundant hyalinized stroma and sparse inflammation; and a myxoid pattern consisting of spindled myofibroblasts with a rich vascular and inflammatory component. Immunohistochemically, over 90% of IMTs express smooth muscle actin [7, 8].

In our practice, we have repeatedly encountered an unusual myxoid mesenchymal lesion arising from the vocal cords that frequently harbored an identical *TIMP3::ALK* gene fusion and showed a diffuse cytoplasmic ALK immunoexpression. However, the lesion lacked a compelling smooth muscle actin staining in most cases, as well as the typical diffuse and prominent inflammatory infiltrate, while exhibiting unusual large atypical cells with prominent nucleoli and single or multiple intranuclear and/or intracytoplasmic vacuoles. Herein, we report our experience with 7 such cases to draw attention to these diagnostically challenging vocal cord lesions.

Materials and methods

Case selection

A retrospective review of personal consultation files was conducted to search for cases of laryngeal IMT and other benign mesenchymal tumors of the larynx with unusual features including areas of abundant myxoid stroma with ganglion-like cells or with large atypical cells harboring nuclear or cytoplasmic vacuoles. The search yielded 7 cases in total. However, NGS analysis was informative in only 5 cases (cases 1–5). The remaining 2 cases were included based on an identical morphology and diffuse cytoplasmic ALK staining (cases 6–7) as efforts to confirm the fusion with FISH failed as well. Case 1 has been published in a previous report by Yorita et al. [9]. One or 2 blocks were available for each case. Clinicopathologic data were obtained from the medical records of the institutions that participated in the study.

Immunohistochemical studies

Immunohistochemical staining was routinely performed at the participating institutions using an automated Ventana BenchMark ULTRA or XT systems (Ventana Medical Systems Inc., Tucson, AZ, USA). The primary antibodies used are summarized in Table 1.

Table 1 Antibodies used for the immunohistochemical examination

	Dilution	Clone	Source
ALK-1	1:50 (cases 1, 4–7), 1:100 (cases 2–3)	D5F3	Cell signaling
SMA	RTU	1A4	Dako
Desmin	RTU	D33	Dako
S100	RTU	polyclonal	Dako
Pan-cytokeratin	RTU	AE1/AE3	Dako
CD34	1:200	QBEnd/10	Dako

Abbreviations: *RTU*, ready to use

Molecular-genetic studies

FISH analysis

FISH analysis of *ALK* rearrangements in case 1 was described previously [9]; the protocol for analysis of *ALK* rearrangements in cases 2–3 is delineated in [10]. For the detection of *ALK* and *TIMP3* rearrangements in cases 6–7, Vysis ALK Break Apart FISH Probe Kit (Vysis/Abbott Molecular, Des Plaines, IL, USA) and Custom-FISH Design 22q12.3 TIMP3 break-apart probe were used (SureFISH/Agilent Technologies, Santa Clara, CA, USA), respectively. The FISH procedure and interpretation of FISH results were performed as described earlier [11].

RNA-sequencing

RNA was extracted using Maxwell RSC RNA FFPE kit (automated on Maxwell RSC 48 Instrument, Promega, Madison, WI, USA). Purified RNA was quantified using the Qubit Broad Range RNA Assay (Thermo Fisher Scientific, Waltham, MA, USA). Cases 4 and 6–7 were analyzed using the TruSight Oncology 500 panel. RNA libraries were prepared using the TruSight Oncology 500 Kit (Illumina, San Diego, CA, USA) according to the manufacturer's protocol. Sequencing was performed on the NovaSeq 6000 sequencer (Illumina) following the manufacturer's recommendations. Data analysis was performed using Trusight Oncology 500 LocalApp. Case 5 was sequenced in accordance with the manufacturer's protocol using the Ion S5 sequencer (Thermo Fisher Scientific) and a custom kit based on Archer FusionPlex Sarcoma kit (Archer DX, Boulder, CO, USA) that detects fusions in 53 genes and mutations in 13 genes, including *ALK*, *BRAF*, *NTRK1-3*, *RAF1*, *RET*, and *ROS1*. Data analysis was performed using the Archer Analysis software version 6.2 (Archer DX). Case 1 was analyzed as described previously [9]; the protocol for analysis of cases 2–3 is delineated in [12].

Results

Clinical data

The main clinical data are summarized in Table 2. Six patients were male; 1 patient was a middle-aged female. Their age ranged from 15 to 65 years (mean 36, median 32). Two patients experienced hoarseness of voice; one of these patients also reported slight dyspnea. One patient had dysphonia and intermittent aphonia as well as the sensation of a foreign body in his throat; he also suffered from moderate dyspnea. Three patients reported previous tobacco use (smoking of cigarettes). All cases affected the superficial portion of the vocal cords, with 2 cases arising from the left vocal cord, while 4 were localized to the right vocal cord and no information on the laterality was available in 1 case. All cases were treated by local excision of unknown extent. In case 5, a small probatory biopsy was taken 2 months prior to the excision. Follow-up information was available for 4 patients. The patient in case 1 had no signs of recurrence at the last video laryngoscopic examination performed 4 months after the surgical intervention and had no clinical signs of recurrence 3 years after the surgery (video laryngoscopy or other imaging examination were, however, not performed at that time due to patient's refusal). No evidence of disease after 11.5 years was reported in case 2. In case 4, there was no evidence of disease 2 months after the excision. The tumor recurred and was treated by re-excision 1 year after the initial excision in case 6. Subsequently, the patient has had no evidence of disease for 14 years. Cases 3 and 5 are recent cases. No follow-up information was available in case 7.

Histological and immunohistochemical findings

Microscopically, the tumors grew as unencapsulated, vaguely nodular lesions in the superficial portions of the vocal cord. When present, the overlying squamous epithelium displayed slight reactive changes. The tumors consisted of various combinations of compact areas and areas with abundant myxoid stroma (Fig. 1A–D). The tumor cells were loosely scattered in the myxoid stroma, sometimes with a haphazard tissue culture-like growth pattern resembling proliferative fasciitis, while in the more compact areas, short irregular fascicles could be appreciated (Fig. 1A). The typical fascicular or storiform growth pattern composed of bland spindled cells typical of IMT was, however, not present. Cytomorphologically, tumor cells had a highly variable appearance. Some cells were bland, oval to spindled or stellate shaped, with moderately sized lightly basophilic nuclei and inconspicuous,

Table 2 Clinical data and histopathologic and molecular-genetic features of the cases

Case no	Clinical features			Molecular-genetic features		Immunohistochemistry						Follow-up information
	Age/sex	Size (mm)	Site	RNA-Seq	FISH ALK/TIMP3 ba	ALK	SMA	Desmin	S100	panCK	CD34	
1	35/M	10	LVC	TIMP3-ALK, Ex1-Ex12	+/ND	+	-	-	-	-	-	NED (3 yr)
2	24/M	20	RVC	TIMP3-ALK, Ex1-Ex12	+/ND	+	Va+	-	-	-	-	NED (11.5 yr)
3	27/M	10	RVC	TIMP3-ALK, Ex1-Ex12	+/ND	+	Va+	-	-	-	-	Recent
4	65/M	9	RVC	TIMP3-ALK, Ex1-Ex12	ND/ND	+	-	-	-	-	-	NED (2 mo)
5	32/M	NA	RVC	TIMP3-ALK, Ex1-Ex12	ND/ND	+	-	-	-	-	ND	Recent
6	54/F	NA	VC	NA	NA/-	+	-	-	-	-	-	Recurrence (1 yr), later NED (14 yr)
7	15/M	NA	LVC	NA	NA/NA	+	-	-	-	-	-	NA

Abbreviations: *ba*, break-apart; *Ex*, exon; *F*, female; *Fo*, focally; *LVC*, left vocal cord; *M*, male; *mo*, months; *NA*, not analyzable or not available; *ND*, not done; *NED*, no evidence of disease; *RVC*, right vocal cord; *yr*, years; *Va*, variably; *VC*, vocal cord; −, negative; +, positive
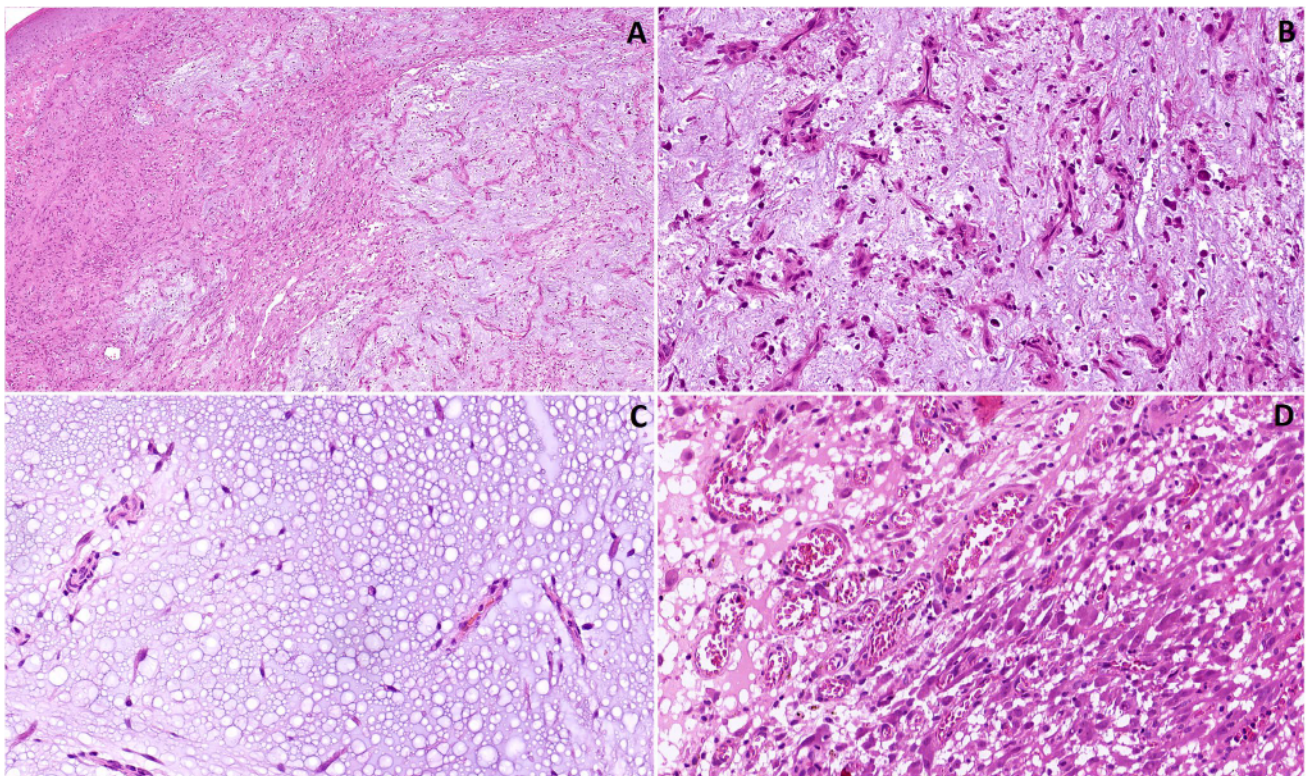
Springer

Fig. 1 Histomorphologic features: **A** low-power view of the alternating myxoid and solid, vaguely fascicular areas in case 2; **B** abundant myxoid stroma with numerous curvy vessels in case 2; **C** hypocellular myxoid "lake" in case 4; **D** gradual transition of the hypocellular myxoid (left) and more compacted (right) areas, with a rich capillary network throughout the lesion in case 7

mildly eosinophilic cytoplasm. However, the typical feature of these tumors was the presence of large atypical cells with prominent nucleoli, often with single or multiple intranuclear and intracytoplasmic vacuoles or intranuclear cytoplasmic pseudoinclusions (Fig. 2A–C, E). Dark basophilic nuclei with indistinct borders and smudged appearance were encountered in some of these cells (Fig. 2C–D). In addition, large ganglion-like cells were present. They had light cytoplasm, medium-sized nuclei with smooth chromatin, and enlarged vividly eosinophilic nucleoli (Fig. 2F, Fig. 2F-inset). Some atypical cells exhibited long bipolar or multipolar dendritic processes that could be best appreciated on ALK immunohistochemical examination (Fig. 3A–B), but were visible even in the hematoxylin and eosin stain. On occasion, these cells acquired a resemblance to Purkinje cells in the cerebellum or rhabdomyoblastic tadpole cells (Fig. 2C). A delicate network of branching small vessels was present throughout the tumors, with a slight cellular condensation around the vessels in some areas and strikingly "curly" vessels in three cases (Fig. 1A–B). Sparse, mostly perivascular inflammatory infiltrate of polymorphonuclear leukocytes, lymphocytes, and plasma cells was present throughout the tumors in 6 cases, while in case 1, only occasional lymphocytes were scattered in the tumor tissue, with a heavier lymphoplasmacytic infiltrate present at the tumor border. Mitotic figures and necrosis were absent in all cases. The recurrent tumor in case 6 was slightly more cellular, with less prominent myxoid areas. The material from the original excision was reviewed in this case, revealing a widely positive resection margin.

ALK immunohistochemical staining was diffusely and strongly positive in the cytoplasm of the tumor cells in all cases, occasionally highlighting their dendritic cytoplasmic processes (Fig. 3A–B). Smooth muscle actin showed a variable positivity in 2 cases; the other 5 cases tested were completely negative. Desmin, S100 protein, pan-cytokeratin (using the AE1/AE3 antibody), and CD34 were negative in all cases tested. On examination by electron microscopy, which was performed in case 1 [9], the tumor cell cytoplasm contained a rich network of rough endoplasmic reticulum with secretory granules and abundant cytoplasmic vacuoles. Intranuclear cytoplasmic pseudoinclusions were revealed as well. Contrarily, myofilaments were completely absent from the tumor cells.
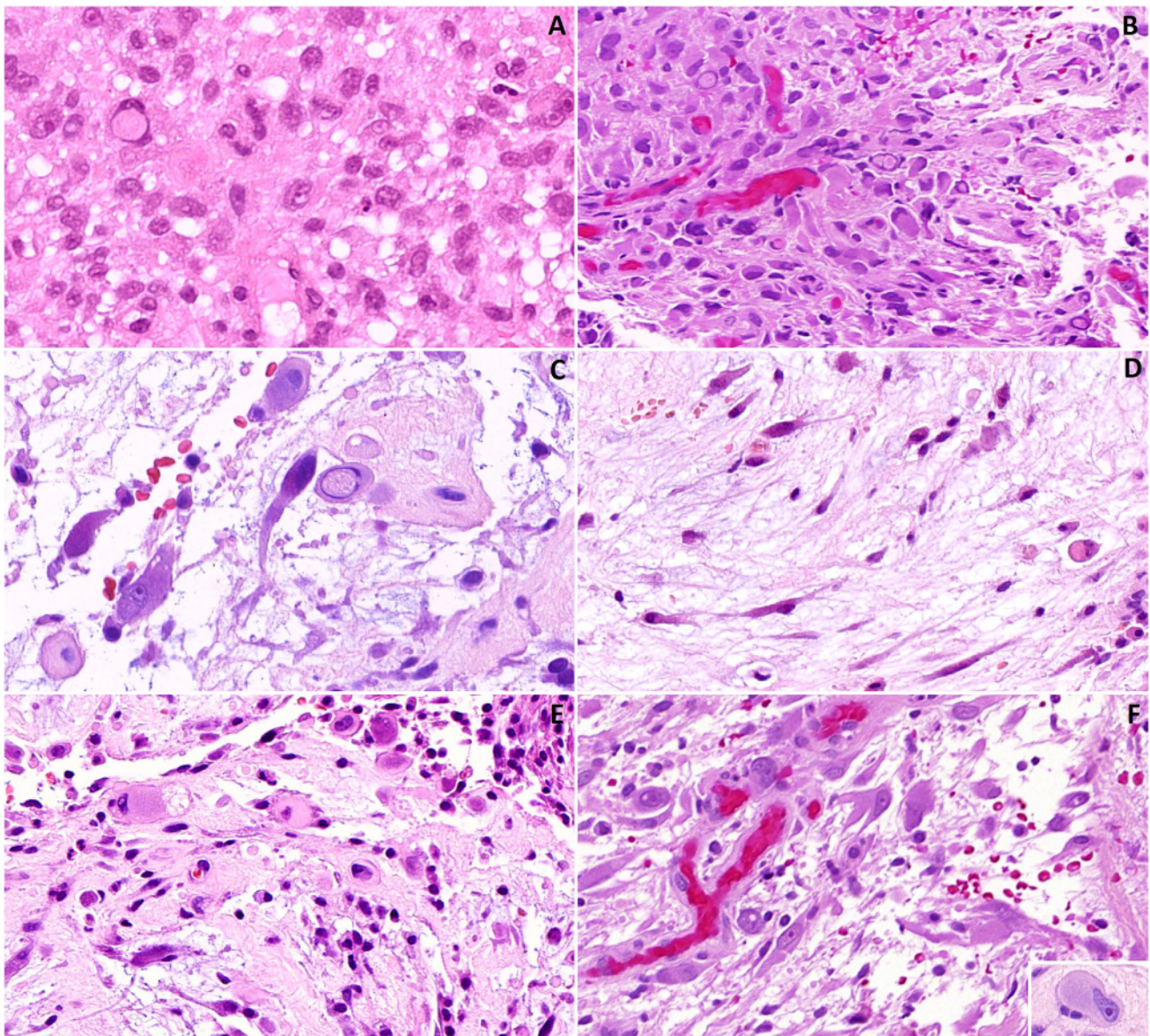
Fig. 2 Atypical tumor cells present in the tumors. Some atypical cells contained intranuclear pseudoinclusions (**A–C**; cases 3, 6, and 4, respectively). Large cells with indistinct nuclear borders and basophilic smudged chromatin (**C–D**; case 4). Intracytoplasmic vacuoles were occasionally seen (**E**; case 4). Tumor cells with a ganglion-like appearance (**F**; case 6, **F-inset**; case 4)

Molecular-genetic findings

The molecular-genetic results are summarized in Table 2. FISH analysis revealed a break in the *ALK* gene in 3/3 of analyzable cases; the method failed in 2 other cases in which the analysis was attempted. *TIMP3* break was not detected by FISH in case 6 and further molecular testing was not possible due to the low quality of the genetic material in this archival biopsy specimen. An identical *TIMP3::ALK* fusion involving exon 1 of the *TIMP3* gene and exon 12 of the *ALK* gene was detected by sequencing methods in all 5 analyzable cases. The reference transcript sequences used for describing *TIMP3* and *ALK* have accession numbers NM_000362.4 and NM_004304.3, respectively; the chromosomal position is described using the reference genome GRCh37 (hg19), with breakpoints at chr22:33198107 and chr2:29474133.

Discussion

We report 7 cases of an unusual vocal cord lesion characterized by various amounts of myxoid stroma, large atypical cells with intranuclear and/or intracytoplasmic vacuoles, sparse inflammatory infiltrate, and a frequent *TIMP3::ALK*
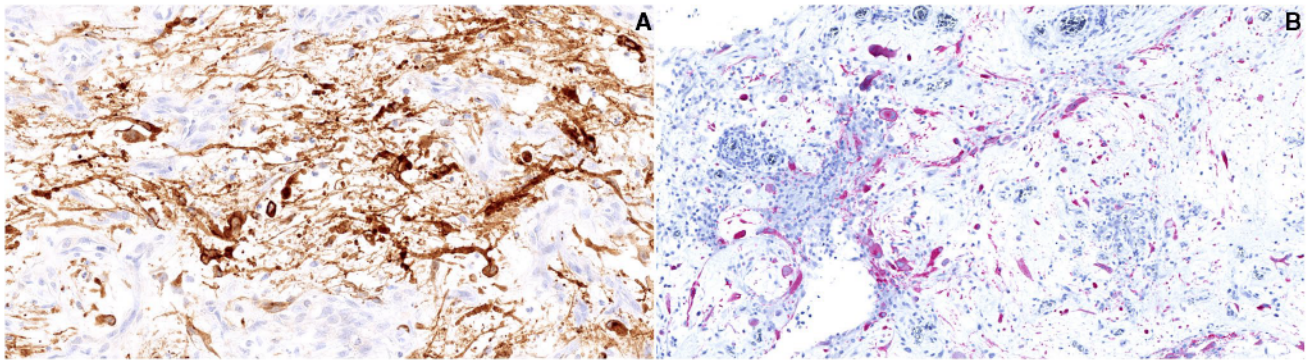
Springer

Fig. 3 Strong cytoplasmatic immunohistochemical positivity with the ALK antibody was present in all cases, occasionally highlighting their dendritic cytoplasmic processes (**A**; case 2, **B**; case 4)

fusion with corresponding ALK immunoexpression. Overall, it is unclear whether this tumor represents a mere subtype of IMT or a distinct entity. While a myxoid pattern is well recognized in IMT, it is often accompanied by fascicular/storiform growth patterns at least in some areas of the tumor. Similarly, while the ganglion-like cells can be found in some IMTs [13], the prominent large cells with intranuclear and cytoplasmic vacuoles or intranuclear cytoplasmic pseudoinclusions are not a feature of IMT. Most IMTs feature an ample and diffuse inflammatory infiltrate which was rather sparse in our cases. Importantly, 70% of the cases presented herein lacked myofibroblastic phenotype by immunohistochemistry. Ultrastructurally, the most striking feature of the tumor cells was the abundant rough endoplasmic reticulum taking up most of the cytoplasm. This is a feature seen in both fibroblasts and myofibroblasts, together with a spindled or stellate shape of the cells [14, 15] which was also observed in our cases. Myofilaments were, however, not present in the examined cells [9], pointing rather towards a fibroblastic differentiation. An identical *TIMP3::ALK* gene fusion detected in all cases analyzable by RNA-sequencing proposes a distinctive pathogenetic pathway for the development of this lesion. However, FISH for a *TIMP3* rearrangement was negative in 1 case which was not analyzable by sequencing methods. Indolent clinical behavior and a favorable outcome can be deduced from the available follow-up information, proposing a risk of overtreatment in case of misdiagnosis. Only 1 case recurred locally, likely due to incomplete removal of the tumor tissue in the original excision.

The activity of the transmembrane receptor tyrosine kinase ALK is key for the development of the neural system under physiological conditions [16], while its genetic alterations are the cause of several neoplastic diseases [17–21]. About three-fifths of IMT cases harbor a driver *ALK* gene fusion [2, 3]. The negative cases often display rearrangements of other receptor tyrosine kinase genes,

including *ROS1*, *RET*, *NTRK3*, or *IGF1R* [2, 3, 22]. ALK contains a receptor domain in the extracellular region, a single hydrophobic transmembrane domain, and a tyrosine kinase domain located in the intracellular part of the protein. Under normal conditions, the kinase dimerizes and autophosphorylates itself after being triggered by an extracellular ligand, and then continues to activate several proteins of various downstream signaling pathways, including but not limited to the RAS/MAPK, PI3K/Akt, and PLCγ pathways [23]. The fusion product in our cases retains the tyrosine kinase domain, which is crucial for its function in carcinogenesis. Translocation of the *ALK* gene to the *TIMP3* gene, coding for a protein involved in the remodelation of extracellular matrix—a process that is universally present during tumorigenesis—likely causes its increased expression, which can be confirmed by immunohistochemistry.

Recently, Kerr et al. [6] reported 13 cases of IMT in the head and neck region. In 4 cases (cases 1, 6, 11, and 13), the tumors occurred in the vocal cords and harbored a *TIMP3::ALK* fusion. Considering this subgroup, both sexes were affected equally; the patients' ages ranged from 25 to 33 years (mean 28.75, median 28.5). Follow-up information was available in 2/4 of cases with a mean of 4.25 years; both patients had no evidence of disease. The tumors contained large ganglion-like cells in 2 cases, as well as cells with intranuclear inclusions in 3 cases, dispersed in a variable mixture of myxoid and compact stroma with moderate to diffuse lymphocytic or lymphoplasmacytic inflammatory infiltrate. Immunohistochemically, all cases displayed cytoplasmic granular or diffuse positivity for ALK. Smooth muscle actin and desmin were negative in 2/3 and 3/4 cases tested, respectively. Conversely, case 13 was immunopositive for smooth muscle actin; rare cells are also stained for desmin. The exact fusion event differed slightly in this group: exon 1 of the *TIMP3* gene was fused to exon 19 of the *ALK* gene in 2 cases; the other 2 cases harbored a fusion of exon 3 of

the *TIMP3* gene to exon 18 of the *ALK* gene. In any event, however, the ALK tyrosine kinase domain is retained in the fusion product, preserving its proposed oncogenic activity.

Similarly, Pierry et al. [4] presented 6 cases of laryngeal IMT with ALK overexpression, three of which were located in the vocal cords and were positively tested for an *ALK* rearrangement by FISH (cases 2, 3, and 6). Two males were affected, and 1 patient was female. Their ages ranged from 40 to 48 years (mean 43.$\overline{3}3$, median 42). Histologically, the tumors consisted of spindle cells with nuclear atypia in a myxoid background, with variably pronounced inflammatory infiltrates of lymphocytes and plasma cells. However, no detailed histomorphologic description was available for each case separately. Case 2 which occurred in the vocal cord of a 40-year-old male did not stain immunohistochemically for smooth muscle actin, while the other 2 cases were positive. Moreover, case 6 was immunopositive for desmin. The patients did not receive any additional treatment after the excision of the tumor and had no evidence of disease in the follow-up period which lasted from 5 to 28 months (mean 15, median 12). One more atypical IMT of the right vocal cord was reported by Völker et al. [24]. The patient was a 34-year-old female who suffered a recurrence 3 months after the initial excision that was considered complete. The patient had no evidence of disease 2.5 years after the excision of the recurrent tumor. Interestingly, the primary tumor consisted of cytomorphologically mostly bland spindled cells in a myxoid stroma; the recurrence displayed more compact growth of mildly atypical cells with prominent nucleoli. The tumor was immunohistochemically positive for ALK, while both smooth muscle actin and desmin were negative.

Even though a detailed review of these previously reported tumors [4, 6, 24] was not available, given the concordant immunoprofile (ALK positivity, common negativity for muscle markers), histomorphologic features (presence of myxoid stroma and atypical cells), and very indolent clinical behavior, as well as the *TIMP3::ALK* driving fusion in the 4 cases reported by Kerr et al. [6], we propose that at least some of these previous cases might represent identical tumors as presented herein by us. We are unable to determine whether this indolent lesion represents a separate diagnostic entity or a subtype of IMT. However, it is morphologically and immunohistochemically unique and needs to be recognized to refrain from overdiagnosis.

Apart from the laryngeal region, *TIMP3::ALK* fusions have been reported in 2 uterine and 12 pregnancy-associated IMT cases [25–29]. The ages of the female patients ranged from 25 to 41 years (mean 34, median 34.5). All of the 7 patients with available follow-up data had no evidence of disease. Interestingly, histomorphologic parallels could be drawn between these IMT cases and the laryngeal lesion presented herein. The majority of cases displayed focal to abundant myxoid stroma interweaved with delicate thin-walled vessels. The tumor cells were described as elongated or spindled, while mild to moderate nuclear atypia and ganglion-like appearance of some cells were common findings. On immunohistochemical examination, ALK was positive in the tumor cell cytoplasm in each case.

A number of entities can be considered in the differential diagnosis of the lesion presented herein. In general, the unusual cytological features and diffuse ALK immunoexpression and/or detection of *ALK* rearrangements are the most helpful diagnostic clues. Firstly, edematous reactive vocal cord nodules and polyps can easily be excluded by the absence of any significant atypia in the non-neoplastic small spindled fibroblasts that are present in these lesions. Similarly, the diagnosis of myxoma, which has been scarcely reported in the vocal cords [30] and which consists of abundant myxoid stroma with dispersed, completely bland spindled or stellate small cells, can be rejected based on the significantly different cytological and immunohistochemical features present in our cases.

Given the previously mentioned cytological atypia, malignant soft tissue tumors should be taken into account during the diagnostic process. Myxofibrosarcoma is a malignant myxoid mesenchymal tumor that affects older adults with no sex predilection [31–34]. Soft tissues of proximal extremities are most commonly affected, with the thigh being the most frequent site [32]. Less than 50 cases of head and neck myxofibrosarcoma cases have been reported in the literature [35, 36] and, to the best of our knowledge, only 1 report of a myxofibrosarcoma occurring in the vocal cord exists [37]. The differentiation between these two entities might be challenging. Just as the herein presented lesions, myxofibrosarcoma is a vaguely nodular lesion with alternating hypocellular myxoid and more cellular solid areas. Notably, the myxoid stroma is predominant in low-grade cases. Solid sheets of spindled cells become more frequent with increasing histological grade. Another common feature of the two lesions is the presence of numerous curvilinear or arched capillaries with perivascular cell compaction [34]. Cytologically, the spindled tumor cells display nuclear pleomorphism and hyperchromasia; some cells might contain intracytoplasmic vacuoles and thus resemble lipoblasts [34]. These changes are very subtle in low-grade myxofibrosarcoma, while in the more high-grade cases, the atypical cells as well as mitotic figures and occasional necrosis are more prominent. The latter aids in the differentiation of myxofibrosarcoma from the lesions presented here, as increased mitotic rate and necrosis were absent in our cohort. Genetically, myxofibrosarcoma harbors complex genetic aberrations, while *ALK* rearrangements have not been detected. Therefore, the detection of an *ALK* rearrangement and/

or immunohistochemical expression of ALK might be diagnostically very useful in ruling out myxofibrosarcoma.

Alternating myxoid and compact whorled areas, together with delicate curvilinear vessels, are also typical for low-grade fibromyxoid sarcoma (LGFMS). Only extremely rare cases are known to appear in the head and neck region, generally in younger adult male patients [38]. Despite its malignant nature, the tumor is cytomorphologically bland, composed of a monotonous proliferation of spindled or fusiform neoplastic cells. This is in contrast to the variably shaped and slightly atypical cells encountered in tumors presented in this report. Moreover, diffuse MUC4 immunoexpression and *FUS::CREB3L1/2* or less commonly *EWSR1::CREB3L1* fusions represent helpful diagnostic features of LGFMS [39–41].

The myxoid stroma, variably inflammatory background, and atypical tumor cells could suggest the possibility that one is dealing with dedifferentiated liposarcoma. Morphologically, the presence of a well-differentiated component as well as the presence of more hyperchromatic spindle cells might help to establish the correct diagnosis. In morphologically challenging cases, CDK4 and MDM2 immunohistochemical markers and, conversely, ALK immunohistochemistry represent very helpful diagnostic aids [42].

In summary, we report 7 cases of an indolent, variably myxoid tumor of the vocal cords, characterized by overt cellular atypia with large cells containing intranuclear and intracytoplasmic vacuoles, delicate curvilinear vessels, and sparse inflammatory infiltrate. A recurrent *TIMP3::ALK* fusion and ALK immunoexpression were present in all cases tested. It remains unclear whether this tumor represents a mere subtype of IMT or a separate entity. Nevertheless, it is a morphologically distinct and diagnostically challenging lesion that needs to be recognized by surgical pathologists in order to prevent overdiagnosis in this clinically very delicate area. We, therefore, suggest the name "Myxoid fibroblastic tumor of the vocal cords with a *TIMP3::ALK* fusion" for the entity.

Data availability Data supporting the findings of this study are available within the article. The complete datasets generated during and/or analyzed during the current study are available from the corresponding author on reasonable request.

Code availability Not applicable.

Declarations

Ethics approval The study was approved by the institutional review board of the Faculty of Medicine in Pilsen, Charles University. The procedures used in this study adhere to the tenets of the Declaration of Helsinki.

Informed consent No patient consent was required for this study.

Conflict of interest The authors declare no competing interests.

References

1. WHO classification of tumours editorial board (2020) WHO classification of tumours of soft tissue and bone, 5th edn. IARC Press, Lyon
2. Yamamoto H, Yoshida A, Taguchi K et al (2016) ALK, ROS1 and NTRK3 gene rearrangements in inflammatory myofibroblastic tumours. Histopathology 69(1):72–83
3. Antonescu CR, Suurmeijer AJ, Zhang L et al (2015) Molecular characterization of inflammatory myofibroblastic tumors with frequent ALK and ROS1 gene fusions and rare novel RET rearrangement. Am J Surg Pathol 39(7):957–967
4. Pierry C, Pérot G, Karanian-Philippe M et al (2015) Polypoid laryngeal inflammatory myofibroblastic tumors: misleading lesions: description of six cases showing ALK overexpression. Am J Clin Pathol 144(3):511–516
5. Coffin CM, Watterson J, Priest JR, Dehner LP (1995) Extrapulmonary inflammatory myofibroblastic tumor (inflammatory pseudotumor). A clinicopathologic and immunohistochemical study of 84 cases. Am J Surg Pathol. 19(8):859–872
6. Kerr DA, Thompson LDR, Tafe LJ et al (2021) Clinicopathologic and genomic characterization of inflammatory myofibroblastic tumors of the head and neck: highlighting a novel fusion and potential diagnostic pitfall. Am J Surg Pathol 45(12):1707–1719
7. Meis JM, Enzinger FM (1991) Inflammatory fibrosarcoma of the mesentery and retroperitoneum. A tumor closely simulating inflammatory pseudotumor. Am J Surg Pathol. 15(12):1146–1156
8. Coffin CM, Humphrey PA, Dehner LP (1998) Extrapulmonary inflammatory myofibroblastic tumor: a clinical and pathological survey. Semin Diagn Pathol 15(2):85–101
9. Yorita K, Togashi Y, Nakagawa H et al (2019) Vocal cord inflammatory myofibroblastic tumor with mucoid deposits harboring TIMP3-ALK fusion: a potential diagnostic pitfall. Pathol Int 69(6):366–371
10. Agaimy A, Baněčková M, Ihrler S et al (2021) ALK Rearrangements characterize 2 distinct types of salivary gland carcinomas: clinicopathologic and molecular analysis of 4 cases and literature review. Am J Surg Pathol 45(9):1166–1178
11. Ptáková N, Miesbauerová M, Kosťun J et al (2018) Immunohistochemical and selected genetic reflex testing of all uterine leiomyosarcomas and STUMPs for ALK gene rearrangement may provide an effective screening tool in identifying uterine ALK-rearranged mesenchymal tumors. Virchows Arch 473(5):583–590
12. Agaimy A, Tögel L, Haller F, Zenk J, Hornung J, Märkl B (2020) YAP1-NUTM1 gene fusion in porocarcinoma of the external auditory canal. Head Neck Pathol 14(4):982–990
13. Coffin CM, Hornick JL, Fletcher CD (2007) Inflammatory myofibroblastic tumor: comparison of clinicopathologic, histologic,

and immunohistochemical features including ALK expression in atypical and aggressive cases. Am J Surg Pathol 31(4):509–520

14. Eyden B (2004) Fibroblast phenotype plasticity: relevance for understanding heterogeneity in "fibroblastic" tumors. Ultrastruct Pathol 28(5–6):307–319

15. Eyden B (2008) The myofibroblast: phenotypic characterization as a prerequisite to understanding its functions in translational medicine. J Cell Mol Med 12(1):22–37

16. Cao Z, Gao Q, Fu M, Ni N, Pei Y, Ou WB (2019) Anaplastic lymphoma kinase fusions: roles in cancer and therapeutic perspectives. Oncol Lett 17(2):2020–2030

17. Gustafson S, Medeiros LJ, Kalhor N, Bueso-Ramos CE (2009) Anaplastic large cell lymphoma: another entity in the differential diagnosis of small round blue cell tumors. Ann Diagn Pathol 13(6):413–427

18. Koivunen JP, Mermel C, Zejnullahu K et al (2008) EML4-ALK fusion gene and efficacy of an ALK kinase inhibitor in lung cancer. Clin Cancer Res 14(13):4275–4283

19. Chou A, Fraser S, Toon CW et al (2015) A detailed clinicopathologic study of ALK-translocated papillary thyroid carcinoma. Am J Surg Pathol 39(5):652–659

20. Janoueix-Lerosey I, Lequin D, Brugières L et al (2008) Somatic and germline activating mutations of the ALK kinase receptor in neuroblastoma. Nature 455(7215):967–970

21. George RE, Sanda T, Hanna M et al (2008) Activating mutations in ALK provide a therapeutic target in neuroblastoma. Nature 455(7215):975–978

22. Piarulli G, Puls F, Wängberg B et al (2019) Gene fusion involving the insulin-like growth factor 1 receptor in an ALK-negative inflammatory myofibroblastic tumour. Histopathology 74(7):1098–1102

23. Huang H (2018) Anaplastic lymphoma kinase (ALK) receptor tyrosine kinase: a catalytic receptor with many faces. Int J Mol Sci 19(11):3448

24. Völker HU, Scheich M, Zettl A, Hagen R, Müller-Hermelink HK, Gattenlöhner S (2010) Laryngeal inflammatory myofibroblastic tumors: different clinical appearance and histomorphologic presentation of one entity. Head Neck 32(11):1573–1578

25. Haimes JD, Stewart CJR, Kudlow BA et al (2017) Uterine inflammatory myofibroblastic tumors frequently harbor ALK fusions with IGFBP5 and THBS1. Am J Surg Pathol 41(6):773–780

26. Bennett JA, Nardi V, Rouzbahman M, Morales-Oyarvide V, Nielsen GP, Oliva E (2017) Inflammatory myofibroblastic tumor of the uterus: a clinicopathological, immunohistochemical, and molecular analysis of 13 cases highlighting their broad morphologic spectrum. Mod Pathol 30(10):1489–1503

27. Devereaux KA, Fitzpatrick MB, Hartinger S, Jones C, Kunder CA, Longacre TA (2020) Pregnancy-associated inflammatory myofibroblastic tumors of the uterus are clinically distinct and highly enriched for TIMP3-ALK and THBS1-ALK fusions. Am J Surg Pathol 44(7):970–981

28. Cheek EH, Fadra N, Jackson RA et al (2020) Uterine inflammatory myofibroblastic tumors in pregnant women with and without involvement of the placenta: a study of 6 cases with identification of a novel TIMP3-RET fusion. Hum Pathol 97:29–39

29. Makhdoum S, Nardi V, Devereaux KA et al (2020) Inflammatory myofibroblastic tumors associated with the placenta: a series of 9 cases. Hum Pathol 106:62–73

30. Val-Bernal JF, Martino M, Longarela MY (2020) Cellular myxoma of the vocal cord: a case report and review of the literature. Turk Patoloji Derg 36(1):77–81

31. Sanfilippo R, Miceli R, Grosso F et al (2011) Myxofibrosarcoma: prognostic factors and survival in a series of patients treated at a single institution. Ann Surg Oncol 18(3):720–725

32. Gilg MM, Sunitsch S, Leitner L et al (2020) Tumor-associated mortality and prognostic factors in myxofibrosarcoma - a retrospective review of 109 patients. Orthop Traumatol Surg Res 106(6):1059–1065

33. Yoshimoto M, Yamada Y, Ishihara S et al (2020) Comparative study of myxofibrosarcoma with undifferentiated pleomorphic sarcoma: histopathologic and clinicopathologic review. Am J Surg Pathol 44(1):87–97

34. Huang HY, Lal P, Qin J, Brennan MF, Antonescu CR (2004) Low-grade myxofibrosarcoma: a clinicopathologic analysis of 49 cases treated at a single institution with simultaneous assessment of the efficacy of 3-tier and 4-tier grading systems. Hum Pathol 35(5):612–621

35. Zhang B, Bai M, Tian R, Hao S (2021) Idiopathic and radiation-induced myxofibrosarcoma in the head and neck-case report and literature review. Chin Neurosurg J 7(1):48

36. Dell'Aversana Orabona G, Iaconetta G, Abbate V et al (2014) Head and neck myxofibrosarcoma: a case report and review of the literature. J Med Case Rep 8:468

37. Gugatschka M, Beham A, Stammberger H, Schmid C, Friedrich G (2010) First case of a myxofibrosarcoma of the vocal folds: case report and review of the literature. J Voice 24(3):374–376

38. Cowan ML, Thompson LD, Leon ME, Bishop JA (2016) Low-Grade Fibromyxoid Sarcoma of the Head and Neck: A Clinicopathologic Series and Review of the Literature. Head Neck Pathol. 10(2):161–6

39. Lau PP, Lui PC, Lau GT, Yau DT, Cheung ET, Chan JK (2013) EWSR1-CREB3L1 gene fusion: a novel alternative molecular aberration of low-grade fibromyxoid sarcoma. Am J Surg Pathol 37(5):734–738

40. Mertens F, Fletcher CD, Antonescu CR et al (2005) Clinicopathologic and molecular genetic characterization of low-grade fibromyxoid sarcoma, and cloning of a novel FUS/CREB3L1 fusion gene. Lab Invest 85(3):408–415

41. Panagopoulos I, Storlazzi CT, Fletcher CD et al (2004) The chimeric FUS/CREB3l2 gene is specific for low-grade fibromyxoid sarcoma. Gene Chromosome Cancer 40(3):218–228

42. Aleixo PB, Hartmann AA, Menezes IC, Meurer RT, Oliveira AM (2009) Can MDM2 and CDK4 make the diagnosis of well differentiated/dedifferentiated liposarcoma? An immunohistochemical study on 129 soft tissue tumours. J Clin Pathol 62(12):1127–1135

🖄 Springer

4.9 Epithelioid soft tissue neoplasm of the soft palate with a *PTCH1::GLI1* fusion: A case report and review of the literature

V práci je popsán vzácný mesenchymální tumor měkkého patra s fúzí *PTCH1::GLI1*. Nádor byl diagnostikován u 34leté ženy, původně byl však považován za zánětlivou lézi a byl léčen antibiotickou terapií. Vzhledem k perzistenci nálezu bylo provedeno CT vyšetření, které prokázalo přítomnost nehomogenního tumoru v oblasti měkkého patra a nasopharyngu, provedená probatorní biopsie byla uzavřena jako low-grade kulatobuněčný sarkom s pozitivitou neuroendokrinních imunohistochemických markerů.

Nádor byl resekován, resekce však nebyla kompletní, proto byla po dvou měsících provedena re-resekce a disekce krčních lymfatických uzlin, další adjuvantní léčba nebyla onkologem doporučena. V době tvorby disertační práce byla pacientka dle posledního dostupného údaje 14 měsíců bez příznaků onemocnění.

Nádorové buňky byly uspořádány ve splývajících hnízdech se solidně-trabekulárním, fascikulárním nebo retikulárním růstovým vzorem, oddělených vazivovými septy. Neoplastické buňky se jevily nápadně uniformní, kulaté až oválně, se středně objemnou, povětšinou jemně granulární eosinofilní cytoplazmou, ložiskově i s cytoplazmou projasněnou, a s centrálně umístěnými jádry s jemným chromatinem a nevýraznými jadérky. Ve fascikulárních oblastech nabývaly buňky vřetenité morfologie. Mitotická aktivita byla nízká (2 mitotické figury na 10 polí velkého zvětšení), nebyly přítomny atypické mitózy a nekróza. V nádoru byly ložiskově hojné tumor-infiltrující nenádorové lymfocyty a bohatá větvená síť kapilár, ve větších cévách byla pozorována protruze tkáně nádoru do cévního lumen, avšak bez pravé lymfovaskulární invaze.

Imunohistochemicky byly nádorové buňky nerovnoměrně pozitivní v průkazu markerů S100 a CD56 a difúzně pozitivní v průkazu D2-40. Široký panel epiteliálních, myogenních, melanocytárních, endoteliálních a dalších markerů byl negativní. Vzhledem k pozitivitě neuroendokrinních markerů v probatorní biopsii byla testována exprese NSE, synaptofyzinu a chromograninu: zatímco NSE byla imunohistochemicky difúzně pozitivní, synaptofyzin a chromogranin byly pozitivní jen v limitovaném rozsahu (do 5 % nádorových buněk).

Vzhledem k podezření na *GLI1*-rearanžovaný tumor byl materiál testován pomocí RNA-seq. Byla prokázána přítomnost fúze *PTCH1::GLI1* mezi exonem 1 genu *PTCH1* a exonem 6 genu *GLI1*. Doposud popsané nádory s fúzí *PTCH1::GLI1* včetně zde prezentovaného případu vykazovaly epiteloidní rysy s multinodulárním nebo plexiformním typem růstu s uspořádáním buněk v hnízdech a s přítomností bohaté jemné a větvené vaskulární sítě. Nádorové buňky měly uniformní cytomorfologii s oválnými jádry, byly přítomny oblasti s projasněním cytoplazmy a fokální vřetenobuněčnou morfologií. Imunohistochemicky bylo možné prokázat expresi S100, exprese SMA a cytokeratinů byla negativní.

CASE REPORTS

Epithelioid Soft Tissue Neoplasm of the Soft Palate with a *PTCH1-GLI1* Fusion: A Case Report and Review of the Literature

Natálie Klubíčková[1,2,8] · Zdeněk Kinkor[1,2] · Michael Michal[1,2] · Martina Baněčková[1,2] · Veronika Hájková[3] · Jaroslav Michálek[4] · Richard Pink[5] · Zdeněk Dvořák[6] · Michal Michal[1,2] · Ilmo Leivo[7] · Alena Skálová[1,2]

Abstract

GLI1 fusions involving *ACTB*, *MALAT1*, *PTCH1* and *FOXO4* genes have been reported in a subset of malignant mesenchymal tumors with a characteristic nested epithelioid morphology and frequent S100 positivity. Typically, these multilobulated tumors consist of uniform epithelioid cells with bland nuclei and are organized into distinct nests and cords with conspicuously rich vasculature. We herein expand earlier findings by reporting a case of a 34-year-old female with an epithelioid mesenchymal tumor of the palate. The neoplastic cells stained positive for S100 protein and D2-40, whereas multiple other markers were negative. Genetic alterations were investigated by targeted RNA sequencing, and a *PTCH1-GLI1* fusion was detected. Epithelioid mesenchymal tumors harboring a *PTCH1-GLI1* fusion are vanishingly rare with only three cases reported so far. Due to the unique location in the mucosa of the soft palate adjacent to minor salivary glands, multilobulated growth, nested epithelioid morphology, focal clearing of the cytoplasm, and immunopositivity for S100 protein and D2-40, the differential diagnoses include primary salivary gland epithelial tumors, in particular myoepithelioma and myoepithelial carcinoma. Another differential diagnostic possibility is the ectomesenchymal chondromyxoid tumor. Useful diagnostic clues for tumors with a *GLI1* rearrangement include a rich vascular network between the nests of neoplastic cells, tumor tissue bulging into vascular spaces, and absence of SOX10, GFAP and cytokeratin immunopositivity. Identifying areas with features of *GLI1*-rearranged tumors should trigger subsequent molecular confirmation. This is important for appropriate treatment measures as *PTCH1-GLI1* positive mesenchymal epithelioid neoplasms have a propensity for locoregional lymph node and distant lung metastases.

Keywords Epithelioid soft tissue neoplasm · Oral cavity · *PTCH1-GLI1* gene fusion · Soft palate · S100 protein · Hedgehog signaling pathway

There are two senior authors of this manuscript (Ilmo Leivo and Alena Skálová).

✉ Natálie Klubíčková
    klubickova@biopticka.cz

1   Department of Pathology, Faculty of Medicine in Pilsen, Charles University, Pilsen, Czech Republic

2   Department of Pathology, Bioptical Laboratory, Ltd., Pilsen, Czech Republic

3   Molecular and Genetic Laboratory, Bioptical Laboratory, Ltd., Pilsen, Czech Republic

4   Department of Clinical and Molecular Pathology, Faculty of Medicine and Dentistry, Palacky University, and University Hospital Olomouc, Olomouc, Czech Republic

5   Department of Oral and Maxillofacial Surgery, University Hospital Olomouc, Olomouc, Czech Republic

6   Department of Plastic and Aesthetic Surgery, St. Anne's University Hospital, and Faculty of Medicine, Masaryk University Brno, Brno, Czech Republic

7   Institute of Biomedicine, Pathology, University of Turku, and Turku University Hospital, Turku, Finland

8   Department of Pathology, Bioptical Laboratory, Ltd., Mikulášské náměstí 4, 326 00 Pilsen, Czech Republic

Ⓐ Springer

Introduction

Fusions or amplifications of the *GLI1* gene have been discovered in soft tissue tumors of variable morphology, immunoprofile and clinical behavior. *GLI1*-fusion positive tumors were initially reported by Dahlen et al. in 2004 as a group of distinctive smooth muscle actin positive mesenchymal neoplasms harboring an *ACTB-GLI1* gene fusion, and they were designated as "pericytoma with t(7;12) translocation" [1]. Three of their five cases were located in the tongue and one each in the stomach and the calf [1]. Subsequently, other *GLI1*-rearranged tumors have been reported to arise in diverse tissues [2, 3], including the ovary [4, 10], the bones [5], the gastrointestinal tract [6–9], the soft tissue of the extremities [10], the retroperitoneum [2], the lung [3] or the kidney [15]. A broad spectrum of malignant mesenchymal neoplasms with relatively monomorphic round cell or epithelioid morphology, with a frequent S100 protein expression, and with recurrent *GLI1* gene fusions with *ACTB*, *MALAT1*, *PTCH1* or *FOXO4* have been characterized [2, 3, 15]. Although sharing some histologic features with pericytoma, including monomorphic and occasionally round cell phenotype, nested growth pattern and an intricate capillary network, these lesions display morphologic variability, lack of actin immunoreactivity, and propensity for locoregional lymph node and distant lung metastases [2].

Even though in the first published series of tumors harboring *ACTB-GLI1* fusions there was a marked predilection for occurrence in the tongue [1], other *GLI1*-rearranged tumors have been later reported to arise in other locations of the head and neck, including the submandibular gland and soft tissues of the neck [11]. However, a mucosal location in the palate has never been reported. Herein, we present a case of a 34-year-old female patient with an epithelioid mesenchymal tumor of the soft palate harboring a *PTCH1-GLI1* fusion. Several cases with *GLI1* rearrangements in the head and neck have been described [11] but to date, only two of them harbored the *PTCH1-GLI1* fusion. They arose in soft tissues of the submandibular region and the neck [2, 11] and the tongue [11]. One additional case with this fusion arose in soft tissues of the thorax [12]. To the best of our knowledge, ours is only the fourth case with the *PTCH1-GLI1* fusion reported so far.

All reported tumors with the *PTCH1-GLI1* rearrangement (including our case) showed prominent epithelioid features with a multinodular or plexiform growth pattern at low magnification and a distinctive nested architecture with a rich, delicate arborizing vascular network. The tumor cells displayed a monomorphic cytomorphology with uniform round to ovoid nuclei, multiple clear-cell areas, a focal spindled morphology, and S100 protein immunopositivity. Conversely, smooth muscle actin and wide-spectrum cytokeratin (AE1/AE3) expressions were negative on immunohistochemical examination. The unusual intraoral mucosal localization of the tumor in the palate and overlapping multilobulated growth, nested epithelioid morphology, clear cytoplasm and S100 protein immunopositivity represent possible differential diagnostic features shared with some primary salivary gland neoplasms, such as myoepithelioma, cellular pleomorphic adenoma, and myoepithelial carcinoma. Useful diagnostic clues for tumors with a *GLI1* rearrangement include a rich vascular network, nested architecture, tumor tissue bulging into vascular spaces, and the absence of cytokeratin, SOX10, GFAP and calponin immunopositivity. Identification of areas with classic histopathologic features of *GLI1*-rearranged tumors should trigger efforts for molecular confirmation of a *GLI1* rearrangement. This aberration has not been reported in the myoepithelial carcinoma of salivary glands [13, 14].

Materials and Methods

The study was approved by the institutional review board of the Faculty of Medicine in Pilsen, Charles University. The case described in this study was retrieved from the consultation files of AS. The clinical follow-up information was obtained from the treating clinicians (RP, ZD) and the referring pathologist (JM).

For conventional microscopy, excised tissues were fixed in formalin, processed routinely, embedded in paraffin (FFPE), cut, and stained with hematoxylin and eosin. For immunohistochemical analysis, 4-μm-thick sections were cut from paraffin blocks and mounted on positively charged slides (TOMO; Matsunami Glass IND, Japan). Sections were processed on a BenchMark ULTRA (Ventana Medical System, Tucson, AZ), deparaffinized, and then subjected to heat-induced epitope retrieval by immersion in CC1 solution at 95 °C and pH 8.6. All primary antibodies used are summarized in Table 1. Bound antibodies were visualized using the UltraView Universal DAB Detection Kit (Roche, Basel, Switzerland) and the UltraView Universal Alkaline Phosphatase Red Detection Kit (Roche). The slides were counterstained with Mayer's hematoxylin. Appropriate positive and negative controls were employed.

Targeted Next-Generation Sequencing

For next-generation sequencing (NGS) RNA was extracted using Total NA Maxwell RSC DNA FFPE kit (automated on Maxwell RSC 48 Instrument, Promega, Madison, WI). Purified RNA was quantified using the Qubit Broad Range RNA Assay (Thermo Fisher Scientific, Waltham, MA). Fusion

Table 1 Antibodies used for the immunohistochemical study

Antibody	Clone	Dilution	Antigen retrieval, time	Source
AE1/AE3	AE1/AE3	RTU	EnVision High pH, 30 min	Dako
CAM5.2	CAM5.2	RTU	CC1, 36 min	Ventana
CD31	JC70A	1:40	CC1, 36 min	Dako
CD34	QBEnd/10	1:100	EnVision High pH, 30 min	Dako
CD56	123C3	RTU	CC1, 52 min	Ventana
CD99	O13	RTU	CC1, 52 min	Ventana
CDK4	DCS-31	1:800	CC1, 52 min	Invitrogen
Chromogranin	DAK-A3	1:200	EnVision High pH, 30 min	Dako
CK5/6	D5/16B4	1:50	EnVision High pH, 30 min	Dako
CK7	OV-TL 12/30	RTU	EnVision High pH, 30 min	Dako
CK14	SP53	RTU	CC1, 36 min	Ventana
DDIT3	9C8	1:200	EnVision High pH, 30 min	AbCam
Desmin	D33	RTU	EnVision High pH, 30 min	Dako
D2-40	D2-40	RTU	EnVision High pH, 30 min	Dako
HHV-8	13B10	RTU	CC1, 52 min	Ventana
Ki-67	MIB-1	RTU	EnVision High pH, 30 min	Dako
MyoD1	EP212	RTU	CC1, 52 min	Ventana
NSE	BBS/NC/VI-H14	1:400	CC1, 36 min	Dako
OSCAR	IsoType:IgG2a	1:100	EnVision High pH, 30 min	Covance
p63	4A4	RTU	EnVision High pH, 30 min	Dako
SOX10	SP267	RTU	CC1, 52 min	Ventana
STAT6	YE361	1:1000	CC1, 52 min	Abcam
Synaptophysin	DAK-SYNAP	RTU	EnVision High pH, 30 min	Dako
S-100	Polyclonal	RTU	EnVision High pH, 30 min	Dako

CC1 EDTA buffer, pH 8.6, 95 °C; *EnVision high pH* EnVision high pH solution, pH 9.0, 97 °C; *min* minutes; *RTU* ready to use

transcript detection and mutational analysis were performed using the customized FusionPlex Sarcoma kit No.6 (Archer DX, Boulder, CO). The process of library preparation and sequencing was done as described previously [14] and data analysis was performed using the Archer Analysis software version 6.2.1. The complete list of genes is available in Online Resource.

Case Presentation

The patient was a 34-year-old female who had observed a stiff lesion in her soft palate 2 months prior to first contact with a maxillofacial surgeon. The lesion was initially considered to be an abscess with partial regression of its size after dental work and an antibiotic treatment. However, a CT angiography revealed a persistent non-homogenous tumorous lesion in the soft palate and lateral nasopharyngeal wall. A preliminary biopsy was inconclusive, but suggestive of a low-grade round-cell sarcoma with immunohistochemical positivity for D2-40 and neuroendocrine markers (a diffuse positivity for synaptophysin and NSE, and a focal positivity for S-100 protein). At the time of excision, the tumor measured $34 \times 21 \times 13$ mm. Oral surface above the tumor was ulcerated in an area of 18×13 mm and to a depth of 4 mm (Fig. 1A). The tumor consisted of soft tan-brown tissue on cut surface, and there was no discernible capsule.

Microscopically, the excision was covered by a superficially ulcerated stratified squamous epithelium with reactive changes and an extensive pseudoepitheliomatous hyperplasia. Underneath, there was inflamed granulation tissue with occasional giant cells attached to the multilobular tumor (Fig. 2A). Invasive tumor front extended into the surrounding small salivary gland (Fig. 2B) and the striated muscle tissue (Fig. 2C), and perineural invasion was noted (Fig. 2D). Tumor cell nests were separated by thick or delicate fibrous septae (Fig. 3A) and occasionally they protruded into vascular spaces (not shown). An abundant arborizing capillary network was seen throughout the neoplastic tissue. The network was well pronounced especially in solid areas of the tumor (Fig. 3A, B). The tumor cells were organized either in a solid-trabecular fashion (Fig. 3B), a fascicular (myoepithelial carcinoma-like) pattern (Fig. 3C, D), or a reticular pattern with a myxoid stroma (Fig. 3E). A minor part of the tumor displayed a pseudoglandular architecture (Fig. 3F). Tumor cells appeared relatively uniform, round
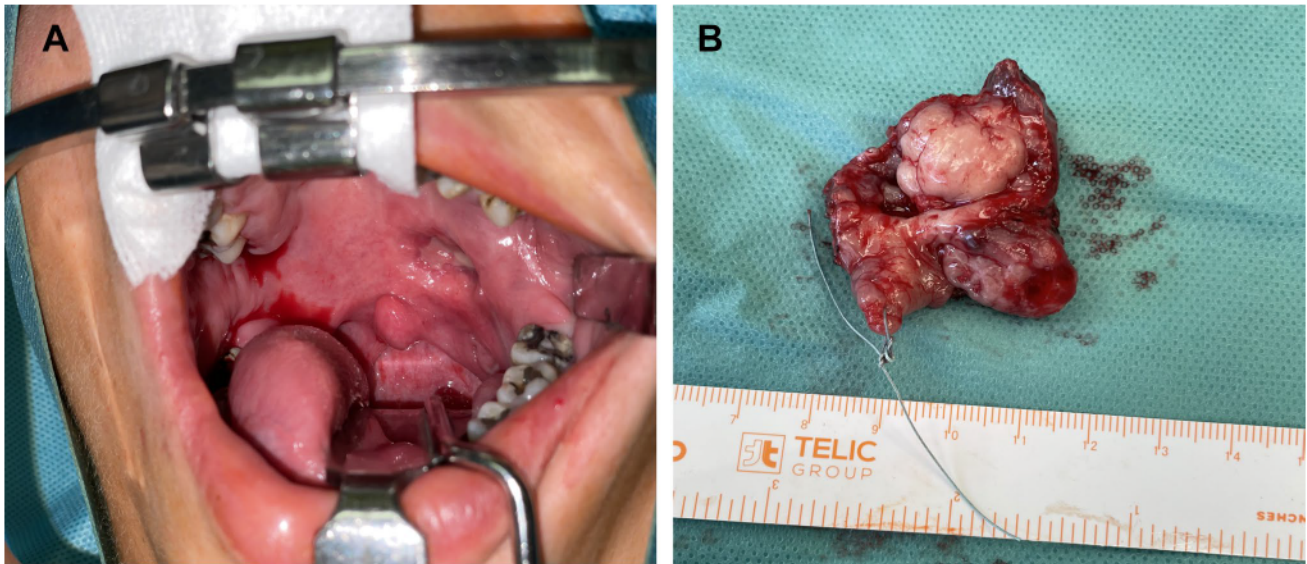
Fig. 1 Macroscopic features of the tumor. **A** The tumor grew on the left side of the soft palate with a superficial ulceration. **B** Residual tumor tissue was resected during second surgery, together with the left palatine tonsil
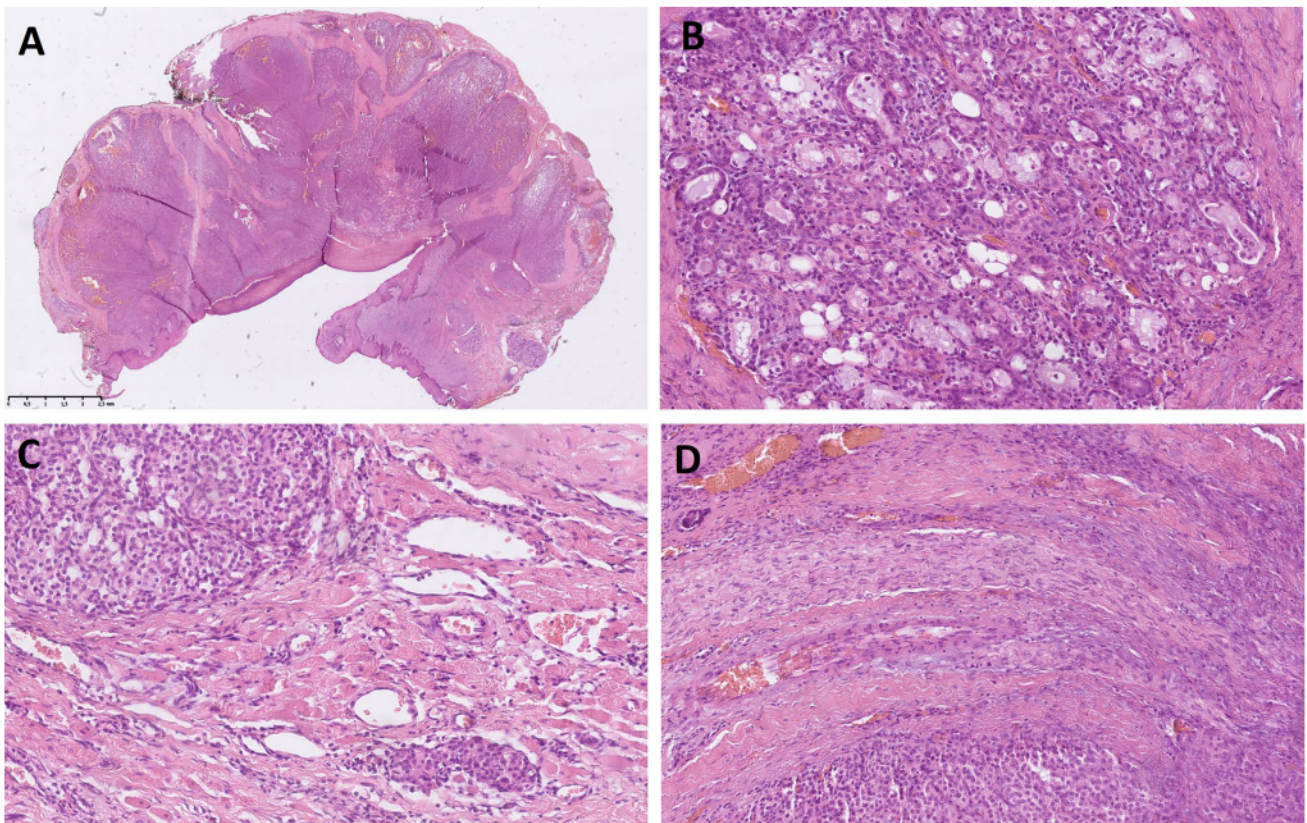

Fig. 2 Low-power microscopic view of the tumor (H&E*). **A** The multilobular tumor grew underneath an ulcerated stratified squamous epithelium of the oropharyngeal mucosa. **B** Tumor cells extended into adjacent minor salivary gland. **C** Tumor cells infiltrated adjacent striated muscle tissue. **D** Perineural infiltration was noted. *Hematoxylin and eosin
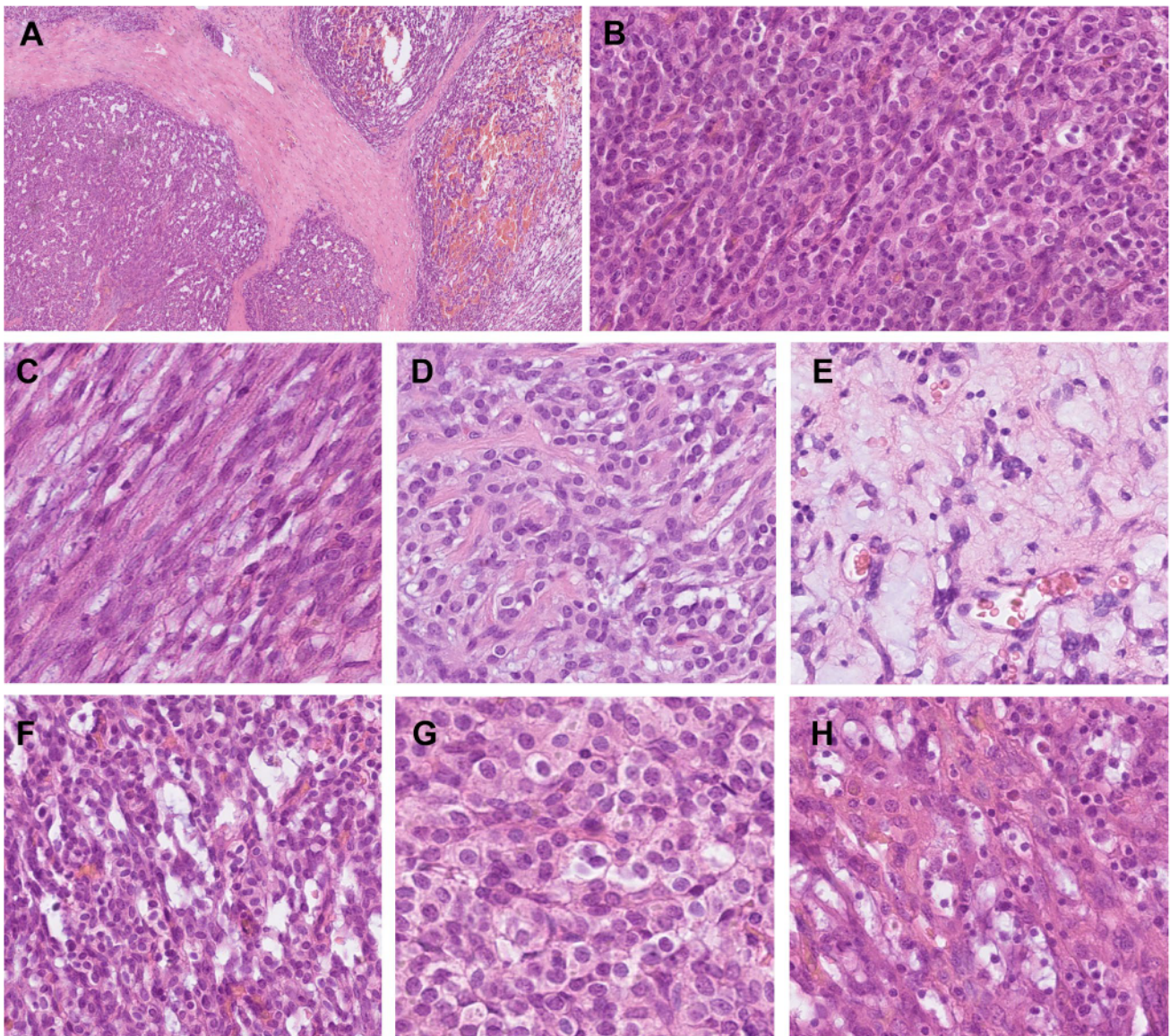
Fig. 3 Histomorphologic features of the tumor (H&E*). Nests of tumor cells were surrounded by thick or delicate fibrous septae (**A**). Arborizing capillary network was interspersed among tumor cells throughout the lesion (**A**, **B**). Tumor cells were relatively uniform, round to oval, occasionally spindled, and with bland basophilic oval nuclei and inconspicuous nucleoli (**B**, **C**). Several architectural patterns were seen. Tumor cells grew predominantly in a solid-trabecular (**B**) and a fascicular, myoepithelial carcinoma-like fashion (**C**, **D**). Less commonly, a reticular pattern with abundant myxoid stroma (**E**) and a pseudoglandular microcystic pattern (**F**) were seen. Focally, tumor cells displayed clearing of the cytoplasm with an infrequent perinuclear halo (**G**). The clear cell change escalated in some areas into a pseudolipoblast-like appearance with marked vacuolization of the cytoplasm (**H**). A focal lymphocytic infiltrate was seen throughout the tumor (**H**). *Hematoxylin and eosin

to oval, with bland centrally located basophilic-staining nuclei, inconspicuous nucleoli and a moderate amount of delicate granular eosinophilic cytoplasm. A spindled cell morphology was present in the fascicular areas. Occasional cells displayed clearing of the cytoplasm, sometimes with a perinuclear halo (Fig. 3G), escalating in some areas into a pseudolipoblast appearance with prominent cytoplasmic vacuolization (Fig. 3H). Tumor-infiltrating lymphocytes were abundant, especially in the solid-trabecular areas of the tumor (Fig. 3H). Cell proliferation was low, reaching 2 mitotic figures per 10 HPF. No tumor necrosis nor any atypical mitoses were seen. The tumor was not completely resected.

Immunohistochemically, a focal and patchy S-100 protein (Fig. 4A) and CD56 (Fig. 4B) positivity, as well as a diffuse and strong D2-40 (Fig. 4C) expression were demonstrated in the tumor cells. A wide spectrum of various markers was negative, including markers of epithelial
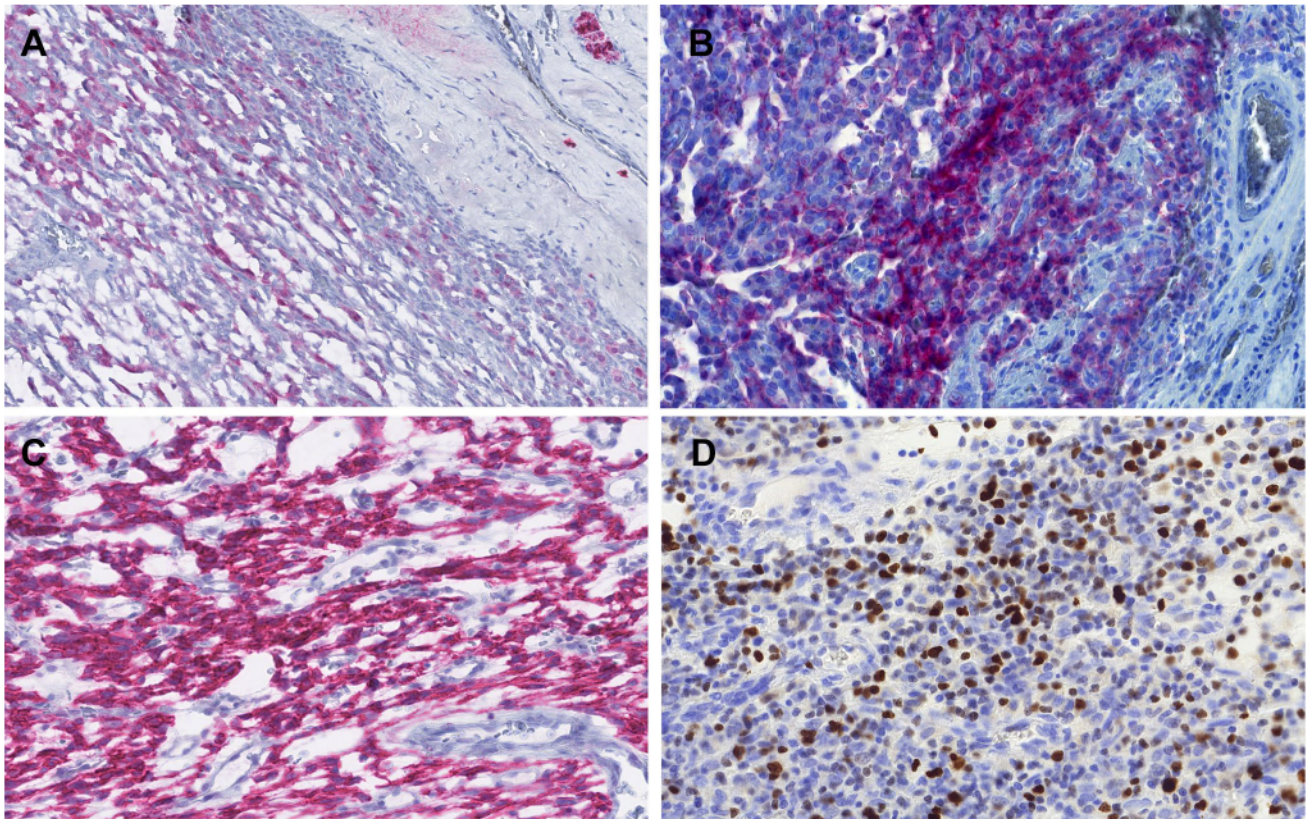
Fig. 4 Immunohistochemical features of the tumor. **A** Immunohistochemical examination revealed focal and patchy S-100 protein expression (positive internal control in a nerve is seen in the upper right corner). **B** Similar pattern was seen with CD56 immunostain. **C** Diffuse and strong D2-40 positivity was present throughout the tumor. **D** Ki-67 stained up to 7% of cells in areas with sparse lymphocytes, while 20–25% of tumor cells were positive in lymphocyte-rich foci

(AE1/AE3, OSCAR, CAM5.2, CK5/6, CK7, CK14), myogenic (myoD1, desmin), melanocytic (SOX10), and endothelial (CD31, CD34) differentiation, as well as various other markers such as CD99, p63, HHV-8, DDIT3, STAT6 and CDK4. Proliferative index was low to intermediate, in lymphocyte-poor areas Ki-67 stained up to 7% of nuclei, while in lymphocyte-rich areas Ki-67 was positive in 20–25% of tumor cells (Fig. 4D). As

the immunohistochemical examination of the probatory biopsy at the referring institution showed diffuse positivity for synaptophysin and NSE, we conducted an additional analysis of the expression of neuroendocrine markers. While NSE was strongly diffusely positive, patchy synaptophysin expression was detected in up to 5% cells and chromogranin was positive in one focus. However,

PTCH1-GLI1 fusion transcript:

PTCH1 NM_001083602.1: exon 1 (chr9:98278751) - **GLI1** NM_005269.2: exon6 (chr12:57859390)

Fig. 5 *PTCH1-GLI1* fusion transcript. Exon 1a of *PTCH1* gene containing a Gli1 binding site (black arrow) is fused (red arrow) to exon 6 of *GLI1* gene. Gli1 part of the fusion protein retains its FOXP coiled-coil domain (FOXP-CC) and three zinc fingers of C2H2 type (C2H2 Zn fingers), which may enable dimerization and binding to Gli1 target genes

multiple blocks had to be examined to demonstrate the positivity of synaptophysin and chromogranin.

Using the Archer FusionPlex custom panel, a *PTCH1-GLI1* fusion involving exon 1 of the *PTCH1* gene and exon 6 of the *GLI1* gene was detected. The reference transcript sequences used for describing *PTCH1* and *GLI1* have accession numbers NM_001083602.1 and NM_005269, respectively. The chromosomal position is described using the reference genome GRCh37 (hg19), and breakpoints at chr9:98278751, and chr12:5785939 (Fig. 5).

Re-resection and lateral block neck dissection were performed 2 months after the primary excision (Fig. 1B). Small amounts of residual tumor were identified in the resection sample from the oropharynx, but the margins were clear. Twenty-two neck lymph nodes were identified, and they were free of tumor infiltration. A PET-CT scan was performed before the first surgery, and it did not reveal any suspected metastatic lesions. Subsequent adjuvant therapy was not recommended by an oncologist. The patient is currently in the second trimester of pregnancy. The case is recent and only a limited follow-up of 4 months is available with no evidence of disease.

Discussion

Genetic abnormalities of *GLI1*, including gene fusions and amplification, have been reported recently in a subset of soft tissue tumors with a distinctive epithelioid nested histomorphology and a propensity for locoregional and distant metastasis [2]. To the best of our knowledge, 45 cases of *GLI1*-altered tumors, including 14 cases (31% of all cases) in the head and neck region, have been reported to date. Rearrangements of *GLI1* have been detected in tumors arising from various parts of the body, including soft tissues of extremities or trunk (11/31 cases) [2, 3, 10], gastrointestinal tract (10/31 cases) [6–9], bones (4/31 cases) [2, 5, 10], ovary (2/31 cases) [4, 10], and one case each in intrathoracic soft tissues [12], kidney [15], lung [3], and

retroperitoneum [2]. In the head and neck region, the most common site of origin was tongue (11/14 cases), followed by submandibular and neck soft tissue (3/14 cases) [1–3, 11]. There are no previous reports of a tumor of the soft palate. The tumors were diagnosed either as "pericytoma with t(7,12) translocation" or mesenchymal neoplasm with *GLI1* gene alterations (the name malignant epithelioid neoplasm with GLI1 gene rearrangements was also used for this entity in the past [2]). Additionally, two cases of gastroblastoma with a *MALAT1-GLI1* fusion [7] and five cases of gastric plexiform fibromyxoma with the same fusion or *GLI1* amplification were reported recently [8]. Strikingly, with the exception of the plexiform fibromyxoma cases, most tumors demonstrated similar histopathologic features and were described as vaguely lobular proliferations of bland spindled to ovoid epithelioid cells with pale eosinophilic or clear cytoplasm, often with some myxoid areas and delicate arborizing vasculature. Even though the first reported cases of *GLI1*-altered tumors stained positive for smooth muscle actin, leading to their diagnosis as pericytoma, much higher variability in the immunoprofile of these tumors was later noted. In addition to the actin, the tumors are frequently positive for CD56 (16/19 cases tested, 84%), S100 protein (17/43 cases tested, 39.5%) and, less commonly, wide spectrum cytokeratins (AE1/AE3) (8/39 cases tested, 20.5%). Although a wide age range has been observed in patients with *GLI1*-rearranged tumors (ranging from 1 to 79 years), patients in their 4th decade seem to be most commonly affected (median 32 years). The situation is very similar with regards specifically to the head and neck tumors, where the age of the patients has ranged from 1 to 65 years, with a median of 34.5 years. According to the obtainable data, local recurrence and/or distant metastasis occurred in 36% cases with follow-up information available, including two cases in the head and neck area. The tumor in the first case occurred in the submandibular soft tissue and harbored a *PTCH1-GLI1* fusion (discussed further in the next paragraph), in the second case the tumor with a *GLI1* amplification arose

Table 2 *PTCH1-GLI1* positive mesenchymal tumors: clinicopathologic and immunophenotypic characteristics

Case #	Age/Sex	Site	IHC	Follow-up	References
1	32/F	Submandibular ST/neck	S100 (+)	LR, mets to LN and lung, AWD 123 mo	[2, 11]
2	38/M	Tongue	S100 (+) CD56 (+)	NED 2 mo	[11]
3	13/M	Thorax	S100 (+) CD56 (+)	NED 84 mo	[12]
4	34/F	Soft palate	S100 (F+) CD56 (F+) D2-40 (+)	NED 4 mo	Recent case

AWD alive with disease; *NED* alive with no evidence of disease; *F* female; *F+* focally positive; *LN* lymph nodes; *LR* local recurrence; *M* male; *met* metastasis; *mo* months; *+* positive; *ST* soft tissue

from the neck soft tissue. Both patients developed both local recurrence and distant metastasis.

Presumably, this is only the fourth neoplasm with a *PTCH1-GLI1* fusion reported to date (Table 2). One of the previously described tumors with this fusion grew as an intrathoracic mass in a 13-year-old male [12]. Two tumors with the fusion described by Antonescu and Xu [2, 11] occurred in the head and neck, one appearing in the submandibular soft tissues of a 32-year-old female patient, and the other in the tongue of a 38-year-old male patient. Similarly, the 34-year-old female patient in our case presented with an ulcerated tumor of the soft palate. A stronger predilection for the head and neck can be noted in the *PTCH1-GLI1* fused tumors than in other *GLI1*-rearranged neoplasms, although the number of cases known at present is limited. One of the three previously reported cases with a *PTCH1-GLI1* fusion developed local recurrence and lung metastasis. The mitotic index in this case was high (6 mitoses per 10 HPF), and the tumor also contained areas of necrosis. Conversely, both of these features were lacking in the other cases that did not metastasize, including the case reported here. Even though mitotic activity in our case was rather low and the tumor was ultimately resected with tumor-free margins, a careful follow-up is mandatory.

Considering the histomorphology, tumors with the *PTCH1-FLI1* fusion do not differ greatly from other tumors in the group. As in the other cases of *GLI1*-rearranged tumors reported in the head and neck, the present tumor consisted of monomorphic round cells with epithelioid features and a focal clear-cell change that were organized into nests interspersed with delicate capillary networks. Only limited information is available in the literature on histomorphology of the pediatric tumor occurring in the 13-year-old male. The authors describe a tumor consisting of uniform small round cells organized into cord-like structures [12]. In rough agreement with the immunoprofile of all *GLI1* rearranged tumors, the *PTCH1-GLI1* fused tumors reported to date were at least focally positive for CD56 and negative for AE1/3, while S100 protein, which is only positive in approximately 40% of all *GLI1*-rearranged tumors, was expressed at least in some cells in each tumor with the *PTCH1-GLI1* fusion. At least focal expression of CD56 and S100 protein (observed in 3/3 and 4/4 analyzed cases, respectively) with consistently negative cytokeratins and smooth muscle actin, together with the typical histomorphology, seems to be a common denominator for *PTCH1-GLI1* fused tumors [11].

The transcription factor Gli1 is a nuclear effector of the Hedgehog signaling pathway, which under normal conditions plays important roles in organogenesis during embryonic development. The pathway is deregulated in various cancers, for instance a *GLI2* amplification has been demonstrated in some medulloblastomas, while a proportion of rhabdomyosarcomas reportedly harbor inactivating

mutations in genes of tumor suppressor proteins Patched and Sufu [16]. The significance of the Hedgehog signaling pathway during embryonic development and in carcinogenesis is evident in patients with the nevoid basal cell carcinoma syndrome, who suffer from multiple basal cell carcinomas and various congenital abnormalities caused by an inactivating germline mutation in the *PTCH1* gene. This gene encodes the Patched protein, a tumor suppressor localized in the cell membrane, where it binds and inhibits the Smoothened receptor. When any of the Hedgehog signaling proteins binds Patched, it is inactivated and Smoothened is released. Consequently, a signaling cascade leads to the activation of Gli1. In deregulated signaling during tumorigenesis, various proteins involved in cell proliferation, loss of cell adhesion, increased motility or cancer cell stemness belong to Gli1 targets [16, 17]. Importantly, the Patched-encoding gene *PTCH1* contains a Gli1 binding site in its exon 1. The proposed gene product of the *PTCH1-GLI1* fusion retains the Gli1 binding site in the *PTCH1* part, while the proposed fusion protein contains zinc fingers in the Gli1 part that provide binding to specific regulatory sequences of genes downstream of the Hedgehog pathway, including *PTCH1* (Fig. 5). In neoplastic cells, this might in turn create a positive feedback loop, in contrast to the opposing relationship between Gli1 and Patched in normal tissues. This would increase the expression of the fusion protein which remains an active transcription factor for other targets in the Hedgehog pathway.

The differential diagnosis of a *GLI1*-rearranged mesenchymal epithelioid neoplasm is challenging. Due to an overall bland morphology with monomorphic round to epithelioid cells, multilobulated growth, nested architecture, clear cytoplasm and S100 protein immunopositivity, these tumors are strongly reminiscent of primary epithelial and/or myoepithelial neoplasms of the salivary glands. In the present case, due to the corded, microglandular or reticular growth patterns within a myxoid stroma, the epithelioid and spindle-shaped uniform neoplastic cells, and the unique mucosal location in the palate in close proximity to minor salivary glands, the resemblance to myoepithelial neoplasms including myoepithelioma, cellular pleomorphic adenoma, and myoepithelial carcinoma, was particularly intriguing. Importantly, in contrast to the multinodular and infiltrative growth pattern of the *GLI1*-rearranged mesenchymal neoplasm, a benign myoepithelioma is well-circumscribed. Moreover, pleomorphic adenoma shows a biphasic phenotype with both ductal and myoepithelial differentiation, whereas all *GLI1*-rearranged tumors were composed of a single cell type. Myoepithelial carcinoma shows at least focally invasive features and is characterized by a multinodular architecture divided by fibrous bands in a zonal arrangement and a hypercellular peripheral rim surrounding a hypocellular, usually myxoid

and/or necrotic center. Useful diagnostic clues for tumors with a *GLI1* rearrangement include a rich vascular network among nests of tumor cells, tumor tissue bulging into vascular spaces, and absence of cytokeratin, SOX10, GFAP and calponin immunopositivity. Identification of areas with these classic features of *GLI1*-rearranged tumors should trigger efforts for molecular confirmation of a *GLI1* rearrangement, which in contrast has not been reported in myoepithelial carcinomas of salivary glands [13, 14].

Ectomesenchymal chondromyxoid tumor is another tumor included in the differential diagnosis of *GLI1*-rearranged tumors. It is a rare mesenchymal neoplasm characterized by a striking predilection for the anterior dorsal tongue. It has a multilobulated growth pattern and is immunohistochemically positive for S100 protein, CD56, cytokeratin, and SMA [18, 19]. However, ectomesenchymal chondromyxoid tumor typically shows a more spindled cytomorphology and an abundant myxoid stroma, it lacks an arborizing capillary network and may express other myoepithelial markers such as calponin and GFAP [18]. At the molecular level, these tumors harbor a characteristic *RREB1-MKL2* fusion. Thus, molecular testing can be used in differential diagnosis in challenging cases [19].

In a tumor with positive neuroendocrine markers and a prominent vascular network in between round to oval cells with moderate amounts of pale eosinophilic cytoplasm organized in a solid-trabecular pattern, the differential diagnosis of paraganglioma could be considered. Nonetheless, a more solidly nested growth pattern is usually present in paraganglioma. Furthermore, S100 protein immunohistochemistry displays a distinct pattern in paragangliomas, with only the sustentacular cells staining positive. Whereas CD56 immunopositivity is very frequent in epithelioid soft tissue tumors with *GLI1* rearrangements, other neuroendocrine markers are typically negative. In fact, there have only been four other cases thus far with a reported positivity for any neuroendocrine markers. These include a case of a 57-year-old female with a tibial tumor with rare cells staining with an antibody against synaptophysin [10], two cases diffusely positive for NSE, including a 67-year-old male with a bone (talus) tumor [5] and a 48-year-old male with a jejunal tumor [6], and an additional case of a 28-year-old male with a gastroblastoma positive for NSE in the epithelial component of the tumor [6]. All but one of these patients later suffered distant metastases [6, 7, 10], possibly linking such neuroendocrine features to a more aggressive clinical behavior. This further highlights the importance of careful follow-up of the patient in the case presented here.

A correct diagnosis supported by the detection of a *GLI1* gene rearrangement may have therapeutic implications, as tumors with *GLI1* oncogenic activation and subsequent *PTCH1* overexpression may be sensitive to SHH pathway inhibitors [20]. Identification of *GLI1* alterations and oncogenic activation in this unique tumor entity may, therefore, allow patients, especially those with advanced disease, to gain access to Hedgehog or *GLI1*-targeted therapies.

In summary, the presented case improves our understanding of the emerging group of *GLI1*-rearranged tumors. The tumor consisted of nests of relatively uniform round to spindled cells with bland basophilic nuclei, an occasional clearing of tumor cell cytoplasm and focal immunohistochemical positivity for S-100 protein and CD56. A reticular, trabecular, pseudoglandular or fascicular architecture was present in different parts of the tumor. A delicate branching vasculature permeated the lesion. Molecular genetic testing revealed a *PTCH1-GLI1* fusion. *GLI1*-rearranged tumors usually have an indolent behavior; however, propensity for locoregional recurrence and distant metastatic spread should not be underscored. Information about molecular genetic background of the tumor is of great clinical importance, especially for patients with advanced disease who could benefit from treatment with selective Hedgehog pathway inhibitors.

Declarations

References

1. Dahlén A, Fletcher CD, Mertens F, et al. Activation of the GLI oncogene through fusion with the beta-actin gene (ACTB) in a group of distinctive pericytic neoplasms: pericytoma with t(7;12). Am J Pathol. 2004;164(5):1645–53.

2. Antonescu CR, Agaram NP, Sung YS, Zhang L, Swanson D, Dickson BC. A distinct malignant epithelioid neoplasm with GLI1 gene rearrangements, frequent S100 protein expression, and metastatic potential: expanding the spectrum of pathologic entities with *ACTB/MALAT1/PTCH1-GLI1* fusions. Am J Surg Pathol. 2018;42(4):553–60.

3. Agaram NP, Zhang L, Sung YS, et al. GLI1-amplifications expand the spectrum of soft tissue neoplasms defined by GLI1 gene fusions. Mod Pathol. 2019;32:1617–26.

4. Koh NWC, Seow WY, Lee YT, Lam JCM, Lian DWQ. Pericytoma with t(7;12): the first ovarian case reported and a review of the literature. Int J Gynecol Pathol. 2019;38(5):479–84.

5. Bridge JA, Sanders K, Huang D, et al. Pericytoma with t(7;12) and ACTB-GLI1 fusion arising in bone. Hum Pathol. 2012;43(9):1524–9.

6. Prall OWJ, McEvoy CRE, Byrne DJ, et al. A malignant neoplasm from the jejunum with a MALAT1-GLI1 fusion and 26-year survival history. Int J Surg Pathol. 2020;28(5):553–62.

7. Graham RP, Nair AA, Davila JI, et al. Gastroblastoma harbors a recurrent somatic MALAT1–GLI1 fusion gene. Mod Pathol. 2017;30(10):1443–52.

8. Spans L, Fletcher CDM, Antonescu CR, et al. Recurrent MALAT1–GLI1 oncogenic fusion and GLI1 up-regulation define a subset of plexiform fibromyxoma. J Pathol. 2016;239(3):335–43.

9. Castro E, Cortes-Santiago N, Suarez Ferguson LM, Rao PH, Venkatramani R, López-Terrada D. Translocation t(7;12) as the sole chromosomal abnormality resulting in ACTB-GLI1 fusion in pediatric gastric pericytoma. Hum Pathol. 2016;53:137–41.

10. Kerr DA, Pinto A, Subhawong TK, et al. Pericytoma with t(7;12) and ACTB-GLI1 fusion: reevaluation of an unusual entity and its relationship to the spectrum of GLI1 fusion-related neoplasms. Am J Surg Pathol. 2019;43(12):1682–92.

11. Xu B, Chang K, Fople AL, et al. Head and neck mesenchymal neoplasms with *GLI1* gene alterations: a pathologic entity with distinct histologic features and potential for distant metastasis. Am J Surg Pathol. 2020;44(6):729–36.

12. Ichikawa D, Yamashita K, Okuno Y, et al. Integrated diagnosis based on transcriptome analysis in suspected pediatric sarcomas. NPJ Genomic Med. 2021;6:49.

13. Dalin MG, Katabi N, Persson M, et al. Multi-dimensional genomic analysis of myoepithelial carcinoma identifies prevalent oncogenic gene fusions. Nat Commun. 2017;8(1):1197.

14. Skálová A, Agaimy A, Vanecek T, et al. Molecular profiling of clear cell myoepithelial carcinoma of salivary glands with *EWSR1* rearrangement identifies frequent *PLAG1* gene fusions but no *EWSR1* fusion transcripts. Am J Surg Pathol. 2021;45(1):1–13.

15. Pettus JR, Kerr DA, Stan RV, et al. Primary myxoid and epithelioid mesenchymal tumor of the kidney with a novel GLI1-FOXO4 fusion. Genes Chromosom Cancer. 2021;60(2):116–22.

16. Sari IN, Phi LTH, Jun N, Wijaya YT, Lee S, Kwon HY. Hedgehog signaling in cancer: a prospective therapeutic target for eradicating cancer stem cells. Cells. 2018;7(11):208.

17. Carpenter RL, Lo HW. Hedgehog pathway and GLI1 isoforms in human cancer. Discov Med. 2012;13(69):105–13.

18. Laco J, Mottl R, Höbling W, et al. Cyclin D1 expression in ectomesenchymal chondromyxoid tumor of the anterior tongue. Int J Surg Pathol. 2016;24(7):586–94.

19. Dickson BC, Antonescu CR, Argyris PP, et al. Ectomesenchymal chondromyxoid tumor: a neoplasm characterized by recurrent *RREB1-MKL2* fusions. Am J Surg Pathol. 2018;42(10):1297–305.

20. Rimkus TK, Carpenter RL, Qasem S, Chan M, Lo HW. Targeting the sonic hedgehog signaling pathway: review of smoothened and GLI inhibitors. Cancers (Basel). 2016;8(2):22.

Springer

5   Závěr

V disertační práci jsou diskutovány vzácné a nově definované jednotky v nádorové patologii hlavy a krku, se zaměřením na jejich molekulárně-genetické pozadí, imunoprofil, diferenciální diagnózu a klinické implikace.

Autorka se během doktorského studia podílela na 16 publikacích vydaných v časopisech s impact factorem, na 8 z nich jako první autor. Součástí akademického působení autorky byla také aktivní účast na 11 domácích a zahraničních konferencích či seminářích.

V oblasti salivární patologie jsou uvedeny dvě studie zabývající se acinickým karcinomem a sklerózujícím polycystickým adenomem. Následují studie zabývající se vzácnými sinonasálními adenokarcinomy, v oblasti sinonasální patologie je dále diskutován bifenotypický sinonasální sarkom transformující v agresivní rhabdomyosarkom a rovněž prognosticky značně nepříznivý *EWSR1::POU2AF3* sarkom. Poté jsou předloženy nové poznatky včetně dat z metylačního profilování u souboru mesenchymálních nádorů s aberacemi genů kódujících proteinkinázy, popis souboru 7 unikátních myxoidních fibroblastických tumorů hlasivky, a nakonec je referován vzácný tumor měkkého patra s *PTCH1:GLI1* fúzí.

6   Reference

1. Speight PM, Barrett AW. Salivary gland tumours. Oral Dis. 2002;8(5):229–40.
2. Alsanie I, Rajab S, Cottom H, et al. Distribution and Frequency of Salivary Gland Tumours: An International Multicenter Study. Head Neck Pathol. 2022;16(4):1043-1054.
3. Ferlay J, Ervik M, Lam F, et al. Global Cancer Observatory: Cancer Today. Lyon, France: International Agency for Research on Cancer, 2024 [cited 2024 Feb 19]. Available from: https://gco.iarc.who.int/today.
4. WHO Classification of Tumours Editorial Board. Head and neck tumours [Internet; beta version ahead of print]. Lyon, France: International Agency for Research on Cancer, 2022 [cited 2024 Feb 19]. (WHO classification of tumours series, 5th ed.; vol. 9). Available from: https://tumourclassification.iarc.who.int/chapters/52.
5. Patel NR, Sanghvi S, Khan MN, Husain Q, Baredes S, Eloy JA. Demographic trends and disease-specific survival in salivary acinic cell carcinoma: an analysis of 1129 cases. Laryngoscope. 2014;124(1):172-178.
6. Skálová A, Sima R, Vanecek T, et al. Acinic cell carcinoma with high-grade transformation: a report of 9 cases with immunohistochemical study and analysis of TP53 and HER-2/neu genes. Am J Surg Pathol. 2009;33(8):1137-1145.
7. Haller F, Bieg M, Will R, et al. Enhancer hijacking activates oncogenic transcription factor NR4A3 in acinic cell carcinomas of the salivary glands. Nat Commun. 2019;10(1):368. Published 2019 Jan 21.
8. Skálová A, Gnepp DR, Simpson RH, et al. Clonal nature of sclerosing polycystic adenosis of salivary glands demonstrated by using the polymorphism of the human androgen receptor (HUMARA) locus as a marker. Am J Surg Pathol. 2006;30(8):939-944.
9. Bishop JA, Gagan J, Baumhoer D, et al. Sclerosing Polycystic "Adenosis" of Salivary Glands: A Neoplasm Characterized by PI3K Pathway Alterations More Correctly Named Sclerosing Polycystic Adenoma. Head Neck Pathol. 2020;14(3):630-636.
10. Skálová A, Baněčková M, Laco J, et al. Sclerosing Polycystic Adenoma of Salivary Glands: A Novel Neoplasm Characterized by PI3K-AKT Pathway Alterations-New Insights Into a Challenging Entity. Am J Surg Pathol. 2022;46(2):268-280.
11. Turner JH, Reh DD. Incidence and survival in patients with sinonasal cancer: a historical analysis of population-based data. Head Neck. 2012;34(6):877-885.
12. Youlden DR, Cramb SM, Peters S, et al. International comparisons of the incidence and mortality of sinonasal cancer. Cancer Epidemiol. 2013;37(6):770-779.
13. Kennedy MT, Jordan RC, Berean KW, Perez-Ordoñez B. Expression pattern of CK7, CK20, CDX-2, and villin in intestinal-type sinonasal adenocarcinoma. J Clin Pathol. 2004;57(9):932-937.
14. Skalova A, Sar A, Laco J, et al. The Role of SATB2 as a Diagnostic Marker of Sinonasal Intestinal-type Adenocarcinoma. Appl Immunohistochem Mol Morphol. 2018;26(2):140-146.
15. Donhuijsen K, Kollecker I, Petersen P, Gaßler N, Wolf J, Schroeder HG. Clinical and morphological aspects of adenocarcinomas of the intestinal type in the inner nose: a retrospective multicenter analysis. Eur Arch Otorhinolaryngol. 2016;273(10):3207-3213.

16. Heffner DK, Hyams VJ, Hauck KW, Lingeman C. Low-grade adenocarcinoma of the nasal cavity and paranasal sinuses. Cancer. 1982;50(2):312-322.

17. Shah AA, Jain D, Ababneh E, et al. SMARCB1 (INI-1)-Deficient Adenocarcinoma of the Sinonasal Tract: A Potentially Under-Recognized form of Sinonasal Adenocarcinoma with Occasional Yolk Sac Tumor-Like Features. Head Neck Pathol. 2020;14(2):465-472.

18. Le Loarer F, Laffont S, Lesluyes T, et al. Clinicopathologic and Molecular Features of a Series of 41 Biphenotypic Sinonasal Sarcomas Expanding Their Molecular Spectrum. Am J Surg Pathol. 2019;43(6):747-754.

19. Huang SC, Ghossein RA, Bishop JA, et al. Novel PAX3-NCOA1 Fusions in Biphenotypic Sinonasal Sarcoma With Focal Rhabdomyoblastic Differentiation. Am J Surg Pathol. 2016;40(1):51-59.

20. Fritchie KJ, Jin L, Wang X, et al. Fusion gene profile of biphenotypic sinonasal sarcoma: an analysis of 44 cases. Histopathology. 2016;69(6):930-936.

21. Agaimy A, Baněčková M, De Almeida J, et al. Recurrent EWSR1::COLCA2 Fusions Define a Novel Sarcoma With Spindle/Round Cell Morphology and Strong Predilection for the Sinonasal Tract. Am J Surg Pathol. 2023;47(3):361-369.

22. Hiemenz MC, Kaur J, Kuang Z, et al. POU2AF3-rearranged sarcomas: A novel tumor defined by fusions of EWSR1 or FUS to a gene formerly designated COLCA2. Genes Chromosomes Cancer. 2023;62(8):460-470.

23. Schwartz JC, Cech TR, Parker RR. Biochemical Properties and Biological Functions of FET Proteins. Annu Rev Biochem. 2015;84:355-379.

24. Myhre-Jensen O. A consecutive 7-year series of 1331 benign soft tissue tumours. Clinicopathologic data. Comparison with sarcomas. Acta Orthop Scand. 1981;52(3):287-293.

25. WHO Classification of Tumours Editorial Board. Soft tissue and bone tumours [Internet]. Lyon, France: International Agency for Research on Cancer; 2020 [cited 2024 Feb 21]. (WHO classification of tumours series, 5th ed.; vol. 3). Available from: https://tumourclassification.iarc.who.int/chapters/33.

26. Gatta G, Capocaccia R, Botta L, et al. Burden and centralised treatment in Europe of rare tumours: results of RARECAREnet-a population-based study [published correction appears in Lancet Oncol. 2017 Aug;18(8):e433]. Lancet Oncol. 2017;18(8):1022-1039.

27. Fletcher CD. Distinctive soft tissue tumors of the head and neck. Mod Pathol. 2002;15(3):324-330.

28. Antonescu CR. Emerging soft tissue tumors with kinase fusions: An overview of the recent literature with an emphasis on diagnostic criteria. Genes Chromosomes Cancer. 2020;59(8):437-444.

29. Davis JL, Al-Ibraheemi A, Rudzinski ER, Surrey LF. Mesenchymal neoplasms with NTRK and other kinase gene alterations. Histopathology. 2022;80(1):4-18.

30. Coffin CM, Watterson J, Priest JR, Dehner LP. Extrapulmonary inflammatory myofibroblastic tumor (inflammatory pseudotumor). A clinicopathologic and immunohistochemical study of 84 cases. Am J Surg Pathol. 1995;19(8):859-872.

31. Gleason BC, Hornick JL. Inflammatory myofibroblastic tumours: where are we now?. J Clin Pathol. 2008;61(4):428-437.

32. Kerr DA, Thompson LDR, Tafe LJ, et al. Clinicopathologic and Genomic Characterization of Inflammatory Myofibroblastic Tumors of the Head and Neck: Highlighting a Novel Fusion and Potential Diagnostic Pitfall. Am J Surg Pathol. 2021;45(12):1707-1719.

33. Antonescu CR, Suurmeijer AJ, Zhang L, et al. Molecular characterization of inflammatory myofibroblastic tumors with frequent ALK and ROS1 gene fusions and rare novel RET rearrangement. Am J Surg Pathol. 2015;39(7):957-967.

34. Yamamoto H, Yoshida A, Taguchi K, et al. ALK, ROS1 and NTRK3 gene rearrangements in inflammatory myofibroblastic tumours. Histopathology. 2016;69(1):72-83.

35. Xu B, Chang K, Folpe AL, et al. Head and Neck Mesenchymal Neoplasms With GLI1 Gene Alterations: A Pathologic Entity With Distinct Histologic Features and Potential for Distant Metastasis. Am J Surg Pathol. 2020;44(6):729-737.

36. Agaram NP, Zhang L, Sung YS, et al. GLI1-amplifications expand the spectrum of soft tissue neoplasms defined by GLI1 gene fusions. Mod Pathol. 2019;32(11):1617-1626.

37. Parrack PH, Mariño-Enríquez A, Fletcher CDM, Hornick JL, Papke DJ Jr. GLI1 Immunohistochemistry Distinguishes Mesenchymal Neoplasms With GLI1 Alterations From Morphologic Mimics. Am J Surg Pathol. 2023;47(4):453-460.

38. Nitta Y, Takeda M, Fujii T, et al. A case of pericytic neoplasm in the shoulder with a novel DERA-GLI1 gene fusion. Histopathology. 2021;78(3):466-469.

39. Skálová A, Vanecek T, Sima R, et al. Mammary analogue secretory carcinoma of salivary glands, containing the ETV6-NTRK3 fusion gene: a hitherto undescribed salivary gland tumor entity. Am J Surg Pathol. 2010;34(5):599-608.

40. Baneckova M, Agaimy A, Andreasen S, et al. Mammary Analog Secretory Carcinoma of the Nasal Cavity: Characterization of 2 Cases and Their Distinction From Other Low-grade Sinonasal Adenocarcinomas. Am J Surg Pathol. 2018;42(6):735-743.

41. Skálová A, Vanecek T, Majewska H, et al. Mammary analogue secretory carcinoma of salivary glands with high-grade transformation: report of 3 cases with the ETV6-NTRK3 gene fusion and analysis of TP53, β-catenin, EGFR, and CCND1 genes. Am J Surg Pathol. 2014;38(1):23-33.

42. Andreasen S, Skálová A, Agaimy A, et al. ETV6 Gene Rearrangements Characterize a Morphologically Distinct Subset of Sinonasal Low-grade Non-intestinal-type Adenocarcinoma: A Novel Translocation-associated Carcinoma Restricted to the Sinonasal Tract. Am J Surg Pathol. 2017;41(11):1552-1560.

43. Andreasen S, Kiss K, Melchior LC, Laco J. The ETV6-RET Gene Fusion Is Found in ETV6-rearranged Low-grade Sinonasal Adenocarcinoma Without NTRK3 Involvement. Am J Surg Pathol. 2018;42(7):985-988.

44. Kishikawa S, Hayashi T, Shimizu J, et al. Low-grade tracheal adenocarcinoma with ETV6::NTRK3 fusion: unique morphology akin to subsets of sinonasal low-grade non-intestinal-type adenocarcinoma. Virchows Arch. 2022;481(5):793-797.

45. Charville GW, Varma S, Forgó E, et al. PAX7 Expression in Rhabdomyosarcoma, Related Soft Tissue Tumors, and Small Round Blue Cell Neoplasms. Am J Surg Pathol. 2016;40(10):1305-1315.

46. Folpe AL. MyoD1 and myogenin expression in human neoplasia: a review and update. Adv Anat Pathol. 2002;9(3):198-203.

47. Bell D, Phan J, DeMonte F, Hanna EY. High-grade transformation of low-grade biphenotypic sinonasal sarcoma: Radiological, morphophenotypic variation and confirmatory molecular analysis. Ann Diagn Pathol. 2022;57:151889.
48. Hasnie S, Glenn C, Peterson JEG, El Rassi ET, McKinney KA. High-Grade Biphenotypic Sinonasal Sarcoma: A Case Report. J Neurol Surg Rep. 2022;83(3):e105-e109. Published 2022 Sep 13.
49. Yorita K, Togashi Y, Nakagawa H, et al. Vocal cord inflammatory myofibroblastic tumor with mucoid deposits harboring TIMP3-ALK fusion: A potential diagnostic pitfall. Pathol Int. 2019;69(6):366-371.

7   Souhrn díla autorky

7.1   Publikace tvořící podklad disertační práce

Klubíčková N, Grossmann P, Šteiner P, et al. A minority of cases of acinic cell carcinoma of the salivary glands are driven by an NR4A2 rearrangement: the diagnostic utility of the assessment of NR4A2 and NR4A3 alterations in salivary gland tumors. Virchows Arch. 2023;482(2):339-345.

Skálová A, Baněčková M, Laco J, **et al**. Sclerosing polycystic adenoma of salivary glands: A novel neoplasm characterized by PI3K-AKT pathway alterations – New insights into a challenging entity. Am J Surg Pathol. 2022;46(2):268-280.

Klubíčková N, Mosaieby E, Ptáková N, et al. High-grade non-intestinal type sinonasal adenocarcinoma with ETV6::NTRK3 fusion, distinct from secretory carcinoma by immunoprofile and morphology. Virchows Arch. 2023;483(2):187-195.

Skálová A, Taheri T, Bradová M, **et al**. SMARCB1-deficient sinonasal adenocarcinoma: a rare variant of SWI/SNF-deficient malignancy often misclassified as high-grade non-intestinal-type sinonasal adenocarcinoma or myoepithelial carcinoma. Virchows Arch. Published online December 12, 2023.

Meyer A, **Klubíčková N**, Mosaieby E, et al. Biphenotypic sinonasal sarcoma with PAX3::MAML3 fusion transforming into high-grade rhabdomyosarcoma: report of an emerging rare phenomenon. Virchows Arch. 2023;482(4):777-782.

Koshyk O, Dehner CA, van den Hout MFCM, **et al**. EWSR1::POU2AF3(COLCA2) sarcoma: An aggressive, polyphenotypic sarcoma with a head and neck predilection. Mod Pathol. 2023;36(12):100337.

Klubíčková N, Dermawan JK, Mosaieby E, et al. Comprehensive clinicopathological, molecular, and methylation analysis of mesenchymal tumors with NTRK and other kinase gene aberrations. J Pathol. Published online February 9, 2024.

Klubíčková N, Michal M, Agaimy A, et al. TIMP3::ALK fusions characterize a distinctive myxoid fibroblastic tumor of the vocal cords: a report of 7 cases. Virchows Arch. 2022;481(5):721-729.

Klubíčková N, Kinkor Z, Michal M, et al. Epithelioid soft tissue neoplasm of the soft palate with a PTCH1-GLI1 fusion: A case report and review of the literature. Head Neck Pathol. 2022;16(2):621-630.

7.2 Další publikace související s tématem disertační práce

Klubíčková N, Gross JM, Comová K, Kuruc J, Michal M. A novel FUS::NFATC4 fusion detected in a sarcoma with morphological features overlapping with NFATC2 sarcomas. Histopathology. 2024;84(2):413-415.

Skálová A, Bradová M, Michal M Jr, **et al**. Molecular pathology in diagnosis and prognostication of head and neck tumors. Virchows Arch. Published online January 13, 2024.

7.3 Publikace nesouvisející s tématem disertační práce

Klubíčková N, Michal M, Kinkor Z, et al. Poorly differentiated extra-axial extraskeletal chordoma diagnosed by methylation profiling: case report and analysis of brachyury expression in SWI/SNF-deficient tumors. Virchows Arch. Published online August 18, 2023.

Klubíčková N, Agaimy A, Hájková V, et al. RNA-sequencing of myxoinflammatory fibroblastic sarcomas reveals a novel SND1::BRAF fusion and 3 different molecular aberrations with the potential to upregulate the TEAD1 gene including SEC23IP::VGLL3 and TEAD1::MRTFB gene fusions. Virchows Arch. 2022;481(4):613-620.

Lenz J, **Klubíčková N**, Ptáková N, et al. Extraskeletal myxoid chondrosarcoma: A study of 17 cases focusing on the diagnostic utility of INSM1 expression and presenting rare morphological variants associated with non-EWSR1::NR4A3 fusions. Hum Pathol. 2023;134:19-29.

Lasota J, Chłopek M, Kaczorowski M, **et al**. Utility of immunohistochemistry with antibodies to SS18-SSX chimeric proteins and C-terminus of SSX protein for synovial sarcoma differential diagnosis. Am J Surg Pathol. 2024;48(1):97-105.

Michal M, Ud Din N, Švajdler M, **et al**. TFG::MET-rearranged soft tissue tumor: A rare infantile neoplasm with a distinct low-grade triphasic morphology. Genes Chromosomes Cancer. 2023;62(5):290-296.

7.4 Účast na vědeckých konferencích

7.4.1 Přednášky

Sklíčkový seminář patologických pracovišť, 30.9.-1.10.2021, Lednice
Přednáška: Tumor hlasivky s *TIMP3::ALK* fúzí.

34th European Congress of Pathology, 3-7.9.2022, Basilej
Přednáška 1: A single-institution experience with 128 cases of acinic cell carcinoma: Diagnostic utility of NR4A3 and NR4A2 immunohistochemistry in salivary gland pathology.
Přednáška 2: A single institution experience with 17 cases of extraskeletal myxoid chondrosarcoma: Rare fusions, unusual morphology and the utility of INSM1 immunohistochemistry.

47. sjezd českých patologů, 3.-5.11.2022, Praha
Přednáška: Tumory s diferenciací do příčně pruhované svaloviny: Přehled novinek a diferenciální diagnostika.

Sklíčkový seminář patologických pracovišť, 10.-11.11.2022, Mikulov
Přednáška 1: Novinky v mesenchymálních lézích s diferenciací do příčně pruhované svaloviny.
Přednáška 2: Hyalinizující světlobuněčný karcinom slinné žlázy rtu s fúzí *SMARCA2::CREM*.
Přednáška 3: Sinonasální solitární fibrózní tumor.

Večer Šiklova ústavu patologie, 26.4.2023, Plzeň
Přednáška: Kaposiho sarkom jako komplikace dlouhodobé kortikoterapie.

Studentská vědecká konference Lékařské fakulty v Plzni, 17.5.2023, Plzeň
Přednáška: Targeted RNA sequencing of ossifying fibromyxoid tumor reveals novel *PHF1::AFF3*, *PHF1::KLF15*, *BMI1::EPC1*, and *SUZ12::EPC1* gene fusions and unusual morphological features.

48. sjezd českých patologů, 26.-28.10.2023, Zlín
Přednáška: Přednáška k převzetí Lamblovy ceny za nejlepší původní práci v oboru patologie publikovanou v předchozím roce členem Společnosti českých patologů ČLS JEP ve věku do 35 let.

Sklíčkový seminář patologických pracovišť, 9.-10.11.2023, Mikulov
Přednáška 1: Mesenchymální vřetenobuněčné tumory s alteracemi genů pro proteinkinázy: Přehled a nové poznatky.
Přednáška 2: Metatypický adenoidně cystický karcinom parotis.
Přednáška 3: Palisádující adenokarcinom submandibulární žlázy.

7.4.2 Postery

111th USCAP, 19.-24.3.2022, Los Angeles, CA, USA
Poster 1: Targeted DNA and RNA sequencing of soft tissue spindle cell tumors reveals a rare *MET::TFG* and a novel *PWWP2A::RET* gene fusions as well as additional recurrent *PIK3CA* point mutations.
Poster 2: Solitary fibrous tumor with pure round cell morphology: Immunohistochemical and molecular study of 15 cases.

112th USCAP, 11.-16.3.2023, New Orleans, LA, USA
Poster 1: Targeted RNA sequencing of ossifying fibromyxoid tumors reveals novel *PHF1* gene fusions and unusual morphologic features.
Poster 2: SMARCB1-deficient sinonasal adenocarcinoma: Rare variant of SWI/SNF-deficient malignancy often misclassified as high-grade non-intestinal adenocarcinoma or myoepithelial carcinoma.

113th USCAP, 23.-28.3.2024, Baltimore, MD, USA
Poster 1: Ossifying fibromyxoid tumors with lipomatous and chondroid differentiation: A diagnostic pitfall [accepted for poster presentation].
Poster 2: *HMGA2* gene alterations define a distinctive canalicular subtype of salivary pleomorphic adenoma [accepted for poster presentation].